Low-Frequency Variability of Sea Level Along the Coast of India

D. Shankar

Thesis

submitted to Goa University

for the Degree of

Doctor of Philosophy

in

Marine Sciences

Goa University

December 1998

Statement

As required under the University ordinance 0.19.8.(vi), I state that this thesis entitled *Low-frequency variability of sea level along the coast of India* is my original contribution and it has not been submitted on any previous occasion.

The literature related to the problem investigated has been cited. Due acknowledgements have been made wherever facilities and suggestions have been availed of.

D. SHANKAR

National Institute of Oceanography, Goa
December 1998

Certificate

This is to certify that the thesis entitled *Low-frequency variability of sea level along the coast of India*, submitted by D. Shankar to Goa University for the degree of Doctor of Philosophy, is based on his original studies carried out under my supervision. The thesis or any part thereof has not been previously submitted for any other degree or diploma in any university or institution.

S. R. Shetye

SATISH R. SHETYE

National Institute of Oceanography, Goa
December 1998

All the corrections suggested by the experts are incorporated

22/1/2000

HEAD
DEPARTMENT OF MARINE SCIENCE
&
~~MARINE~~ BIOTECHNOLOGY
GOA UNIVERSITY.

S. R. Shetye

~~वैज्ञानिक~~ / Scientist
राष्ट्रीय समुद्र विज्ञान संस्थान
National Institute of Oceanography
दोना पावला, गोवा – ४०३ ००४
Dona Paula, Goa 403 004.

Vita

Name	Shankar Doraiswamy
Born	9 August 1967, Bangalore
Education	
B. Tech.	Aerospace Engineering Indian Institute of Technology, Madras (Chennai) June 1989
M.Sc. (Engg.)	Atmospheric Sciences Indian Institute of Science, Bangalore November 1991
Work	
Research Fellow	Centre for Mathematical Modelling and Computer Simulation (C-MMACS), Bangalore November 1991 to August 1994
Scientist	Centre for Mathematical Modelling and Computer Simulation (C-MMACS), Bangalore September 1994 to January 1995
Scientist	National Institute of Oceanography, Goa January 1995 to date
Address for communication	
By post	Physical Oceanography Division, National Institute of Oceanography, Dona Paula, Goa 403 004, India.
By e-mail	`shankar@csnio.ren.nic.in`, `shankar@darya.nio.org`.

List of Publications

- **D. Shankar**. *Seasonal cycle of the zonally symmetric tropical circulation in a simple climate model.* M.Sc. thesis, Indian Institute of Science, Bangalore, 1991.
- **D. Shankar**, J. P. McCreary, W. Han, and S. R. Shetye. Dynamics of the East India Coastal Current, 1. Analytic solutions forced by interior Ekman pumping and local alongshore winds. *Journal of Geophysical Research*, 101:13,975–13,991, 1996.
- J. P. McCreary, W. Han, **D. Shankar**, and S. R. Shetye. Dynamics of the East India Coastal Current, 2. Numerical solutions. *Journal of Geophysical Research*, 101:13,993–14,010, 1996.
- S. R. Shetye, A. D. Gouveia, **D. Shankar**, S. S. C. Shenoi, P. N. Vinayachandran, D. Sundar, G. S. Michael, and G. Nampoothiri. Hydrography and circulation in the western Bay of Bengal during the northeast monsoon. *Journal of Geophysical Research*, 101:14,011–14,025, 1996.
- **D. Shankar** and S. R. Shetye. On the dynamics of the Lakshadweep high and low in the southeastern Arabian Sea. *Journal of Geophysical Research*, 102:12,551–12,562, 1996.
- S. S. C. Shenoi, **D. Shankar** and S. R. Shetye. On the sea surface temperature high in the Lakshadweep Sea before the onset of the southwest monsoon. *Journal of Geophysical Research*, 104:15,703–15,712, 1999.
- **D. Shankar** and S. R. Shetye. Are interdecadal sea level changes along the Indian coast influenced by variability of monsoon rainfall? *Journal of Geophysical Research*, 104:26,031–26,042, 1999.
- D. Sundar, **D. Shankar**, and S. R. Shetye. Sea level during storm surges as seen in tide-gauge records along the east coast of India. *Current Science*, 77:1325–1332, 1999.
- **D. Shankar**. Seasonal cycle of sea level and currents along the coast of India. *Current Science*. (In press.)

Acknowledgements

It was on a warm afternoon in May 1991, when I was finishing my M.Sc. thesis at the Indian Institute of Science (IISc) and looking for a job, that I first met Satish Shetye. The meeting led me first to a fellowship in C-MMACS and then to a job at the National Institute of Oceanography (NIO). In the seven years that I have spent in the warm waters of the tropical oceans, he has been a teacher and a friend, and has spent more time thinking of my career than I have. We have been co-authors on all but one of my publications, and the use of the first-person plural in this thesis may be interpreted as such.

When he started out on his cruises in the Indian coastal waters in the 1980s, Satish formed a small group, which I joined on coming to Goa in January 1995. They have been pleasant company, both professionally and otherwise. Shenoi, Michael, Unni, Sundar, Albert, and Pradnya helped generate the vibrations that made work possible on hot, summer afternoons. Shenoi, by introducing me to the notion of an outlier, breathed life into a stillborn Chapter 6, enabling me to wind up the thesis. Michael is the local *GMT guru* and several figures in the thesis bear his stamp.

Others in the Physical Oceanography Division helped too. Suryachandra Rao took time off from his own thesis to enable the synthesis of a climatology of temperature and salinity in the coastal waters of India[1], Saji taught me how to draw a curve using *GMT*, making it easy to draw schematics of currents in the ocean, and Fernandes, Anselm, and Navelkar were among those who put up with my babble about *Linux* and LaTeX.

At Goa University, which I visited mainly to submit the half-yearly progress reports and pay the fees, Sandra always helped with a smile.

All the work reported in this thesis was carried out at NIO under a project on sea-level variability sponsored by the Department of Ocean Development, Government of India. The sources of data and software that made this thesis possible are acknowledged in Appendix D. Many of these data sets and softwares were obtained over the Internet, this being possible because of the efforts of those who maintain the network in NIO. When I came to NIO in January 1995, there was but a rudimentary e-mail service here. In these four years, there has been a virtual revolution

[1] See Chapter 4.

in our computing facilities; this was made possible by the efforts of several colleagues and of the director of the institute.

The revolution in communication, especially the Internet, made it possible to keep in touch with, be helped by, and to help friends and colleagues outside Goa. Vinayachandran, Asha Guruprasad, and Ravi Nanjundiah (IISc) made available data and patiently answered my many questions. Julian McCreary (Jay), Weiqing Han, and Kevin Kohler (Nova Southeastern University) were always helpful. Kevin made available the results of their numerical simulations. Despite his busy schedule, Jay was always willing to review our manuscripts and we eagerly awaited his criticism; he and Weiqing helped Satish and me hone our arguments and improve our manuscripts.

This thesis was typed using LaTeX 2ε[2]. The "style file", `guthesis.sty`, was hacked from `utthesis.sty` by Dinesh Das; `utthesis.sty` was brought to my notice by N. H. Saji at a time when I was not getting anywhere with a template for the thesis, and it proved an invaluable starting point. And, as the saying goes, well begun is half done.

Finally, those who generated good vibrations around me! There are many, but I do not want to catalogue names here. Two, however, are special. My father was more interested in my becoming a *doctor* than I ever have been; he passed away before he could realise his dream. My mother has made life more than easy during her stay in Goa and has put up, without a murmur, with more than just my absurd schedule; but for her, I would still be plodding through the thesis. To her, and to my late father, I dedicate this thesis.

D. SHANKAR

National Institute of Oceanography, Goa
December 1998

[2] LaTeX 2ε is an extension of LaTeX, a collection of macros for TeX. TeX is a trademark of the American Mathematical Society.

Synopsis

Coastal sea level is one of the better documented oceanic variables, there being several tide-gauge records of hourly sea level that stretch back to the last century. This, together with the fact that geostrophic, low-frequency coastal currents leave their signatures on sea level, makes tide-gauge data an excellent source of information for the study of coastal circulation over a vast range of sub-inertial frequencies. Low-frequency variability of sea level along the coast of India forms the subject of this thesis. "Low" is defined to exclude frequencies higher than those described by monthly sea level. The seasonal cycle is the highest frequency studied in this thesis, which examines the variability of sea level along the coast of India on seasonal through interdecadal time scales and determines the causes of the observed variability.

After the introduction in Chapter 1 of the thesis, the observational and theoretical background is presented in Chapter 2. The focus is on the literature on the seasonal cycle. The seasonal cycle of sea level, corrected for the effect of atmospheric pressure using the Inverse-Barometer approximation, is coherent along the coast; its range is 45 cm on the east coast and 30 cm on the west coast. Along the east coast, the maximum sea level occurs in November and the minimum during March–April; along the west coast, the maximum occurs in December and the minimum during the southwest monsoon. The seasonal cycle of corrected sea level is in good agreement with that of the observed alongshore ship drifts, implying a link between the large-scale coastal circulation and coastal sea level. It does not, however, match that of the local alongshore winds, showing that the circulation along the coast of India is influenced considerably by remote forcing. This inability to model the circulation along the coast of India by invoking purely local causes leads to a theoretical framework, developed over the last decade, for describing the large-scale circulation in the north Indian Ocean.

This theoretical framework merges the Bay of Bengal, the Arabian Sea, and the equatorial Indian Ocean into a single dynamical entity, which must be modelled as a whole even to simulate the circulation in its parts. It is applied in Chapter 3 to the Lakshadweep high and low, a high and low in sea level that form off southwest India during the northeast and southwest monsoons, respectively, and propagate westward. The dynamics of the high and low is modelled using a dynamical $1\frac{1}{2}$-layer reduced-gravity model. The simulations show that the high and low are explicable by

linear theory and do not owe their existence to nonlinearity. Simple numerical and analytic solutions show that a Kelvin wave propagating along the east coast of India can generate the high and low, implying that the essential elements of the high and low are contained in coastal Kelvin and equatorial Rossby waves, both of which arise from linear dynamics on an equatorial β-plane. They are forced by the radiation of Rossby waves from Kelvin waves propagating poleward along the west coast of India. The Kelvin waves must have a period greater than about 50 days to radiate Rossby waves and force the high and low; at lower periods, they are trapped at the coast. Among the mechanisms forcing these Kelvin waves along the west coast of India, most important are the winds along the east coast of India and Sri Lanka, which by themselves can force the high and low. The winds along the west coast of India and Sri Lanka, especially along the southern margin of the Indian subcontinent, contribute to the formation of the low, but cannot force a high. Other processes contribute marginally to the Lakshadweep high, but they force a westward Southwest Monsoon Current during the southwest monsoon, and the low does not form.

Though the dynamical reduced-gravity model is successful in simulating the essential features of the circulation in the north Indian Ocean, including the currents along the coast of India, it fails to simulate the seasonal cycle of coastal sea level; this is the subject of Chapter 4. The wind-forced model fails to simulate the winter peak along the east coast, and as a result, forces a higher range of the seasonal cycle along the west coast than along the east coast. Simulations in which temperature and salinity vary in the active model layer, these fields being prescribed from a climatology, show that the drop in salinity along the east coast after the southwest monsoon raises steric sea level and is the cause of the maximum in November. This low salinity is the result of runoff from the Ganga and the Brahmaputra into the northern Bay of Bengal during the southwest monsoon. Thus, three mechanisms — atmospheric pressure, winds on the scale of the basin, and salinity — contribute to the seasonal cycle of sea level along the coast of India.

A lower frequency, the annual mean sea level, is the subject of Chapter 5. Levelling observations conducted during the Great Trigonometrical Survey of India (1858–1909) showed that the annual mean sea level is higher along the east coast of India than along the west, the difference between Vishakhapatnam and Mumbai (Bombay) being about 30 cm. Simulations with the $1\frac{1}{2}$-layer reduced-gravity model show that purely wind-forced circulation accounts for half this difference, the other half being due to the gradient in salinity along the coast.

The variability of annual sea level on interannual and interdecadal time scales is the subject of Chapter 6. Annual mean sea level along the coast is significantly correlated with the annual extrema and seasonal averages. Cross-correlations of annual mean sea level at the stations along the coast are statistically significant, showing that these changes are coherent and are part of a basin-scale response. The annual mean and extrema of sea level are also correlated with annual all-India rainfall, as is the local rainfall at Mumbai with the annual sea level there. These correlations

retain their significance when the rainfall and sea-level data are decimated with a 10-year running mean. The interdecadal changes in monsoon rainfall are reflected in sea-level changes at Mumbai, which has the only century-long tide-gauge record in the Indian Ocean; both increase from a low in the first quarter of this century to a high in the 1950s and decrease thereafter.

Our hypothesis is that the seasonal inflow of the monsoon rainfall into the seas around India and the dynamics of the East and West India Coastal Currents (EICC and WICC) provide the link between monsoon rainfall and coastal sea level, the coastal salinity field playing an intermediate role. The seasonal EICC and WICC spread the runoff along the coast, creating a cross-shore salinity gradient; the time scale associated with this gradient is much longer than an year because mixing is slow in the ocean, which responds as a two-layer system to this quasi-steady cross-shore gradient in salinity. When salinity, and hence, density, decreases coastward in the upper layer, sea level rises at the coast, and this is accompanied by a weak, geostrophic, surface current that flows with the lighter water on its right; below it is an undercurrent. Geostrophy also requires that the pycnocline slope up towards the coast.

There are two main conclusions of this thesis, which is summarized in Chapter 7.

1. There are three causes of the low-frequency variability of sea level along the coast of India.

   (a) The large-scale wind-forced circulation of the upper ocean.

   (b) The large changes in salinity that are a result of the high rainfall over the Indian sub-continent and the surrounding seas.

   (c) Atmospheric pressure.

   The first two causes are important at periods ranging from a season to decades; atmospheric pressure contributes significantly only to the seasonal cycle.

2. We propose a hypothesis connecting the interdecadal changes in sea level along the coast of India to the variability of the monsoon, the major aspect of the climate of the region. This hypothesis is different from those generally proposed to link sea level to climate change; these hypotheses invoke the increase in volume due to the change in temperature of the upper ocean and the addition of freshwater because of the melting of polar ice caps.

Contents

List of Tables

List of Figures

Chapter 1

Introduction

The surface of the sea deforms continuously under various influences. Its level, measured relative to an arbitrary datum, is called sea level, which changes with time and is the grossest, and most obvious, indicator of change in the oceans. Changes in sea level are greater in the shallow waters in the vicinity of a coast than they are in the open sea, and since a large fraction of the human population resides in coastal areas, variations in sea level have aroused interest for a long time. A reasonably accurate prediction of sea level was also necessary for safe navigation of boats and ships in harbours. This, and the relative ease of measuring sea level as compared to measuring, say, temperature or currents, has led to it being one of the better documented oceanic variables. Hourly measurements of sea level are available at several places over the globe, some of the records stretching back to the last century.

A tide gauge measures sea level relative to land; an increase in sea level may either be due to an absolute rise in sea level, or due to a sinking of land. The largest changes evident in a typical sea-level record are those due to astronomical tides. These regular, periodic patterns are modified by the effects of the weather; exchange of energy between the atmosphere and the ocean occurs at all space and time scales, from the generation of short-period wind-waves to the slow transfer of energy, over a century, from the tropics to the poles by the global ocean circulation. The sea-level record also includes the effect of secular changes in sea level, forced by changes in the volume of ice locked in major ice caps and glaciers.

India, with its long coastline, lies in the Indian Ocean (Figure 1.1), which is much smaller than the Pacific or the north Atlantic. Unlike these two basins, it is bounded in the north by Asia; this makes it a tropical basin. This has profound consequences for the meteorology and oceanography of this region: the land-ocean contrast forces seasonally reversing winds, the monsoons, over the north Indian Ocean (Figure 1.2), unlike in the north Atlantic or the north Pacific. The north Indian Ocean responds to this forcing, resulting in the significant seasonal cycle of sea level seen in the tide-gauge records along the coast of India.

Figure 1.1 The geography of the Indian Ocean. The zonal extent of the Indian Ocean is much less than that of the Pacific or the north Atlantic. Its southern boundary is arbitrary, but is chosen to distinguish it from the Antarctic, or southern, Ocean. Unlike the Pacific and the Atlantic, the Indian Ocean is bounded in the north by Asia; this makes it a tropical basin. This has profound consequences for the meteorology and oceanography of this region: the land-ocean contrast forces seasonally reversing winds, the monsoons, over the north Indian Ocean, unlike in the north Atlantic or the north Pacific. The north Indian Ocean responds to this forcing, resulting in the significant seasonal cycle of sea level seen in the tide-gauge records along the coast of India.

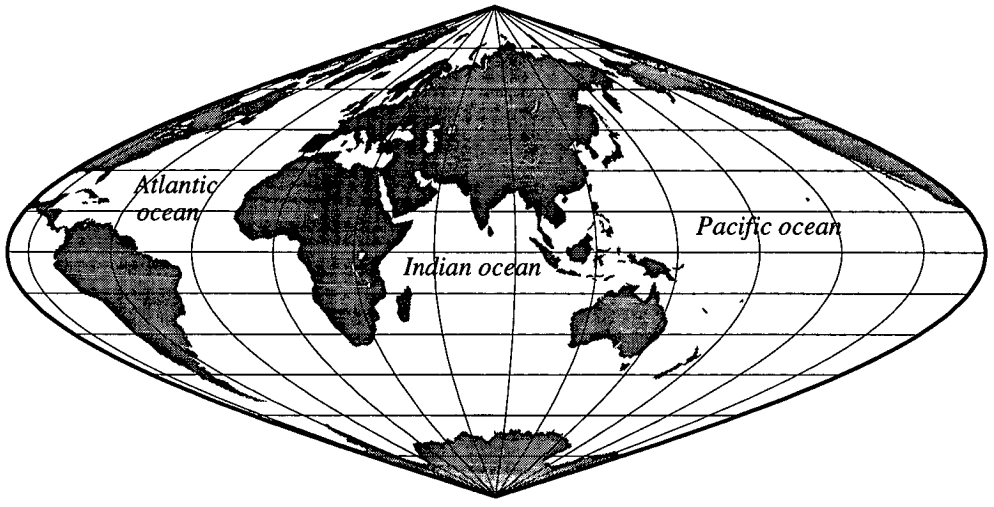

Mumbai, on the west coast of India (Figure 1.2), has the longest tide-gauge record in the Indian Ocean. Like tide-gauge records elsewhere in the world, that at Mumbai exhibits variability over a range of frequencies (Figure 1.3). The change in sea level due to tides is much greater than those related to the weather; the latter are obtained by filtering the the hourly sea level with a 3-day low-pass filter [Doodson, 1921]. Tidal and non-tidal sea-level oscillations are usually studied separately because of the vastly different ways in which they are forced. We ignore tides in this thesis, focussing instead on weather-related sea-level changes at "low" frequencies. Though these are much smaller than the tides, the related movement of the thermocline is important. Defining "low" to exclude all frequencies higher than seasonal, we study the variability of sea level along the coast of India on seasonal through interdecadal time scales, mapping one end of the spectrum of sea-level variability. For this, it is necessary to filter the tides and high-frequency oscillations related to the weather out of the sea-level data. This is most easily achieved by averaging the hourly sea level over a month to obtain monthly sea level[1]; this does almost as good a job at

[1]Throughout this thesis, the term "monthly sea level" is used to denote the mean of hourly sea level over a given calendar month. Likewise, "annual sea level" is used to denote the mean of monthly sea level over a calendar year. What we call monthly and annual sea level are often called monthly mean and annual mean sea level; we drop the "mean", using it only when its absence can lead to ambiguity.

Figure 1.2 The geography of the north Indian Ocean. The north Indian Ocean is split by the Indian peninsula into two parts, the Bay of Bengal in the east and the Arabian Sea in the west. The equatorial Indian Ocean, the Bay of Bengal, and the Arabian Sea are contiguous basins because the southern tip of the Indian subcontinent lies well north of the equator. Together, they form one dynamical entity, the north Indian Ocean.

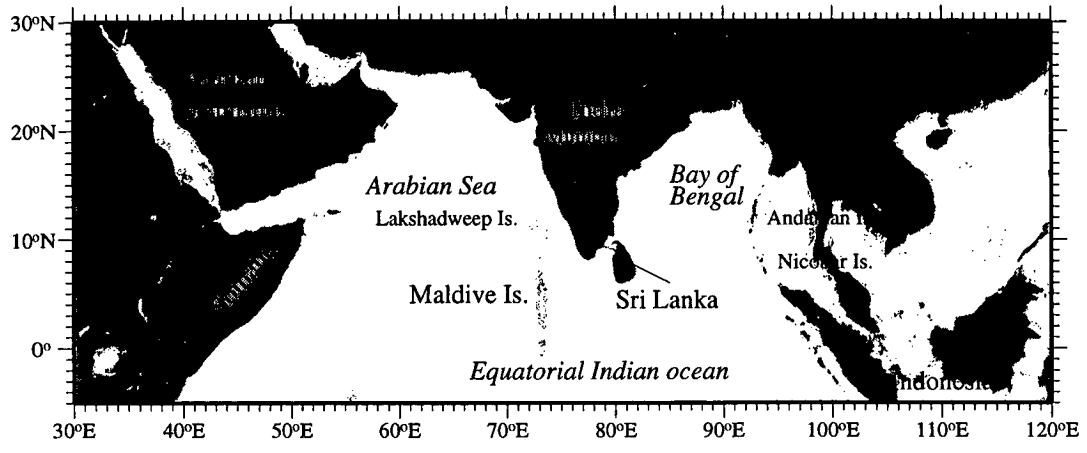

filtering out the higher frequencies, especially the tides, as do more complex techniques [Pugh, 1987]. In this thesis, we use monthly sea level to study the low-frequency variability of sea level along the coast of India.

The tide gauges along the coast of mainland India are important for estimating low-frequency changes because they represent half of those for the entire Indian Ocean [Emery and Aubrey, 1989]. A brief description of this network of tide gauges is given in Chapter 2, which presents the observational and theoretical background for this thesis. At the low frequencies of interest, the sea level along the coast is related to alongshore currents, which are forced by winds acting on the scale of the basin. This leads to a theoretical framework, developed during this decade, for the wind-forced circulation in the north Indian Ocean. The framework is applied in Chapter 3 to the dynamics of the Lakshadweep high and low, a high and low in sea level that form off southwest India. The next three chapters are devoted to the low-frequency variability of coastal sea level, of which the seasonal cycle is the highest frequency. Since it is the most prominent of the regular oscillations related to the weather, it is seen even in a climatology of monthly sea level; this climatological seasonal cycle is studied in Chapter 4. A lower frequency is described by annual sea level, the mean of monthly sea level over an year. The alongshore variation of annual sea level is the subject of Chapter 5. Departures from climatology and sub-annual changes are studied in Chapter 6. Chapter 7 summarizes and concludes the thesis.

Figure 1.3 Sea level variability at Mumbai on the west coast of India. Hourly, daily, monthly, and annual sea level (cm) are plotted as a function of time to reveal the variability over a range of frequencies; the mean, defined over the duration for which the sea level is plotted, is subtracted before plotting each curve. **(a)** Hourly sea level (dashed curve) and daily sea level (solid curve) during 16 May to 15 June, 1976. Daily sea level, which is mostly related to weather, is computed by de-tiding the hourly sea level with a 3-day low-pass filter. **(b)** Daily sea level, as in (a), but with an increase in the scale of the ordinate. **(c)** Daily sea level (dashed curve) and monthly sea level (solid curve) for 1976. Monthly sea level, obtained by averaging the hourly sea level over a month, essentially describes the seasonal cycle. **(d)** Annual sea level (dashed curve) is the average of monthly sea level over an year. Filtering annual sea level with a 10-year running mean (solid curve) reveals interdecadal changes.

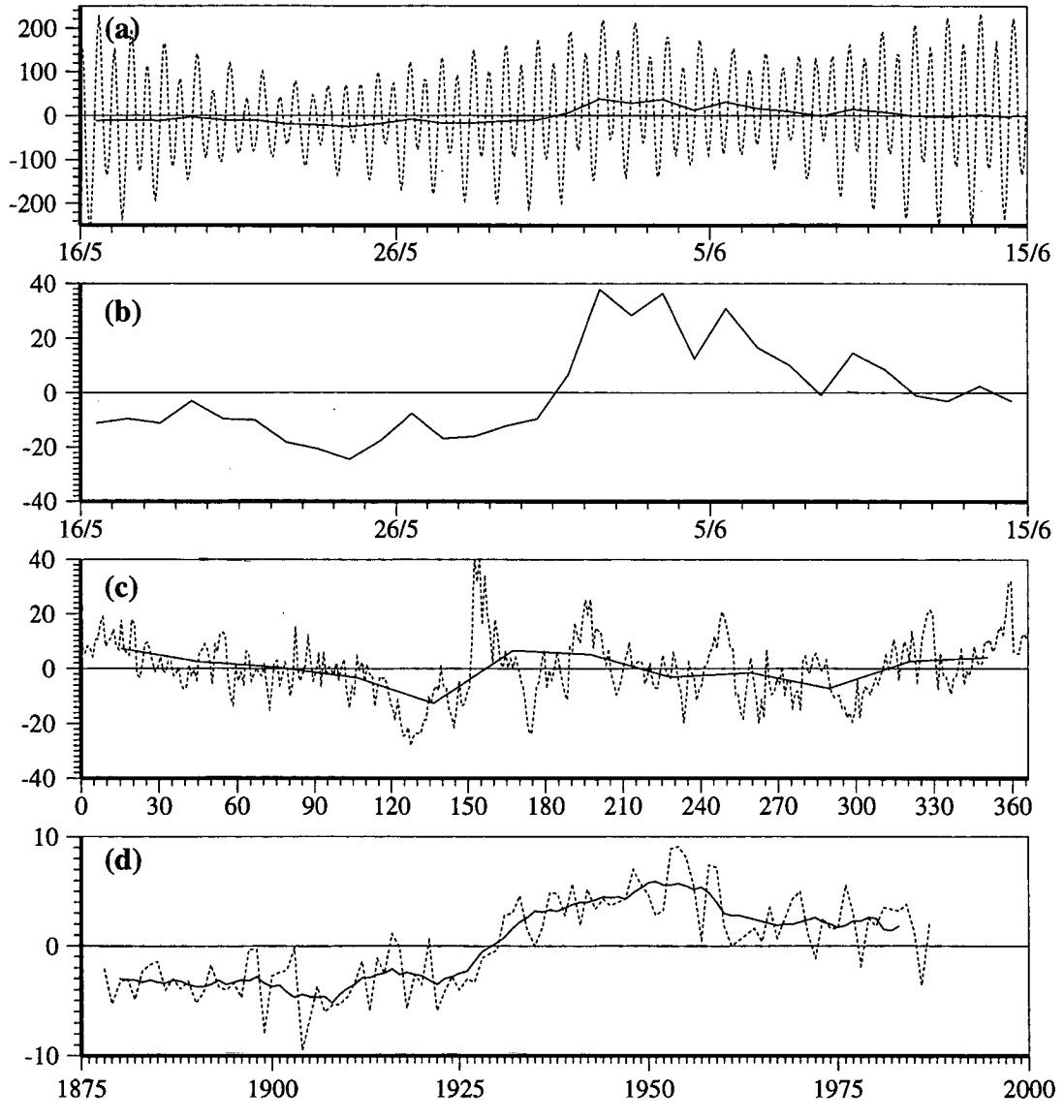

Chapter 2

Observational and Theoretical Background

In this chapter, we examine the observational and theoretical background for this thesis. Most of the literature on the low-frequency variability of sea level along the coast of India deals with the seasonal cycle, the outstanding low-frequency signal in the sea-level records; hence, before surveying the literature, we describe the observed seasonal cycle of sea level, beginning with a description of the tide-gauge network along the coast of India.

2.1 The Tide-Gauge Network Along the Coast of India

The Geodetic and Research Branch of the Survey of India monitors the network of tide gauges along the coast of mainland India and at a few offshore island stations [Roy, 1994]. The measurements are made using a float-type automatic mechanical tide gauge with an accuracy[1] of 1 cm; since the oscillations studied in this thesis are at least an order of magnitude greater, this accuracy is sufficient for our purpose. The measured sea level is recorded by a stylus on charts, which are later digitised into hourly values of sea level. Monthly sea level is computed from these hourly values by averaging over a month, and annual sea level is obtained by averaging the monthly sea levels over an year. These monthly and annual sea-level data are supplied by the Survey of India to the Permanent Service for Mean Sea Level (PSMSL) along with the datum to which the measurement is referred. Since the datum history is known for the tide gauges of India, a homogeneous series of levels can be prepared. These levels are adjusted by the PSMSL to a Revised

[1] Although the hourly sea level may be accurate only to 1 cm, the mean of several hourly values is potentially much more accurate, provided that the error in each reading has a random probability distribution. If this distribution is statistically normal, the mean of n independent readings is more accurate than a single reading by a factor of $n^{-\frac{1}{2}}$. On this basis, 100 readings would reduce the error from 1 cm to 1 mm [Pugh, 1987].

Local Reference (RLR) datum, which is defined relative to the tide-gauge benchmark so that the mean sea level in a specified year[2] is approximately 7 m. Defining sea levels relative to the tide-gauge benchmark has the advantage of separating the oceanographic and the geodetic aspects of the problem of sea-level trends [Pugh, 1987].

The traditional Indian tide-gauge network has been used primarily for establishing the datum for vertical control network of India and to determine various tidal constituents for tide tables [Roy, 1994]. As a result, many of the records are short, and only 12 [Emery and Aubrey, 1989] are acceptable for estimating sea-level variability on seasonal and higher time scales. Some of these, however, are situated on the banks of major rivers, or in narrow gulfs, making them unsuitable for the study of low-frequency variability on the scale of a basin. Five of these gauges were found by Emery and Aubrey to have acceptable confidence levels; these gauges are located at Mumbai (Bombay), Mangalore, and Kochi (Cochin) on the Indian west coast, and at Vishakhapatnam and Chennai (Madras) on the Indian east coast (Figure 2.1, Table 2.1). In addition, we use data from Marmagao[3] on the west coast and Paradip[4] on the east coast. Apart from the Indian tide gauges, that at Colombo in Sri Lanka is considered because it lies close to the southern tip of the Indian subcontinent, the junction between the Bay of Bengal and the Arabian Sea.

Table 2.1 Tide-gauge stations along the coast of the Indian subcontinent. N_{yr} is the number of years of data available. The monthly mean sea-level data for all stations are with respect to the Revised Local Reference, i.e., all the sea-level data used in this thesis are RLR data. The Permanent Service for Mean Sea Level (PSMSL) is the source for the monthly sea-level data.

Station	Longitude (°E)	Latitude (°N)	Time span	N_{yr}
Paradip	86.70	20.26	1966–1988	22
Vishakhapatnam	83.28	17.68	1937–1989	52
Chennai (Madras)	80.30	13.10	1916–1989	43
Colombo	79.85	6.95	1953–1965	13
Kochi (Cochin)	76.26	9.96	1939–1989	50
Mangalore	74.80	12.92	1952–1976	23
Marmagao	73.80	15.42	1969–1989	15
Mumbai (Bombay)	72.83	18.92	1878–1988	111

[2]Henceforth, we refer to such sea-level data as "RLR data".

[3]The record at Marmagao was considered too short by Emery and Aubrey, but more data has since become available.

[4]For reasons not known, Paradip was ignored by Emery and Aubrey.

Figure 2.1 Tide-gauge stations along the coast of the Indian subcontinent. "Indian subcontinent" implies India and some neighbouring countries, including Sri Lanka. In the figure, the solid line is the 200 m isobath, which usually marks the shelf-break, and the dashed line is the 1000 m isobath. The shelf is narrow along the east coast of the Indian subcontinent, except in the northern Bay of Bengal; it is wider along the west coast, especially off Mumbai.

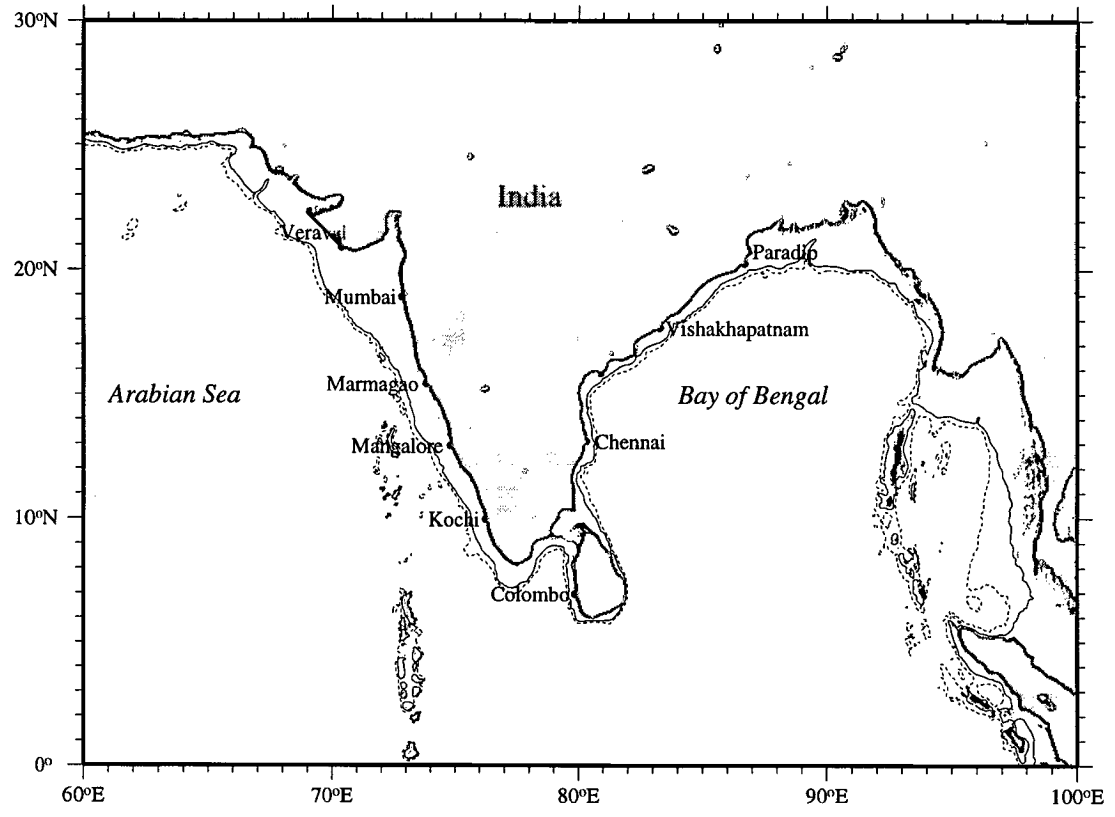

2.2 The Climatological Seasonal Cycle of Sea Level

The dominant frequency of the wind-stress forcing over the north Indian Ocean is the annual harmonic [Rao, 1998], a consequence of the seasonally reversing monsoon winds. These large-scale winds force a pronounced seasonal cycle of circulation in the basin, and hence, a seasonal cycle of sea level along the coast of India[5]. The seasonal cycle is the highest frequency adequately resolved by monthly sea level. A climatology is obtained from monthly sea level by averaging the data for a particular month, say January, over all the years of the record. A monthly climatology of anomalies is then obtained by removing the annual mean from the monthly climatology.

There are three causes of the seasonal cycle of sea level at a coast: astronomic tides, atmo-

[5]Strictly, we should say "coast of the Indian subcontinent" because the coast of Sri Lanka forms part of it. With due apologies to the Sri Lankans, we use "coast of India" in the rest of this thesis.

spheric pressure, and "steric oscillations" [Patullo et al., 1955]. Steric oscillations are due to changes in specific volume; the steric sea level is low (high) when the water is cold (warm), or has high (low) salinity. Changes in steric sea level are forced by surface fluxes and horizontal and vertical advection of heat and salt. Even in the absence of horizontal advection and of fluxes across the boundaries of the ocean, coastal currents forced by winds cause changes in the local mass field by forcing coastal upwelling or downwelling, thereby influencing the steric sea level (Figure 2.2). We distinguish between this and the changes in steric sea level caused by horizon-

Figure 2.2 Effect of winds and coastal currents on steric sea level. This schematic of a section normal to the coast shows the relation between winds, coastal currents, and sea level. The ocean is considered a two-layer system, the denser lower layer being much deeper than the shallow upper layer. The interface between the two layers represents the pycnocline, the density-equivalent of the thermocline. In the northern hemisphere, wind blowing with the coast on its right (left) forces Ekman flow into (out of) the coast, causing coastal downwelling (upwelling); sea level rises (falls) at the coast and the pycnocline slopes down (up) towards the coast. This sets up a cross-shore pressure gradient that drives a geostrophic alongshore current. In the figure, the current shown by "x" ("·") within a circle is into (out of) the plane of the paper. Thus, when there is downwelling (upwelling) at the coast, the current flows with the coast on its right (left), sea level rises (falls) at the coast, and the pycnocline slopes down (up) towards the coast. The change in sea level is given by $\eta = -\left(\frac{\rho_2 - \rho_1}{\rho_2}\right) h$, where h is the change in the thickness of the upper layer from the mean, or undisturbed, state.

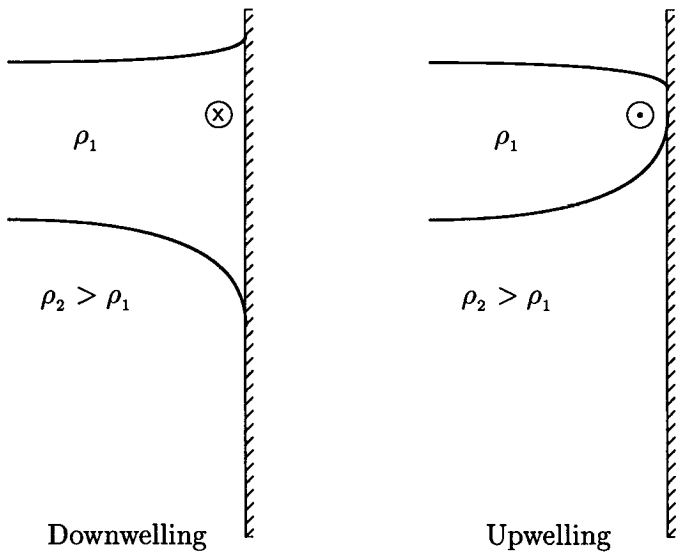

tal advection of heat and salt and by the exchange of heat and salt across the boundaries of the ocean; the former are considered the effect of wind-forced coastal currents, and the latter that of thermohaline forcing. Therefore, there are four causes of changes in monthly sea level at a coast:

astronomic tides, atmospheric pressure, wind-forced coastal currents, and thermohaline effects. Of these, the astronomic tides contribute around 1 cm, which is an order of magnitude less than the meteorological effects [Patullo et al., 1955; Shetye and Almeida, 1985]; hence, we ignore their effect.

2.2.1 The Inverse-Barometer Effect

At the low frequencies of interest, the effect of atmospheric-pressure variations in the tropics can be "corrected" by using the Inverse-Barometer (IB) approximation. Following Ponte [1993], the corrected sea level is given by

$$\eta_c = \eta_o + \frac{1}{\rho g}(p_{\text{atm}} - \overline{p}_{\text{atm}}), \tag{2.1}$$

where η_o and η_c are the observed and corrected sea levels. $\rho = 1026$ kg m^{-3} is the oceanic surface density, g the acceleration due to gravity, p_{atm} the local atmospheric pressure, and $\overline{p}_{\text{atm}}$ the spatial average of the atmospheric pressure over the global ocean. Since $\overline{p}_{\text{atm}}$ is a function of time because of a shift in air mass towards Siberia in winter [Patullo et al., 1955], the IB approximation involves an adjustment of sea level to both local and nonlocal pressure fluctuations [Ponte, 1993]. It is isostatic, i.e., it does not lead to pressure changes in the deeper ocean. The IB effect, computed using climatological monthly atmospheric pressure data from the Comprehensive Ocean-Atmosphere Data Set (COADS), is more pronounced towards the north of the basin and along the east coast of India (Figure 2.3). Seasonal sea-level changes due to variations of atmospheric pressure vary from about 3 cm at Colombo to 13 cm at Paradip. The corrected sea level is lower (higher) than the observed sea level during the southwest (northeast) monsoon[6], when the local atmospheric pressure is low (high). The seasonal changes observed in the corrected sea level are caused by the two remaining processes: wind-forced coastal currents and thermohaline effects. It is these changes, which are linked to the basin-scale dynamics of the north Indian Ocean, that form the subject of this thesis.

2.2.2 Major Features of the Seasonal Cycle of Sea Level

The climatological seasonal cycle of sea level, corrected for the effect of atmospheric pressure[7], is visually coherent along the east and west coasts of India and shows the following features (Figure 2.3[8]).

[6]The southwest monsoon lasts from June to September, the northeast monsoon from November to January. October and February–May are the transition months, when the winds are weak over the north Indian Ocean.

[7]Hereafter, sea level corrected for the effect of atmospheric pressure is referred to as "corrected sea level"; when the correction is not applied, it is called "observed sea level", or "uncorrected sea level", or just "sea level".

[8]In this figure, as in all subsequent figures of this kind, the variables plotted are monthly anomalies. The local annual mean is subtracted from the monthly values to compute the anomalies. Therefore, the anomalies at one station may be compared with those at another.

Figure 2.3 The climatological seasonal cycle of sea level (cm) along the coast of India. The stations on the right (except Colombo) are on the east coast, and those on the left are on the west coast. The figure shows the monthly anomalies of observed and corrected sea level; the local annual mean has been subtracted from the monthly climatology to compute these anomalies. The correction for atmospheric pressure was applied using the Inverse-Barometer approximation. The effect of atmospheric pressure on sea level varies from 3 cm at Colombo to 13 cm at Paradip. The seasonal cycle of corrected sea level is coherent along the coast. Its range is greater along the east coast (45 cm) than along the west coast (30 cm). Along the east (west) coast, the corrected sea level is maximum in November (December) and minimum during March–April (the southwest monsoon).

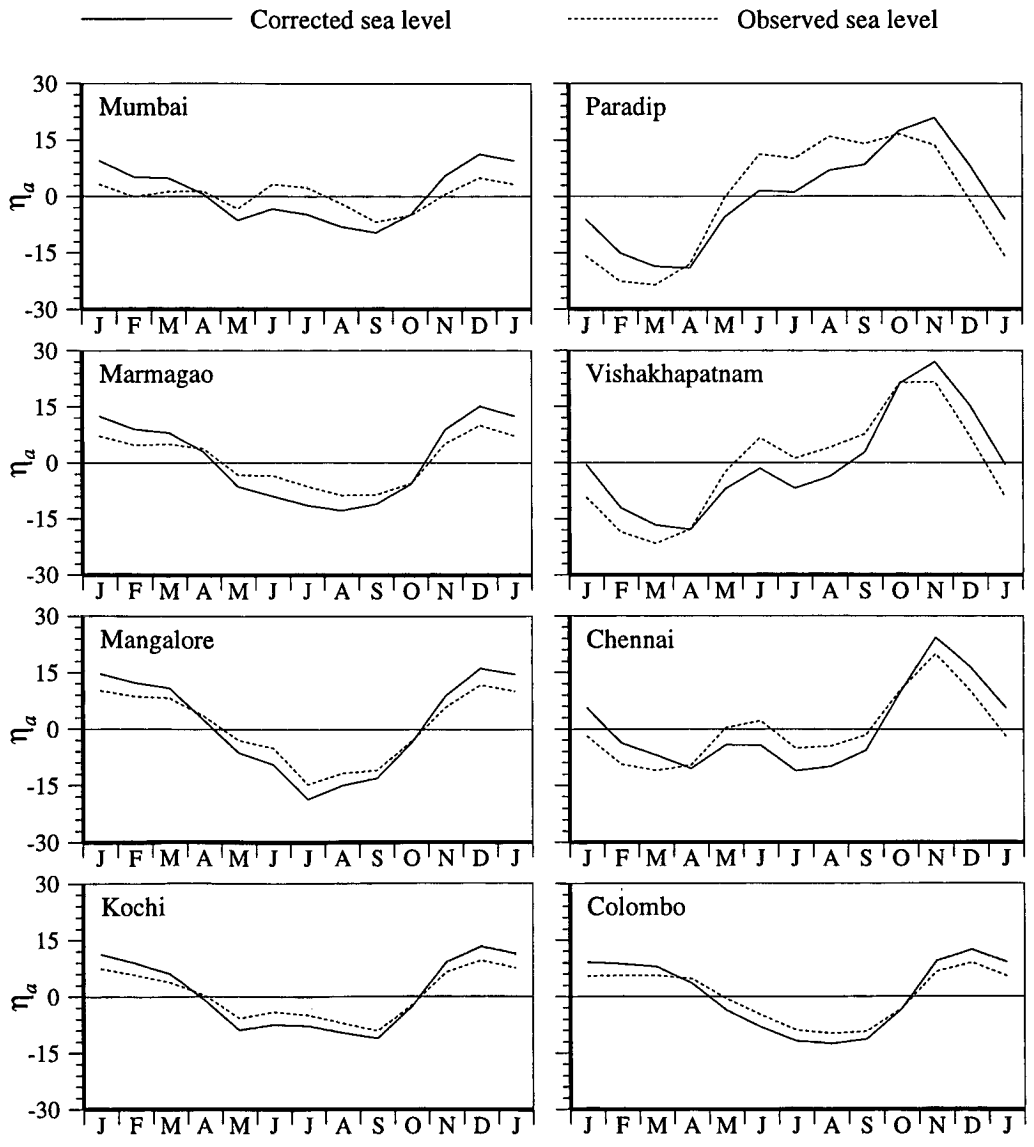

1. The range is greater along the east coast (45 cm) than along the west coast (30 cm). The drop in the range from Chennai to Kochi is because of a decrease in the maximum; the minimum does not change as much from the east to the west coast.

2. Along the east coast, there are two maxima, a minor peak during the southwest monsoon and a major peak during November; the winter peak is broad (in time) at Paradip and narrows equatorward along the coast. The minimum occurs during April.

3. Along the west coast, sea level peaks during December, the peak being broader than along the east coast, making the seasonal cycle more symmetric; there is also a minor secondary peak at Kochi and Mumbai during the southwest monsoon, when the minimum occurs along the west coast.

Some hypotheses have been proffered to explain the seasonal and lower frequencies seen in the sea-level records along the Indian coast; the available literature is surveyed in the following section.

2.3 A Brief Survey of the Literature

The first study of the seasonal cycle of sea level along the Indian coast was by Patullo et al. [1955], who examined the climatological seasonal cycle of sea level measured by tide gauges all over the world and compared them to the height of the sea surface arising from seasonal variations in specific volume; these were computed using data from bathythermograms and Nansen bottle casts. There was a good correlation between the tide-gauge sea level and the steric oscillations at low and temperate latitudes. The sea-level anomalies were nearly equal to the sum of the steric anomalies and the atmospheric-pressure effect, implying that a pressure sensor in the deep ocean would show very small seasonal fluctuations; this condition was termed "isostasy". Patullo et al. also noted that actual current measurements tallied well with currents computed from dynamic topography (or steric heights), implying a link between the large-scale coastal currents and sea level measured by coastal tide gauges.

Varadarajulu et al. [1982] used tide-gauge data for 10 years (1966–1975) at Paradip and concluded that the variations in monthly sea levels were related to variations in heating and cooling during summer and winter, respectively, in addition to the influence of rainfall and the seasonally reversing monsoon winds. Prasad and Reddy [1985] used the same method to study sea-level variability over 10 years (1970–1979) at Chennai. They too linked the observed variability to the physical properties of sea water and the climate in the neighbourhood of Chennai. Both these studies related sea-level changes purely to local causes.

Shetye and Almeida [1985] compared the seasonal cycle of sea level at several stations along the coast of India with those of local rainfall and the large-scale coastal current in the vicinity of the gauge. The seasonal cycle of corrected sea level and that of the alongshore current followed a similar pattern at most stations, Mumbai being an exception; Das [1979] also noted the connection between the seasonal cycle of sea level and that of the alongshore current at Marmagao. Therefore, while not ruling out the possible influence of runoff on the sea level along the east coast, Shetye and Almeida concluded that coastal sea level may be a good tool for monitoring the large-scale, wind-forced geostrophic currents along the coast.

Emery and Aubrey [1989] noted that the monthly sea level at different stations along the Indian coast reveals close relationships. They attributed the maxima in the seasonal cycle to storm surges and to monsoonal floods, or river runoff. Their main focus, however, was on the long-term changes in sea level. Five stations — Mumbai, Kochi, Mangalore, Chennai, and Vishakhapatnam — were found to be reliable indicators of long-term changes. Of these, Mangalore showed a decrease in relative sea level (1.3 mm $year^{-1}$), while the others showed an increase in sea level relative to land, the rate varying from 0.36 mm $year^{-1}$ at Chennai to 2.1 mm $year^{-1}$ at Kochi. This indicates either marginal subsidence of land, or a slow rise in sea level. These results are similar to those obtained for Australia [Aubrey and Emery, 1986], where eight acceptable station records averaged 2.2 mm $year^{-1}$ of land subsidence or sea-level rise. This similarity is striking because Australia is known for its tectonic stability and India for its nearness to a belt of tectonic instability. Other coastal regions of the world exhibit more erratic and local changes ascribable to tectonics associated with folding, faulting, melting of ice caps, volcanic activity, and delta growth, only the last of which can be important along the western and southeastern coasts of India and Australia. Hence, Emery and Aubrey concluded that these two regions may be the best indicators of long-term, relative sea-level change.

Tsimplis and Woodworth [1994] updated the work of Patullo et al. [1955], using three times the quantity of data used in the earlier work. They decomposed the climatological seasonal cycle into annual and semiannual harmonics, presenting the worldwide distribution of the amplitudes and phases of both. There is a difference in annual phase between the east and west coasts of India; the annual phase progressively increases from the east to the west coast. The annual amplitude is much larger than the semiannual amplitude. A large semiannual amplitude, however, may not imply a realistic semiannual oscillation, but can be the result of irregularities in the annual cycle, caused, for example, by the sudden onset of the monsoon.

Clarke and Liu [1994] used monthly sea level along the Indian coast to study interannual variability. They found a significant correlation between the sea level at Vishakhapatnam and that at Chennai, Kochi, and Mumbai. The correlation is maximum at non-zero lags, hinting at the possibility of wave propagation along the coast. Based on a model study, they concluded that

an interannual sea-level signal occurs along more than 8000 km of the Indian Ocean coastline, extending from southern Java to Mumbai, and is generated remotely by zonal interannual winds along the equator. Clarke and Liu [1993] used the same model to study the annual and semiannual sea levels along the eastern boundary of the equatorial Indian Ocean. They concluded that atmospheric pressure, local alongshore winds, and remote forcing by equatorial Kelvin waves were the causes of the observed oscillations.

Thus, these studies show that the sea levels at different stations along the Indian coast reveal close relationships. However, the causes of the observed variability, seasonal or interannual, are not clear. Atmospheric pressure has an effect on sea level, but this is easily accounted for by the Inverse-Barometer approximation. There is also some similarity between the seasonal cycle of local rainfall, and hence of river runoff, and that of sea level. Most crucial, however, is the striking resemblance of the seasonal cycle of coastal currents to that of sea level along the Indian coast. This, and the significant correlation between interannual variations in sea level at Vishakhapatnam and at other stations, suggests that the low-frequency variability of sea level along the Indian coast is linked to the large-scale circulation in the north Indian Ocean. This is not surprising, given that a similar relationship has been noted elsewhere too [Patullo et al., 1955].

2.4 The Large-Scale Circulation Along the Coast of India

Oceanographers have traditionally relied on hydrographic data to estimate currents in the ocean [Pickard and Emery, 1982]. The first major hydrographic survey of the north Indian Ocean was made during the International Indian Ocean Expedition (IIOE) in the late 1960s [Wyrtki, 1971]. Several hydrographic surveys have been carried out in the north Indian Ocean since then, and a coherent picture of the large-scale coastal circulation around India emerged during the 1990s[9]. We use the data collected during six hydrographic surveys during 1987–1994 in the Exclusive Economic Zone (EEZ) of India, in conjunction with ship drifts, to describe the large-scale circulation off the Indian coast. Each of these methods has its own drawbacks. Dynamic topographies constructed from hydrographic data assume a level of no motion, typically 1000 m, and are therefore unreliable in the vicinity of a coast. Ship drifts, on the other hand, are influenced by wind and usually are too noisy to yield a coherent picture of the basin-scale circulation. Nevertheless, in the absence of direct current-meter measurements, these are the only means of estimating currents along the Indian coast.

[9] An extensive bibliography for the Bay of Bengal is given by Varkey et al. [1996].

2.4.1 Hydrography of the Coastal Waters of India

Three cruises surveyed the coastal waters off the Indian west coast during June–August 1987 [Shetye et al., 1990], December-1987–January-1988 [Shetye et al., 1991a], and March–April 1994, and three cruises surveyed the coastal waters off the Indian east coast during July–August 1989 [Shetye et al., 1991b], March–April 1991 [Shetye et al., 1993], and November–December 1991 [Shetye et al., 1996]. These cruises[10] followed near-identical tracks, measurements being made along sections (also called legs) normal to the coast or to the shelf-break.

The dynamic topography with respect to 1000 dbar for these six cruises is shown in Figure 2.4. The dynamic height field is a measure of the geostrophic transport in the top 1000 m of the water column; the smaller the spacing between the contours of dynamic height, the larger is the transport of the associated current, which, in the northern hemisphere, flows with the higher dynamic height on its right. The dynamic topographies in Figure 2.4 are but snapshots, representative of the large-scale circulation during the period of the survey, but they provide the only coherent hydrographic observations in the region. The schematic in Figure 2.5 shows the transports associated with these coastal currents over the top 1000 m of the water column. Interannual variability is expected to cause changes in the transports of these current systems, but they still provide a rough picture of the climatological seasonal cycle of the coastal currents around India.

The currents along the coast of India change direction with season. From November to January, the current along the east coast, the East India Coastal Current (EICC), is equatorward all along the coast [Shetye et al., 1996]. It bends around Sri Lanka to flow along the Indian west coast [Shetye et al., 1991a] as a poleward West India Coastal Current (WICC). Off southwest India, the poleward flow is along the western flank of an anticyclonic high that forms in the region; a geostrophic current completes the circulation around the high, forcing an equatorward WICC off southwest India[11]. The EICC reverses in February, and it flows poleward during March–May, forming the western boundary current of a basin-wide anticyclonic gyre [Shetye et al., 1993]. The anticyclonic high off southwest India persists through March–April, weakening thereafter and giving way to a cyclonic low during the southwest monsoon (June–September); during this period, the WICC flows equatorward along most of the Indian west coast [Shetye et al., 1990]. The EICC is weak during the southwest monsoon; it is poleward in the south, but is equatorward in the north [Shetye et al., 1991b].

Since the dynamic heights do not represent a climatology, we refrain from comparing them with tide-gauge sea level; this has been done elsewhere, and the agreement found to be good

[10] Hereafter, we refer to these six cruises as the "EEZ cruises" because they surveyed the Exclusive Economic Zone (EEZ) of mainland India. A summary of these observations is available in Shetye and Gouveia [1998].

[11] Shetye et al. [1990, 1991a] do not define the WICC the way we do; they compute the transport by integrating across the high. Therefore, the transport estimates given here are different. So are the current widths; for example, Shetye et al. describe a coastal current that is 400 km wide off southwest India. We define the EICC and WICC more precisely in the next chapter.

[Patullo et al., 1955]. A better comparison is afforded by ship drifts because the far larger number of observations, spread over several years, makes it possible to define a climatology. This was done by Shetye and Almeida [1985] and we repeat the exercise, but with a more extensive ship-drift data set.

2.4.2 Coastal Sea Level, Coastal Currents, and Local Alongshore Winds

We use the ship-drift climatology compiled by Rao et al. [1989], which was not available to Shetye and Almeida [1985], to compute the alongshore coastal current. Since the ship drifts are averaged over $2^\circ \times 2^\circ$ bins, the alongshore coastal currents computed from them represent the large-scale coastal circulation. The climatological seasonal cycle of corrected sea level and that of the alongshore coastal current computed from ship drifts are shown in Figure 2.6. The agreement between the two is excellent, except at Colombo. The only major discrepancy is that the alongshore current peaks a month before the sea level does on the west coast. The seasonal cycle of surface circulation in the north Indian Ocean, as revealed by ship drifts (Figure 2.7), also agrees fairly well with the current systems outlined in Figure 2.5.

Since the local alongshore coastal currents match tide-gauge sea level very well, it is possible that the local winds, which must play a role in forcing these currents, also play a role in forcing the seasonal cycle of sea level. The seasonal cycle of corrected sea level is compared with that of the local alongshore wind stress, computed from the climatology of Hellerman and Rosenstein [1983], in Figure 2.8. The annual mean of the wind stress at each location is removed to obtain the monthly anomalies that are plotted in the figure; this is done because the sea-level data plotted are also anomalies. The mean wind-stress field, which is not negligible, can set up a steady alongshore sea-level gradient, but it cannot force time-dependent changes in sea level.

The local alongshore winds and corrected sea level are in phase along most of the west coast, but are in phase only during winter along the east coast, where the strongest upwelling-favourable winds blow during the southwest monsoon, but sea level is lowest earlier in the year. The sea-level range along the east coast is about twice that along the west coast, but the range of alongshore wind stress along the east coast is about 5–6 times that along the west coast. Along the west coast, the range of sea level does not change significantly from Colombo in the south to Mumbai in the north, but there is a large change in the wind stress, especially from Colombo to Kochi. The wind stress at Colombo matches that along the Indian east coast, but the sea level cycle at Colombo is more akin to that along the Indian west coast; the ship drifts at Colombo are influenced more by the strong local winds than by the currents, leading to the mismatch between ship drifts and sea level there (Figure 2.6). These discrepancies imply that the seasonal cycle of sea level along the coast of India is not forced merely by local winds. The coherence in the seasonal cycle of sea level and ship drifts along the coast points to organization on the scale of the basin; it also suggests that

Figure 2.4 Dynamic topography in the coastal waters of India, based on six cruises in the Indian EEZ during 1987–1994. The contour interval is 5 cm^2s^{-2}. The minimum and maximum dynamic height for each cruise are listed in the figure. The "+" indicate the locations at which the hydrographic profiles were obtained. The time of the cruises are mentioned in addition to the months they are considered representative of.

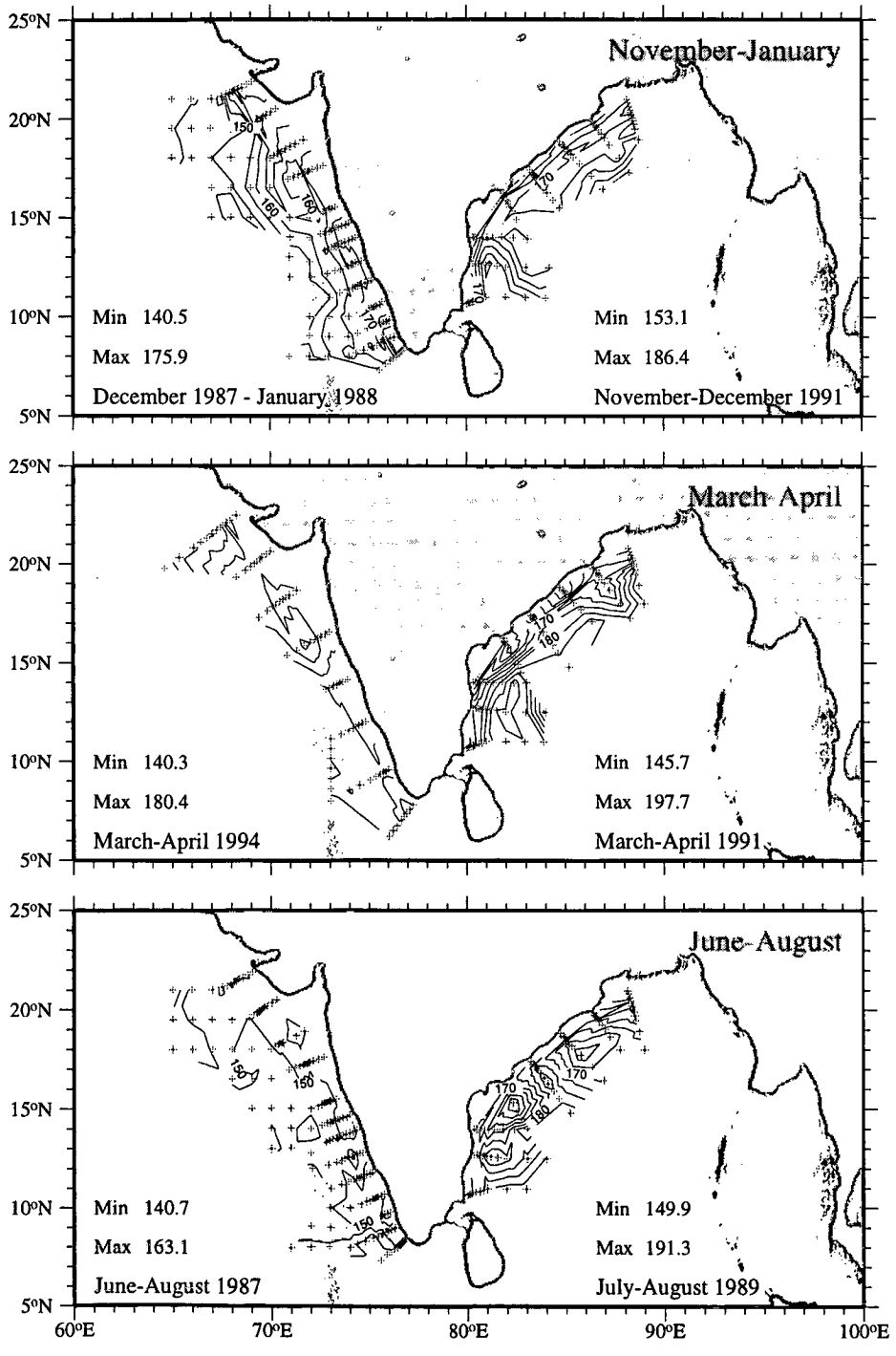

Figure 2.5 A schematic of the current systems along the coast of India. The number against each current indicates the transport (in Sv; 1 Sv = 10^6 m^3 s^{-1}) associated with it in the top 1000 m of the water column. These estimates, based on the six EEZ cruises, provide but an idea of the coastal circulation off India; interannual variability will change the magnitude of these currents, and in the case of the weak currents, even the direction.

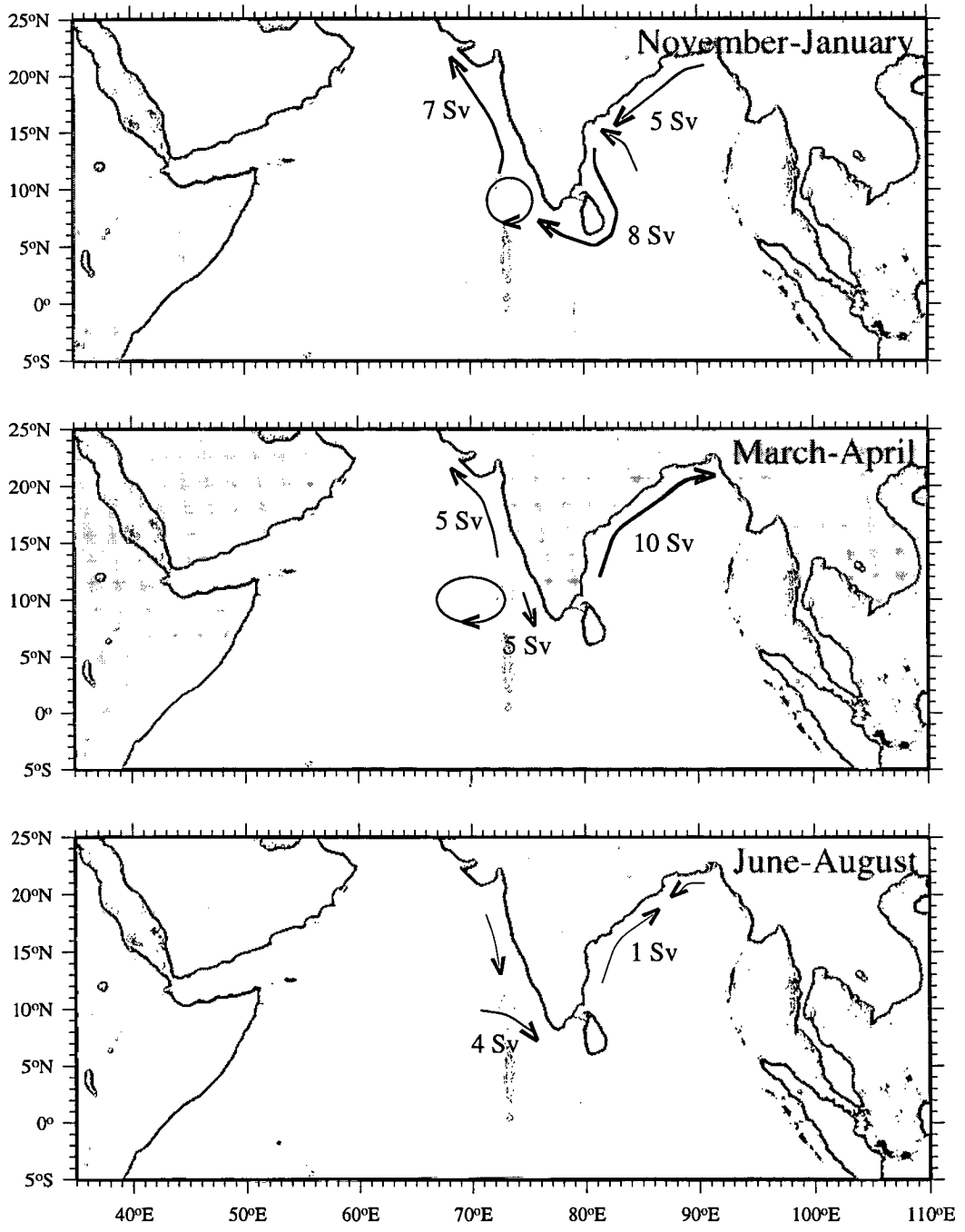

Figure 2.6 Seasonal cycle of corrected sea level (cm) and alongshore ship drifts (cm s^{-1}) along the coast of India. The ship drifts are from the climatology of Rao et al. [1989]. These data are not available at Mumbai and Paradip. The annual mean of the ship drift at each location has been removed to obtain the monthly anomalies that are plotted; this was done because the sea level data plotted are also monthly anomalies. Downwelling- (upwelling-) favourable anomalies are positive (negative); these currents flow with the coast on their right (left) in the northern hemisphere. The ship drifts match the sea level at the coast, except at Colombo, where the strong local winds (see Figure 2.8) influence the ship drifts more than the currents do.

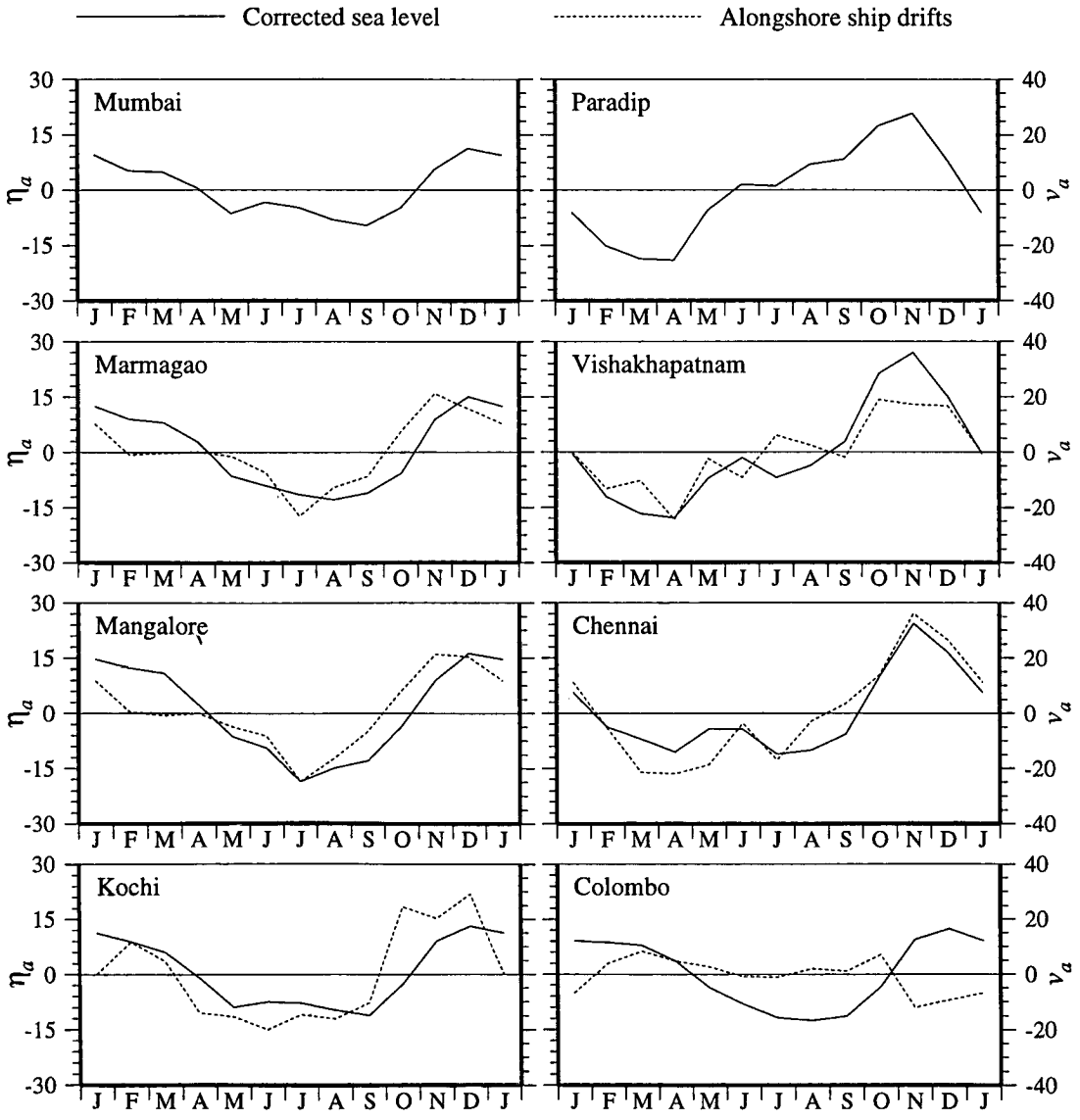

Figure 2.7 Seasonal cycle of surface circulation in the north Indian Ocean, as revealed by ship drifts [Rao et al., 1989]. The currents (cm s^{-1}) were interpolated to the grid used by the numerical model (see Chapter 3) from the original 2° × 2° bins. In January, the EICC is weak; during February–May, it flows poleward and forms the western boundary current of a basin-wide anticyclonic gyre. The WICC is poleward during January–April, except off southwest India, where it flows equatorward to close the geostrophic circulation around a high. The westward Northeast Monsoon Current (NMC) connects the EICC and the WICC.

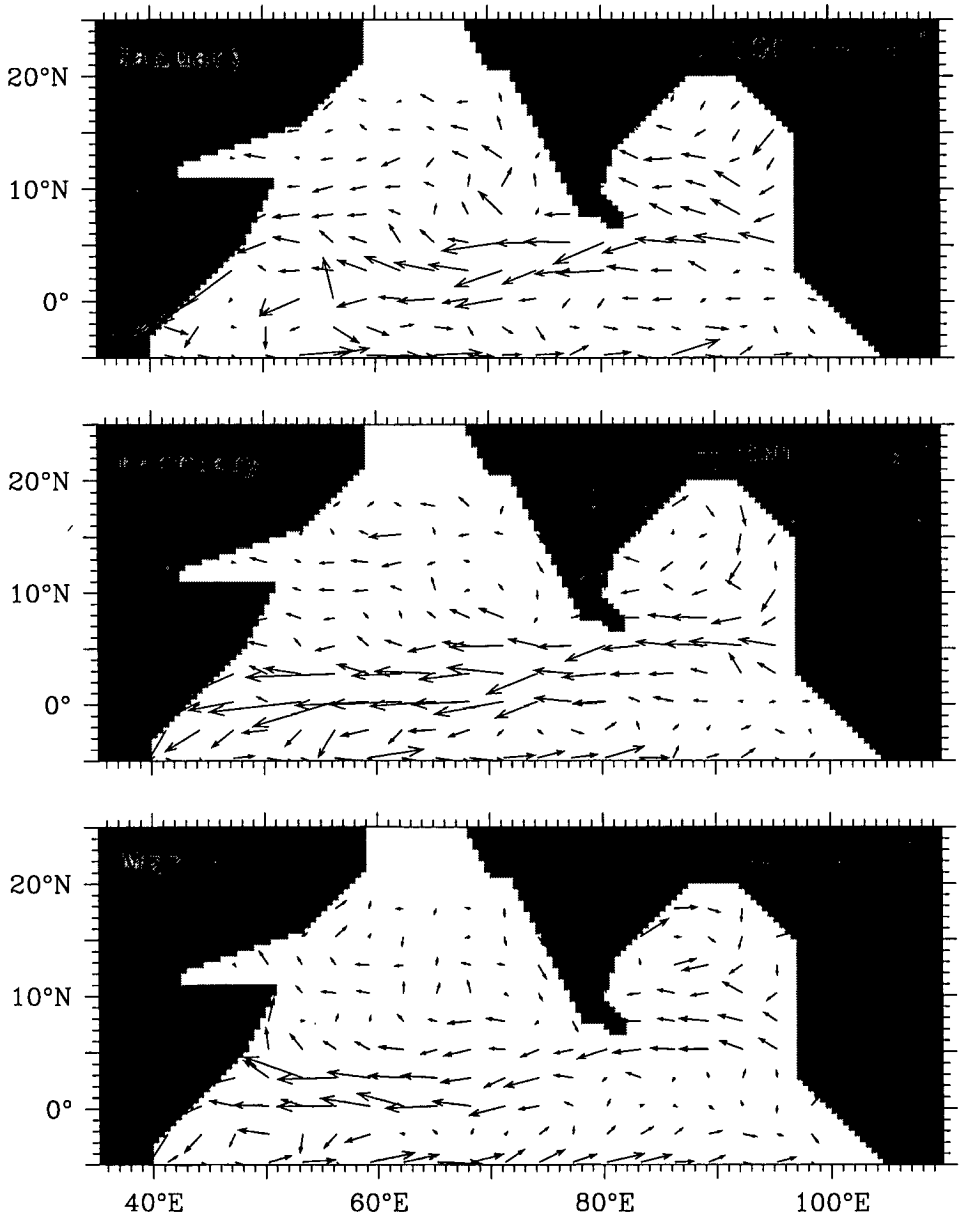

Figure 2.7 (continued) Seasonal cycle of surface circulation in the north Indian Ocean, as revealed by ship drifts [Rao et al., 1989]. The currents (cm s^{-1}) were interpolated to the grid used by the numerical model (see Chapter 3) from the original 2° × 2° bins. During February–May, the EICC flows poleward, forming the western boundary current of a basin-wide anticyclonic gyre. The gyre breaks up in May and the EICC weakens, but it continues to flow poleward till September. The WICC reverses to flow equatorward during the southwest monsoon. The monsoon winds bring about dramatic changes, forcing an eastward jet at the equator during April–May and a strong, poleward current off Somalia during May–September.

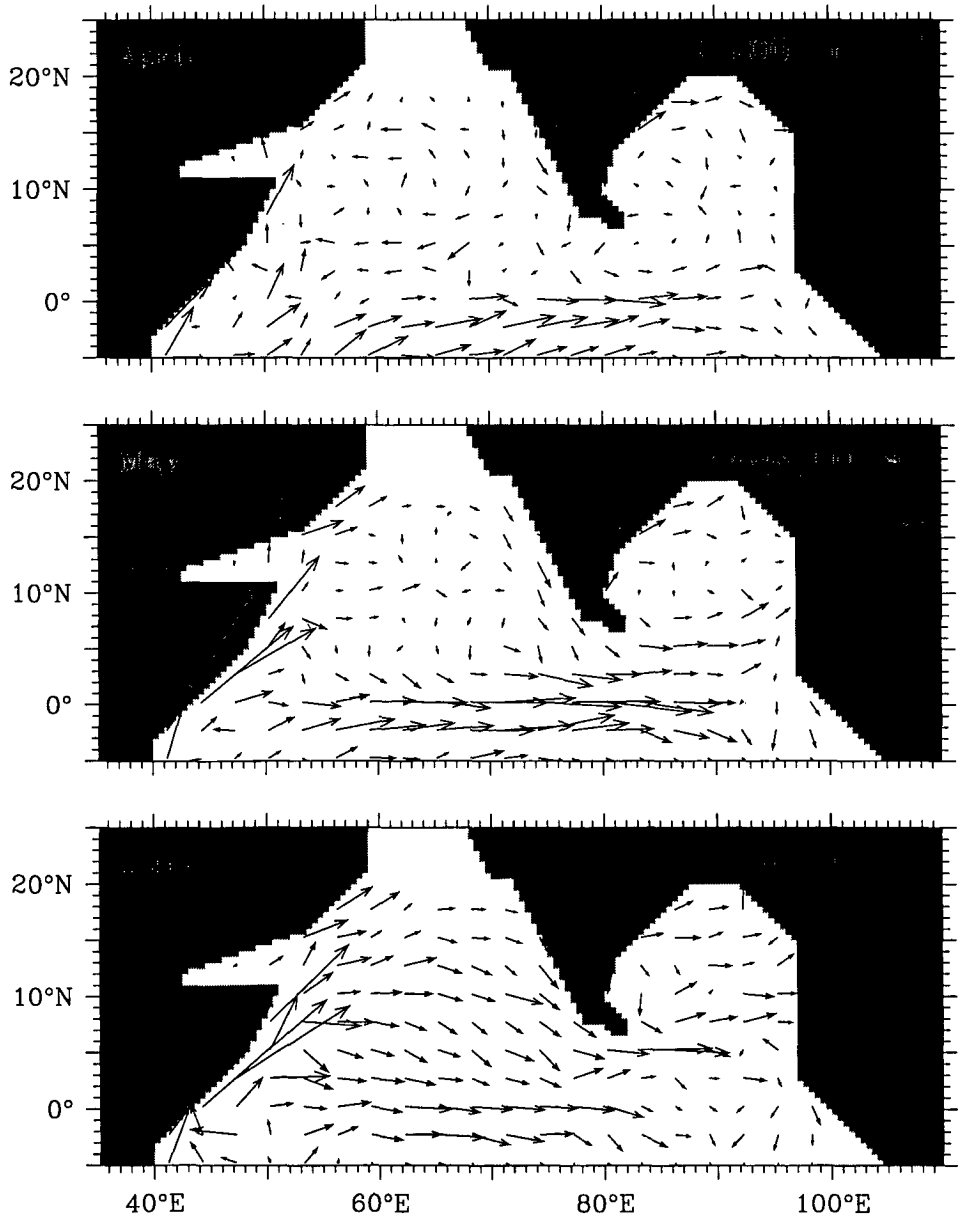

Figure 2.7 (continued) Seasonal cycle of surface circulation in the north Indian Ocean, as revealed by ship drifts [Rao et al., 1989]. The currents (cm s^{-1}) were interpolated to the grid used by the numerical model (see Chapter 3) from the original 2° × 2° bins. During the southwest monsoon, the strong, poleward Somali Current feeds into the the Southwest Monsoon Current (SMC), which spans the basin, flowing across the Arabian Sea and the southern Bay of Bengal. In the Bay of Bengal, a weak EICC flows poleward, but the Ekman drift dominates the ship-drift data. The WICC flows equatorward.

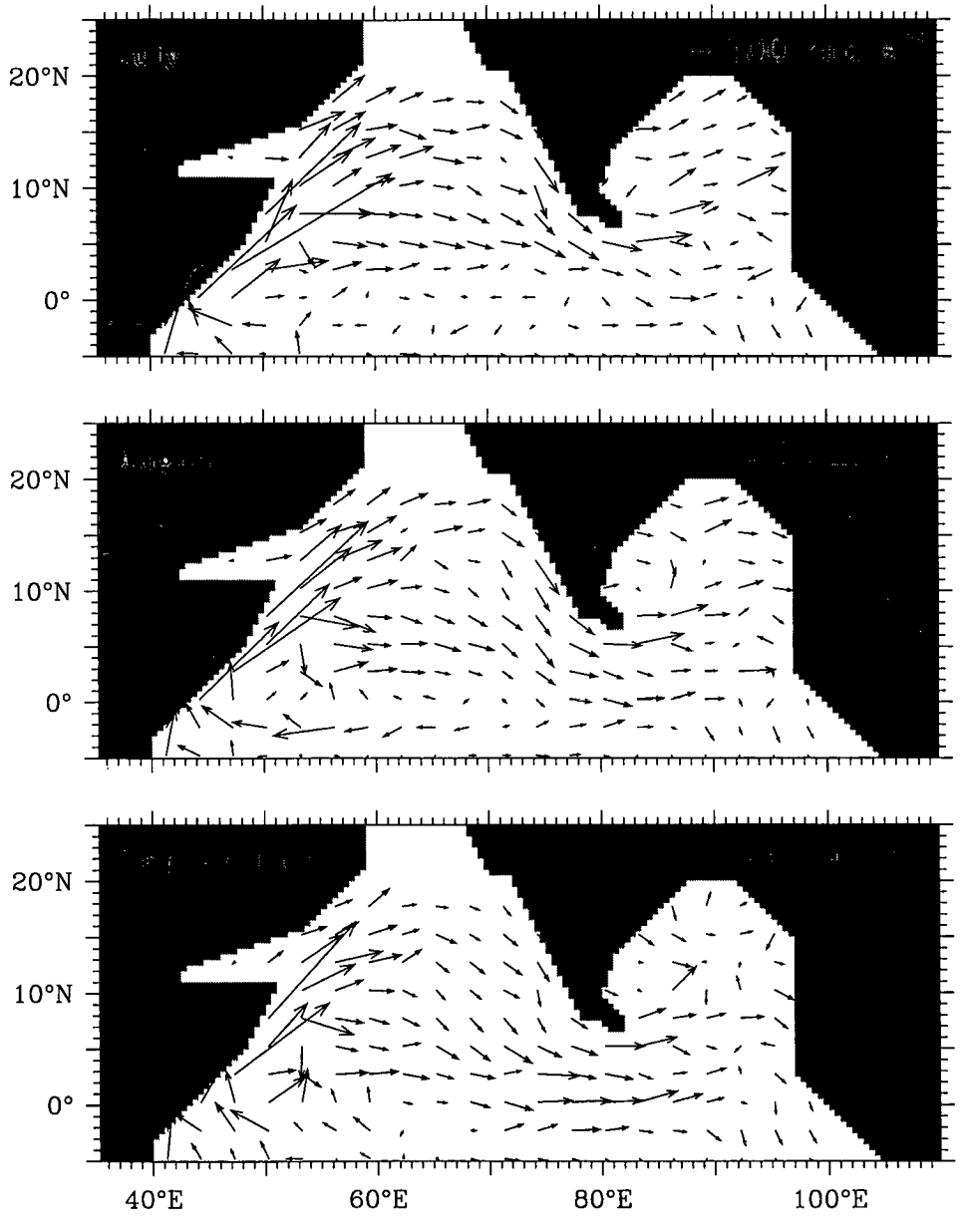

Figure 2.7 (continued) Seasonal cycle of surface circulation in the north Indian Ocean, as revealed by ship drifts [Rao et al., 1989]. The currents (cm s^{-1}) were interpolated to the grid used by the numerical model (see Chapter 3) from the original 2° × 2° bins. With the collapse of the southwest monsoon winds in September, the major currents in the north Indian Ocean reverse direction. The EICC reverses to flow equatorward, the WICC reverses to flow poleward. The Somali Current weakens and reverses in November, when an eastward jet forms again at the equator. By December, the NMC appears in the southern bay.

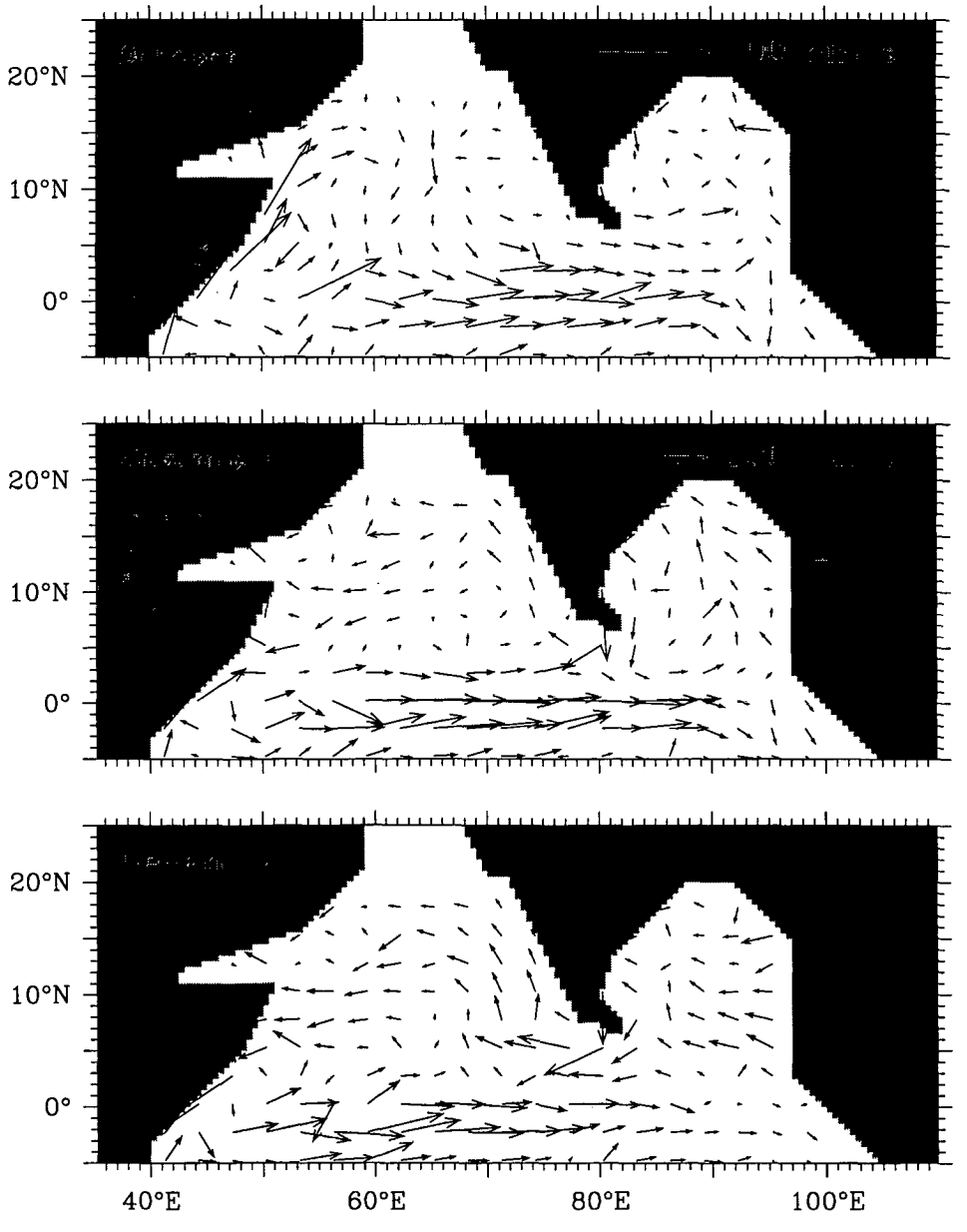

Figure 2.8 Seasonal cycle of corrected sea level (cm) and local alongshore wind stress (dyne cm^{-2}). The wind-stress data are from Hellerman and Rosenstein [1983]. The annual mean of the wind stress at each location has been removed to obtain the monthly anomalies that are plotted; this has been done because the sea-level data plotted are also monthly anomalies. The mean wind-stress field, which is not negligible, can set up a steady alongshore sea-level gradient, but it cannot force time-dependent changes in sea level. Downwelling- (upwelling-) favourable anomalies are positive (negative); looking downwind, these winds blow with the coast on their right (left) in the northern hemisphere. The lack of agreement between the local winds and sea level implies that remote forcing is important for the seasonal cycle of sea level and currents along the coast of India.

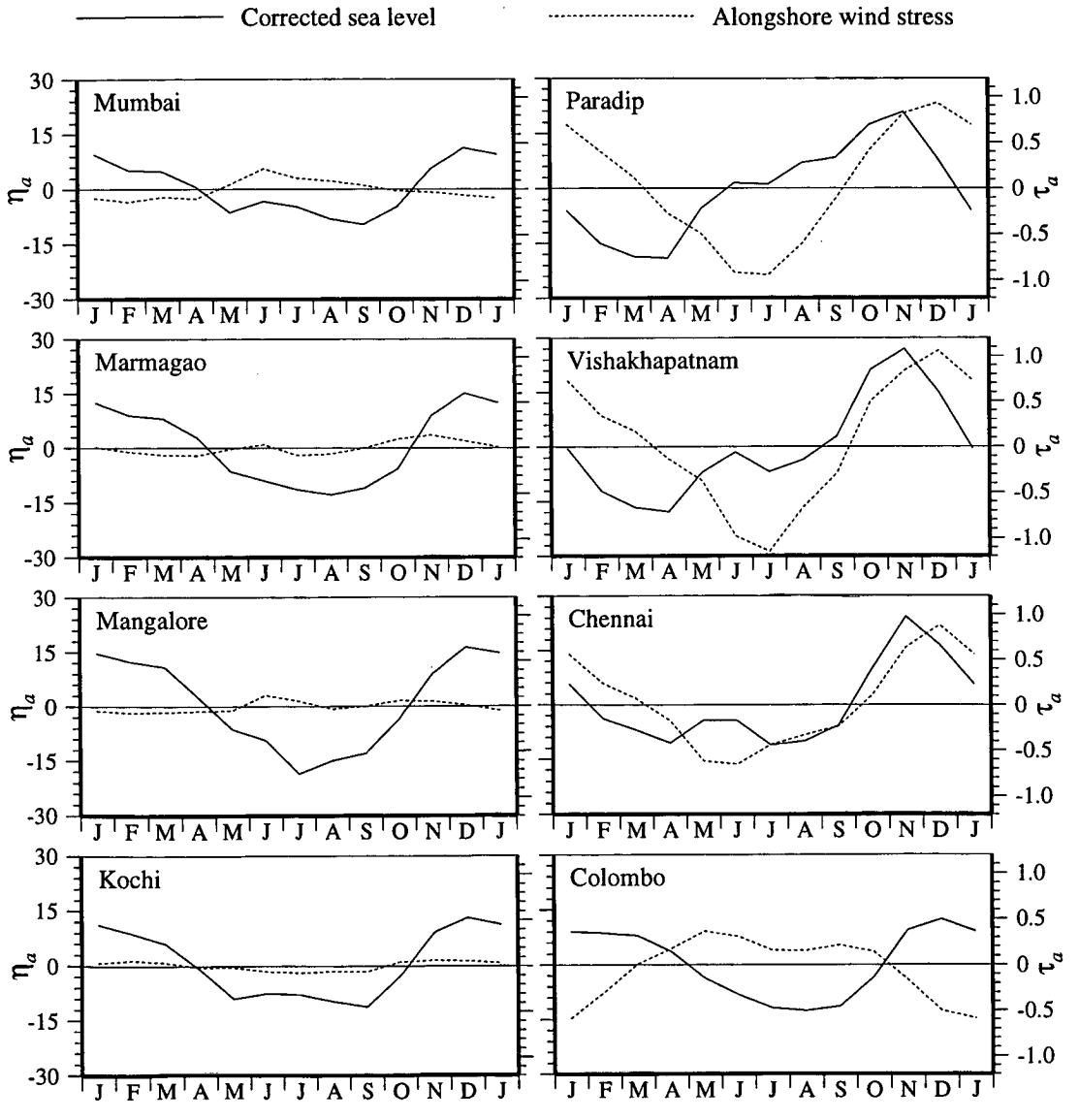

the circulation along the coast of India is, at least in part, forced remotely.

2.5 Basin-Scale Dynamics of the North Indian Ocean

The need to explain the seasonal cycle of circulation off the Indian coast led, during the 1990s, to the development of a framework involving long baroclinic waves, which had been invoked earlier to explain the sea-level variability along the west coast of the American continent. Anomalies of monthly sea level along the eastern boundary of the Pacific are visually coherent and statistically well-correlated from Valparaiso in Chile to the Canadian border [Enfield and Allen, 1980; Chelton and Davis, 1982], the anomalies propagating poleward in both hemispheres. These anomalies are linked to El Niño, whose domain extends across the equatorial Pacific Ocean. The link is provided by equatorial Kelvin and Rossby waves and coastal Kelvin waves, which propagate long distances, carrying information across the equatorial Pacific and forcing changes in locations far removed from the winds that force these changes in the ocean.

The success of this theory in the Pacific Ocean appears to have prompted its application in the Indian Ocean; this development was synchronous with the hydrographic surveys described earlier. Since these waves communicate changes in sea level or currents forced by winds in one region to remote locations, they merge the equatorial Indian Ocean, the Bay of Bengal and the Arabian Sea into a single dynamical entity, the north Indian Ocean, whose dynamics must be modelled as a whole even to simulate the circulation in its parts. The numerical models developed in the 1990s have been fairly successful in simulating the basic features of the observed circulation in the north Indian Ocean; their success implies that the circulation along the Indian coast must, at least in part, be remotely forced. Though there are some studies using Ocean General Circulation Models (OGCMs), most have used reduced-gravity models[12], which had been used with success in studying the El-Niño phenomenon in the Pacific Ocean.

In the following chapter, we use a reduced-gravity model to simulate the circulation in the north Indian Ocean. We focus our attention on the high and low that form off southwest India (see Section 2.4.1) because these cannot be explained without invoking the long baroclinic waves[13] and the connection they establish between the Bay of Bengal, the Arabian Sea, and the equatorial Indian Ocean. Called the Lakshadweep high and low after the islands in whose vicinity they form (Figure 1.2), they also have the benefit of novelty, having been discovered recently by Bruce et al. [1994][14]. Shankar and Shetye [1997] studied the dynamics of the Lakshadweep high and low, and the following chapter is based largely on their work.

[12]The reduced-gravity model is described in Appendix A.

[13]See Appendix B for a brief description of these waves.

[14]Bruce et al. used the name "Laccadive", an anglicized form of "Lakshadweep", which literally means "a hundred thousand islands". Lakshadweep is the official name of this group of islands.

Chapter 3

The Lakshadweep High and Low

3.1 Observational Background

The monsoon winds that sweep across the north Indian Ocean force considerable seasonal changes in surface circulation. The most prominent and the best documented of these is seen off the coast of Somalia [Schott, 1986]. The Somali Current (Figure 3.1), which flows along the coast, is poleward during the southwest monsoon (June–September) and equatorward during the northeast monsoon (November–March). Other currents too, though not as energetic, reverse seasonally; for example, the Southwest Monsoon Current (SMC[1]) and the Northeast Monsoon Current (NMC) south of Sri Lanka, the equatorial jet along the equator [Wyrtki, 1973], and the currents along the east and west coasts of India [Shetye et al., 1990, 1991a,b, 1993, 1996]. Associated with the changes in surface currents are variations in patterns of sea-surface topography, which appear, strengthen, and either decay or propagate away from the region of genesis year after year. The best studied amongst these is the Great Whirl, an anticyclonic gyre, with a high in surface topography, that forms between 5° and 10°N off Somalia with the onset of the southwest monsoon in June [Bruce, 1968]. It peaks during July–August and decays in September. The occurrence of another such high, though not as energetic, was discovered by Bruce et al. [1994]; using hydrographic data collected during the IIOE, they showed that a high forms off southwest India during the northeast monsoon. A low forms in the same region during the southwest monsoon (Figure 3.1). It was mentioned by Bruce [1968] and Bruce et al. [1994] and is seen in maps of geopotential topography [Wyrtki, 1971].

Though the occurrence of the high and low off southwest India was established using traditional hydrographic data, its annual cycle in relation to the annual cycle of sea-level perturbations in the rest of the Indian Ocean was appreciated better only after data from satellite altimetry

[1]The Southwest Monsoon Current is often, perhaps usually, referred to as the Indian Monsoon Current (IMC). SMC appears to be a better acronym, given that its counterpart during the northeast monsoon is called NMC (Northeast Monsoon Current).

Figure 3.1 A schematic of the surface circulation in the north Indian Ocean during January and July. Abbreviations are as follows: LH, Lakshadweep high; LL: Lakshadweep low; GW, Great Whirl; SH, Socotra high; EICC, East India Coastal Current; WICC, West India Coastal Current; SC, Somali Current; NMC, Northeast Monsoon Current; and SMC, Southwest Monsoon Current. In January, the equatorward EICC and poleward WICC are connected by the NMC. In July, there is no apparent connection between the EICC, which flows poleward along the coast of India, and the equatorward WICC because the EICC is equatorward off Sri Lanka [Vinayachandran and Yamagata, 1998]. The WICC flows into the eastward SMC; the WICC in July is often considered part of the SMC because this is a continuous current flowing across the Arabian Sea into the Bay of Bengal. Consistency, however, requires that the current be called WICC when it flows along the west coast of India.

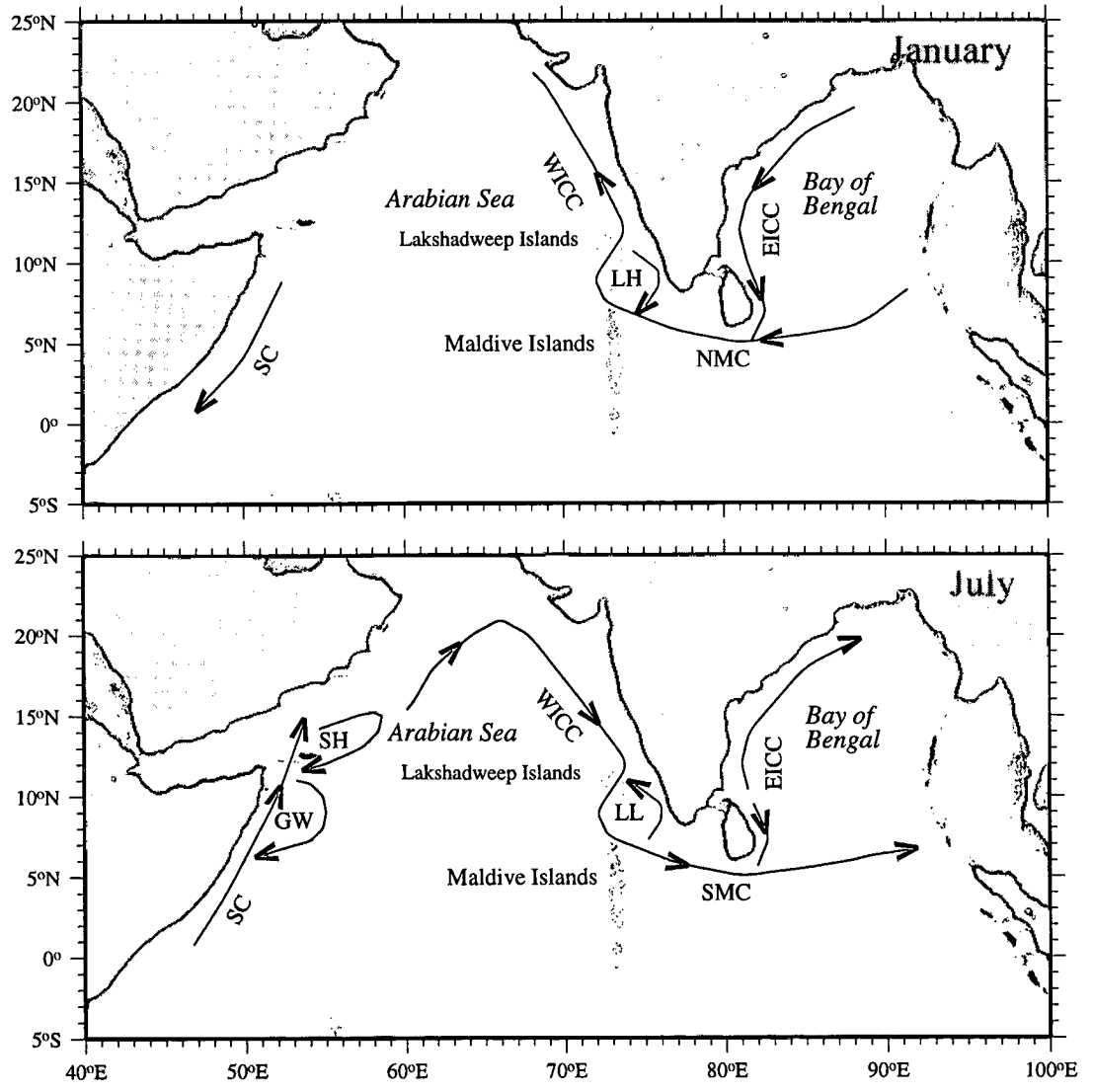

became available. Bruce et al. [1994] used Geosat altimetry to support inferences drawn from hydrography; Perigaud and Delecluse [1992] also used Geosat data to describe the annual cycle of sea level in the Indian Ocean.

The high and low off southwest India are seen in TOPEX/POSEIDON altimetry [Tapley et al., 1994; Nerem et al., 1994]. The altimeter data show that sea level starts rising off southwest India during December, when the East India Coastal Current (EICC[2]) is equatorward [Shetye et al., 1996]. The EICC flows into the NMC, which turns around the southern tip of Sri Lanka [Rao et al., 1989; Cutler and Swallow, 1984] and joins the poleward West India Coastal Current (WICC[3]) [Shetye et al., 1991a]. By early January, the positive anomalies of sea level spread offshore and northward along the west coast of India, and a circular high forms to the east of the Lakshadweep islands. By February, the high is no longer circular: it has stretched westward. By April, positive anomalies in sea level are seen all over the Arabian Sea. The evolution of the low proceeds in a similar fashion. First, sea level drops off southwest India in June, when the WICC is equatorward [Shetye et al., 1990]; the WICC turns around Sri Lanka and joins the eastward SMC. The EICC is poleward off the Indian coast at this time [Shetye et al., 1991b], but it is equatorward off Sri Lanka [Rao et al., 1989; Cutler and Swallow, 1984; McCreary et al., 1996; Vinayachandran and Yamagata, 1998]. Second, the negative anomalies spread offshore and along the coast, and a circular low forms to the east of the Lakshadweep islands during July–August. Third, the low stretches westward, and by the end of October, negative anomalies in sea level occur all over the Arabian Sea. This series of events is also seen in altimeter sea level for other years. These observations suggest that the formation of the high (low) off southwest India during the northeast (southwest) monsoon is one manifestation of an annual cycle of events that are linked not only to the coastal currents around India, but also to the circulation in the southern Arabian Sea as a whole.

3.2 Theoretical Background

A tropical ocean responds rapidly to a change in winds; Lighthill [1969] showed that the equatorial Rossby waves excited by the onset of the southwest monsoon reach the African coast in less than a month. The rest of the north Indian Ocean responds similarly to the monsoon winds: Rossby

[2]The EICC is the current along the east coast of India and Sri Lanka; the name remains the same irrespective of the season and the direction of the current. The EICC also flows along the east coast of Sri Lanka, and its direction along the Lankan coast is often different from that along the Indian coast farther north [McCreary et al., 1996; Vinayachandran and Yamagata, 1998].

[3]The WICC is the west-coast counterpart of the EICC; the name remains the same irrespective of the season and the direction of the current. The existence of the Lakshadweep high and low lead to the WICC being poleward over a part of the coast and equatorward over another part of the coast. There is some ambiguity about the name during the southwest monsoon; the equatorward WICC in July is often considered part of the SMC because this is a continuous current flowing across the Arabian Sea into the Bay of Bengal (Figure 3.1). Consistency, however, requires that the current be called WICC when it flows along the west coast of India.

waves and equatorial and coastal Kelvin waves have a profound effect on its dynamics, forcing changes not only locally in the region of generation, but also remotely. Investigations over the last decade have shown that these waves link the circulation in the Bay of Bengal, the Arabian Sea, and the equatorial Indian Ocean [Potemra et al., 1991; Yu et al., 1991; Perigaud and Delecluse, 1992; McCreary et al., 1993; Shankar et al., 1996; McCreary et al., 1996; Shankar and Shetye, 1997; Vinayachandran, 1995; Vinayachandran et al., 1996; Vinayachandran and Yamagata, 1998].

Yu et al. [1991] showed that an annual equatorial Kelvin wave, on reflection from the eastern boundary, propagates along the perimeter of the Bay of Bengal as a coastal Kelvin wave, radiating westward propagating Rossby waves in the process, and forces changes in the EICC. McCreary et al. [1993] showed that the winds along the eastern boundary of the bay also set up a similar Kelvin wave. They concluded that these Kelvin waves, besides contributing to the dynamics of the EICC [McCreary et al., 1996], bend around Sri Lanka to propagate along the Indian west coast, forcing changes in the WICC. Their simulations produce the high in January and the low in October. The idealized simulations of Yu et al. [1991] also produce the high and low, indicating an annual cycle. Bruce et al. [1994] noted that the high of Yu et al. appears to be a consequence of Rossby wave radiation by coastal Kelvin waves off southwest India. They also pointed out another possible mechanism for the high: a patch of anticyclonic wind-stress curl off the southern tip of India during the northeast monsoon. The wind-stress curl is cyclonic in this region during the southwest monsoon.

In the remainder of this chapter, we study the dynamics of the high and low, specifically addressing the following issues.

1. Many highs and lows that form in the world ocean, particularly those that have been described as eddies (the Gulf Stream eddies, the Great Whirl, etc.), are nonlinear in character. It is the nonlinearity in their dynamics that spins off these systems. Are the Lakshadweep high and low too of a similar kind?

2. How are they linked to the coastal currents off India? Are they forced primarily by winds local to the region, or is remote forcing significant?

Our primary tool in this study is a dynamical $1\frac{1}{2}$-layer reduced-gravity model, which is the simplest realistic model of the surface circulation in the ocean. Experiments with both nonlinear and linear versions of the model indicate that nonlinearity in the momentum balance is not essential to simulate the high and the low, allowing us to simplify the problem. Simulations with a linear reduced-gravity model, shorn of the complexity inherent in the wind forcing, show that a Kelvin wave propagating along the Indian east coast can lead to the high and low. Then we simplify the dynamics further and obtain an analytic solution, showing that the dynamics of linear waves on an equatorial β-plane can simulate the high and low. This leads to a discussion on the forcing

mechanisms, where we examine the effects of local and remote forcing. We conclude the chapter with a discussion on the implications of the Lakshadweep high and low.

3.3 Numerical Simulation of the Lakshadweep High and Low

3.3.1 The Numerical Model

We use a dynamical $1\frac{1}{2}$-layer reduced-gravity model to simulate the seasonal cycle of circulation in the southeastern Arabian Sea. The density of the model layers does not vary in space or time. The equations for the active upper layer[4], are

$$(H\mathbf{v})_t + \nabla\cdot(\mathbf{v}H\mathbf{v}) + f\mathbf{k}\times(H\mathbf{v}) + g\overline{\Gamma}H\nabla H = \tau/\rho_1 + \nu\nabla^2(H\mathbf{v}) - \chi\mathbf{i}\cdot(H\mathbf{v}) \tag{3.1a}$$

$$H_t + \nabla\cdot(H\mathbf{v}) = \kappa\nabla^2 H \tag{3.1b}$$

$$\eta = \overline{\Gamma}\left(H - \overline{H}\right) \tag{3.1c}$$

where H is the instantaneous layer thickness, $\overline{H}$ the initial layer thickness, $\mathbf{v} = (u, v)$ the velocity, $f = \beta y$ the Coriolis parameter, $\tau = (\tau^x, \tau^y)$ the wind stress, g the acceleration due to gravity, and $\overline{\Gamma} = \Delta\rho/\overline{\rho}$ the reduced-gravity parameter, with $\Delta\rho = \rho_2 - \rho_1$. $\overline{\rho}$ is an average density that is representative of the ocean. ν and κ are the Laplacian mixing coefficients for momentum and thickness, the latter being included to damp the small-scale noise in the H field, and χ is a Rayleigh friction coefficient. η is the deviation of model dynamic height, computed with respect to the motionless deep ocean, from the initial state. In the discussion that follows, we refer to η as the model sea level rather than as dynamic height. The model parameters are listed in Table 3.1.

Equations (3.1) are integrated numerically on a staggered Arakawa-C grid using the leapfrog scheme; diffusive terms are evaluated at the backward time level and all other terms at the central time level. To inhibit time-splitting instability, the fields are averaged between successive time levels every 41 time steps. The model domain, shown in Figure 3.2, is as in McCreary et al. [1993]. The upper layer thickness is not allowed to shallow beyond 10 m or deepen beyond 190 m. The no-slip condition is applied at continental boundaries and the gradient boundary condition [Chapman, 1985] is applied at the open southern boundary at 29°S. The open boundary condition and the restrictions on upper layer thickness force changes in the total mass in the basin; to conserve mass, a uniform correction is applied to the upper layer thickness after each time-step. A linear damper (Rayleigh friction) is applied on the zonal velocity field near the southern boundary; it is required to inhibit the development of large-scale instability along the boundary

[4]These equations are derived in Appendix A.

Table 3.1 Model parameters for the $1\frac{1}{2}$-layer reduced-gravity model.

Parameter (units)	Symbol	Value
Laplacian mixing coefficient for momentum ($cm^2\ s^{-1}$)	ν	5×10^7
Laplacian mixing coefficient for thickness ($cm^2\ s^{-1}$)	κ	1×10^7
Thermal expansion coefficient ($°C^{-1}$)	α_T	-0.00025
Haline contraction coefficient (PSU^{-1})	α_S	0.00125
Reduced-gravity parameter	$\overline{\Gamma}$	0.0035
Initial upper layer thickness (m)	$\overline{H}$	100
Minimum upper layer thickness (m)	$H_{\min}$	10
Maximum upper layer thickness (m)	$H_{\max}$	190
Linear Kelvin wave speed for $\overline{H} = 100$ m ($cm\ s^{-1}$)	c	185
Rossby wave speed at 10°N ($cm\ s^{-1}$)	c_R	12.2
Grid size (km)	$\Delta x, \Delta y$	55
Time step (minutes)	Δt	72

caused by the application of the gradient boundary condition on u. The damper is present only near the boundary, with $\chi = 1\ day^{-1}$ within 150 km of the boundary, and decreasing to zero linearly in the interval from 150 km to 300 km. There is no corresponding damper on v and H, so that fluid can pass freely through the boundary.

The forcing is derived from the wind-stress climatology of Hellerman and Rosenstein [1983], their wind stress being interpolated linearly to the model grid and then smoothed [McCreary et al., 1993]. Monthly plots of the wind stress in the north Indian Ocean are shown in Figure 3.3. The model is spun up from a state of rest, the winds being ramped up from zero to the appropriate level over five days to damp inertial oscillations. Results discussed below are from the tenth year of the simulation, by when the the model approaches stationarity.

3.3.2 Role of Nonlinearity

Annual sea-level[5] deviation and velocity over the domain are shown in Figure 3.4 and monthly plots of η and $\mathbf{v}$ are shown in Figure 3.5. The circulation in the eastern Arabian Sea shows a

[5]By annual sea level, we actually mean annual (mean) sea level. It is the mean of monthly sea level over an year. In the model, monthly sea level is computed in two ways. In the figures that show sea-level deviation over the domain, or over the north Indian Ocean, monthly sea level is just the instantaneous sea level in the middle of the model month (day 15). In the figures that show "line-plots" of coastal sea level, it is the mean of daily sea level over a model month (30 days); daily sea level is just the instantaneous sea level at the end of a model day (24 hours). Similarly, by annual velocity, we mean annual mean velocity, the mean of monthly velocity over an year. Monthly velocity is just the instantaneous velocity in the middle of a model month. Note the difference between η_a, which is plotted in the line-plots, and η, which is plotted in the figures that cover the domain or the north Indian Ocean. η_a is the deviation, or anomaly, of the monthly value from the *local* annual mean; η is the deviation from the initial surface. Therefore, the mean of η_a over an year is zero at any location, but that of η is not necessarily so.

Figure 3.2 The domain of the reduced-gravity model for the Indian Ocean. The model domain is identical to that in McCreary et al. [1993]. In some subsequent simulations, the Lakshadweep and Maldive islands are included too; the rest of the domain remains unchanged through all the model results presented in this thesis.

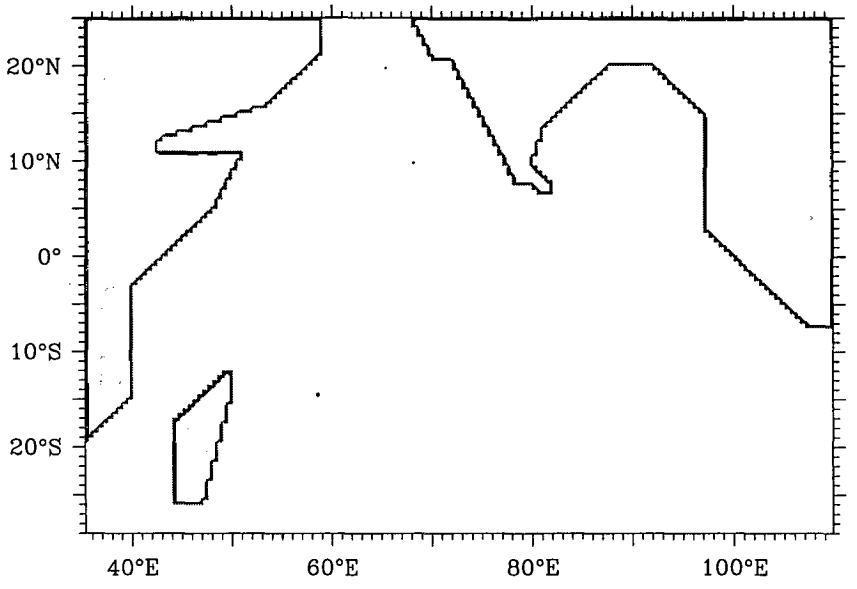

seasonal oscillation in the interface (the model pycnocline), and hence in sea level; a sequence of highs and lows is generated off the west coast of India and the highs and lows propagate westward, as in the altimeter data [Tapley et al., 1994].

In December, the EICC is equatorward; it flows into the westward NMC, which turns around Sri Lanka to join the poleward WICC. In January, a high forms off southwest India. The NMC flows around the high, joining the coastal current, the WICC, at about 12°N. The WICC is poleward north of 12°N and equatorward to the south; the equatorward coastal flow implies coastal downwelling. The high then stretches westward, and the NMC and the high extend across the southern Arabian Sea by March.

By May, the WICC is equatorward all along the coast; it flows into the eastward equatorial jet, which bifurcates near the eastern boundary of the basin. A low forms off southwest India by July. The WICC is equatorward only north of 12°N, where it moves offshore to flow as the Southwest Monsoon Current (SMC) around the western slope of the low; the SMC continues as an eastward current on the southern flank of the low and flows into the Bay of Bengal. South of 12°N, the WICC is poleward, implying coastal downwelling. The low too stretches westward, extending across the southern Arabian Sea by November.

The solution described above reproduces virtually all the significant observed features of the

Figure 3.3 Seasonal cycle of wind stress (dyne cm^{-2}) in the north Indian Ocean. The wind stress is derived from the climatology of Hellerman and Rosenstein [1983]. January marks the end of the northeast monsoon in the Bay of Bengal, where the winds are weak during February–April, these months marking the transition between the northeast and southwest monsoons. The winds weaken over the eastern Arabian Sea too, but they continue to blow from the northeast in the west.

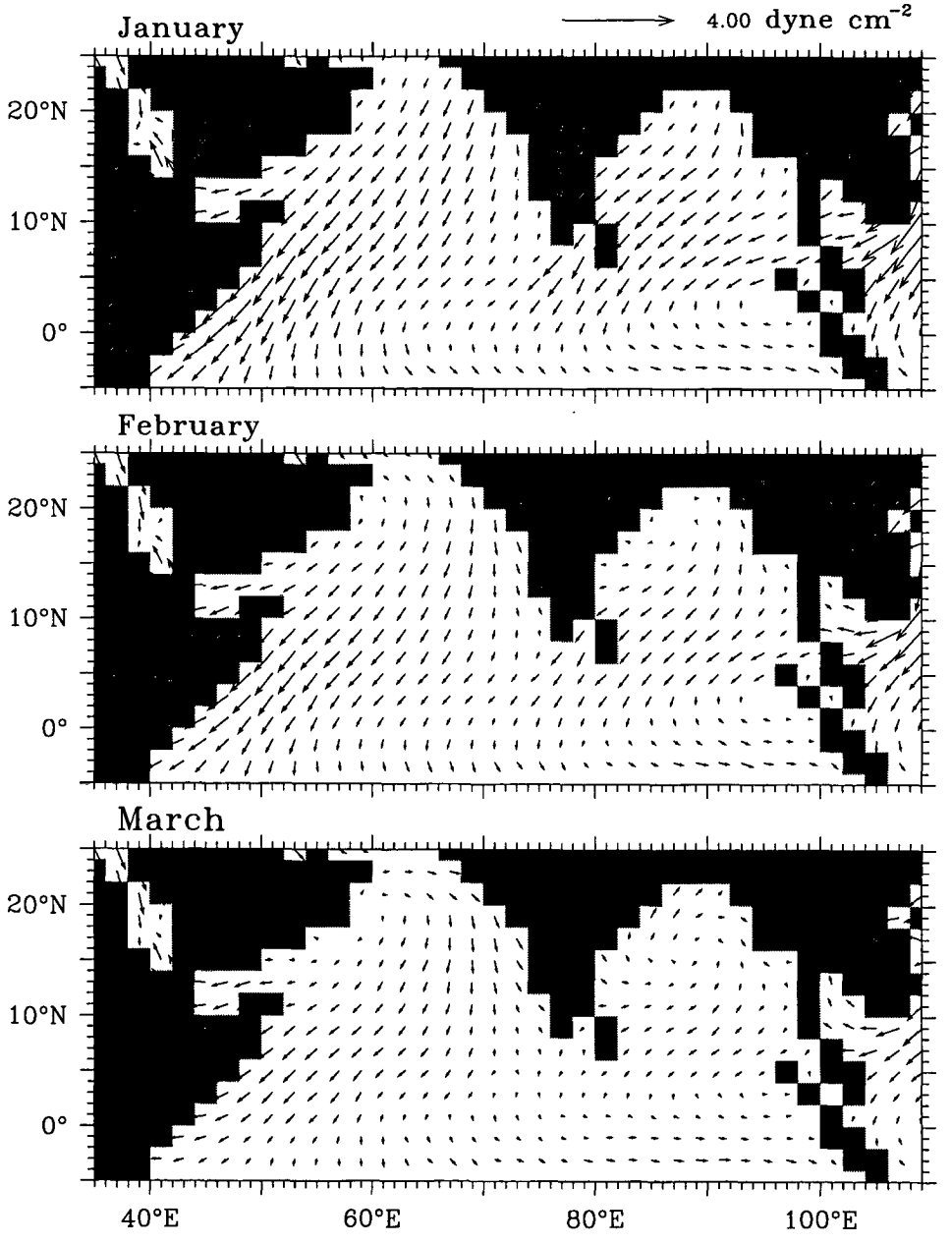

Figure 3.3 (continued) Seasonal cycle of wind stress (dyne cm^{-2}) in the north Indian Ocean. The wind stress is derived from the climatology of Hellerman and Rosenstein [1983]. In April, the winds are at their weakest over the north Indian Ocean. They strengthen in May, blowing from the southwest over the basin, except along the Indian west coast, where they blow from the northwest. The winds are strongest along the east coast of Africa and the central Arabian Sea, where the Findlater jet forms.

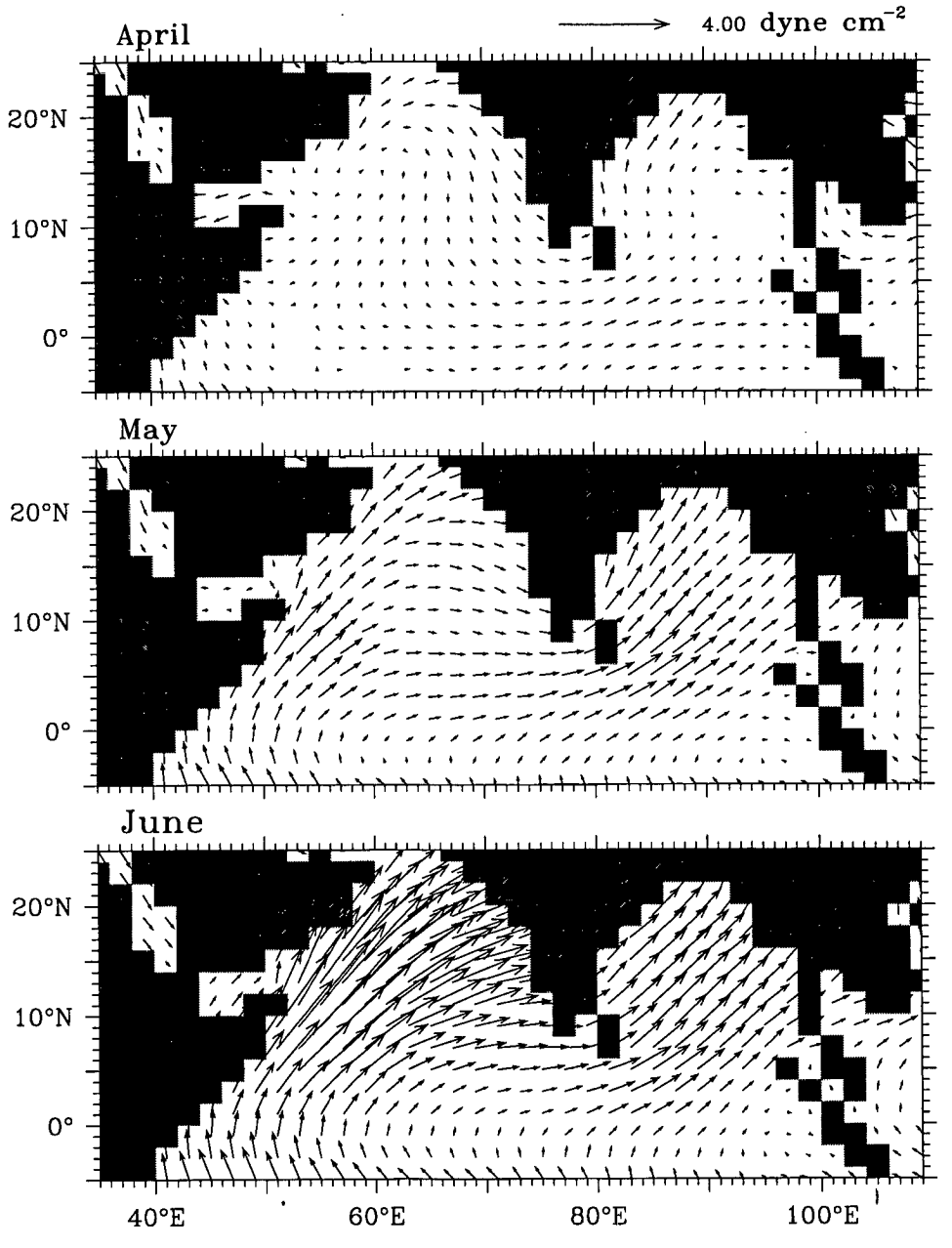

Figure 3.3 (continued) Seasonal cycle of wind stress (dyne cm^{-2}) in the north Indian Ocean. The wind stress is derived from the climatology of Hellerman and Rosenstein [1983]. The southwest monsoon is at its peak in July, with strong winds blowing all over the north Indian Ocean. The winds blow from the southwest over the western Arabian Sea and over the bay, and from the west or northwest over the eastern Arabian Sea. They weaken after July, and October is again a month of transition, with weak winds all over the basin.

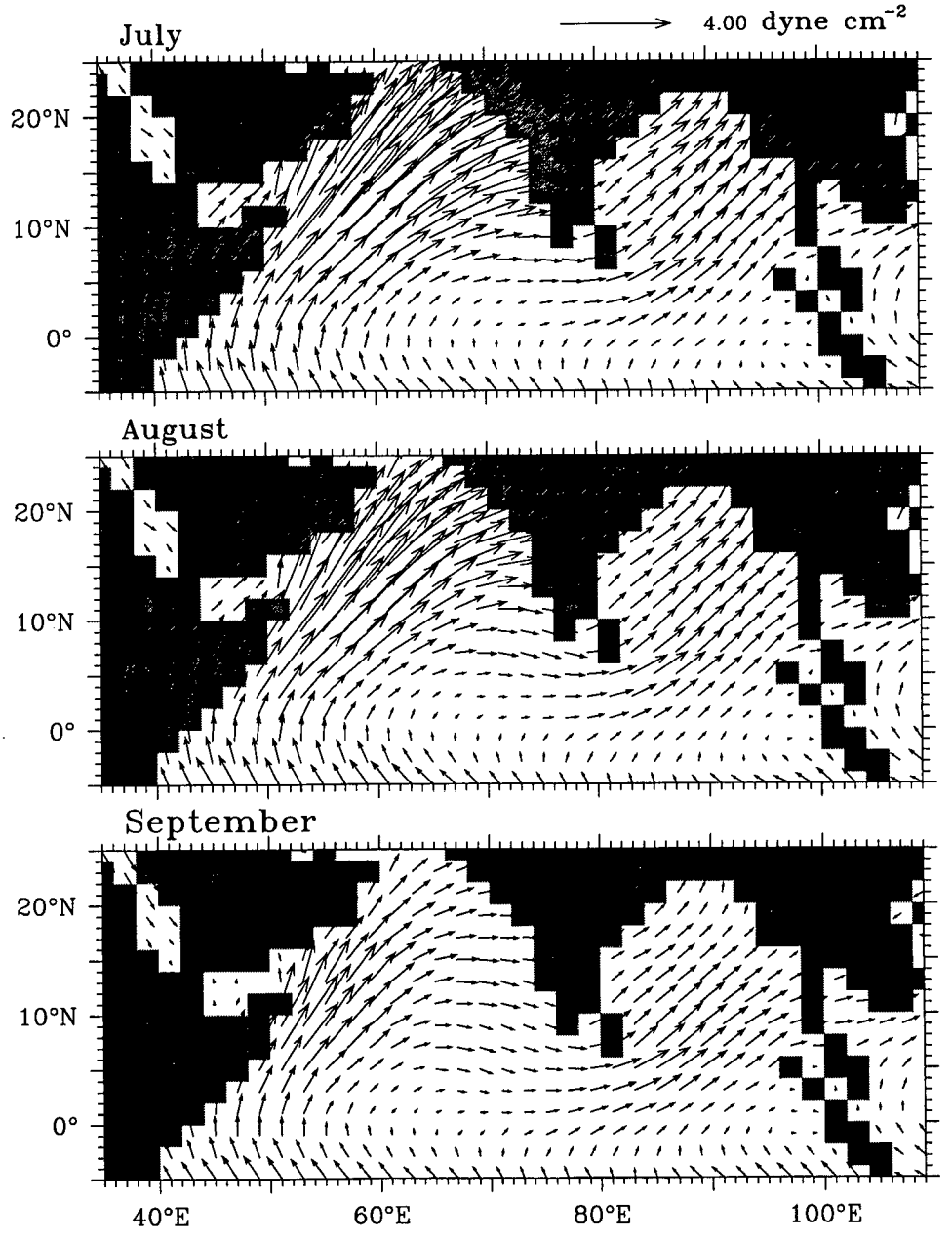

Figure 3.3 (continued) Seasonal cycle of wind stress (dyne cm^{-2}) in the north Indian Ocean. The wind stress is derived from the climatology of Hellerman and Rosenstein [1983]. October is a month of transition between the southwest and northeast monsoons. The winds reverse to blow from the northeast in November, peaking a month later. The northeast monsoon is much weaker than the southwest, resulting in a strong mean wind field over the north Indian Ocean.

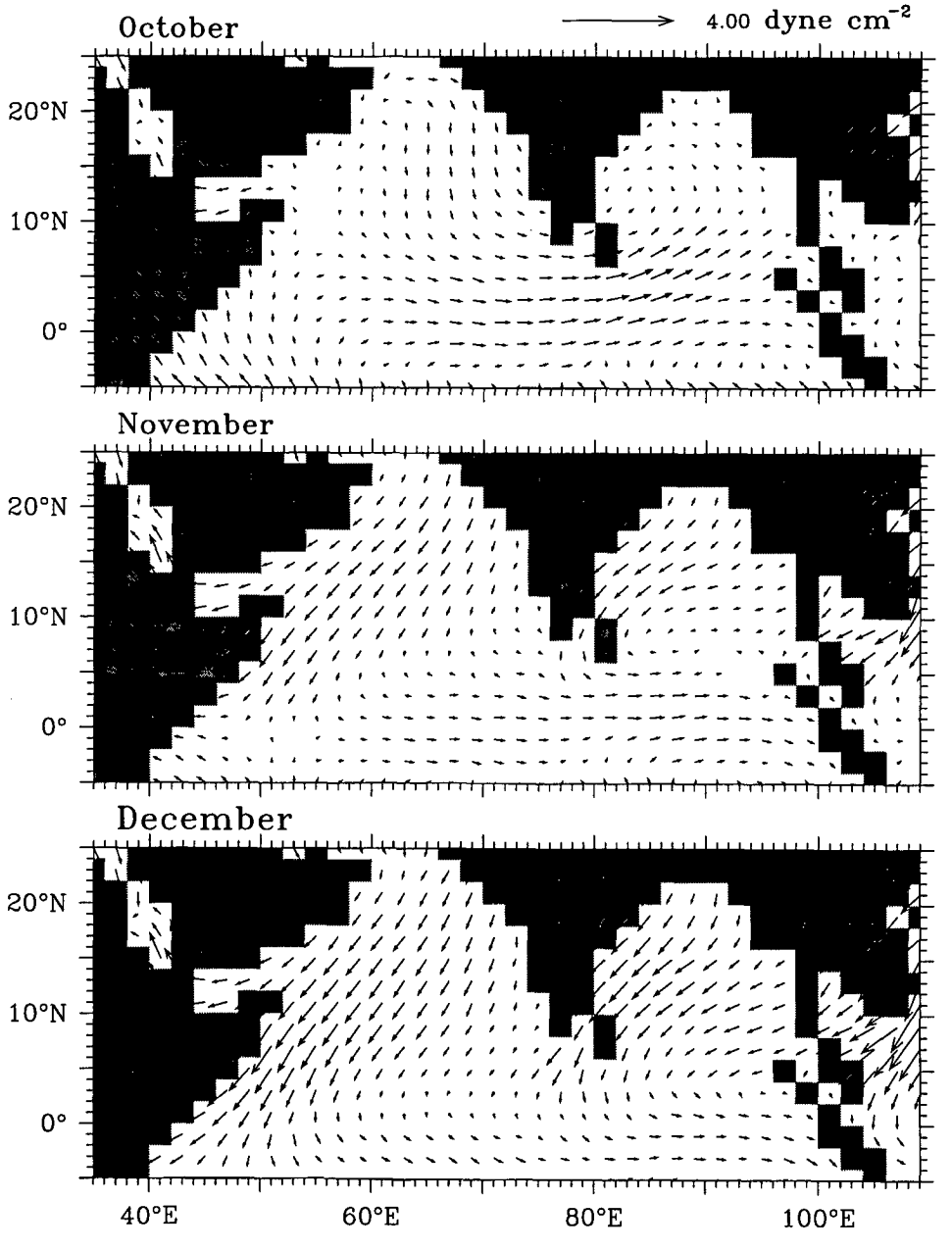

Figure 3.4 Annual sea-level deviation η (cm) and velocity $\mathbf{v}$ (cm s^{-1}) over the model domain. The level of the undisturbed sea surface is removed to obtain the sea-level deviation. This η is different from the η_a that is plotted in the line-plots in Chapters 2 and 4. η_a is the deviation, or anomaly, of the monthly value from the local annual mean. Therefore, the mean of η_a over an year is zero at any location, but that of η is not necessarily so. The solution shows one of the limitations of this model. In the tropical gyre that forms between 5°S and 15°S, the upper layer thickness is at the minimum value, H_{min}, over a large area. This distorts the momentum balance in the region because the pressure-gradient force, which requires a gradient in H, vanishes, implying a breakdown in the geostrophic balance that should apply in the region and leading to the currents flowing across the contours of H, as in an Ekman balance. A similar distortion occurs in the anticyclonic gyre in the south Indian Ocean, where the upper layer thickness is at its maximum value, H_{max}, over a large region. Seasonal distortions of this kind occur in the north Indian Ocean too, especially in the strong upwelling regimes off Somalia and Arabia. These distortions are not crucial because their effects are easily seen, but, along with the absence of the Indonesian Throughflow, they make the simulated flow-field different from that observed over a large part of the south Indian Ocean. Hence, our focus in this thesis is on the north Indian Ocean, where the model, despite its simplicity, performs remarkably well; subsequent figures cover only this part of the basin.

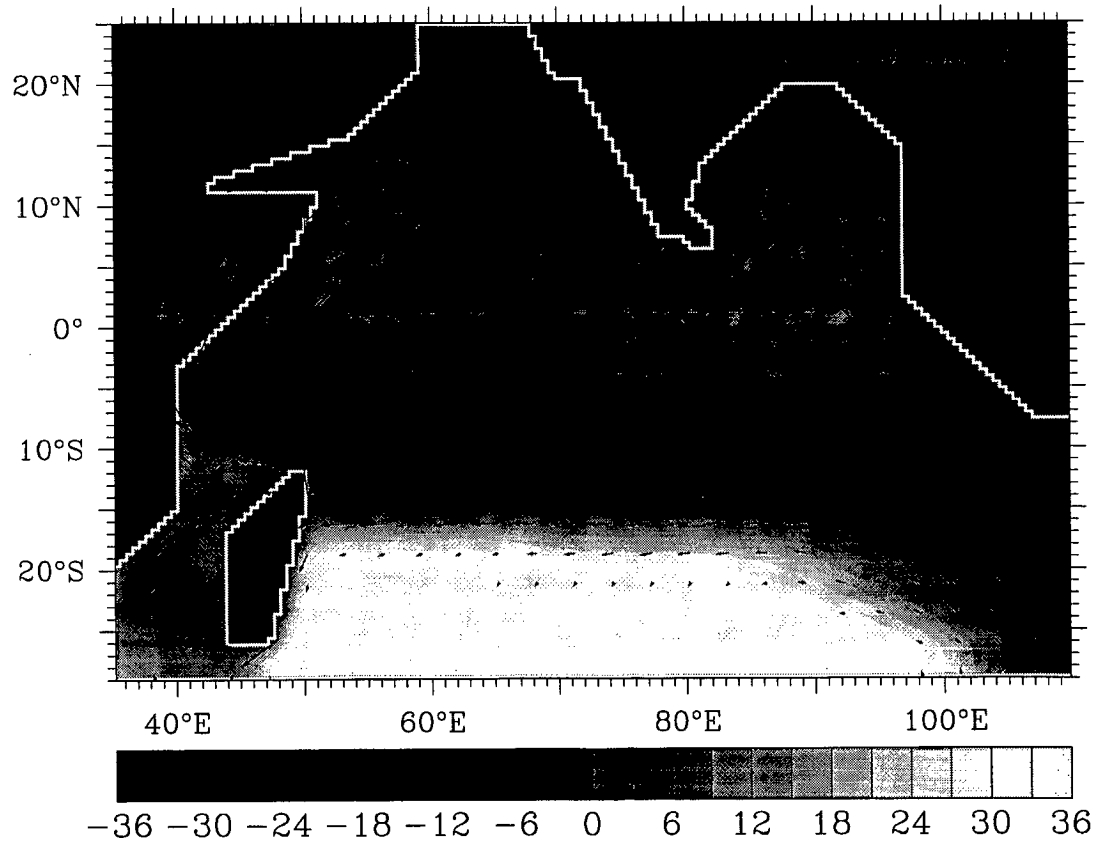

Figure 3.5 Seasonal cycle of surface circulation: nonlinear simulation. Sea-level deviation η (cm) and velocity $\mathbf{v}$ (cm s^{-1}) are shown. In January, the NMC flows around the western flank of the Lakshadweep high off southwest India, joining the poleward WICC at 12°N; the WICC is equatorward to the south, closing the geostrophic circulation around the high. The high stretches westward, extending across the southern Arabian Sea by April. The EICC flows poleward during February–May, forming the western boundary current of a basin-wide anticyclonic gyre in the Bay of Bengal.

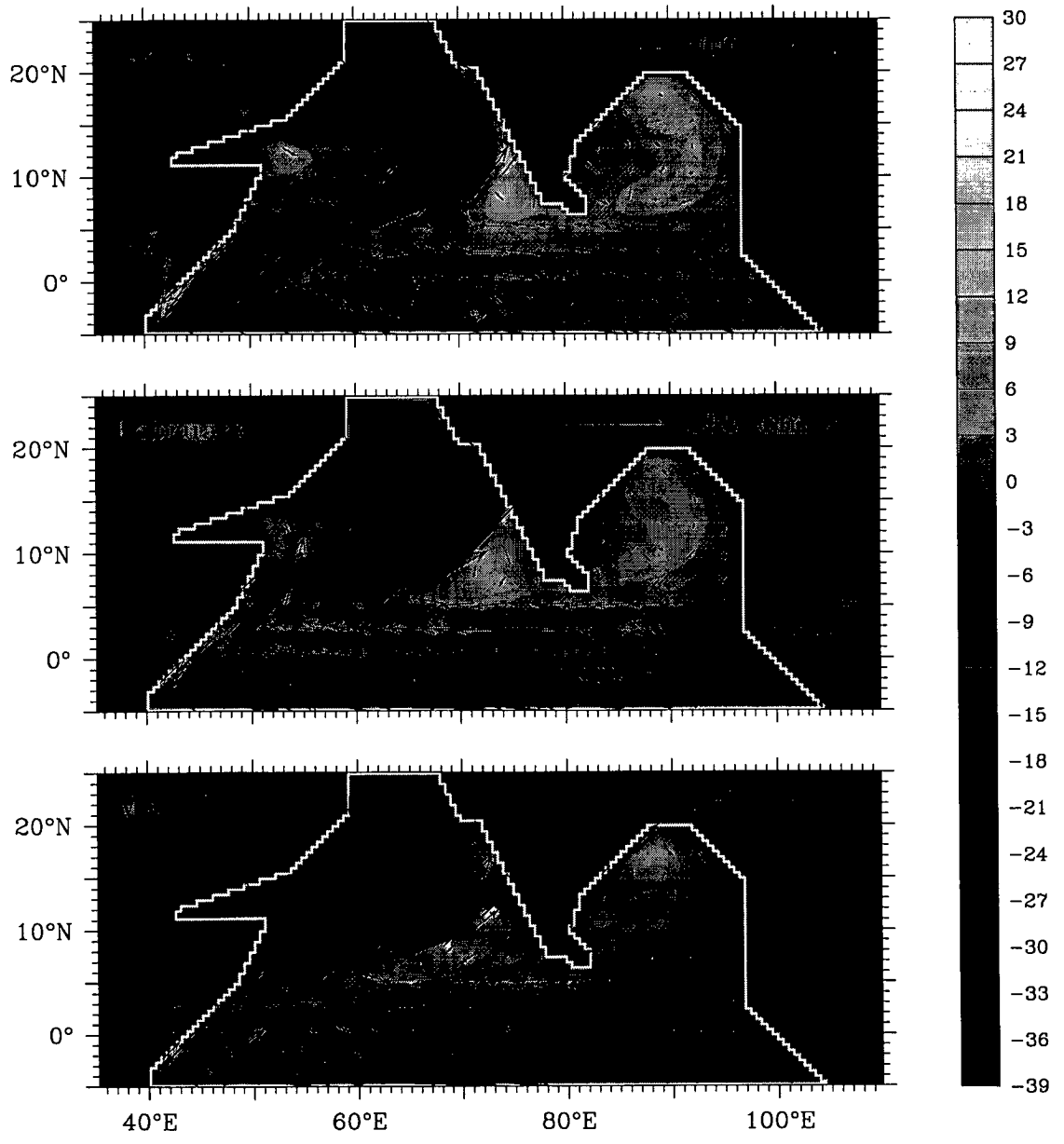

Figure 3.5 (continued) Seasonal cycle of surface circulation: nonlinear simulation. Sea-level deviation η (cm) and velocity $\mathbf{v}$ (cm s^{-1}) are shown. In April, the equatorward WICC off southwest India expands poleward. By June, the WICC is equatorward north of 12°N, where it flows offshore into the SMC, which flows around a low in sea level off southwest India. An eastward jet forms at the equator during April–May. The EICC weakens after April and the anticyclonic gyre vanishes. A weak EICC flows poleward during the southwest monsoon; off Sri Lanka and towards the north of the coast, however, the EICC flows equatorward.

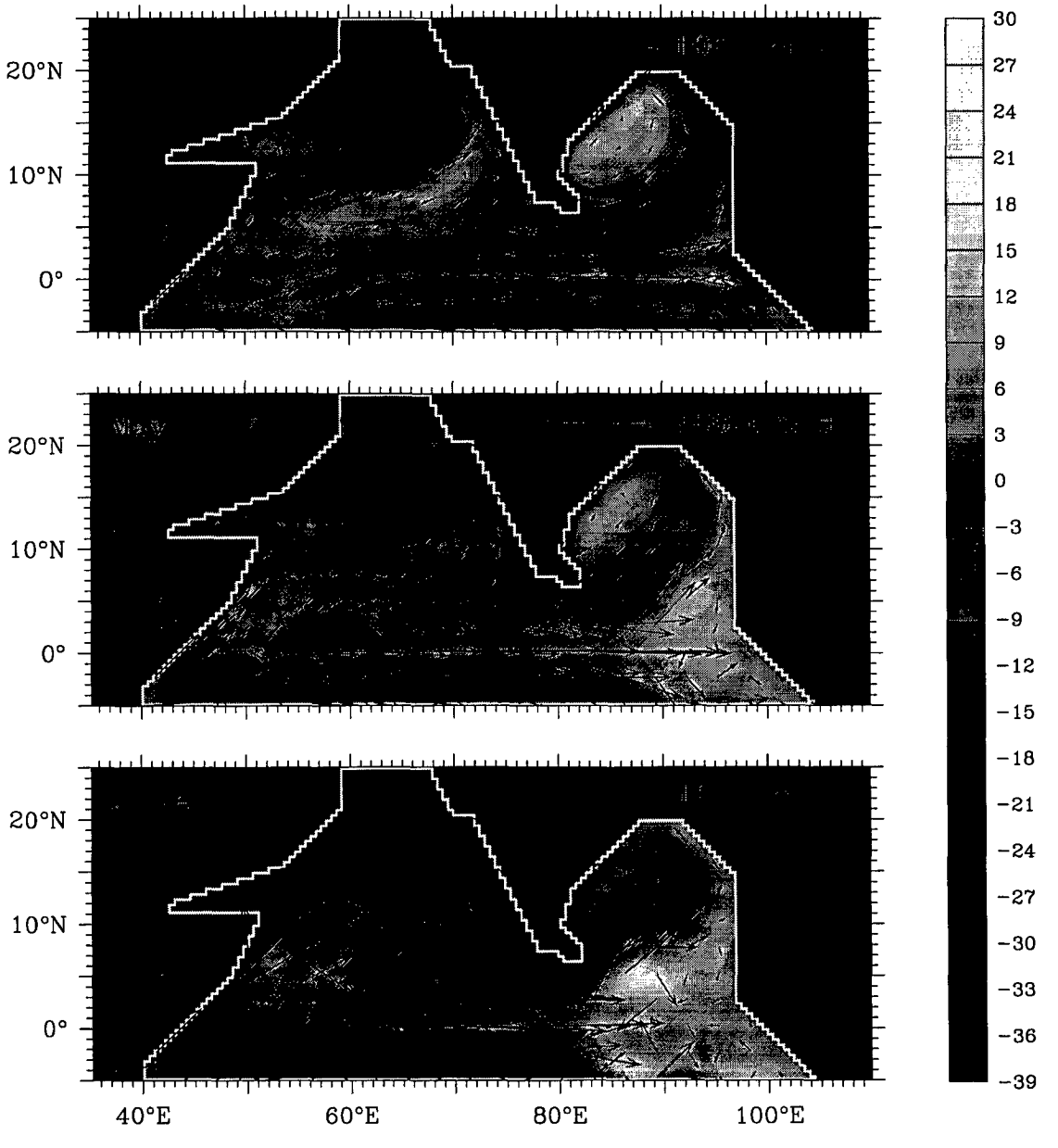

Figure 3.5 (continued) Seasonal cycle of surface circulation: nonlinear simulation. Sea-level deviation η (cm) and velocity $\mathbf{v}$ (cm s^{-1}) are shown. During the southwest monsoon, the Lakshadweep low forms off southwest India and propagates westward. The most vigorous circulation is in the western Arabian Sea, where the Great Whirl forms by July. Another anticyclonic high in sea level, the Socotra high, forms to the north of the Great Whirl. The circulation in the bay lacks organization during the southwest monsoon. The EICC is weak; it is poleward in the south and equatorward in the north and off Sri Lanka.

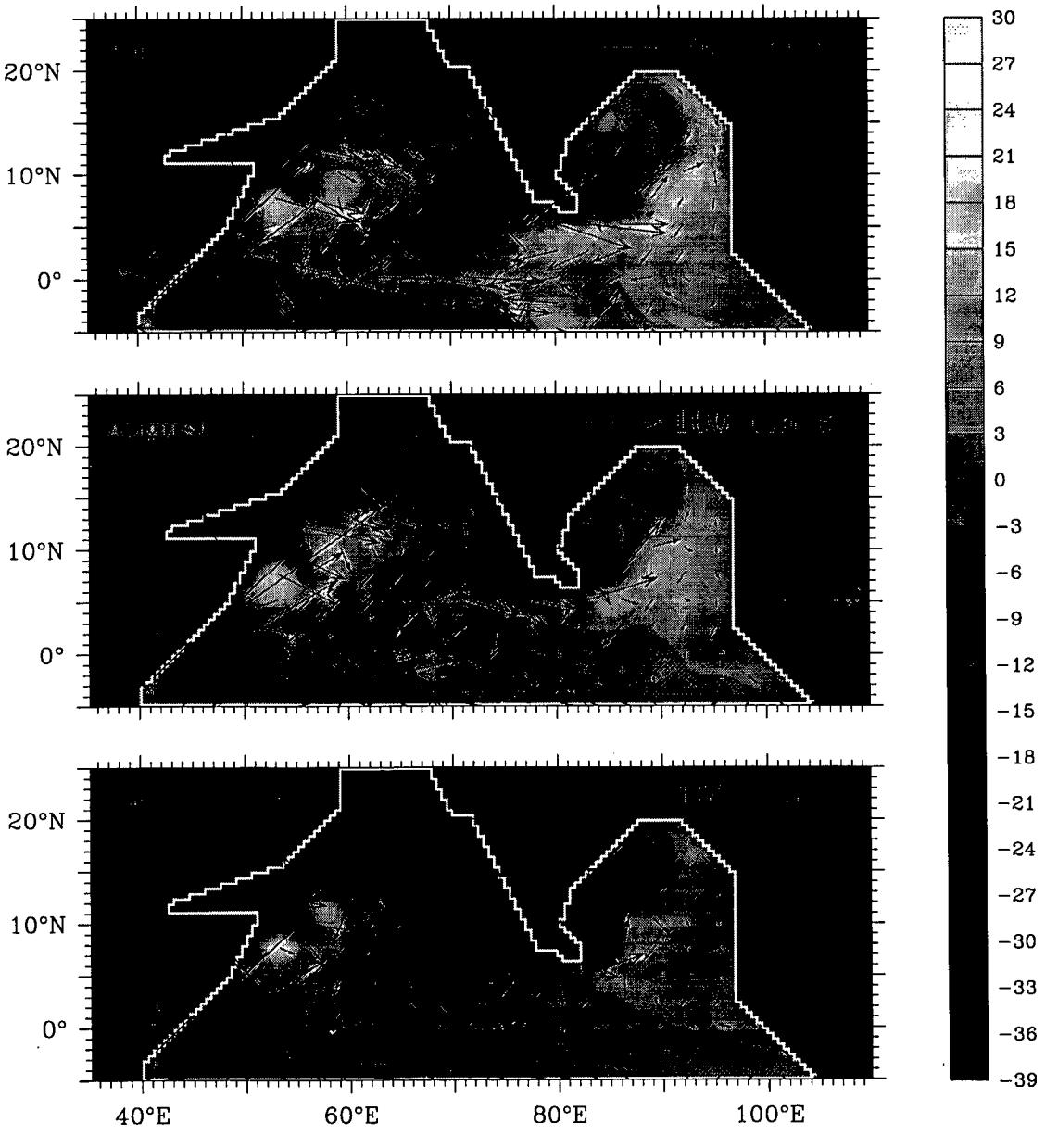

Figure 3.5 (continued) Seasonal cycle of surface circulation: nonlinear simulation. Sea-level deviation η (cm) and velocity $\mathbf{v}$ (cm s^{-1}) are shown. With the collapse of the southwest monsoon in September, the EICC reverses to flow equatorward. It flows into the NMC, which turns around Sri Lanka to join the poleward WICC. In December, the incipient Lakshadweep high is seen off southwest India. Another eastward jet forms at the equator in November, but the model jet does not extend to the eastern boundary.

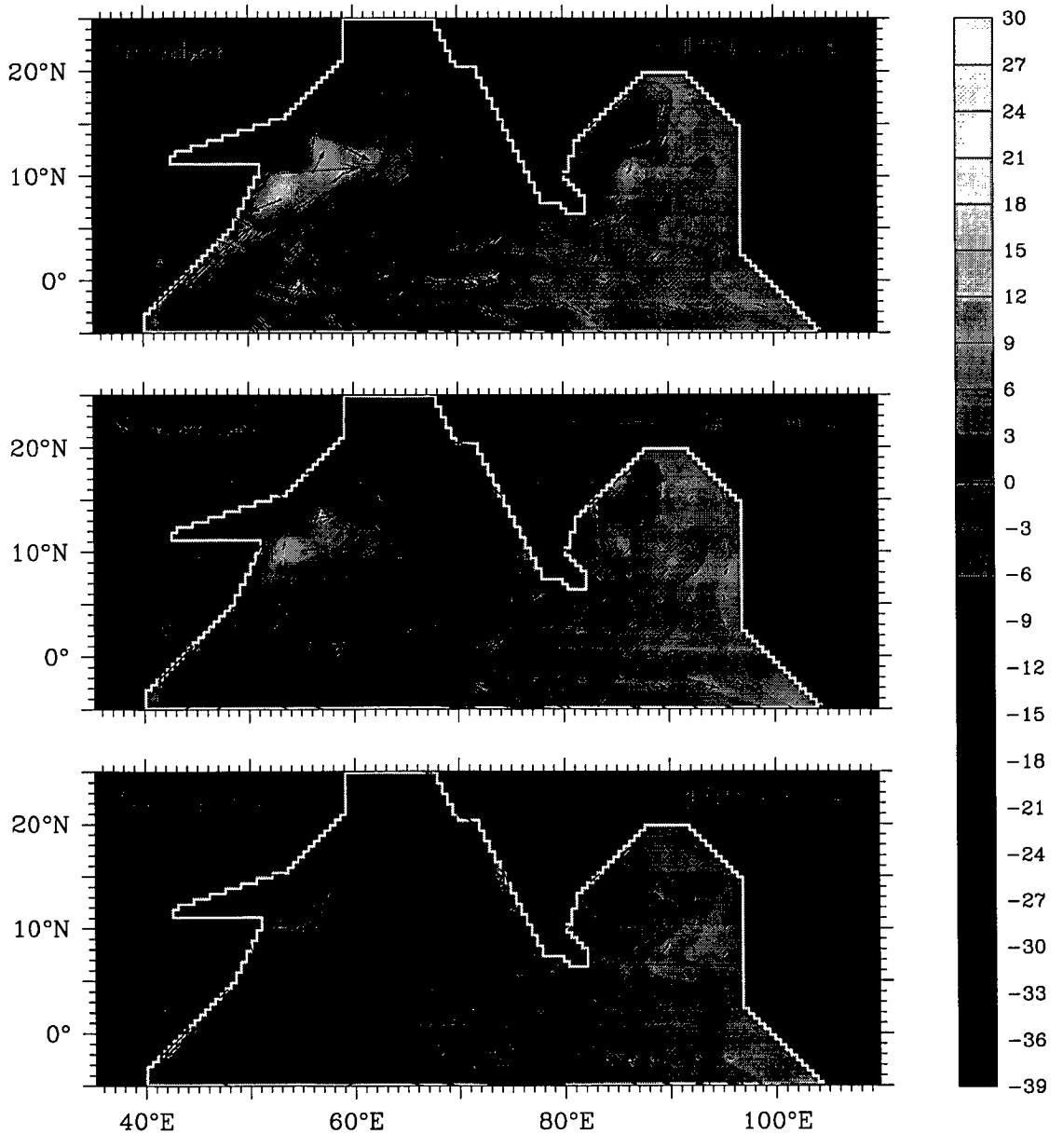

Figure 3.6 Seasonal cycle of surface circulation: linear simulation. Sea-level deviation η (cm) and velocity $\mathbf{v}$ (cm s^{-1}) are shown. The linear solution is virtually identical to the nonlinear solution. Linearization only distorts the highs and lows, stretching them out. The phase speed is constant and the highs and lows propagate at the same speed.

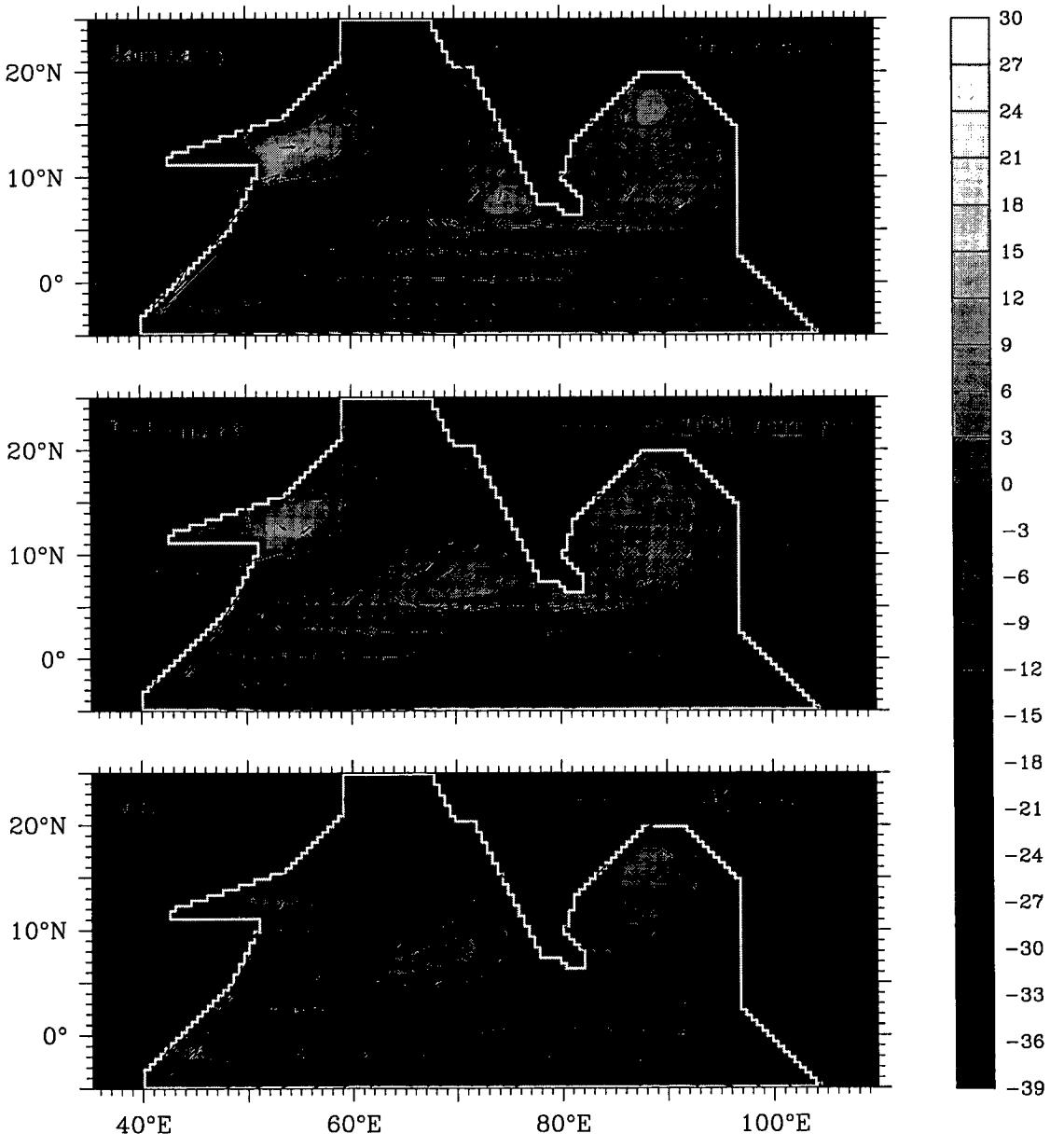

Figure 3.6 (continued) Seasonal cycle of surface circulation: linear simulation. Sea-level deviation η (cm) and velocity $\mathbf{v}$ (cm s^{-1}) are shown. The linear solution is virtually identical to the nonlinear solution. Linearization only distorts the highs and lows, stretching them out. The phase speed is constant and the highs and lows propagate at the same speed.

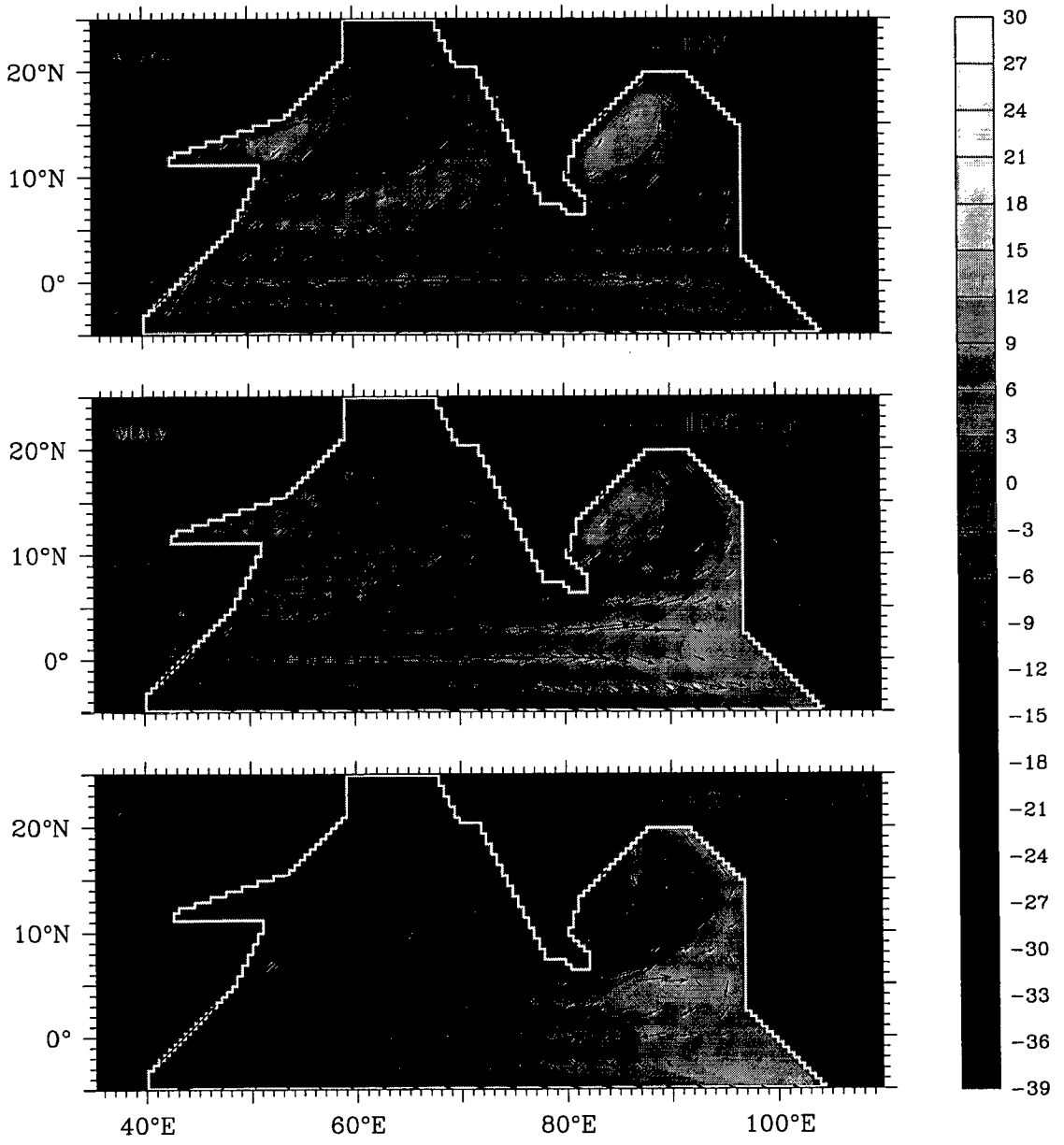

Figure 3.6 (continued) Seasonal cycle of surface circulation: linear simulation. Sea-level deviation η (cm) and velocity $\mathbf{v}$ (cm s^{-1}) are shown. The linear solution is virtually identical to the nonlinear solution, with one major exception. The Great Whirl does not form off Somalia during the southwest monsoon. The two anticyclonic circulations in the region, the Great Whirl and the Socotra high, merge to form a single high in sea level. The Somali Current is also "smoother" in the absence of nonlinearity.

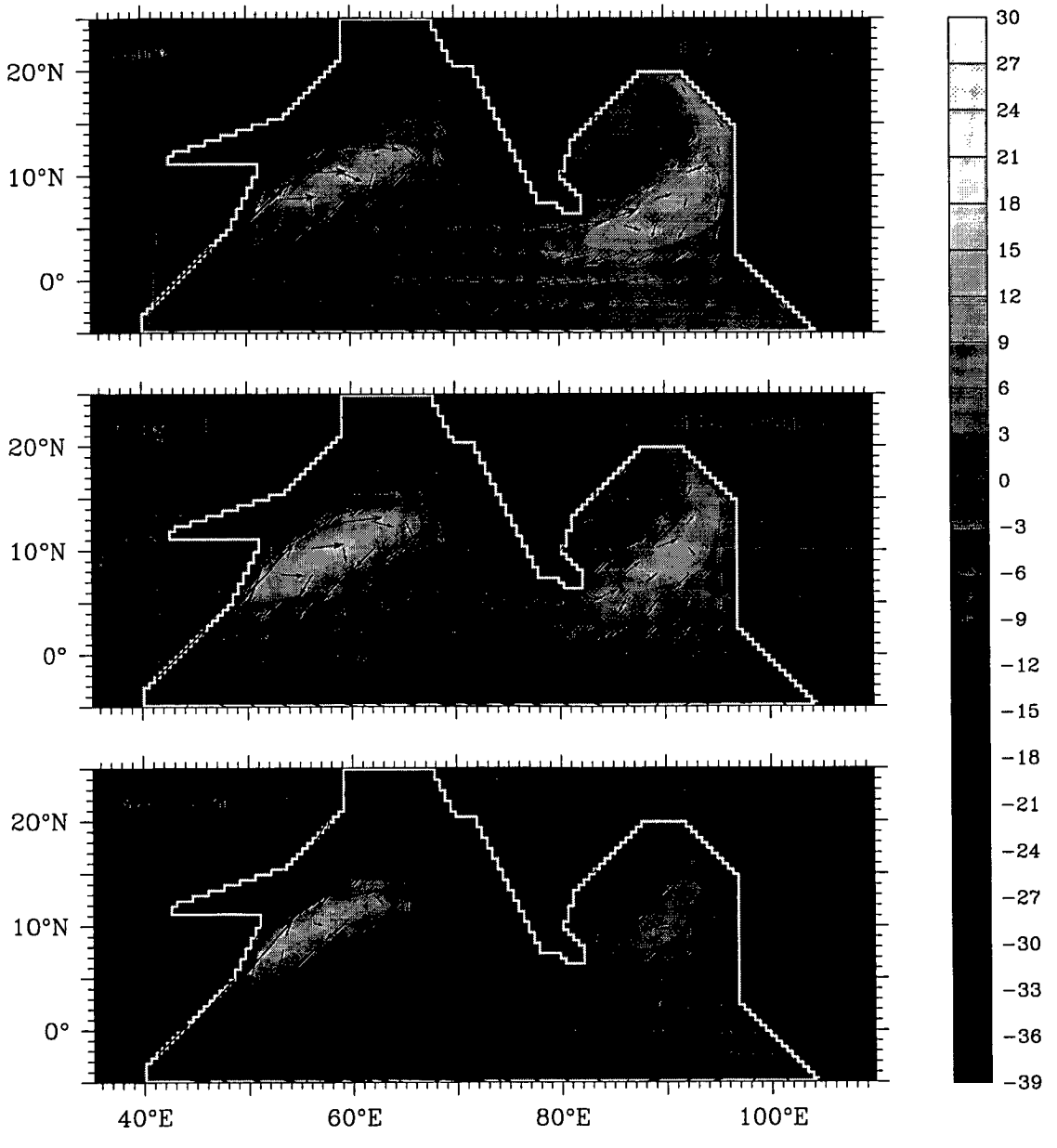

Figure 3.6 (continued) Seasonal cycle of surface circulation: linear simulation. Sea-level deviation η (cm) and velocity $\mathbf{v}$ (cm s^{-1}) are shown. The linear solution is virtually identical to the nonlinear solution. Linearization only distorts the highs and lows, stretching them out. The phase speed is constant and the highs and lows propagate at the same speed.

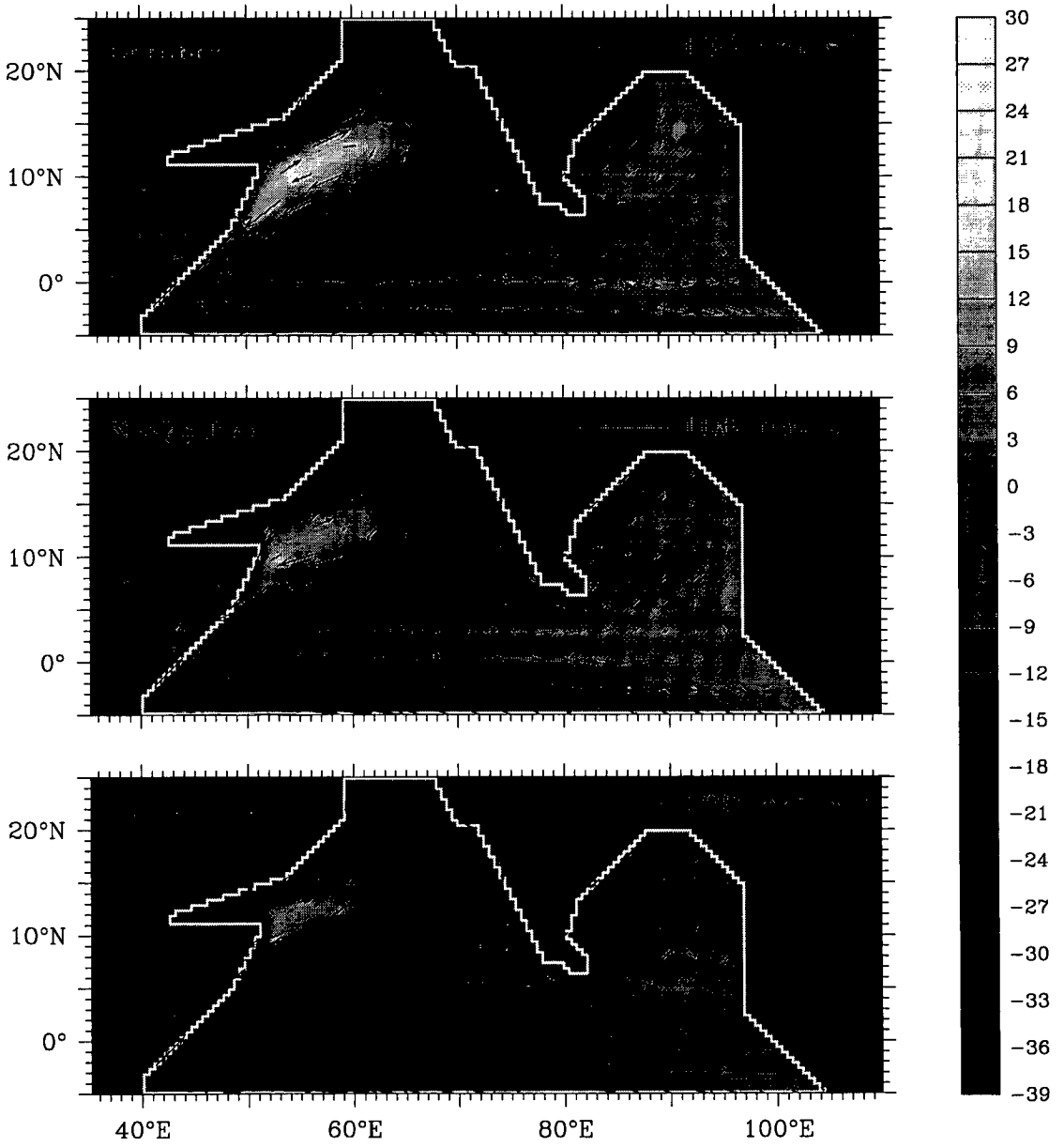

seasonal cycle of the high and low and of the surface circulation in the vicinity of India. To what extent do these features depend on the nonlinearity in the momentum equations? To answer this question, we linearize model equations[6]. The linear simulation reproduces the seasonal cycle of the Lakshadweep high and low and of the circulation in their vicinity (Figure 3.6). In fact, the linear solution is virtually identical to the nonlinear solution, with one notable exception: the Great Whirl does not form[7].

This implies that nonlinearity is crucial to the dynamics of the Great Whirl, but not to that of the Lakshadweep high and low. In its absence, they could be generated by the following causes, either individually or in conjunction with the others: Ekman pumping off the southern tip of India, locally forced coastal Kelvin waves or Rossby waves, and Kelvin waves that reach the west coast of India after making their way around Sri Lanka. McCreary et al. [1993] showed the last of these to be particularly important to the circulation off the Indian west coast. Hence, in the following section, we shall study the circulation off southwest India in the presence of only these remotely triggered waves. Before doing so, however, we examine the possible effects of the Lakshadweep and Maldive[8] islands on the high and low.

3.3.3 Role of Island Chains

We repeat the linear simulation of Section 3.3.2, with but one modification: the Lakshadweep and Maldive island chains are represented as rectangular blocks and the no-slip condition is applied at their boundaries, which correspond roughly to an idealization of the 200 m isobath. Monthly plots of η and $\mathbf{v}$ are shown in Figure 3.7. The island chains slow down the westward progress of the high and low. There is also some distortion of the flow-field to the east of the Maldive islands, which are sufficiently long to reflect the westward propagating Rossby waves; this forces a western boundary current along the east coast of the Maldives, and the poleward reflected current strengthens the flow around the high. The Lakshadweep islands, however, are smaller than the meridional wavelength of the Rossby waves, which pass round, or "through", these islands. Other than these, there are no significant differences introduced by the island chains. They do modify the high and low, but are not, by themselves, responsible for their existence.

[6] See Appendix A, equations (A.13).

[7] Linearization, however, does have other subtle effects. For example, it increases the length scales of highs and lows, stretching them out. It also distorts the phase speeds of the Kelvin and Rossby waves; the highs propagate slower than they do in a nonlinear simulation, and the lows propagate faster.

[8] Like Laccadive, "Maldive" is a distortion of "Maladweep", literally a "garland of islands". The Maldive government, however, uses the anglicized form — at least in English — and we see no reason to do otherwise.

Figure 3.7 Effect of the Lakshadweep and Maldive islands on the Lakshadweep high and low. The simulation is linear and identical to that in Figure 3.6, but for the inclusion of the island chains in the Arabian Sea. Plots of sea-level deviation η (cm) and velocity $\mathbf{v}$ (cm s^{-1}) are shown. The presence of the island chains slows down the westward propagation of the Lakshadweep high. The NMC reflects off the Maldives and the current bifurcates, the northern branch flowing poleward, strengthening the flow around the high. The southern branch bends around the Maldives and flows westward along the equator; the axis of the NMC is displaced southward.

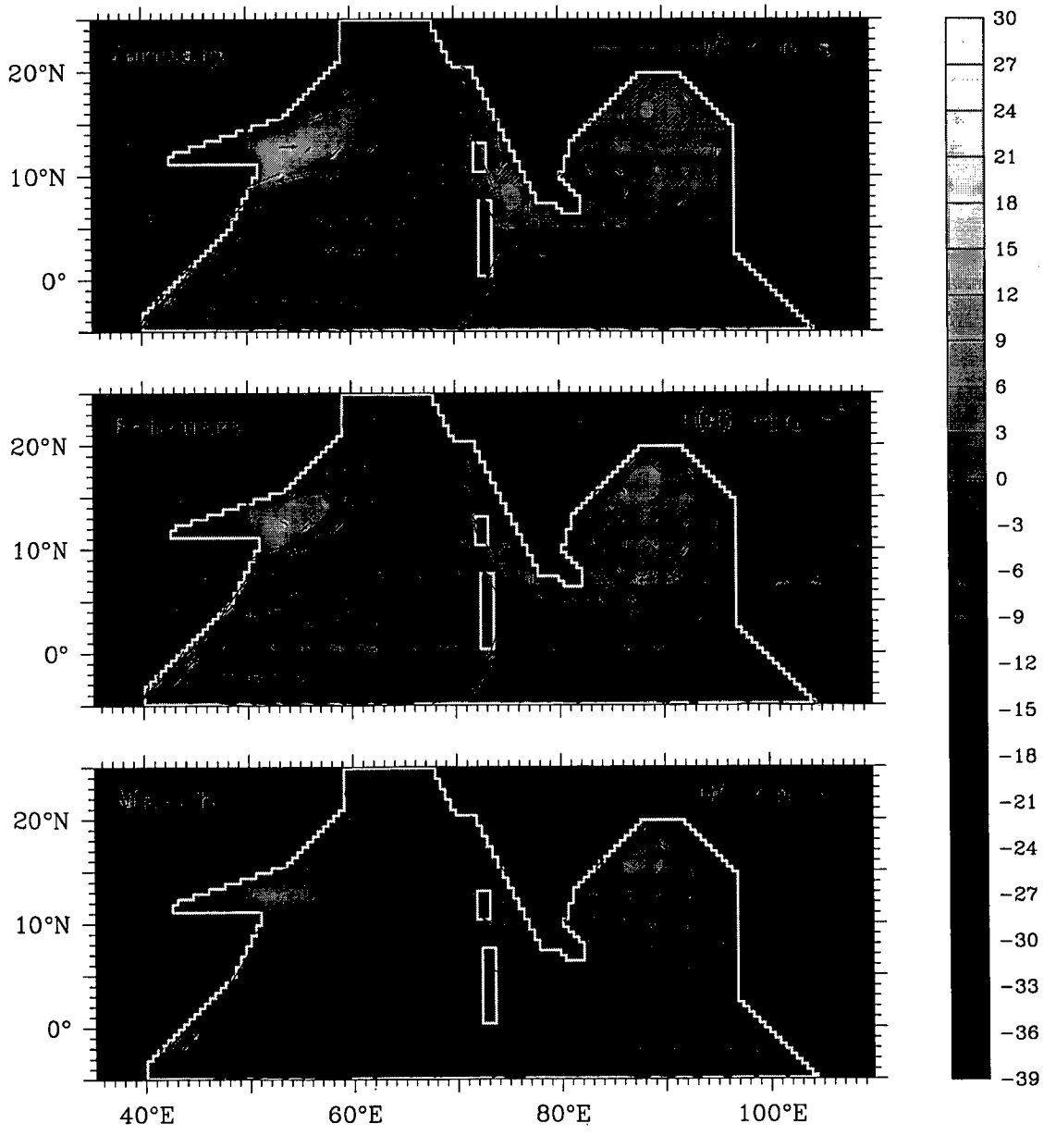

Figure 3.7 (continued) Effect of the Lakshadweep and Maldive islands on the Lakshadweep high and low. The simulation is linear and identical to that in Figure 3.6, but for the inclusion of the island chains in the Arabian Sea. Plots of sea-level deviation η (cm) and velocity $\mathbf{v}$ (cm s^{-1}) are shown. The Lakshadweep islands are smaller than the meridional wavelength of the Rossby waves, which pass round, or "through", these islands. The islands merely displace the high northward. The Rossby waves in the eastern equatorial Indian Ocean force the SMC in the Bay of Bengal [Vinayachandran and Yamagata, 1998]. These waves also reflect at the east coast of the Maldives, forcing a western boundary current that is a continuation of the equatorward WICC.

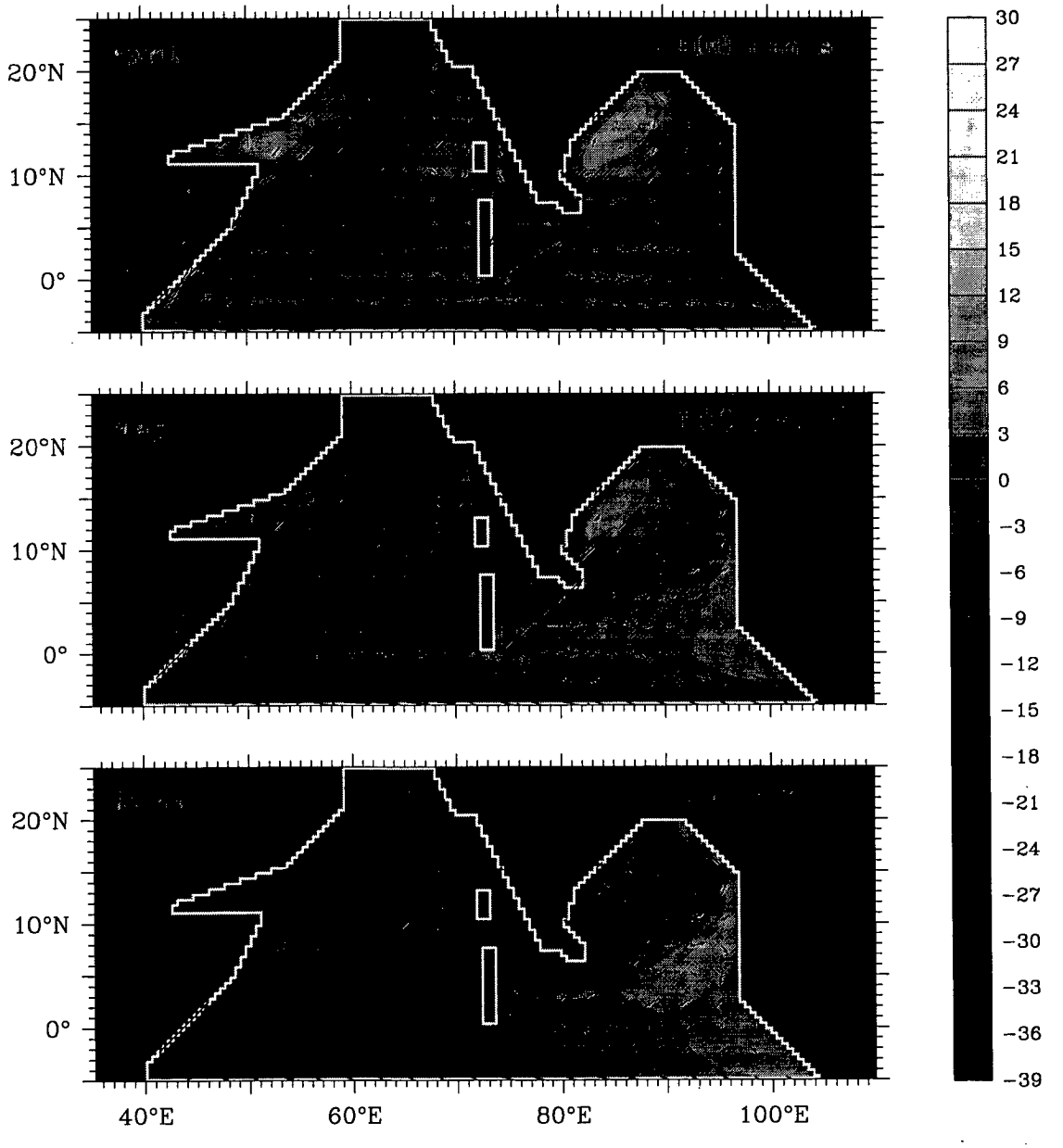

Figure 3.7 (continued) Effect of the Lakshadweep and Maldive islands on the Lakshadweep high and low. The simulation is linear and identical to that in Figure 3.6, but for the inclusion of the island chains in the Arabian Sea. Plots of sea-level deviation η (cm) and velocity $\mathbf{v}$ (cm s^{-1}) are shown. The presence of the islands distorts the SMC; it flows around the Lakshadweep low and turns eastward in the channel between the two island chains. The low propagates faster than in the nonlinear simulation, but is slowed down by the Lakshadweep islands.

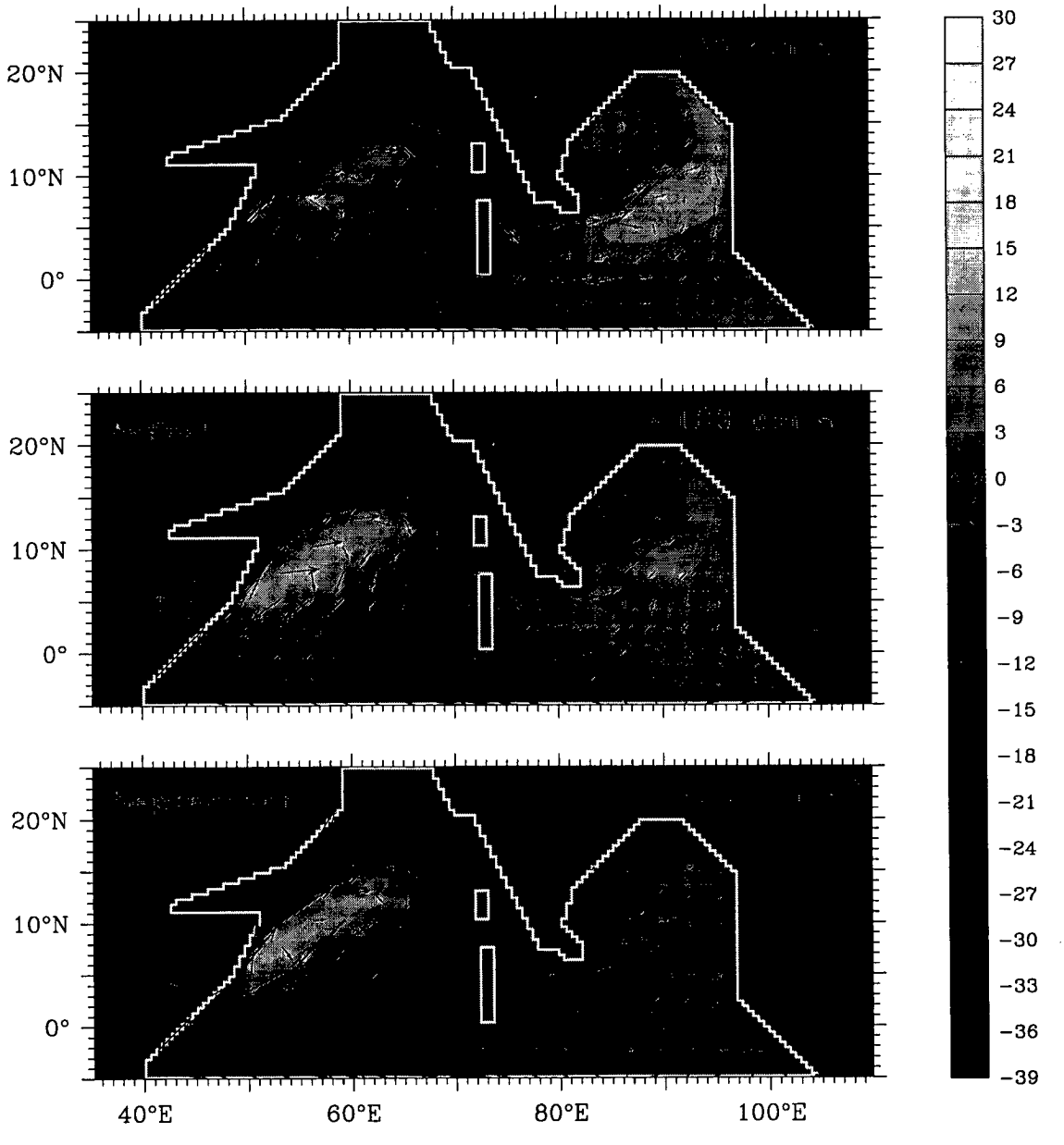

Figure 3.7 (continued) Effect of the Lakshadweep and Maldive islands on the Lakshadweep high and low. The simulation is linear and identical to that in Figure 3.6, but for the inclusion of the island chains in the Arabian Sea. Plots of sea-level deviation η (cm) and velocity $\mathbf{v}$ (cm s^{-1}) are shown. Only a vestige of the SMC remains in October. The NMC begins forming in December and is deflected by the Maldives; the poleward flow strengthens the Lakshadweep high in January.

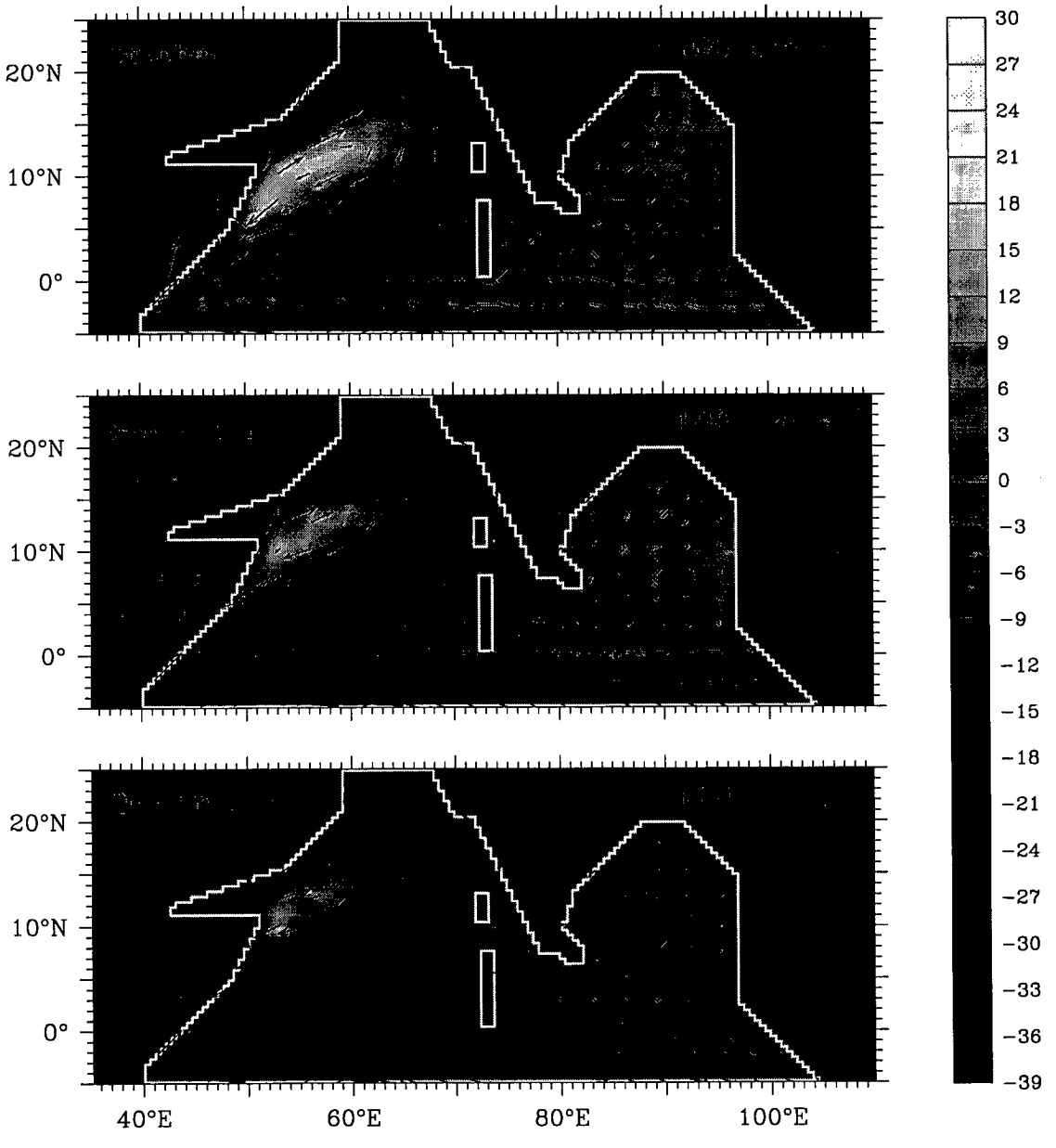

3.4 Role of Remotely Forced Kelvin Waves

Coastal Kelvin waves in the Bay of Bengal are forced primarily by alongshore winds in the bay or by winds in the equatorial waveguide [McCreary et al., 1993, 1996; Shankar et al., 1996; Yu et al., 1991]. These winds also generate Rossby waves. Our objective in this section is to examine the consequence of a coastal Kelvin wave that reaches the southern tip of India after making its way around Sri Lanka; hence, we use the linearized reduced-gravity model and eliminate all other forcing mechanisms by prescribing an oscillatory boundary forcing. First, we obtain numerical solutions for a realistic basin geometry, but now without any forcing by winds; instead, we generate a coastal Kelvin wave along the east coast of India by prescribing a velocity at the northern boundary of the bay. Second, we obtain an analytic solution for a rectangular basin, in which the arrival of a Kelvin wave at the southern tip of India is mimicked by an oscillating zonal current.

3.4.1 Numerical Experiments

We generate a Kelvin wave along the east coast of India by prescribing a periodic current normal to the northern boundary of the Bay of Bengal in the linearized version of the model. At 20°N, the northern boundary of the bay, the slip-flow condition is used for the zonal velocity, and a periodic meridional (normal) velocity is prescribed as follows:

$$v(x,20^\circ,t) = -0.4v_0\cos(\sigma t)\mid x-90^\circ\mid, \qquad 87.5^\circ \le x \le 90^\circ, \tag{3.2}$$

where x is in degrees longitude, $\sigma = 2\pi$ year^{-1}, and $v_0 = 40$ cm s^{-1}. There is flow into (out of) the bay during October–March (April–September), generating a coastal Kelvin wave of period $T = 2\pi\sigma^{-1}$ along the east coast of India; this wave bends around Sri Lanka and propagates poleward along the west coast, radiating a Rossby wave in the process. The pattern seen off the west coast of India is the result of the coastal Kelvin wave and the Rossby wave. The current associated with the Kelvin wave along the east coast, the model EICC, is connected to the current along the western edge of the Rossby wave.

Monthly plots of η and $\mathbf{v}$ for October–March from the fifth year of the simulation are shown in Figure 3.8, which depicts one half of an annual cycle of events that results in the formation of a high off southwest India. Inflow into the northern bay starts on 1 October, beginning the downwelling phase of the Kelvin wave at the east coast. By mid-October, there is equatorward flow in the northern half of the east coast, but the current is still poleward in the south. This is the continuation of a current along the western edge of a low in the Arabian Sea, which formed off southwest India in July and moved offshore. This current bifurcates at the southern tip of Sri Lanka, part of the flow being deflected poleward along the west coast and the rest bending around Sri Lanka to flow poleward along the east coast. By mid-November, the downwelling phase of the

Figure 3.8 The role of remotely forced Kelvin waves. Sea-level deviation η (cm) and velocity **v** (cm s^{-1}) are shown for the linear simulation forced by an oscillatory current at the northern boundary of the Bay of Bengal. The boundary forcing sets up a Kelvin wave along the east coast of India. The downwelling phase begins on 1 October, forcing an equatorward EICC. Off Sri Lanka, the EICC is poleward; it is the continuation of a current that flows along the western edge of a low off southwest India. The low propagates westward and the poleward WICC along its eastern flank extends all along the coast by December.

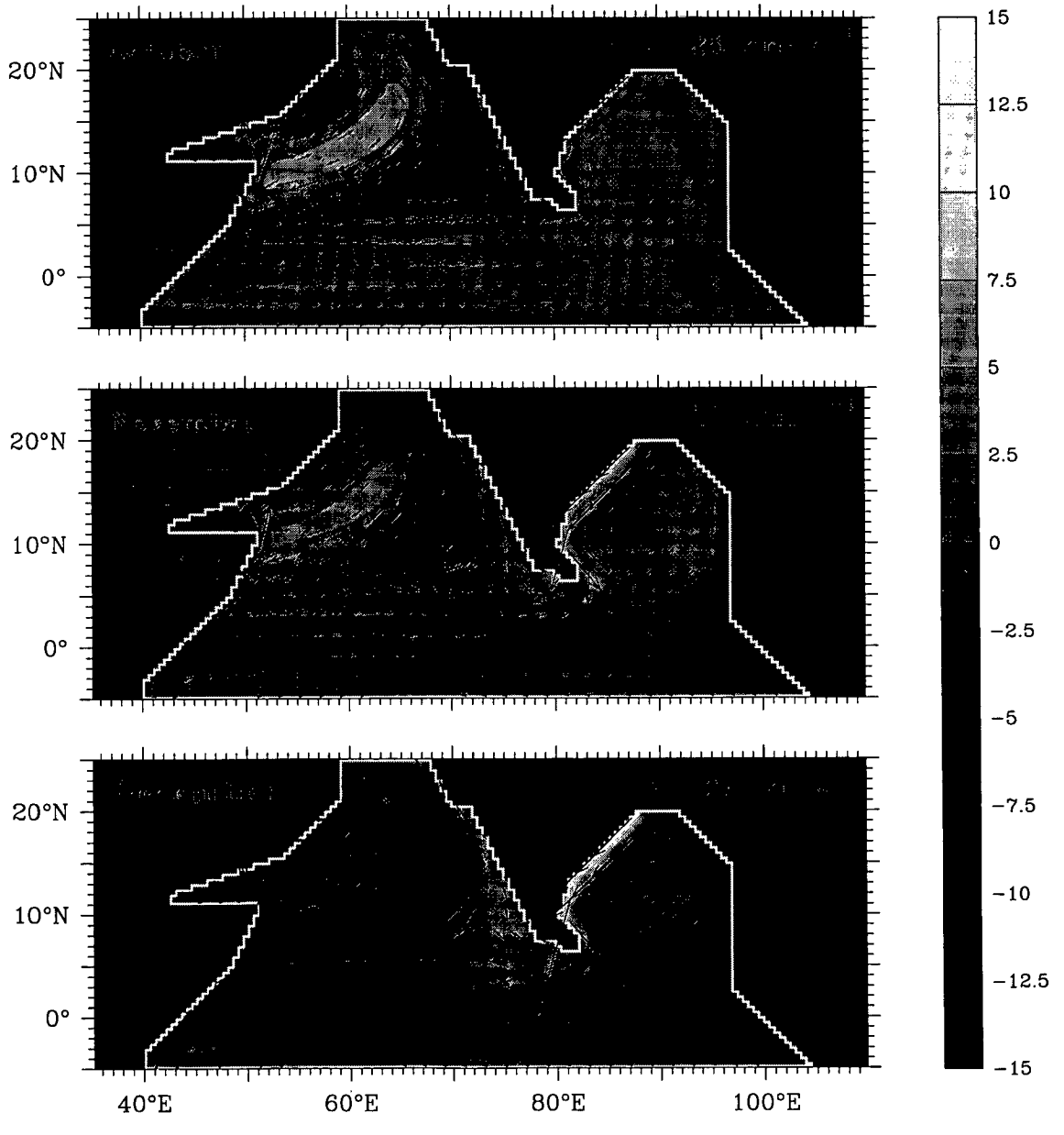

Figure 3.8 (continued) The role of remotely forced Kelvin waves. Sea-level deviation η (cm) and velocity $\mathbf{v}$ (cm s^{-1}) are shown for the linear simulation forced by an oscillatory current at the northern boundary of the Bay of Bengal. The Kelvin wave along the east coast bends around Sri Lanka to propagate poleward along the west coast, radiating westward propagating Rossby waves in the process. The high off southwest India is the result of the coastal Kelvin wave and the Rossby waves. It drifts westward together with the Rossby waves that constitute it, spreading across the southern Arabian Sea by March.

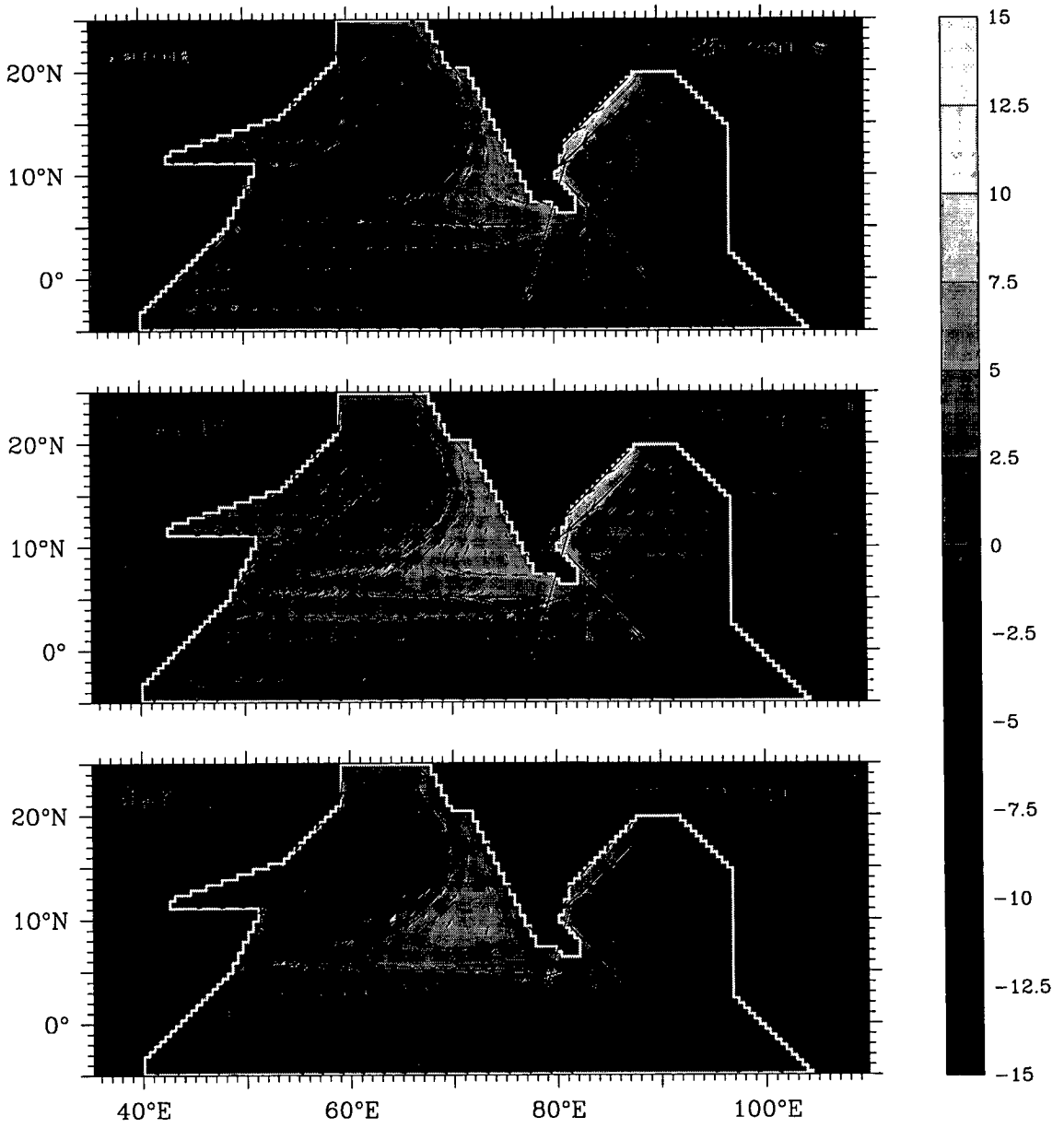

Kelvin wave manifests all along the coastline and the equatorward EICC bends around Sri Lanka to flow on as a poleward WICC. Radiation of Rossby waves weakens the WICC off southwest India even as the equatorward EICC peaks (1 January). By February, there is a weak equatorward, upwelling-favourable current off southwest India, closing the circulation around a high. This cycle of events comes to a close by March, when the high drifts westward together with the Rossby waves that constitute it, spreading across the southern Arabian Sea; the Rossby wave signature now appears in the form of a westward current in the vicinity of 5°N and northeastward velocities to the north of this latitude. By the end of March, the inflow in the northern bay vanishes; outflow starts on 1 April, beginning the second half of the annual cycle. This leads to a low off southwest India in August.

Thus, in these experiments, a Kelvin wave along the east coast of India, the model EICC, leads to a symphony of highs and lows off southwest India, these patterns then propagating offshore as Rossby waves.

3.4.2 Analytic Solution

We now obtain a simple analytic solution to show that all the crucial elements of the observed high and low and the associated currents along the west coast of India are contained in coastal Kelvin and equatorial Rossby waves, both of which arise from linear dynamics on an equatorial β-plane. We use the linearized reduced-gravity model without wind stress forcing and replace Laplacian friction by Rayleigh friction. The equations, derived in Appendix A, are

$$\imath\omega u - fv + g\overline{\Gamma}h_x = 0, \tag{3.3a}$$

$$\imath\omega v + fu + g\overline{\Gamma}h_y = 0, \tag{3.3b}$$

$$\imath\omega h + \overline{H}\,(u_x + v_y) = 0, \tag{3.3c}$$

$$\eta = \overline{\Gamma}h, \tag{3.3d}$$

where $H = \overline{H} + h$, $c = (g\overline{\Gamma H})^{\frac{1}{2}}$ is the speed of the Kelvin wave, and

$$\imath\omega = \frac{\partial}{\partial t} + r = \imath\sigma + r. \tag{3.4}$$

r is the Rayleigh friction coefficient and has units of s^{-1}; it is equivalent to Ac_n^{-2} in McCreary [1981] and Shankar and Shetye [1997].

The boundary condition in the meridional direction is that there are no sources of energy at high latitudes: no energy is brought into the ocean by a high-latitude source of Kelvin waves. At the eastern boundary, we impose the condition

$$u(0,y,t) = \Re\left[u_0 e^{-\delta_1(\zeta-\zeta_0)^2+\imath\omega t}\right], \tag{3.5}$$

where $\zeta = \alpha_0 y$, $\alpha_0^2 = \beta/c$, and $\delta_1 > 0$.

For sufficiently large δ_1, (3.5) represents a narrow zonal flow into or out of the domain, the zonal velocity being nearly zero a short distance north or south of the axis of symmetry y_0. The $u \approx 0$ condition to the north of the flow mimics a closed eastern boundary and represents the Indian west coast; the $u \approx 0$ condition to the south of the flow mimics an open boundary with negligible flow and represents the open ocean to the south of Sri Lanka (see Figure 3.9).

Figure 3.9 The eastern boundary condition for the analytic solution, showing $u(0,y,0)$ (cm s^{-1}) for the Gaussian profile in (3.5) (solid curve) and for periods $T = 360$ days (dashed curve) and $T = 30$ days (dotted curve). 7500 meridional modes were summed over to obtain the dashed and dotted curves, which merge in the region where velocity is not negligible, indicating the degree of accuracy achieved in satisfying the eastern boundary condition. At the eastern boundary, the dashed portion is open and the rest is closed.

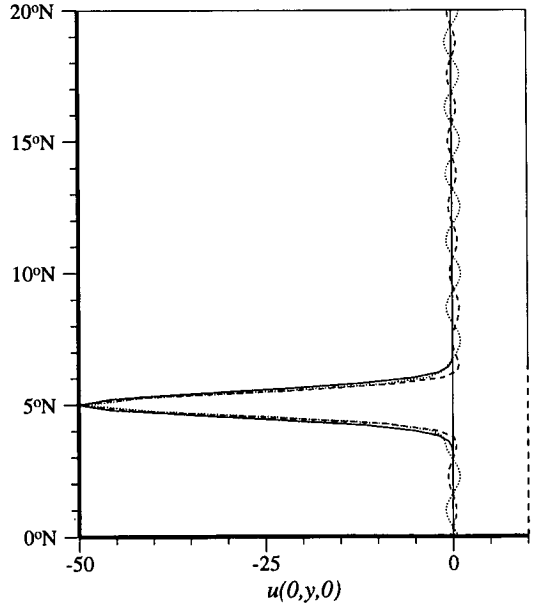

The homogeneous solution to (3.3), subject to the condition (3.5), is given by [McCreary, 1980, 1981]

$$u_m = B_m\left[K_m\phi_{m+1} - \phi_{m-1}\right]e^{\imath k_m(x-x_e)}, \tag{3.6a}$$

$$v_m = B_m \left[\left(\frac{\iota}{c\alpha_0} \right) \frac{(ck_m - \omega)}{(m/2)^{\frac{1}{2}}} \phi_m \right] e^{\iota k_m (x - x_e)}, \tag{3.6b}$$

$$h_m = B_m \left(\frac{c}{g\overline{\Gamma}} \right) [K_m \phi_{m+1} + \phi_{m-1}] e^{\iota k_m (x - x_e)}, \tag{3.6c}$$

where $m = 1, 2, 3, \ldots$; x_e represents the eastern boundary,

$$K_m = \left(\frac{ck_m - \omega}{ck_m + \omega} \right) \left(\frac{m+1}{m} \right)^{\frac{1}{2}},$$

$$k_m = \frac{\beta}{2\omega} \left(1 - \left[1 - \frac{4\omega^2}{\beta^2} \left(\alpha_m^2 - \frac{\omega^2}{c^2} \right) \right]^{\frac{1}{2}} \right),$$

and $\alpha_m = \alpha_0 (2m+1)$. The ϕ_m are the normalized Hermite functions, given by [McCreary, 1981]

$$\phi_m(\zeta) = \frac{(-1)^m}{(2^m m! \pi^{\frac{1}{2}})^{\frac{1}{2}}} e^{\zeta^2/2} \frac{d^m}{d\zeta^m} e^{-\zeta^2}. \tag{3.7}$$

$m = -1$ and $m = 0$ represent the equatorial Kelvin and Yanai waves in the terminology used by McCreary [1981]; both propagate eastward and hence, $B_{-1} = B_0 = 0$. The coefficients with $m \geq 1$ represent westward propagating Rossby waves with complex wavenumber k_m. Since

$$u(0, y, t) = \Re \left[\sum_{m=1}^{M} u_m e^{\iota \omega t} \right], \tag{3.8}$$

and the ϕ_m are orthogonal functions, we multiply both sides of (3.5) and (3.8) by ϕ_m and integrate over $\zeta = (-\infty, \infty)$ to obtain the relation

$$B_m = K_{m-2} B_{m-2} - u_0 (2\pi\delta_2)^{\frac{1}{2}} (1 - 2\delta_2)^{(m-1)/2} e^{(\zeta_{00}^2 - \delta_1 \delta_2 \zeta_0^2)} \phi_{m-1}(\zeta_{00}), \tag{3.9}$$

where

$$\delta_2 = \frac{1}{2(\delta_1 + \frac{1}{2})},$$

$$\zeta_{00} = \frac{2\delta_1 \delta_2 \zeta_0}{(1 - 2\delta_2)^{\frac{1}{2}}},$$

and we have used [Gradshteyn and Ryzhik, 1965, p. 838]

$$\int_{-\infty}^{\infty} e^{\frac{-(\zeta-\zeta_1)^2}{2\delta_2}} H_m(\zeta)d\zeta = (2\pi\delta_2)^{\frac{1}{2}}(1-2\delta_2)^{\frac{m}{2}} H_m\left[\frac{\zeta_1}{(1-2\delta_2)^{\frac{1}{2}}}\right], \tag{3.10a}$$

where $\zeta_1 = 2\delta_1\delta_2\zeta_0$ and

$$H_m(\zeta) = (-1)^m e^{\zeta^2}\frac{d^m}{d\zeta^m}e^{-\zeta^2}. \tag{3.10b}$$

The recursion relation [McCreary, 1981]

$$\zeta\phi_m(\zeta) = \left(\frac{m+1}{2}\right)^{\frac{1}{2}}\phi_{m+1}(\zeta) + \left(\frac{m}{2}\right)^{\frac{1}{2}}\phi_{m-1}(\zeta) \tag{3.10c}$$

and (3.9) are used to estimate the complex coefficients B_m, which when substituted in (3.6) give the required solution.

We compute the solution for the parameters $\overline{H} = 100$ m and $\overline{\Gamma} = 0.0035$, which imply $c = 185$ cm s^{-1}, and $r = 2.1 \times 10^{-9}$ s^{-1}. The solution is not sensitive to the choice of r. To prescribe the eastern boundary condition (3.5), we choose $\delta_1 = 20$, $y_0 = 5°$N, and $u_0 = -40$ cm s^{-1}. Accurate reproduction of the Gaussian velocity profile requires a large value of M in (3.8); the degree of accuracy achieved in satisfying the boundary condition using $M = 7500$ is shown in Figure 3.9.

The solution for a zonal current oscillating with a period $T = 2\pi\sigma^{-1} = 360$ days is shown in Figure 3.10. In the solution, $t = 0$ corresponds to 1 January, when the flow into the basin, the model EICC[9], peaks. Figure 3.10 depicts how η and $\mathbf{v}$ evolve during one half of an annual cycle. The close resemblance of the analytic solution to the evolution depicted in Figure 3.8 implies that it captures the essential elements of the dynamics. As in the numerical experiment with a boundary forcing in lieu of wind stress, the current at the coast reverses to flow equatorward and a high forms by 1 January, when the inflow into the basin peaks. The changes in current and sea level propagate into the open sea. A low forms in like fashion during the second half of the cycle.

The solution for a zonal current of period 60 days is shown in Figure 3.11. The pattern of evolution is virtually identical to that for the annual harmonic. Figure 3.11, however, illustrates two aspects of the dynamics not evident in Figure 3.10. First, the time scale associated with the evolution is a sixth that for the annual harmonic; consequently, the zonal length scale (equal to the product of T and the Rossby wave speed) of patterns seen in the solution is much smaller. Therefore, a series of highs and lows are spread zonally, one high and one low forming at the eastern boundary during one cycle of period T and then migrating westward. Second, the Rossby waves are trapped south of a critical latitude

$$y_c = \frac{c}{2\sigma}. \tag{3.11}$$

[9]Strictly, it is the NMC or the SMC that the zonal current represents.

Propagating Rossby waves cannot exist poleward of the critical latitude[10], which is 7° for T = 60 days. The critical latitude for T = 360 days is 42°, well to the north of the northern boundary of the Arabian Sea; therefore, the waves are not trapped in Figures 3.8 and 3.10.

An extreme case of trapping is shown in Figure 3.12, which depicts the solution for T = 30 days. The critical latitude for this period is 3.5°, to the south of the axis of the zonal current at the eastern boundary. Therefore, Rossby wave radiation is impossible, and the high and low do not form; the zonal flow is deflected north and propagates as a coastal Kelvin wave.

Rossby-wave trapping implies that the location of the southern tip of Sri Lanka is crucial in determining the period of oscillations that will migrate westward into the Arabian Sea from the west coast of the India. At the southern tip of Sri Lanka, 6°N, the critical period is 52 days. Only those disturbances from the Bay of Bengal that have a larger period can generate westward propagating Rossby waves and contribute to the high and low; those with smaller periods will remain trapped at the west coast of Sri Lanka and India. This critical period, however, depends on the Kelvin wave speed c, which depends on stratification and, hence, is a function of time and space[11]. Therefore, the partition between disturbances that are trapped at the coast and those that propagate offshore will not be defined as sharply as in this simple model.

The location of the southern tip of Sri Lanka, at about 6°N, is crucial for another reason too. The internal radius of deformation at this latitude is about 200 km; the radius of deformation at the equator, the e-folding length scale of the equatorial Kelvin wave, is about 300 km. Therefore, the coastal waveguide in which the Kelvin wave propagates is distinct from the equatorial waveguide. This permits the Kelvin waves from the Bay of Bengal to pass unhindered into the Arabian Sea, linking the dynamics of the two basins.

The equatorial waveguide is connected to the bay at its eastern boundary. This link arises as a consequence of the reflection of the equatorial Kelvin wave at the eastern boundary of the basin; the reflected wave is a summation over several meridional modes of the westward propagating Rossby wave, these being required to satisfy the condition of no normal flow at the boundary [Moore, 1968]. The higher meridional modes were shown by Moore to be equivalent to a coastal Kelvin wave, which carries a part of the incident energy poleward along the coast in both hemispheres. This Kelvin wave is trapped at the coast poleward of the critical latitude; equatorward of this latitude, westward radiation of energy is possible, and the coastal Kelvin wave is inseparable from the Rossby wave. The same phenomenon is seen off the Indian west coast. For the seasonal cycle, it is the annual and semiannual harmonics that are most important. The critical latitudes for these periods are 42° and 21°, respectively; the former lies poleward of the northern boundary

[10]The critical latitude is actually smaller (farther south) for the Indian west coast because the boundary is not meridional [Clarke and Shi, 1991]. The critical latitude for a non-meridional boundary is $y_c = \frac{c\cos\theta}{2\sigma}$, where θ is the deviation of the coast from the meridian. For the Indian west coast, $\theta \approx 18°$, which gives a factor of 0.95.

[11]Shankar and Shetye [1997] obtained different values for the critical latitude and period because they used a higher value of c (250 cm s^{-1}).

Figure 3.10 Analytic solution for $T = 360$ days (annual harmonic). Sea-level deviation η (cm) and velocity $\mathbf{v}$ (cm s^{-1}) are plotted for half the annual cycle. As in Figure 3.8, the current at the coast reverses to flow equatorward and a high forms by 1 January, when the inflow into the basin peaks. The changes in current and sea level propagate into the open sea. A low forms in like fashion during the second half of the cycle.

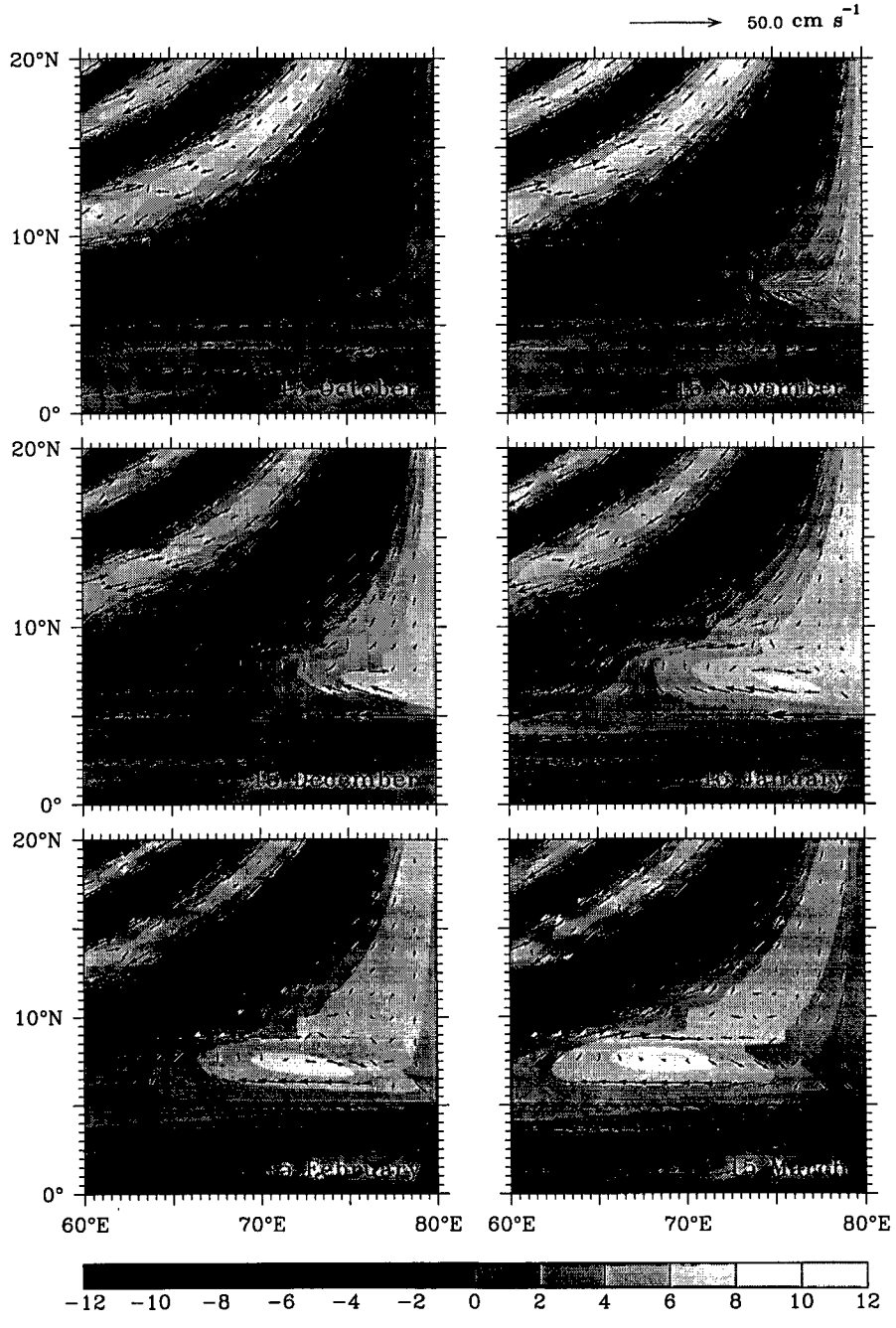

Figure 3.11 Analytic solution for $T = 60$ days; time $t = 0$ and 30 (1 January and 1 February). Sea-level deviation η (cm) and velocity $\mathbf{v}$ (cm s^{-1}) are plotted. A series of highs and lows form at the eastern boundary and propagate westward as Rossby waves; the waves are trapped at the coast north of 7°N.

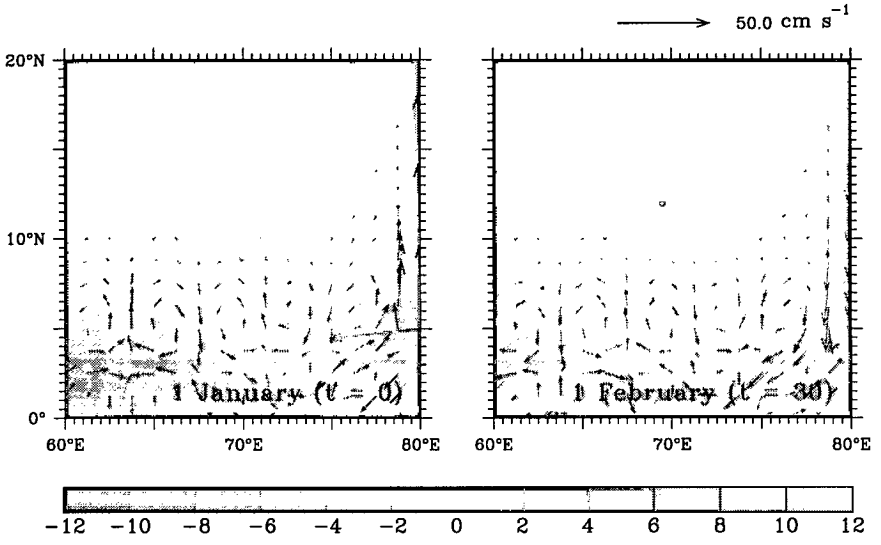

Figure 3.12 Analytic solution for $T = 30$ days; time $t = 0$ and 15 (1 and 16 January). Sea-level deviation η (cm) and velocity $\mathbf{v}$ (cm s^{-1}) are plotted. For a period of 30 days, the critical latitude is 3.5°, to the south of the axis of the zonal current at the eastern boundary. Therefore, Rossby wave radiation is impossible and the high and low do not form.

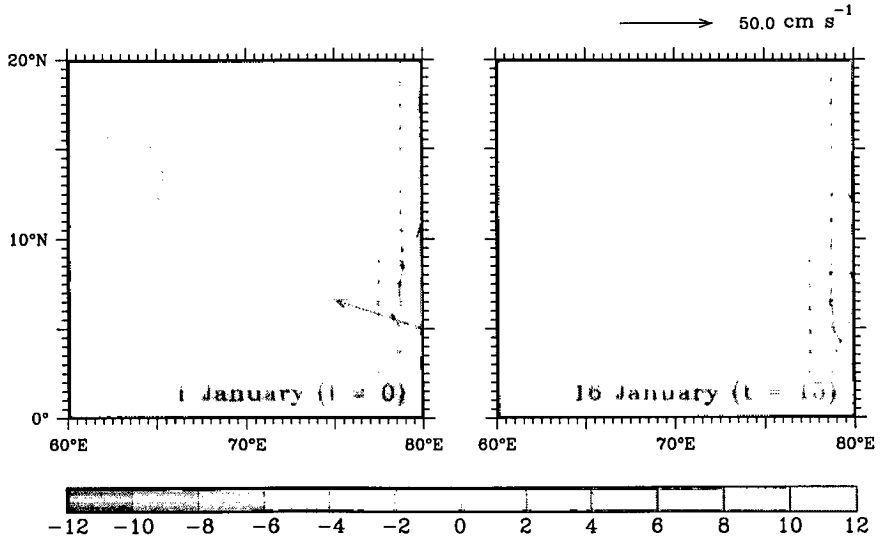

of the basin, and the latter is close to it. Hence, both annual and semiannual Kelvin waves are inseparable from westward propagating Rossby waves in the Bay of Bengal and the Arabian Sea, and energy leaks at these periods from the eastern boundary into the open ocean[12].

3.5 Forcing Mechanisms

The leaky waveguide in the north Indian Ocean makes the Kelvin wave off the east coast of India more complex than the one discussed in Section 3.4; it is the result of Kelvin waves of different frequencies and phases forced by several mechanisms. McCreary et al. [1996] identified three such mechanisms: local alongshore winds (LA) adjacent to the east coasts of India and Sri Lanka, remote alongshore winds (RA) adjacent to the eastern and northern boundaries of the bay [McCreary et al., 1993], and remote forcing from the equatorial waveguide (EQ) [Potemra et al., 1991; Yu et al., 1991]. The resultant Kelvin wave, on reaching the west coast of India, is modified by the local alongshore winds there (WLA), and the Rossby waves radiated from the coast are modified by Ekman pumping [Bruce et al., 1994, 1998]. In addition, the interaction of equatorial Rossby waves with the southern tip of India can also force Kelvin waves along the Indian west coast [Bruce et al., 1998]. All these processes contribute to the formation of the Lakshadweep high and low.

To isolate the effect of the processes on the Lakshadweep high and low and the WICC, two sets of boundary conditions are applied along continental boundaries [Shankar et al., 1996; McCreary et al., 1996]. One set is the usual no-slip condition

$$u = v = 0. \tag{3.12a}$$

The other set,

$$\tilde{u} = \mathbf{n}\cdot\mathbf{v} = -\mathbf{n}\cdot\mathbf{k}\times\frac{\tau}{f}, \quad \tilde{v} = \mathbf{k}\times\mathbf{n}\cdot\mathbf{v}, \tag{3.12b}$$

is applied to the boundaries of the Bay of Bengal and the west coast of India and Sri Lanka in three of the test solutions. In (3.12b), $\mathbf{k}$ is a unit vector directed out of the β-plane and $\mathbf{n}$ is a unit vector normal to the boundary that points into the bay (offshore) along its western and northern margins, out of the bay (inshore) along its northeastern and eastern margins, and out of the sea (inshore) along the southern boundaries of India and Sri Lanka and along their west coast; $\mathbf{v} = (\tilde{u}, \tilde{v})$, where $\tilde{u}$ and $\tilde{v}$ are the velocity components normal to and along the boundary; and $\tau = (\tau^x, \tau^y)$ is the wind stress. Conditions (3.12b) allow Ekman flows to pass through boundaries, and therefore circulations driven by coastal Ekman pumping are filtered out of the solutions.

[12] See Appendix B, Figure B.2.

The solutions for the processes LA, RA, and WLA are found analogous to McCreary et al. [1996]. The main, or control, run is the linear solution described in Section 3.3.3 (Figure 3.7), for which the condition (3.12a) is applied at continental boundaries. The modifications made to obtain the process solutions are described below.

3.5.1 Winds Along the East Coast of India and Sri Lanka (Process LA)

To isolate the effect of the strong winds that blow along the east coast of India and Sri Lanka, we apply conditions (3.12b) along this coast (from 87°E, 20°N to 82°E, 6.5°N), thereby eliminating the effect of the alongshore winds there. The difference between the main run and this run gives the process solution forced by LA (Figure 3.13).

The winds along the east coast are southwesterly during the southwest monsoon and northeasterly during the northeast monsoon. The southwest–northeast alignment of the coast makes the wind vector virtually parallel to the coast and these winds generate strong Kelvin waves; the EICC closely follows the wind field. Northeasterly winds, which force coastal downwelling, set in with the withdrawal of the southwest monsoon and the EICC reverses to flow equatorward. The Kelvin wave that forces this downwelling EICC also forces a downwelling WICC in November. The subsequent radiation of Rossby waves generates a high off southwest India in January, as in the main run, but the high forced by LA is much stronger. The weakening of the northeast monsoon after January forces coastal upwelling along the east coast; the upwelling intensifies with the onset of the southwest monsoon in May. This upwelling Kelvin wave generates a low off southwest India, but it is weaker than in the main run. Thus, the winds along the western boundary of the Bay of Bengal can force both the high and the low. These winds have a stronger impact on the WICC than they have on the EICC; by themselves, they cannot force the seasonal cycle of the EICC, but they can force the seasonal cycle of circulation off southwest India.

3.5.2 Winds Along the Eastern and Northern Boundaries of the Bay of Bengal (Process RA)

To isolate the effect of the winds that blow along the eastern and northern boundaries of the Bay of Bengal, we apply conditions (3.12b) along these coasts (from 97°E, 2.5°N to 87°E, 20°N), thereby eliminating the effect of the alongshore winds there. The difference between the main run and this run gives the process solution forced by RA (Figure 3.14).

These winds also force Kelvin waves, which propagate along the rim of the bay, radiating Rossby waves from the eastern boundary in the process. The Kelvin waves forced by these winds make a weak contribution to the EICC, forcing coastal upwelling during February–September and downwelling during October–January. Their effect on the high and low is also weak. Though

Figure 3.13 Effect of winds along the east coast of India and Sri Lanka (Process LA). Plots of sea-level deviation η (cm) and velocity $\mathbf{v}$ (cm s^{-1}) are shown. Process LA forces a high off southwest India in January; the high propagates westward, as in the main run. The low that formed during the southwest monsoon is also seen in the central Arabian Sea. Its reflection at the coast of Arabia forces an upwelling-favourable current there.

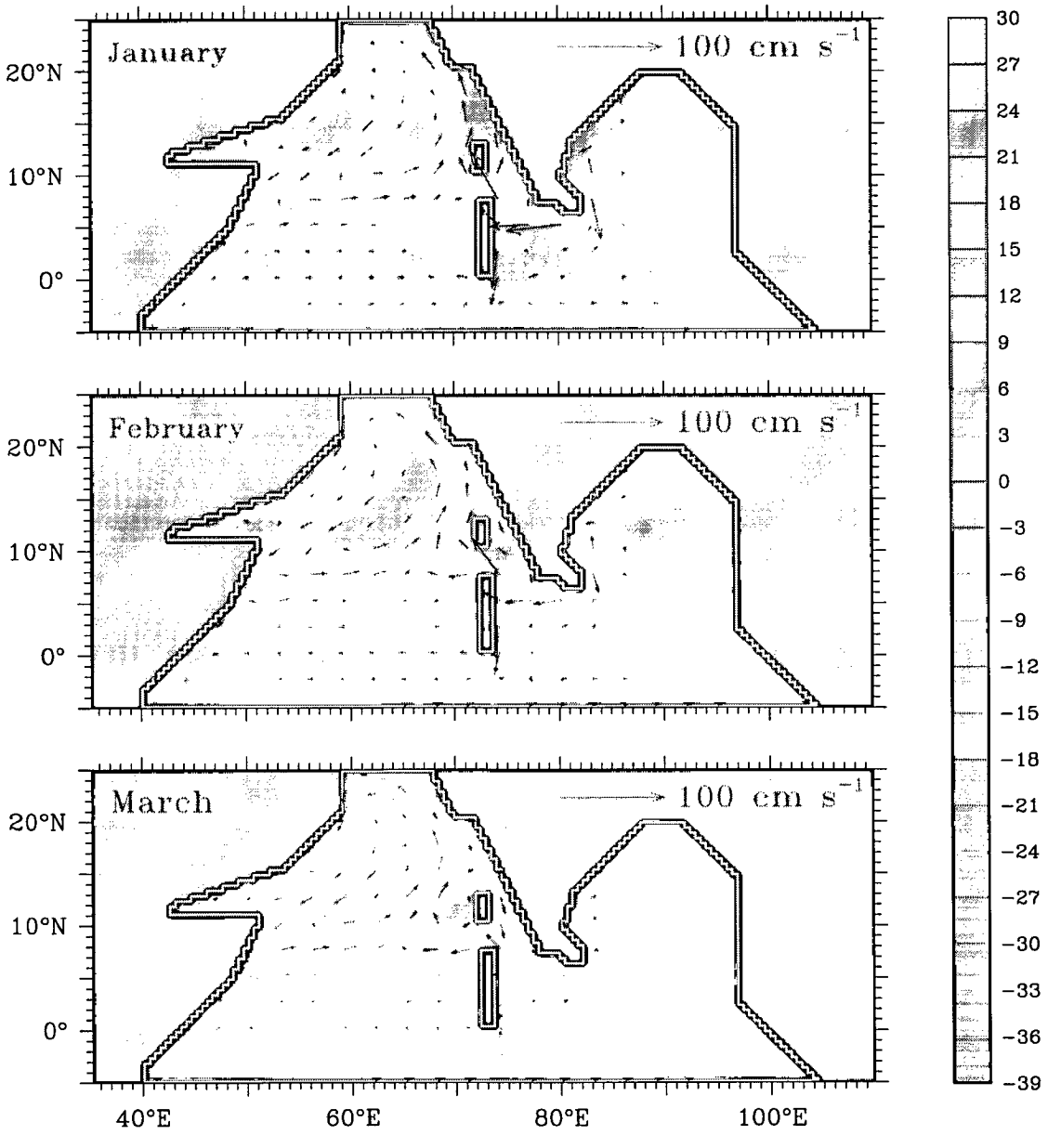

Figure 3.13 (continued) Effect of winds along the east coast of India and Sri Lanka (Process LA). Plots of sea-level deviation η (cm) and velocity $\mathbf{v}$ (cm s^{-1}) are shown. The Lakshadweep high propagates westward; in April, it is located to the west of the Lakshadweep islands. An equatorward WICC forms in May, and by June, the incipient Lakshadweep low is seen off southwest India. The Rossby waves that constitute the Lakshadweep high and low also have an effect on the circulation in the northwestern Arabian Sea.

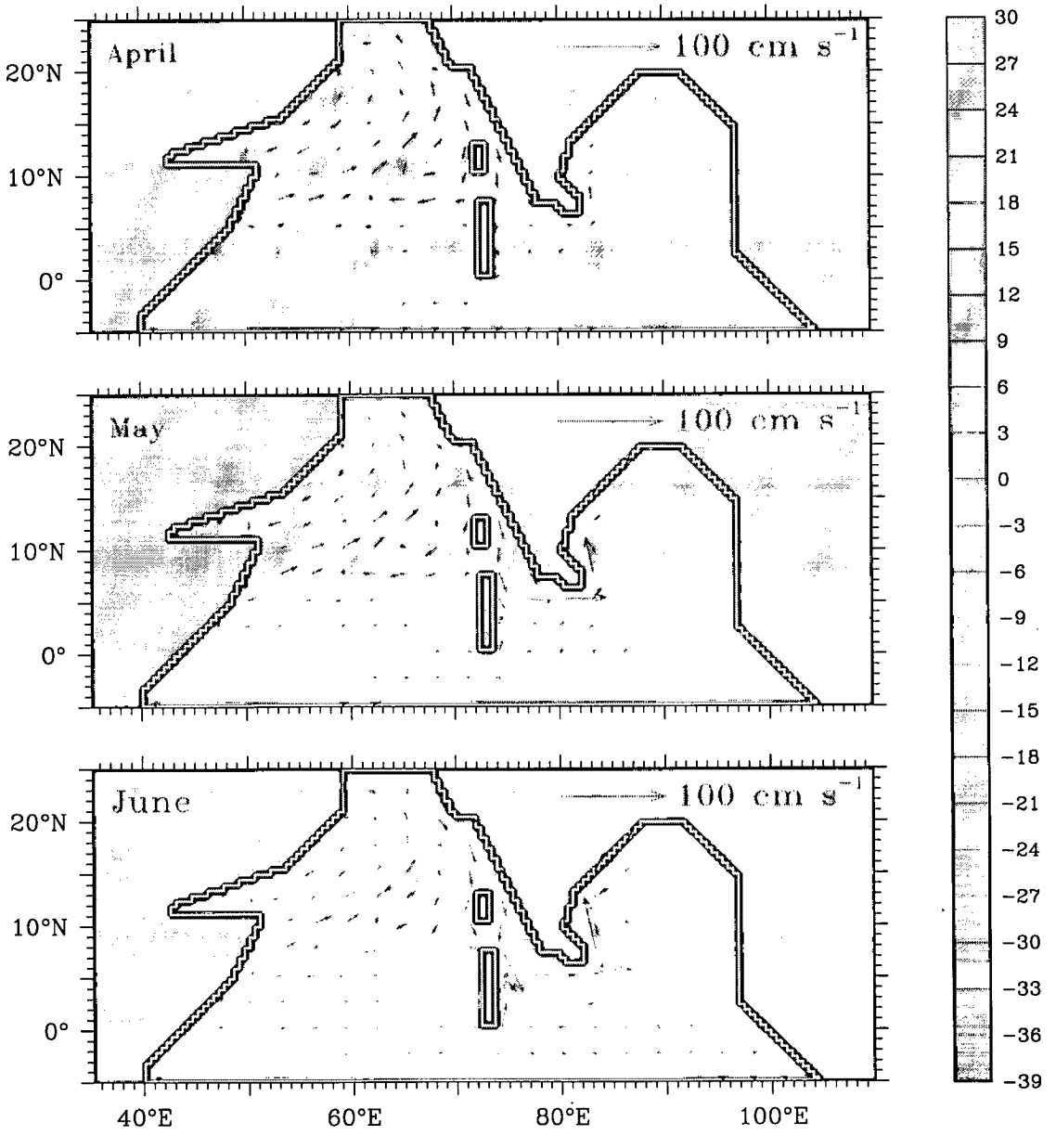

Figure 3.13 (continued) Effect of winds along the east coast of India and Sri Lanka (Process LA). Plots of sea-level deviation η (cm) and velocity $\mathbf{v}$ (cm s^{-1}) are shown. During the southwest monsoon, process LA forces a poleward EICC along the coast of India and Sri Lanka. This current is the continuation of the SMC, whose meandering structure in the Arabian Sea is associated with the Lakshadweep high and low.

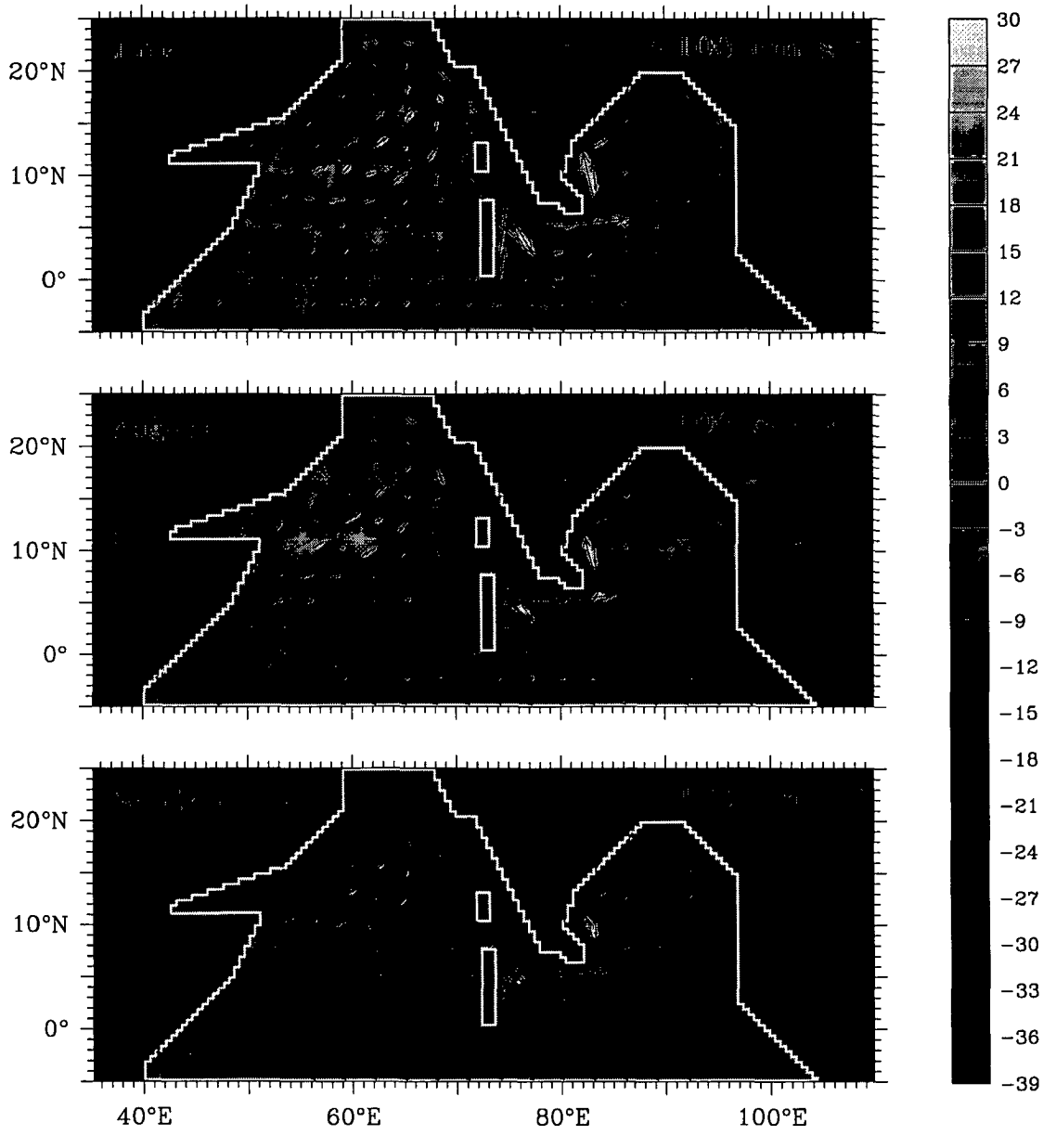

Figure 3.13 (continued) Effect of winds along the east coast of India and Sri Lanka (Process LA). Plots of sea-level deviation η (cm) and velocity $\mathbf{v}$ (cm s^{-1}) are shown. The winds along the east coast of India and Sri Lanka reverse after the collapse of the southwest monsoon, forcing an equatorward EICC. The EICC flows around Sri Lanka into the poleward WICC. By December, the incipient Lakshadweep high is seen off southwest India.

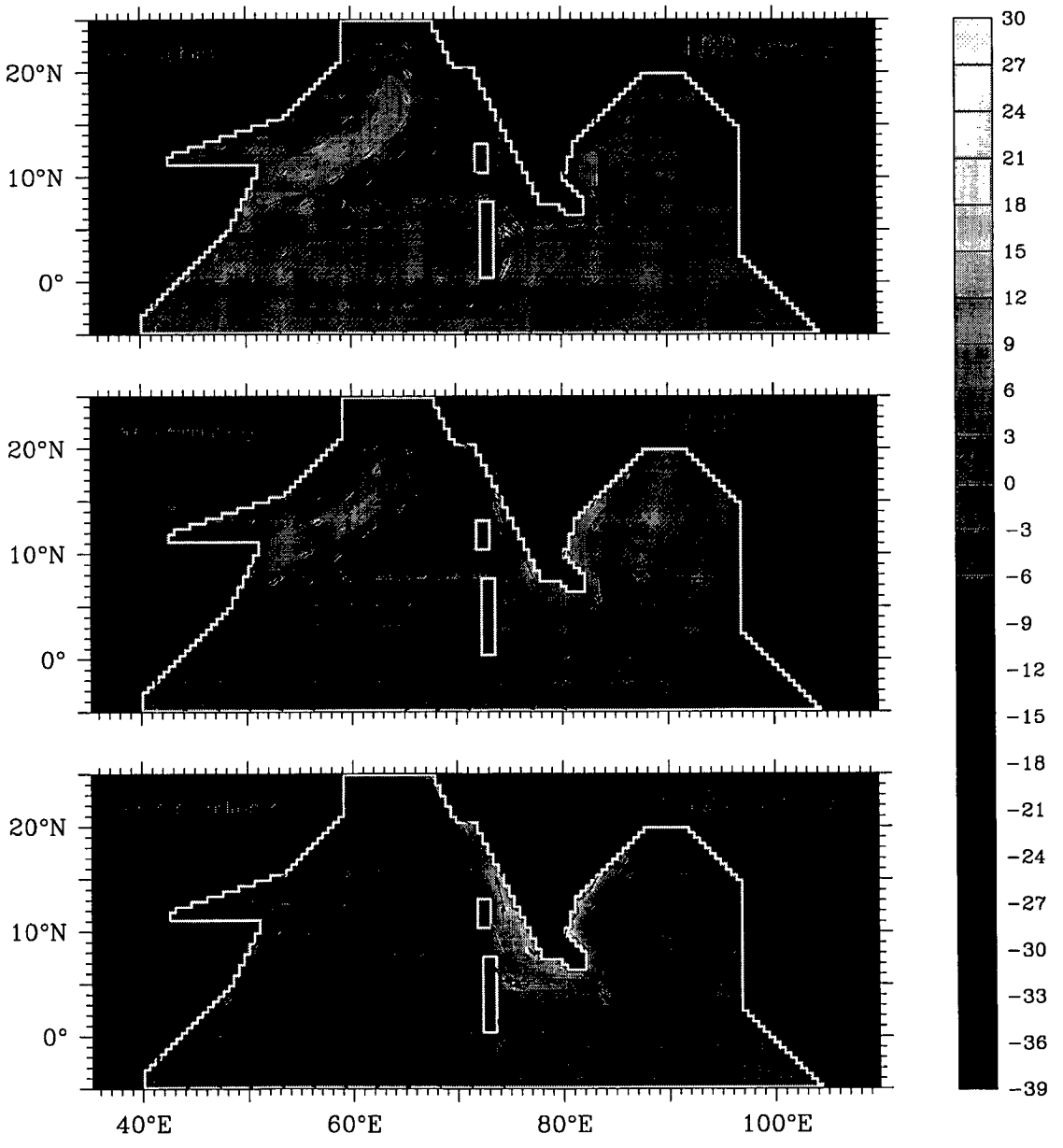

Figure 3.14 Effect of winds along the eastern and northern boundaries of the Bay of Bengal (Process RA). Bimonthly plots of sea-level deviation η (cm) and velocity $\mathbf{v}$ (cm s^{-1}) are shown. Though the winds along the eastern and northern boundaries of the bay are comparable to those along its western boundary, the response to them is weak because these winds blow almost normal to the coast, forcing a weak Kelvin wave.

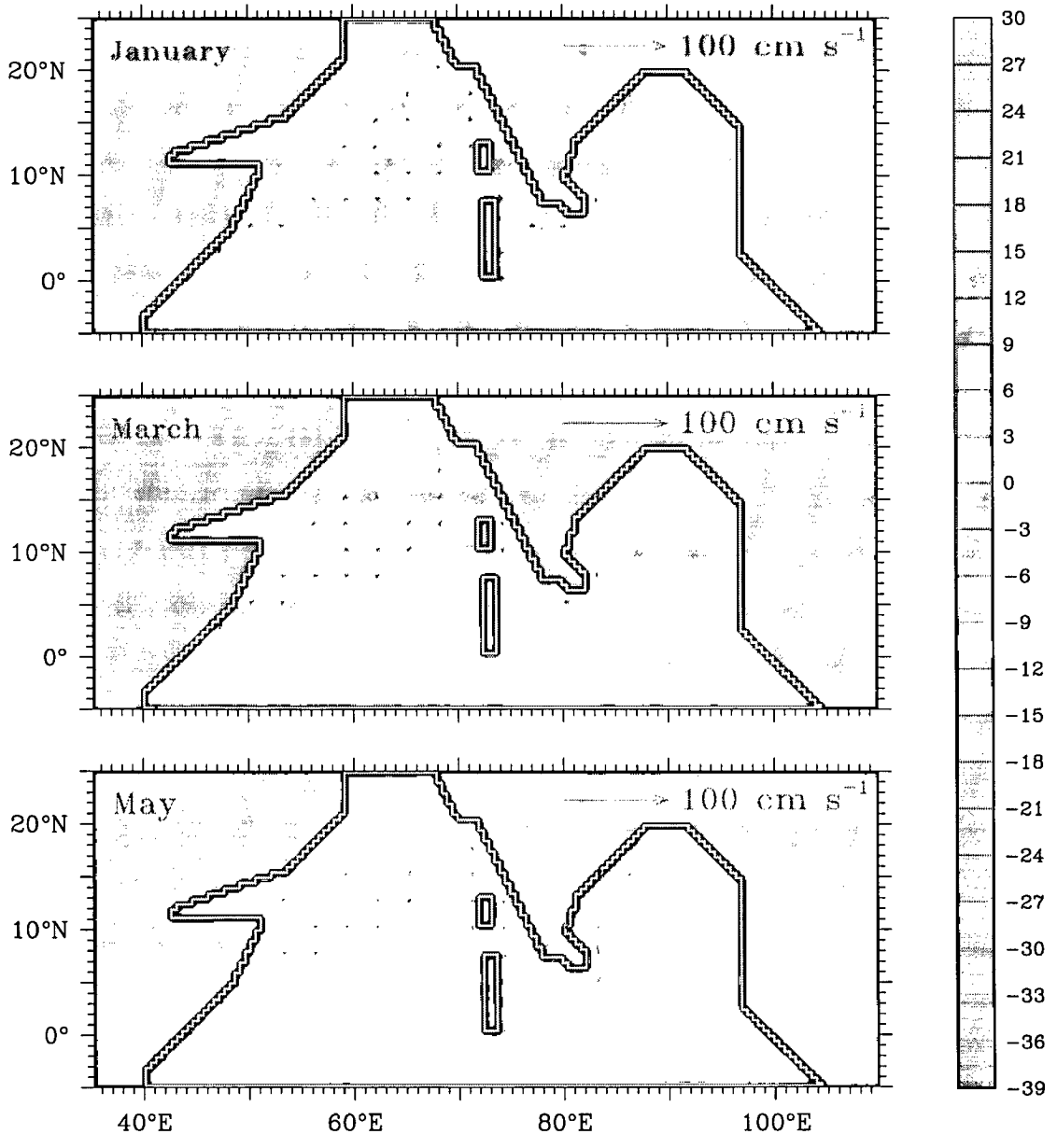

Figure 3.14 (continued) Effect of winds along the eastern and northern boundaries of the Bay of Bengal (Process RA). Bimonthly plots of sea-level deviation η (cm) and velocity $\mathbf{v}$ (cm s^{-1}) are shown. During the southwest monsoon, process RA forces a weak, poleward EICC, complementing process LA; the Kelvin waves that force this EICC also force a weak, equatorward WICC.

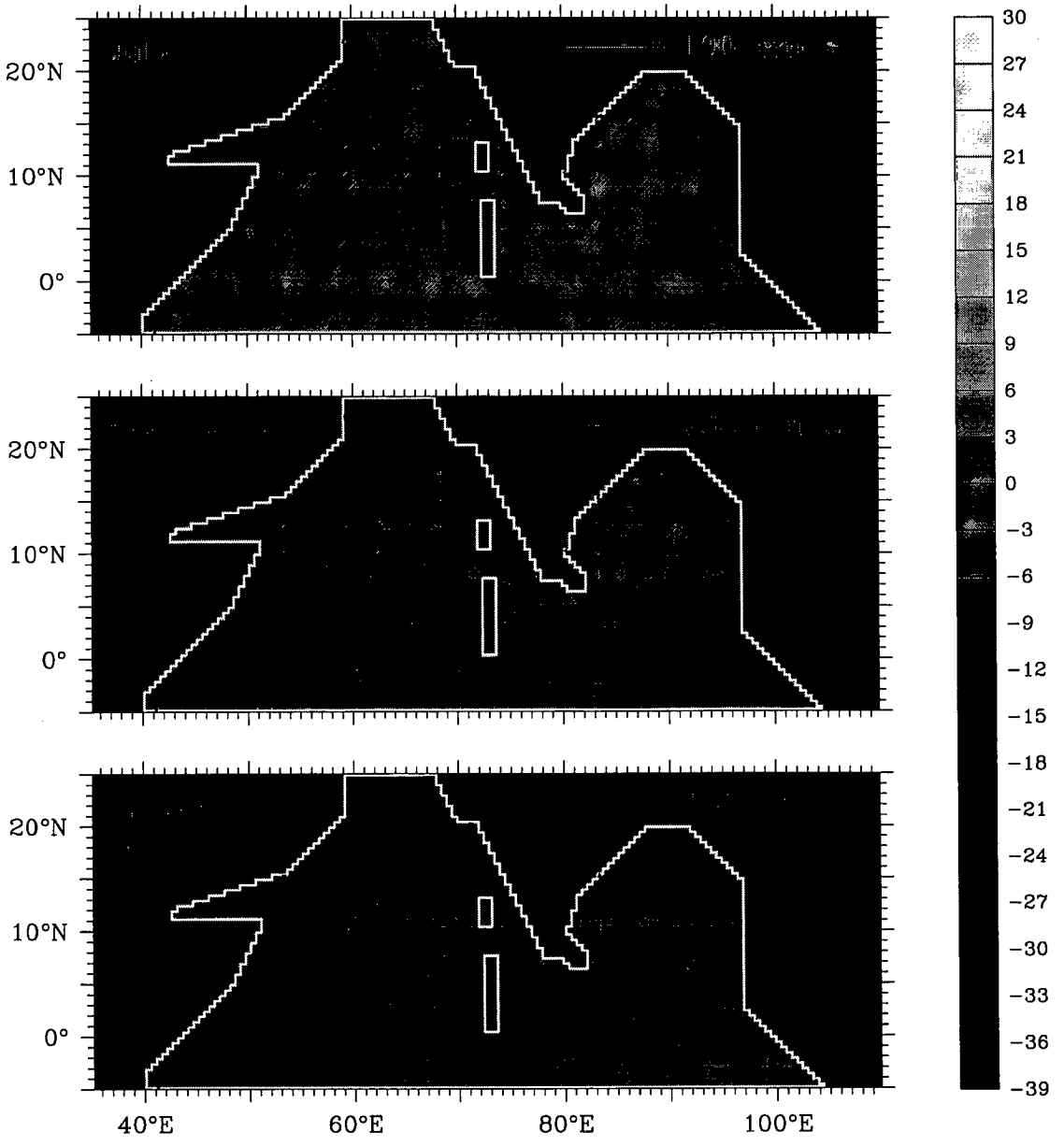

the effect of process RA is much weaker than that of LA, the winds in the eastern bay are not significantly weaker than those in the western bay; it is the alignment of the coast, almost normal to the wind vector, that results in a weak alongshore component, and hence, in a weak response.

3.5.3 Winds Along the West Coast of Sri Lanka and India (Process WLA)

To isolate the effect of the winds that blow along the west coast of Sri Lanka and India, we apply conditions (3.12b) along this coast (from 82°E, 6.5°N to 67.5°E, 25°N), thereby eliminating the effect of the alongshore winds there. The difference between the main run and this run gives the process solution forced by WLA (Figure 3.15).

Along this coast, the winds blow equatorward throughout the year, the winds along the west coast of Sri Lanka being the exception; here, the winds are similar to those along the Indian east coast. During the southwest monsoon, the southwesterlies over the Arabian Sea turn around in the central Arabian Sea to blow from the northwest along the Indian west coast. These winds favour coastal upwelling and are stronger than the equatorward winds during the northeast monsoon. The alignment of the coast also ensures that the winds during the northeast monsoon generate but a weak Kelvin wave. Therefore, though the winds along the eastern boundary of the Arabian Sea do not contribute significantly to the high, they force a low off southwest India and drive the strong upwelling off western and northwestern India during the southwest monsoon.

3.5.4 Other Processes (Processes OP)

The three process solutions described above show that Kelvin waves forced by winds blowing along the east and west coasts of India and Sri Lanka can force the Lakshadweep high and low. To examine the contribution of other processes, we apply conditions (3.12b) from (97°E, 2.5°N) to (67.5°E, 25°N), filtering out processes LA, RA, and WLA. The resulting model response is due to all other processes; these include equatorial Kelvin and Rossby waves, Ekman pumping in the Lakshadweep Sea, and the interaction of equatorial Rossby waves with the southern tip of India (Figure 3.16). The difference between the main run and this run gives the combined effect of LA, RA, and WLA (Figure 3.17).

When the effect of the winds along the coasts of India and Sri Lanka is filtered out of the response, the most striking discrepancies occur in the eastern and northern Arabian Sea. The other processes force but a weak "high" off southwest India. The low does not form during the southwest monsoon, downwelling occurring along most of the west coast instead. This distorts the circulation in the eastern, central, and northern Arabian Sea, with the SMC virtually disappearing to the west of Sri Lanka. This implies that the curious meandering structure of the SMC in the central Arabian Sea is a consequence of the Lakshadweep high and low and is forced by the winds along the coasts of India and Sri Lanka (Figure 3.17). To the east of Sri Lanka, however, the SMC

Figure 3.15 Effect of winds along the west coast of Sri Lanka and India (Process WLA). Plots of sea-level deviation η (cm) and velocity v (cm s^{-1}) are shown. The winds during the northeast monsoon blow normal to the west coast of India and force a weak Kelvin wave; hence, process WLA forces a weak high off southwest India. It has a stronger effect on the low, and the reflection of the low at the coast of Arabia forces an upwelling-favourable current there throughout the year.

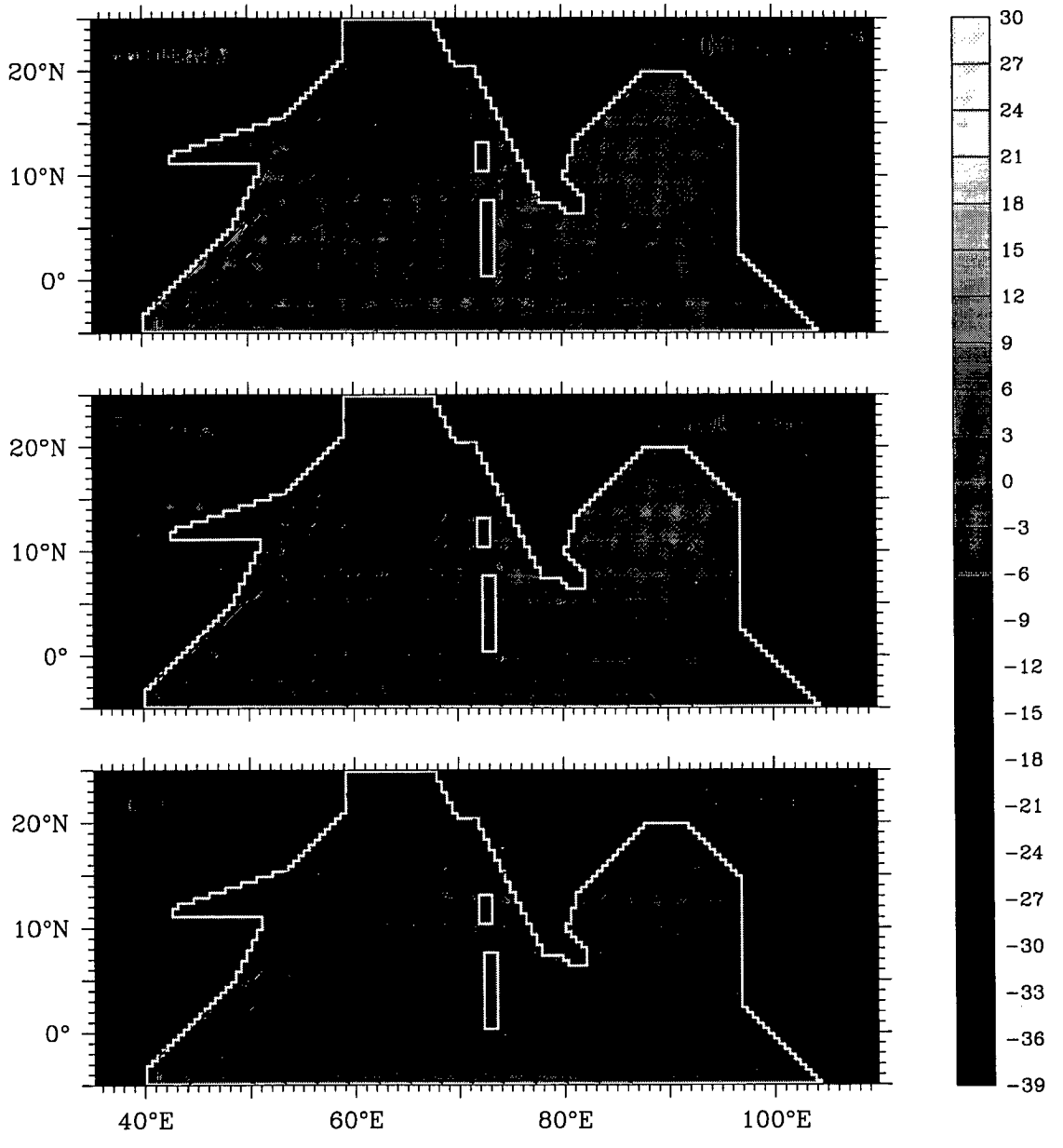

Figure 3.15 (continued) Effect of winds along the west coast of Sri Lanka and India (Process WLA). Plots of sea-level deviation η (cm) and velocity $\mathbf{v}$ (cm s^{-1}) are shown. The effect of the low forced by process WLA and its reflection at the western boundary of the Arabian Sea is felt even in April and May, when process WLA forces a poleward current along the coast of Somalia. This current forces upwelling in the northern part of the Somali coast even before the onset of the southwest monsoon.

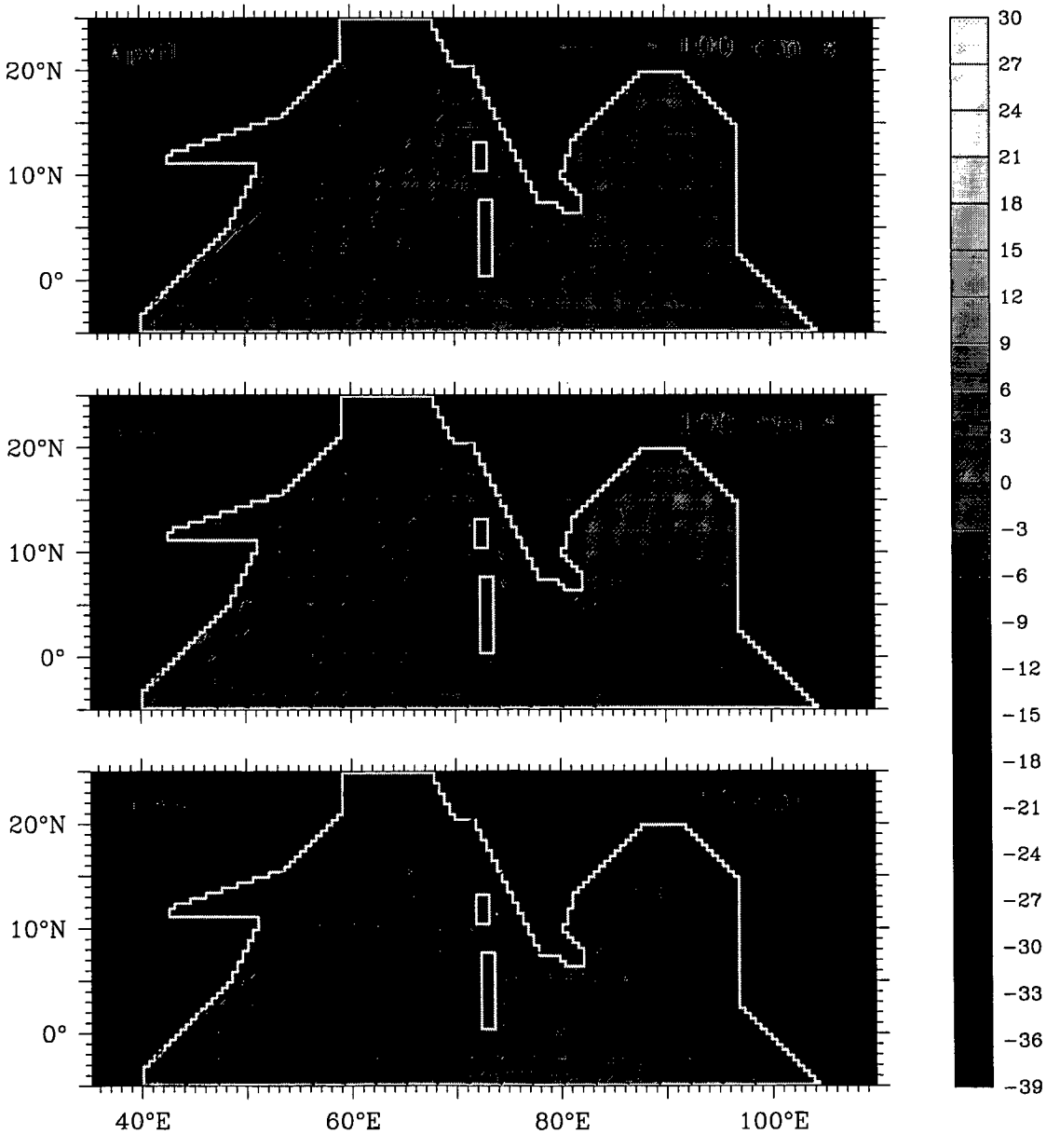

Figure 3.15 (continued) Effect of winds along the west coast of Sri Lanka and India (Process WLA). Plots of sea-level deviation η (cm) and velocity v (cm s^{-1}) are shown. The winds along the west coast of India and Sri Lanka force a low off southwest India by July. The WICC flows equatorward into the SMC. Though process WLA, like LA, can force the SMC, the relatively weak high forced during the northeast monsoon weakens the SMC in the central Arabian Sea.

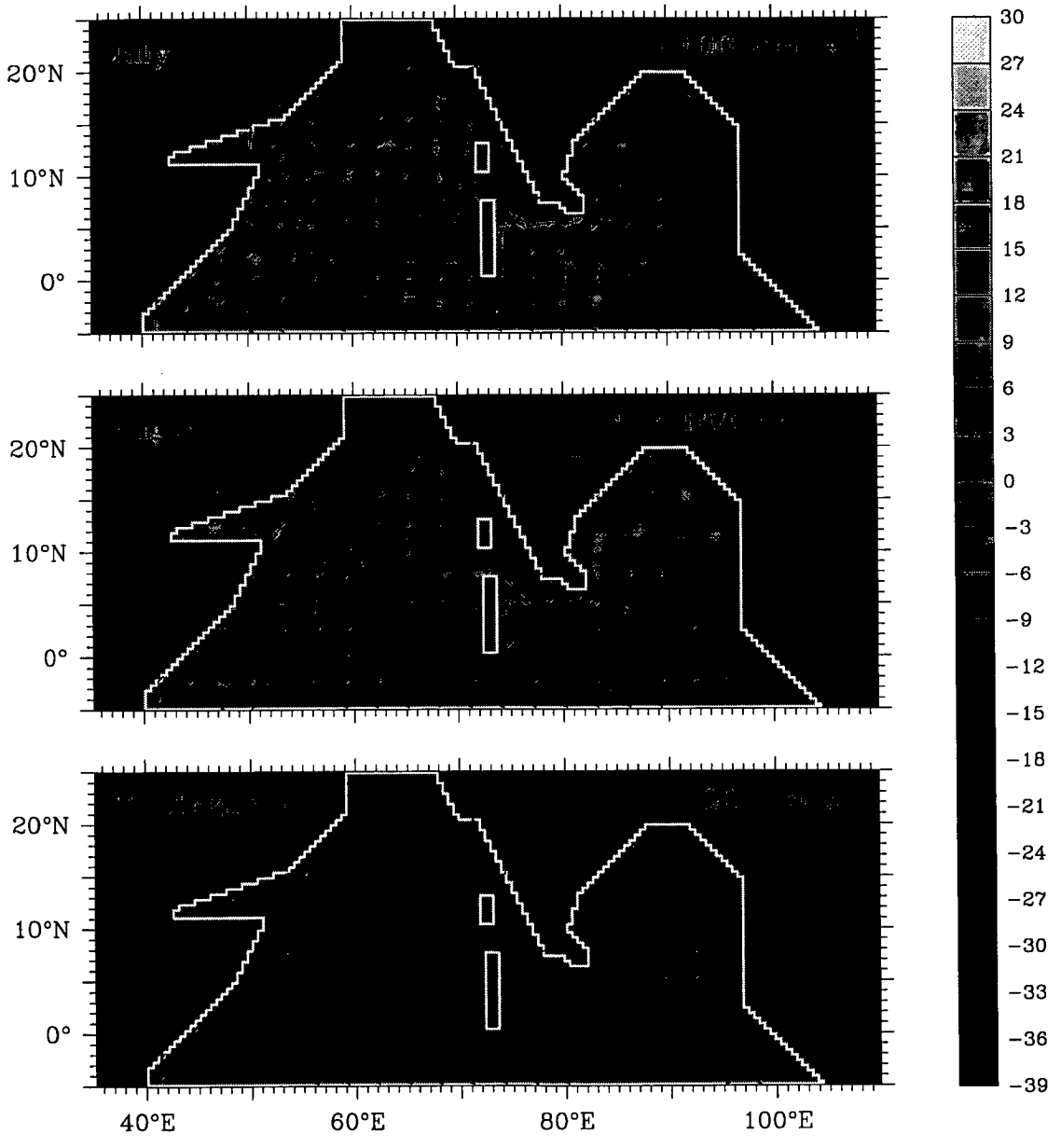

Figure 3.15 (continued) Effect of winds along the west coast of Sri Lanka and India (Process WLA). Plots of sea-level deviation η (cm) and velocity $\mathbf{v}$ (cm s^{-1}) are shown. By October, the low is located to the west of the Lakshadweep islands. The upwelling Kelvin wave forced by process WLA during the southwest monsoon propagates along the rim of the Arabian Sea, forcing upwelling off Arabia and Somalia in winter, opposing the downwelling forced by the local winds.

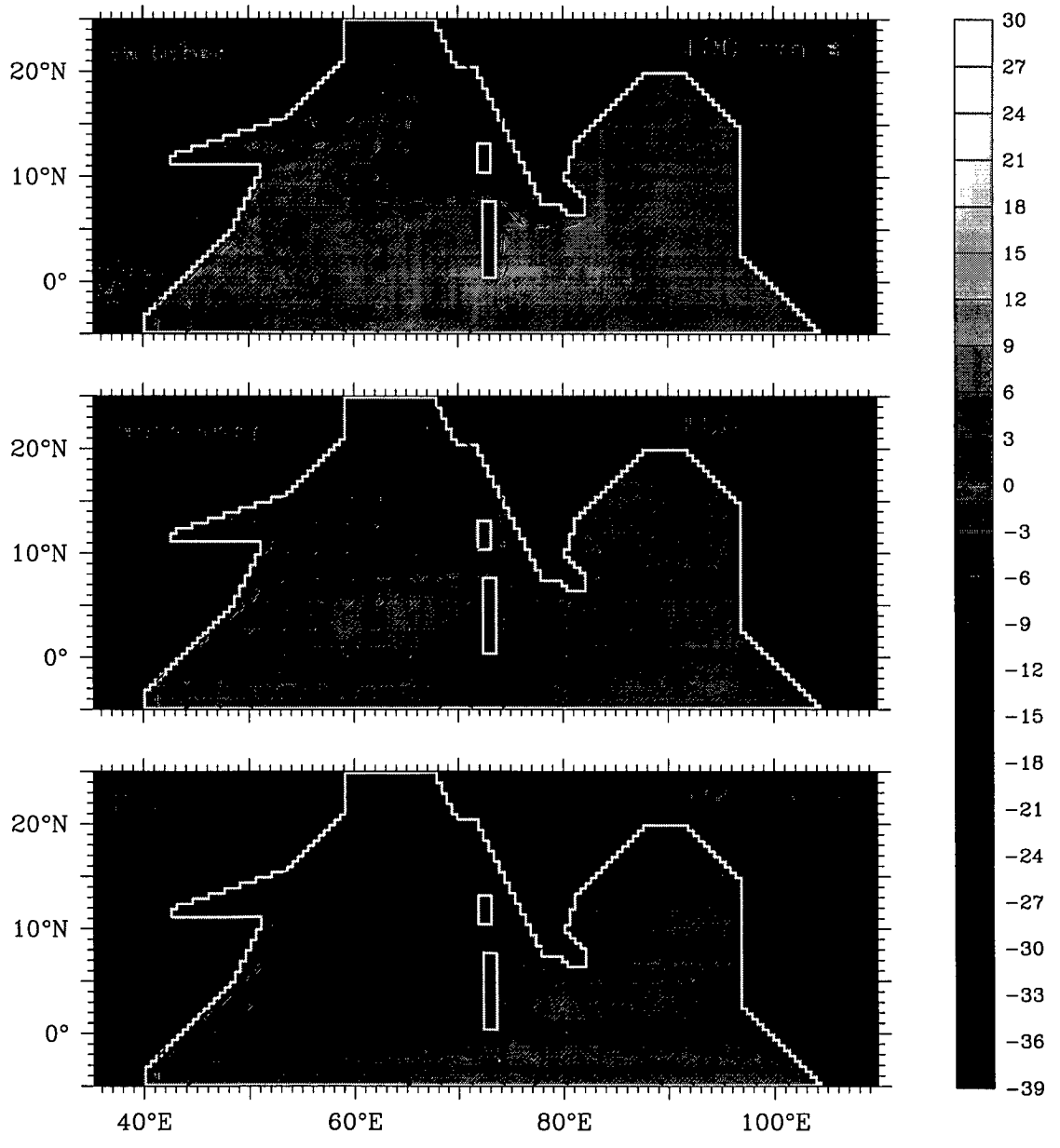

Figure 3.16 Effect of other processes (Processes OP). The effect of processes LA, WLA, and RA has been filtered out of the response. Plots of sea-level deviation η (cm) and velocity $\mathbf{v}$ (cm s^{-1}) are shown. Eliminating the Kelvin waves forced by the alongshore winds in the Bay of Bengal and the eastern Arabian Sea weakens the high off southwest India. Instead, a stronger anticyclonic circulation, with a high in sea level, is seen in the northern Arabian Sea. These processes, however, are responsible for forcing the circulation in the Bay of Bengal throughout the year; the only exception is the EICC, which is also affected by process LA.

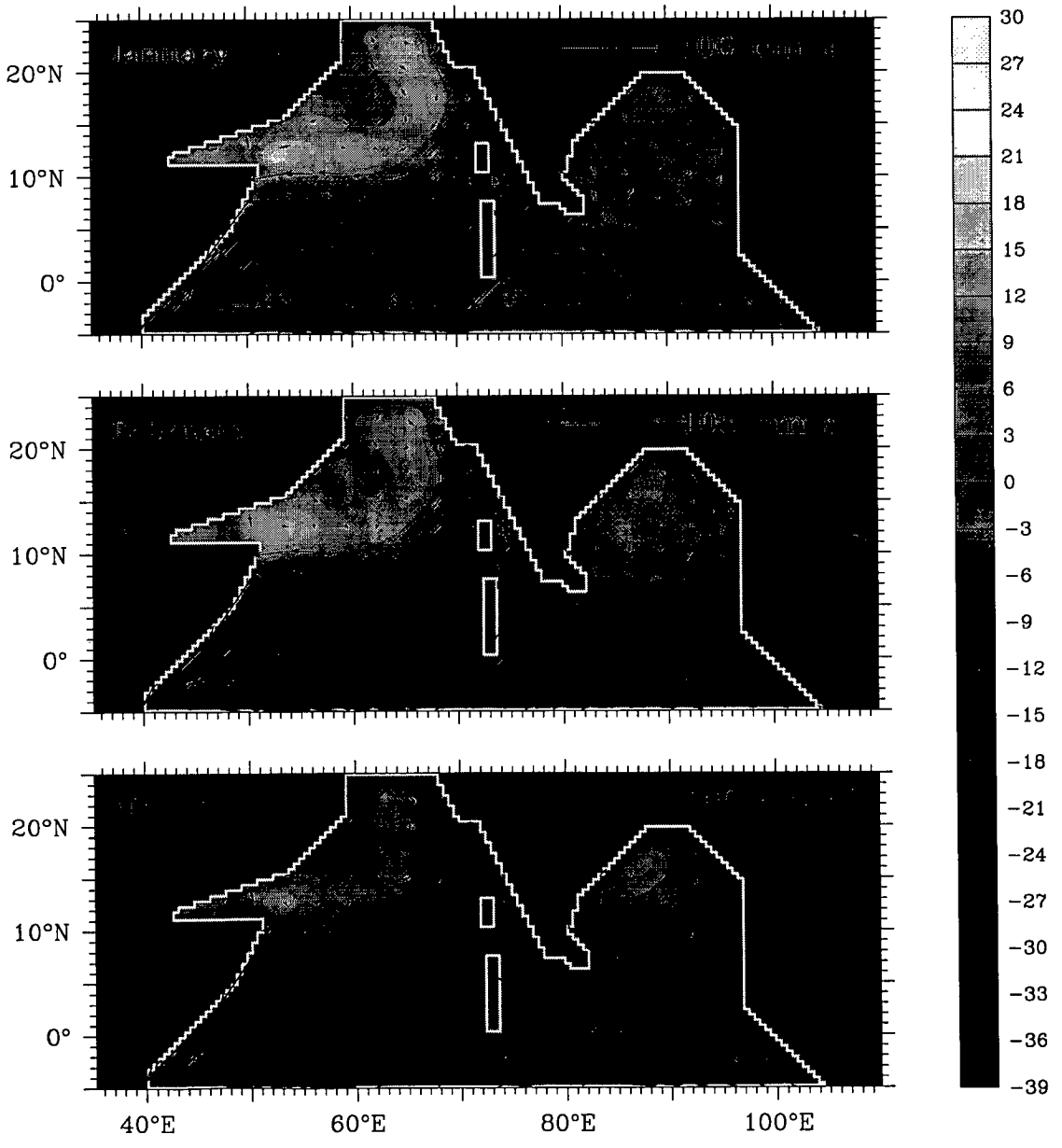

Figure 3.16 (continued) Effect of other processes (OP). The effect of processes LA, WLA, and RA has been filtered out of the response. Plots of sea-level deviation η (cm) and velocity $\mathbf{v}$ (cm s^{-1}) are shown. The absence of the alongshore winds is felt most strongly in the eastern, central, and northern Arabian Sea. The NMC does not weaken in the Arabian Sea and the eastward SMC is restricted to the east of Sri Lanka. The upwelling current off Arabia is weaker than in the main run and the EICC flows equatorward during the southwest monsoon because of Ekman pumping in the interior bay and remote forcing from the equator [Shankar et al., 1996; McCreary et al., 1996].

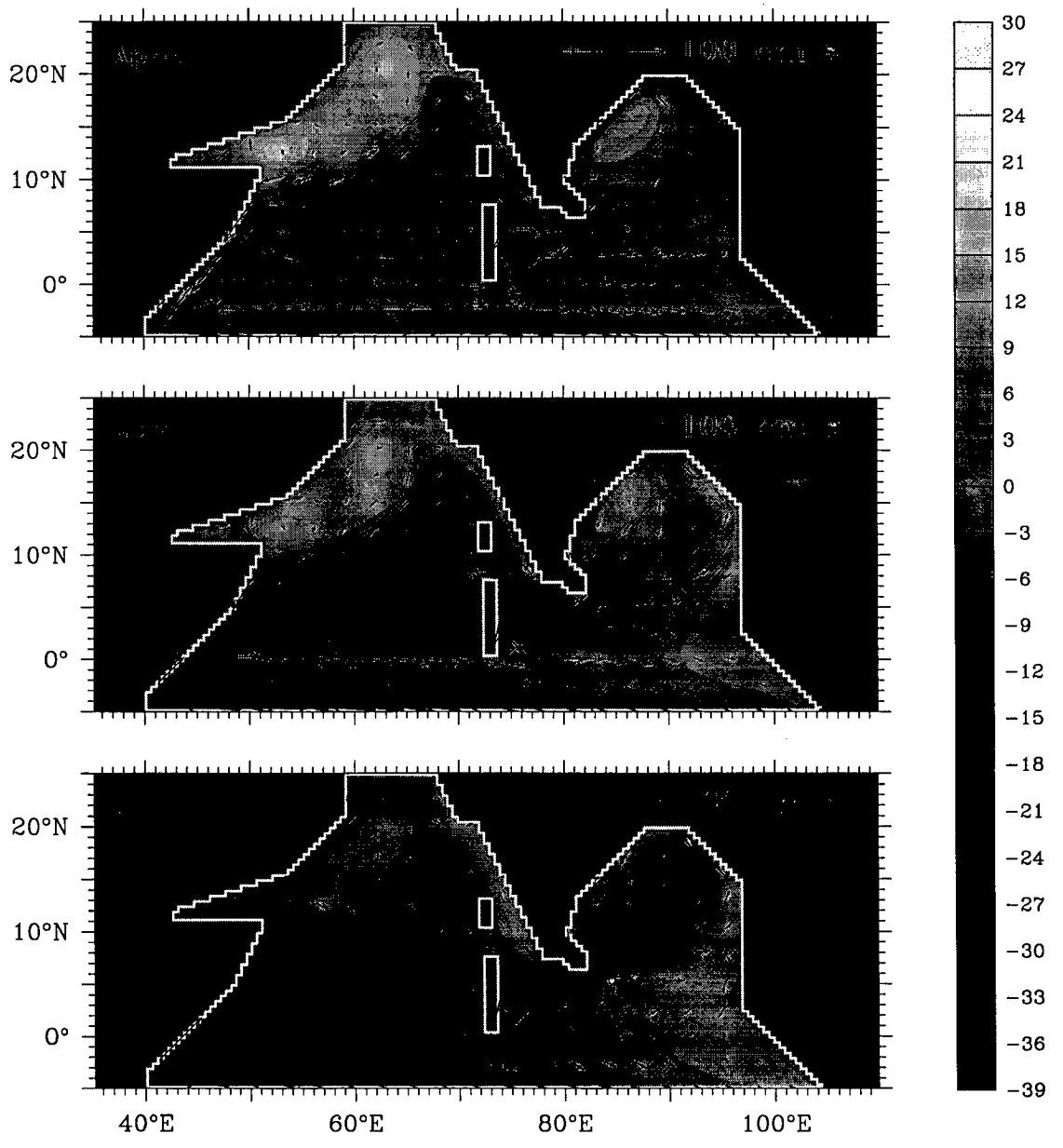

Figure 3.16 (continued) Effect of other processes (Processes OP). The effect of processes LA, WLA, and RA has been filtered out of the response. Plots of sea-level deviation η (cm) and velocity $\mathbf{v}$ (cm s^{-1}) are shown. Processes OP force a westward "SMC" to the west of Sri Lanka. This current flows through the gap between the Lakshadweep and Maldive islands and joins the return flow around the anticyclonic highs in the western Arabian Sea. Processes OP, however, are the principal causes of the circulation in the western Arabian Sea.

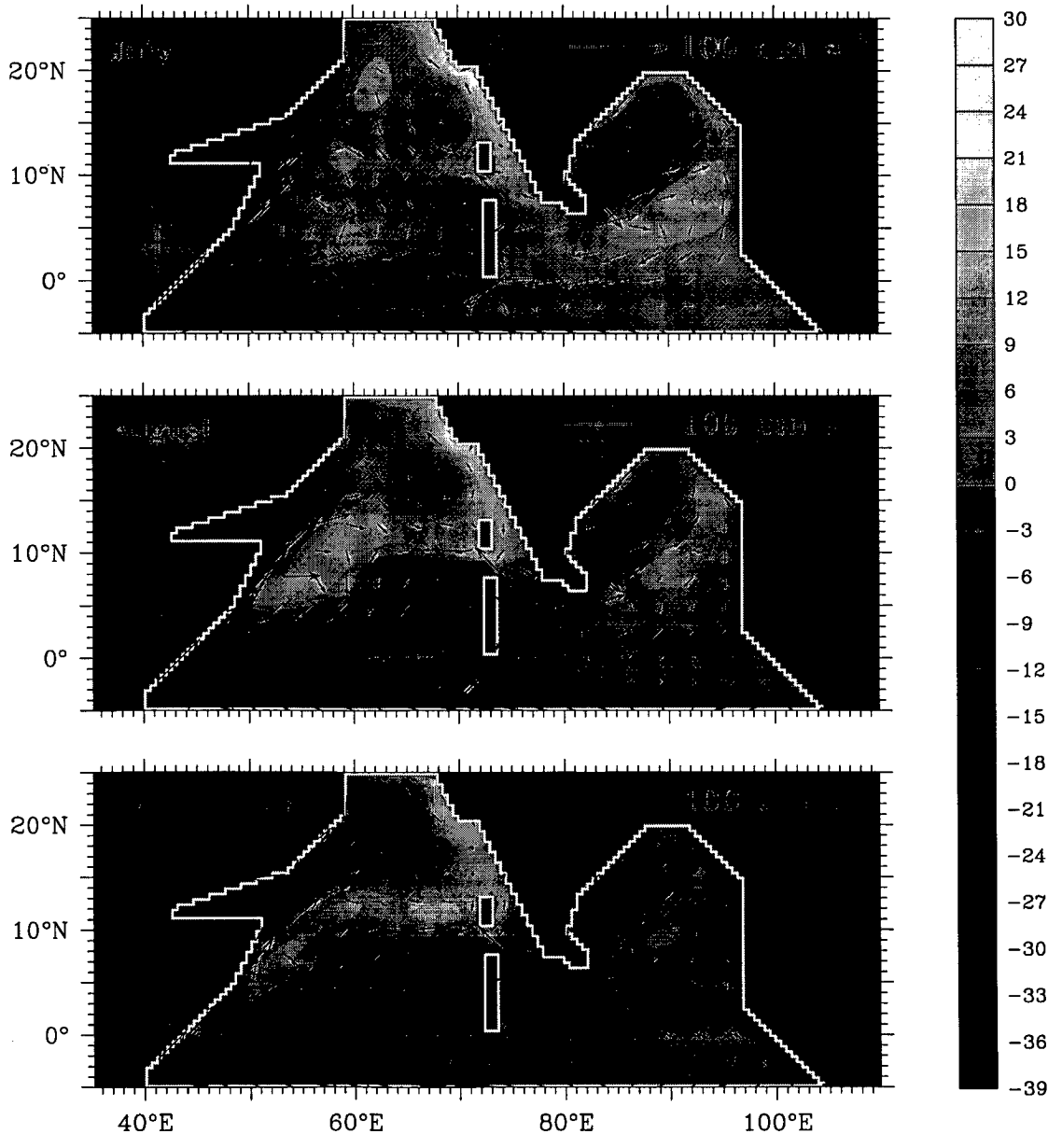

Figure 3.16 (continued) Effect of other processes (Processes OP). The effect of processes LA, WLA, and RA have been filtered out of the response. Plots of sea-level deviation η (cm) and velocity $\mathbf{v}$ (cm s^{-1}) are shown. The major distortion during October–December occurs in the Arabian Sea and off the east coast of Sri Lanka, where a weak EICC flows poleward in the absence of local winds. In the northern and central Arabian Sea, the absence of a low during the southwest monsoon results in a high in sea level. In the rest of the basin, however, it is the processes OP that determine the circulation.

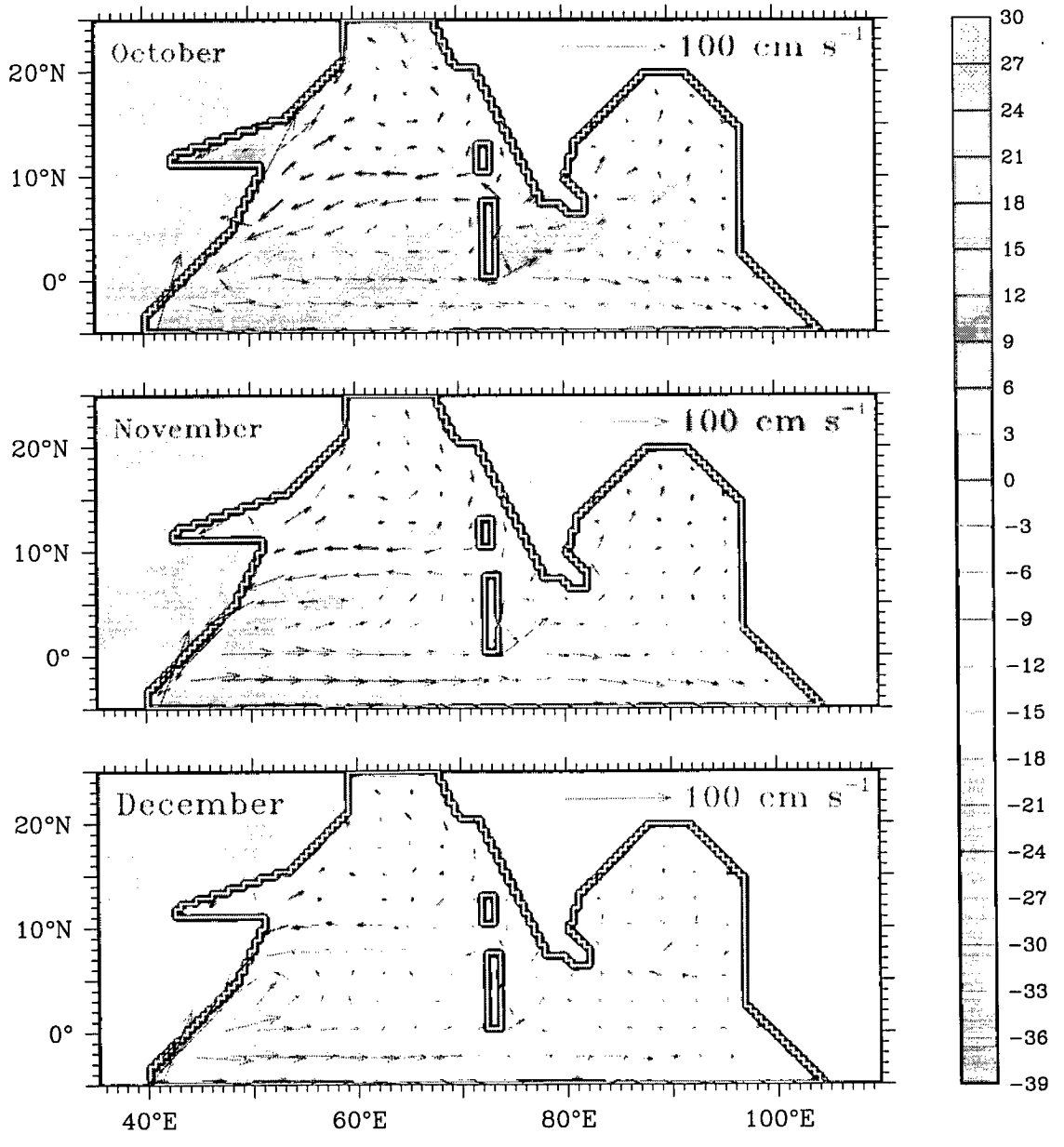

Figure 3.17 Effect of processes LA, RA, and WLA. Only these three processes are retained in this solution. Plots of sea-level deviation η (cm) and velocity $\mathbf{v}$ (cm s^{-1}) are shown. The winds blowing along the coasts of India and Sri Lanka are the principal causes of the circulation in the eastern, central, and northern Arabian Sea. Elsewhere, except for the effect of process LA on the EICC, their impact is small.

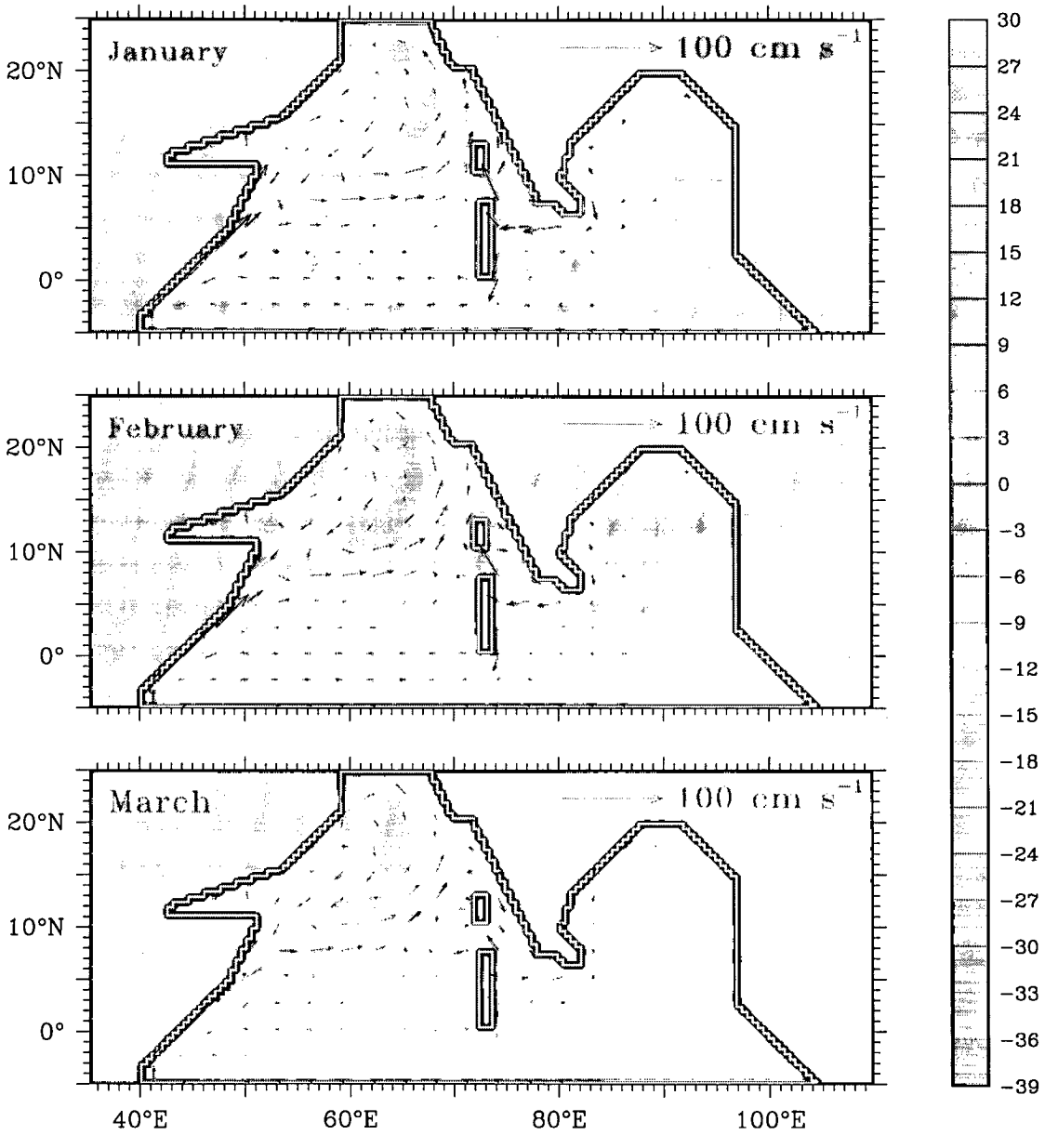

Figure 3.17 (continued) Effect of processes LA, RA, and WLA. Only these three processes are retained in this solution. Plots of sea-level deviation η (cm) and velocity $\mathbf{v}$ (cm s^{-1}) are shown. The Lakshadweep high is forced principally by process LA, with smaller contributions from WLA and OP. The high stretches westward across the southern Arabian Sea by May; its slower propagation in the main run is because of processes OP.

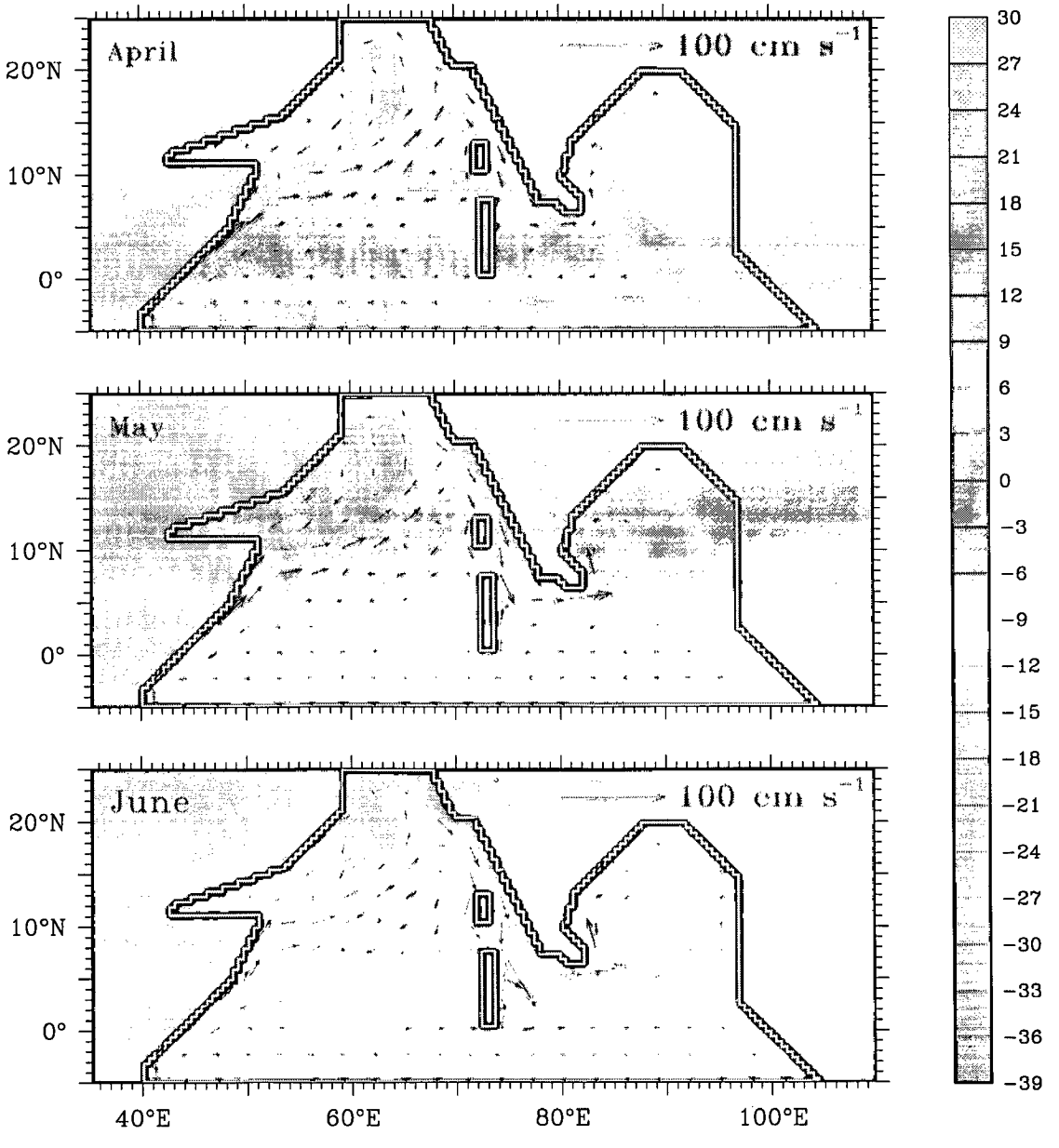

Figure 3.17 (continued) Effect of processes LA, RA, and WLA. Only these three processes are retained in this solution. Plots of sea-level deviation η (cm) and velocity $\mathbf{v}$ (cm s^{-1}) are shown. Processes WLA and LA force strong upwelling off the west coast of India and Sri Lanka during the southwest monsoon. The upwelling signal propagates as a Kelvin wave and complements the local winds that force upwelling off Arabia. The SMC to the west of Sri Lanka is forced by processes LA and WLA; other processes (OP) force a westward current and weaken the SMC forced by LA and WLA. These other processes, however, are the cause of the SMC to the east of Sri Lanka [Vinayachandran and Yamagata, 1998].

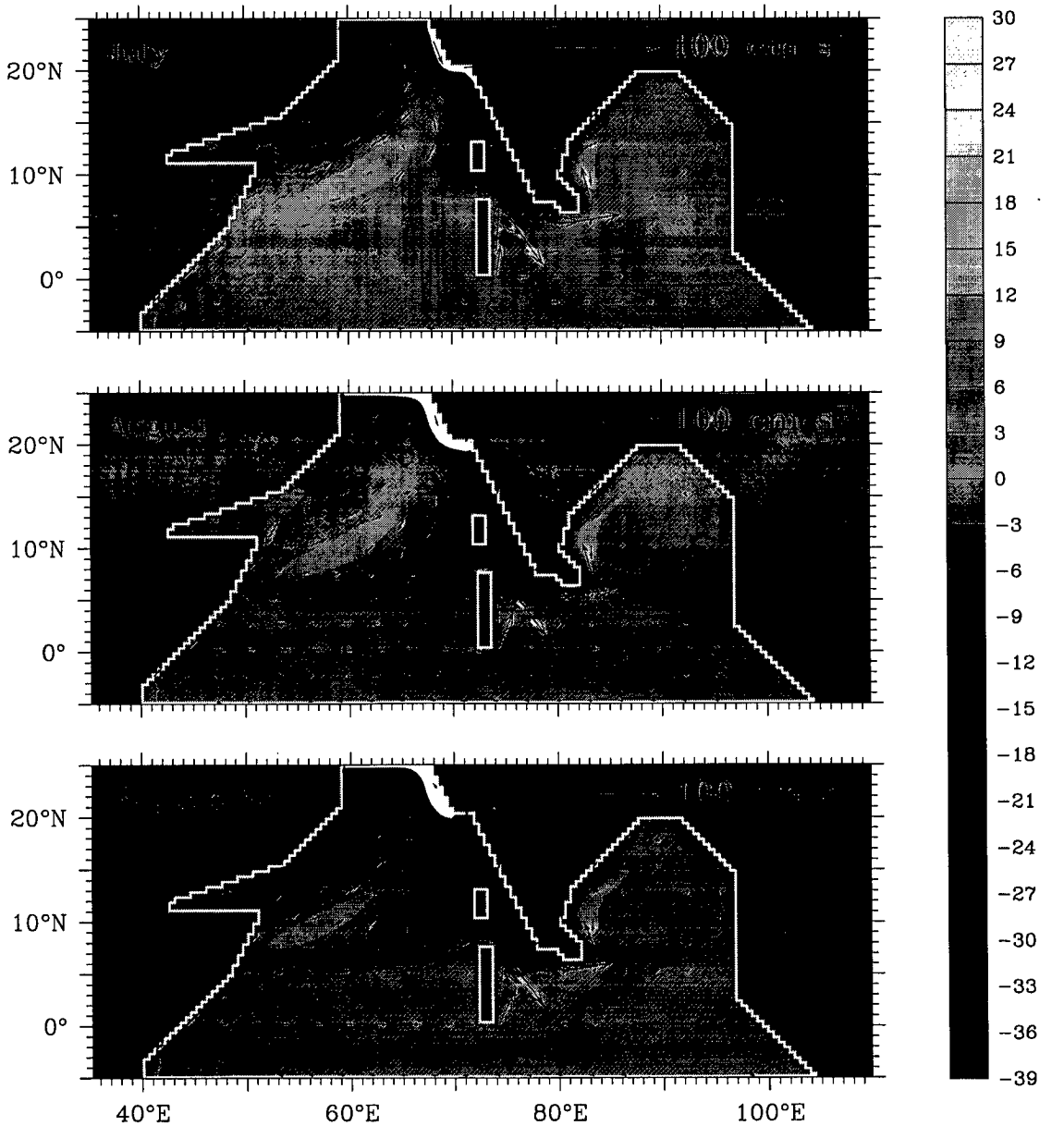

Figure 3.17 (continued) Effect of processes LA, RA, and WLA. Only these three processes are retained in this solution. Plots of sea-level deviation η (cm) and velocity $\mathbf{v}$ (cm s^{-1}) are shown. The low forced by processes LA and WLA propagates westward during October–December and an incipient high forms off southwest India in December. The absence of the local winds off Somalia and the forcing from the equator weakens the flow along the western flank of the low. This flow is enhanced in the main run by the formation of the Great Whirl and the Socotra high; the westward propagation of the Lakshadweep high, which is forced mainly by LA, makes a minor contribution to these highs in September and October..

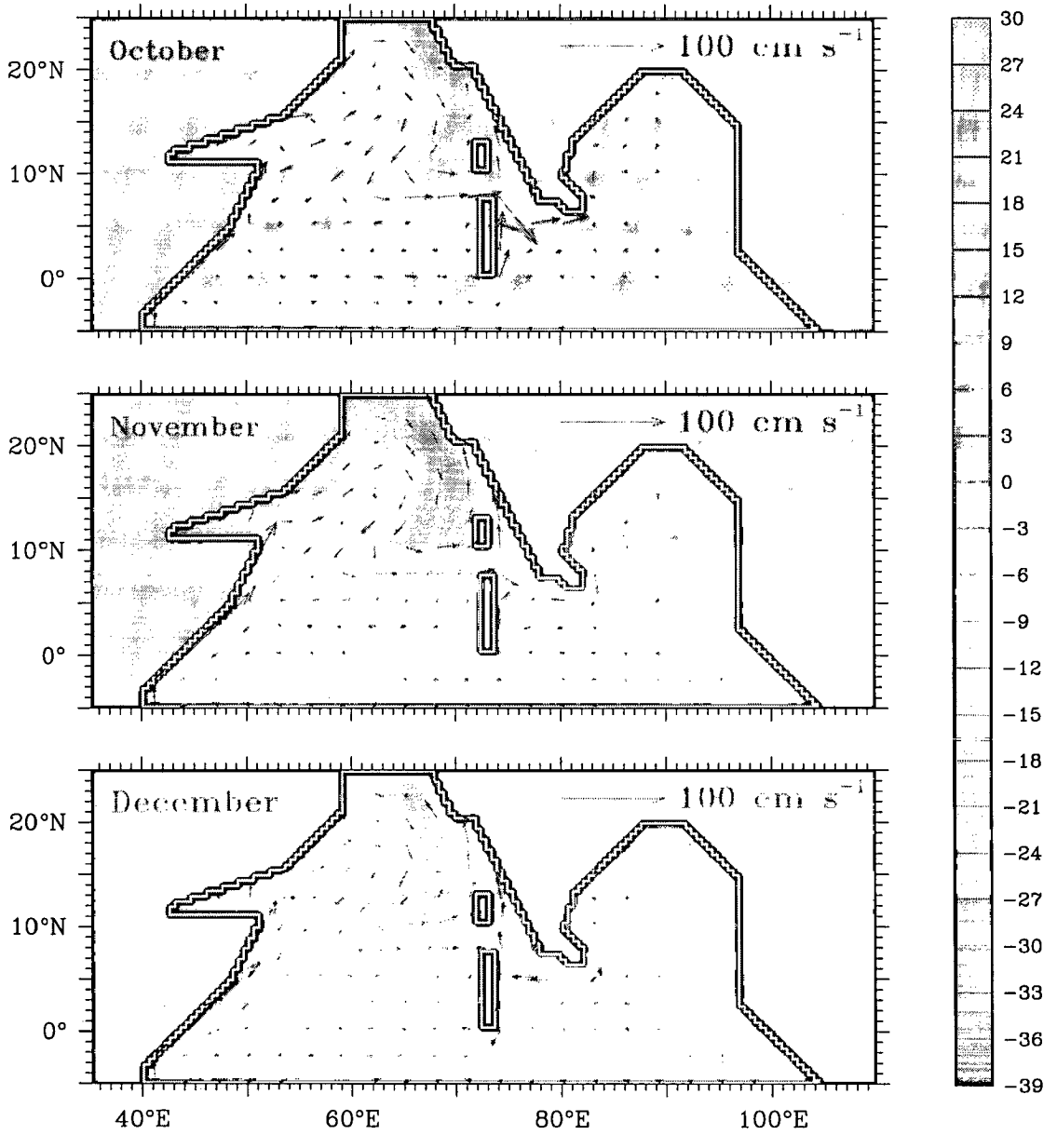

is forced by the equatorial waves and Ekman pumping in the interior bay [Vinayachandran and Yamagata, 1998]. The result of processes OP is a bizarre SMC: it is eastward to the east of Sri Lanka, westward to its west.

These process solutions show that the winds along the coasts of India and Sri Lanka have a strong effect on the circulation in the Arabian Sea; in the Bay of Bengal, their effect is restricted to the east coast of India and Sri Lanka. These winds are the principal mechanisms responsible for the Lakshadweep high and low and the seasonal cycle of circulation in the eastern Arabian Sea. The Kelvin waves forced by these winds also affect the Somali current, but not to the same magnitude. They force an upwelling current off Somalia almost throughout the year, weakening the equatorward Somali current in its northern reaches before the dramatic effect of the equatorial waves and local winds can be felt there with the onset of the southwest monsoon.

Thus, the effect of the processes that lead to the Lakshadweep high and low can be felt over large parts of the Arabian Sea. Since they are forced by the monsoon winds that blow year after year, the high and low must form year after year, and the variability associated with the monsoon must force variations in the high and low over a range of time scales. Such a strong seasonal cycle in the ocean and the variability associated with it must have some effect beyond modifying the circulation of the upper ocean in the region. We conclude this chapter with a brief discussion on some implications of the Lakshadweep high and low.

3.6 Implications of the Lakshadweep High and Low

The Lakshadweep high raises sea level and lowers the pycnocline in the Lakshadweep Sea during January to April. This implies a thick, stable upper layer that can warm more easily. This stability is enhanced by low-salinity water from the Bay of Bengal, brought in by the equatorward EICC and the NMC. Shenoi et al. [1999] argue that the high sea-surface temperatures (SSTs) that occur there as early as March, well before the thermal equator moves over the region, and the monsoon onset vortex that forms there later and heralds the onset of the southwest monsoon over India, are intimately connected to the high. Their hypothesis has all the elements of a classical coupled ocean-atmosphere system. First, an atmospheric event well separated from the eventual region of intense activity triggers events in the ocean. (The collapse of the southwest monsoon in October and the onset of the northeast monsoon generate Kelvin waves in the Bay of Bengal.) Second, response entirely within the ocean produces special conditions at a location remote from the atmospheric event. (The Kelvin waves from the bay lead to downwelling and to a stable surface layer off southwest India, resulting in higher SSTs there.) Third, the ocean triggers an event in the atmosphere. (High SSTs lead to the monsoon onset vortex.)

The Lakshadweep high is also important for the fishery of India. Upwelling along this coast be-

gins sometime in February [Longhurst and Wooster, 1990], well before the onset of the upwelling-favourable southwest monsoon winds. As seen in Figures 3.8 and 3.10, a consequence of the remotely forced Kelvin wave is the formation of a weak, but upwelling-favourable coastal current off southwest India, this current being integral to the dynamics of the high. The early upwelling is therefore one manifestation of the process discussed above. This upwelling current strengthens and leads to the low during the southwest monsoon. The result is an intense upwelling regime in the Lakshadweep Sea and farther north along the Indian west coast, with consequences for the marine chemistry of the region. Upwelling brings up the nutrient-rich deeper water, leading to a growth of phytoplankton, and to the depletion of oxygen in the surface waters due to their mixing with the anoxic deeper waters. These changes in the chemistry and primary productivity have an impact on the fishery of the region [Banse, 1968; Naqvi et al., 1998].

Thus, apart from the physical oceanography of the Arabian Sea, the Lakshadweep high and low have cascading effects on the atmosphere above, and on the marine chemistry and biology of the eastern Arabian Sea. The implications of the high and low are still being unravelled and form an area of active research. Our interest is in the variability of sea level along the Indian coast, and, having described the theoretical framework for studying the dynamics of the north Indian Ocean, it is to the seasonal cycle of coastal sea level that we turn our attention. It is obvious that the dynamics associated with the high and low must have a bearing on the seasonal cycle of sea level along the west coast of India. Most significant is the importance of remote forcing, especially of the high, which appears to be forced primarily by the winds blowing along the east coast of India and Sri Lanka. This bears out our tentative conclusion, drawn earlier on the basis of Figure 2.8, that the winds at a location along the Indian coast are not a sufficient cause of the sea-level changes there; the north Indian Ocean must be considered as a whole to model the observed variability. The $1\frac{1}{2}$-layer reduced-gravity model is successful in simulating the essential features of the circulation in the basin, including the large-scale coastal currents. In the following chapter, we apply it to the study of the seasonal cycle of sea level along the coast of India.

Chapter 4

The Seasonal Cycle of Sea Level Along the Coast

There are four causes of the climatological seasonal cycle of coastal sea level (Section 2.2). Of these four, low-frequency astronomic tides are ignored because they force an oscillation with a range less than 1 cm, much less than the observed variability, and the effect of atmospheric pressure is removed using the Inverse-Barometer (IB) approximation. The seasonal cycle of observed and corrected sea level[1] is plotted in Figure 4.1. The corrected seasonal cycle must be forced by the two remaining processes, which together force changes in steric sea level: wind-forced coastal currents and thermohaline effects due to surface fluxes and horizontal advection of heat and salt. In this chapter, we examine the effect of these two processes within the framework of a reduced-gravity model.

4.1 Effect of Wind-Forced Coastal Currents

The $1\frac{1}{2}$-layer reduced-gravity model used in Chapter 3 is successful in simulating the major observed features of the basin-scale circulation in the north Indian Ocean. It is also able to simulate the seasonal cycle of coastal currents off India (Figure 4.2). Except at Colombo, where the ship drifts are affected more by the strong local winds than by currents[2], the model alongshore currents are in excellent agreement with the observations. This leads us to believe that the model should be able to capture the effect of these large-scale coastal currents, one of the two processes left on eliminating astronomic tides and atmospheric pressure, on sea level along the coast of India.

The model sea level is compared with corrected sea level in Figure 4.3; there is a striking

[1]Observed sea level is the measured sea level; corrected sea level is the sea level corrcted for the effect of atmospheric pressure.

[2]See Figures 2.6 and 2.8.

Figure 4.1 The climatological seasonal cycle of sea level (cm) along the coast of India. The figure shows the observed and corrected sea level; the local annual mean has been subtracted from the monthly climatology to compute these anomalies. The correction for atmospheric pressure was applied using the Inverse-Barometer approximation. The effect of atmospheric pressure on sea level varies from 3 cm at Colombo to 13 cm at Paradip. The seasonal cycle of corrected sea level is coherent along the coast. Its range is greater along the east coast (45 cm) than along the west coast (30 cm). Along the east (west) coast, the corrected sea level is maximum in November (December) and minimum during March–April (the southwest monsoon).

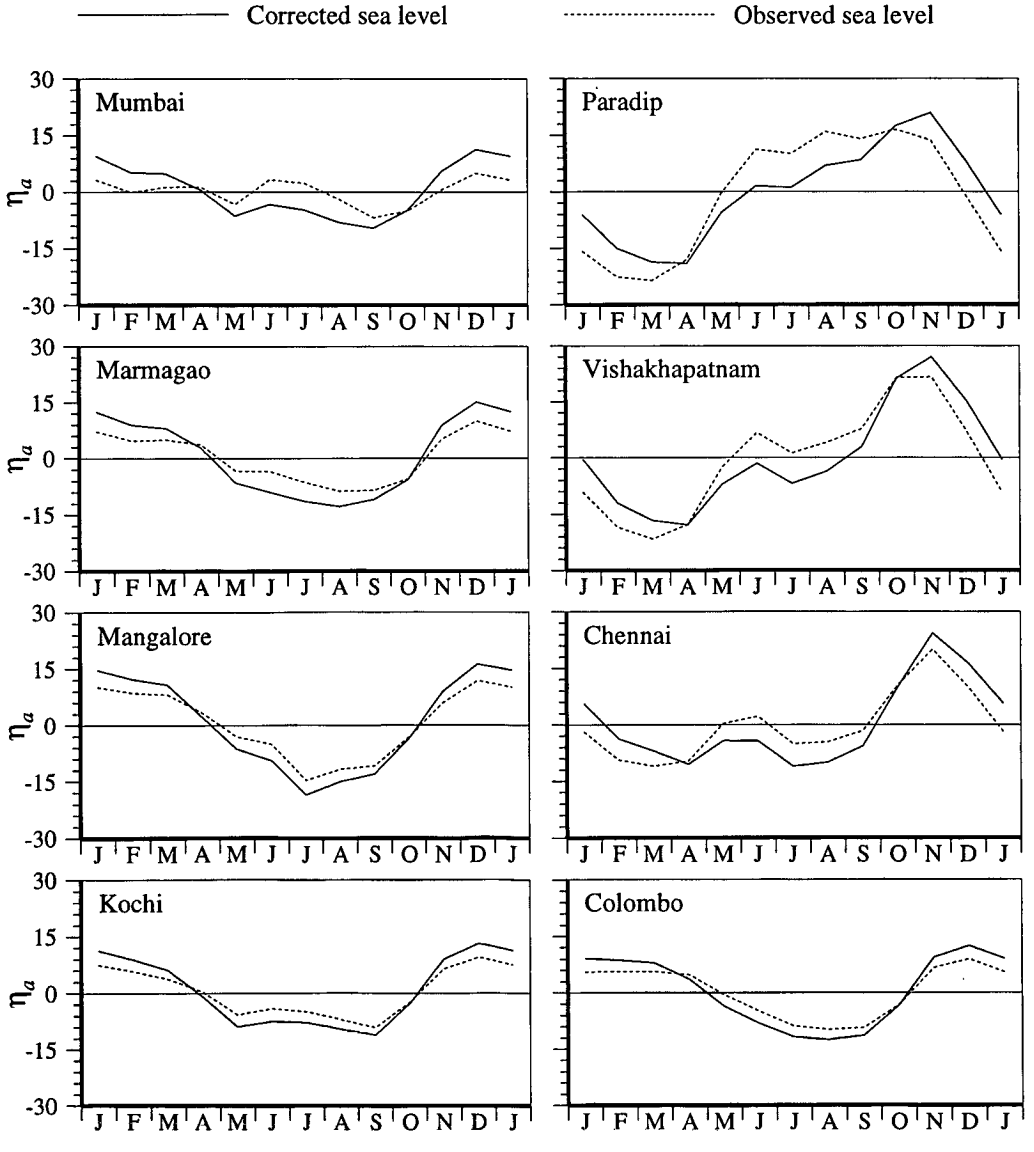

Figure 4.2 The climatological seasonal cycle of alongshore ship drifts, compiled by Rao et al. [1989] (cm s^{-1}), and alongshore currents (cm s^{-1}), simulated by the dynamical $1\frac{1}{2}$-layer reduced-gravity model. Ship-drift data are not available at Paradip and Mumbai. All variables plotted are monthly anomalies; the annual mean has been removed. Downwelling- (upwelling-) favourable anomalies are positive (negative); these currents flow with the coast on their right (left) in the northern hemisphere. The model alongshore currents match the ship drifts, except at Colombo, where the ship drifts are affected more by the strong local winds than by currents (see Figure 2.8).

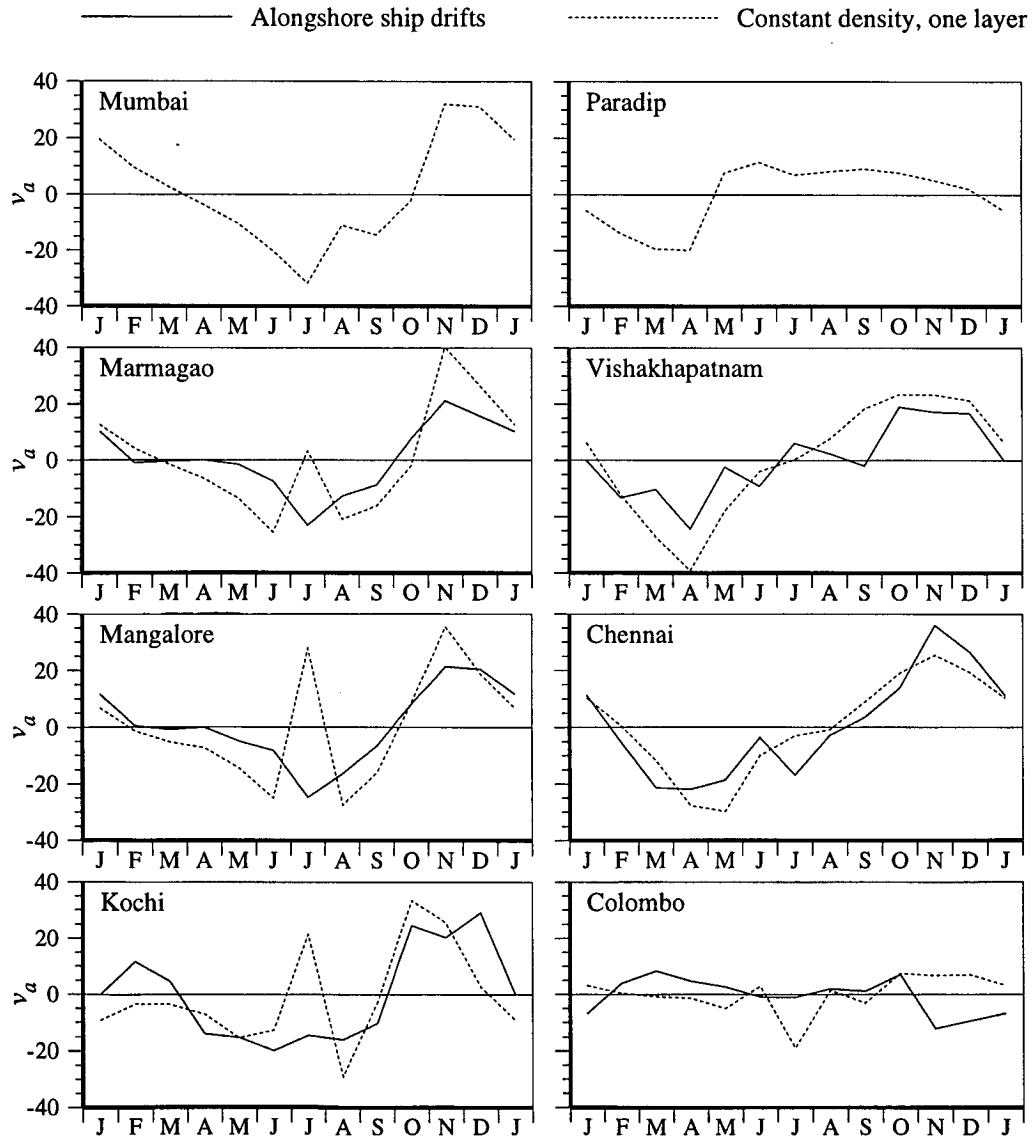

Figure 4.3 Effect of wind-forced coastal currents on the seasonal cycle of sea level (cm). Monthly anomalies of corrected sea level are plotted along with that of the sea level from the $1\frac{1}{2}$-layer and $2\frac{1}{2}$-layer models. The dynamical reduced-gravity model is successful in simulating the seasonal cycle of currents along the coast of India, but it fails to simulate that of sea level. The model fails to simulate the winter peak along the east coast; as a consequence, the simulated seasonal cycle of sea level has a higher range along the west coast.

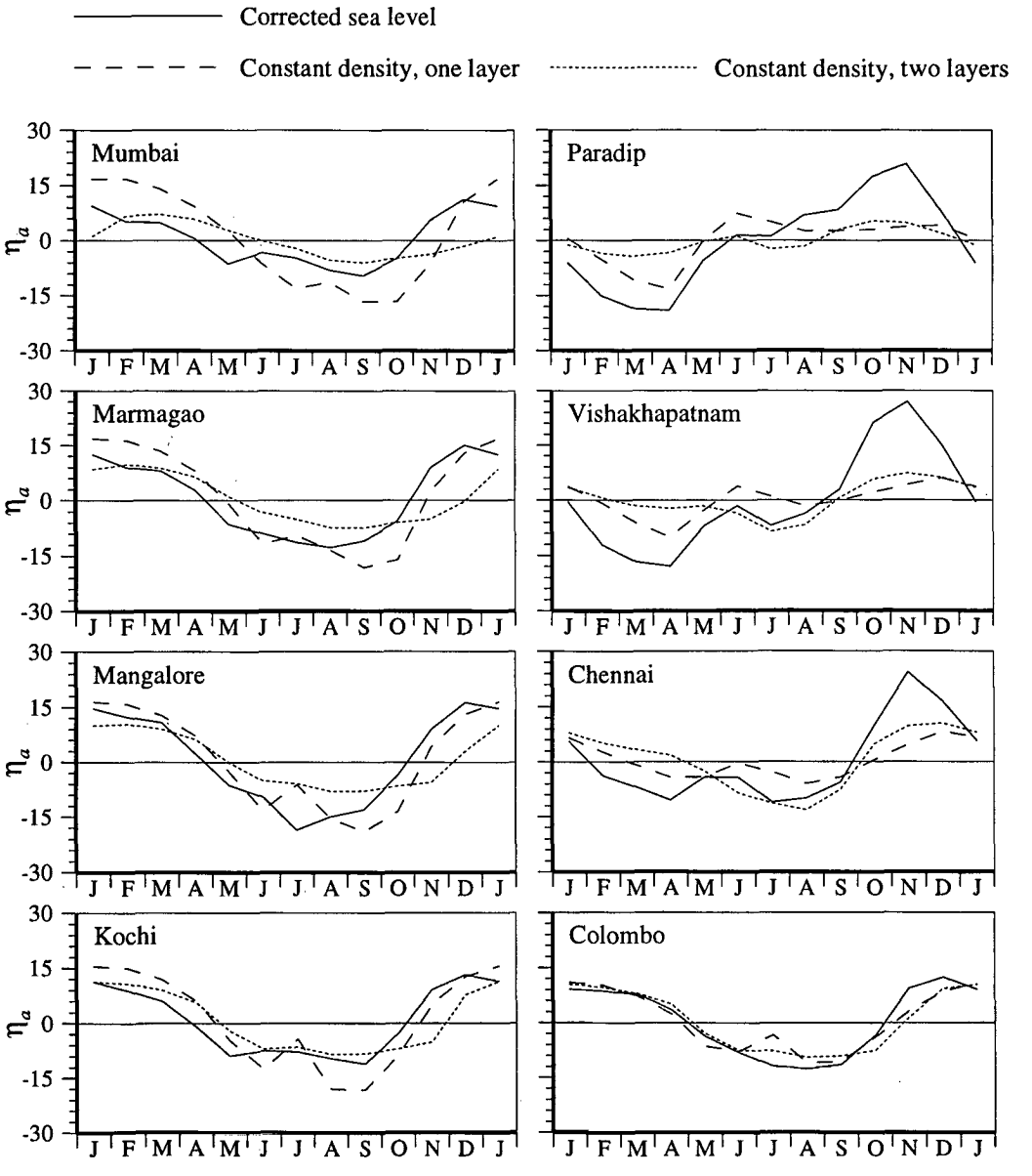

mismatch between the two, especially along the east coast. First, the model is unable to capture the winter peak along the east coast. Second, as a consequence of this, the range of the seasonal cycle along the east coast is much less than that along the west coast.

This failure implies that the model lacks the physics required to simulate the seasonal cycle of coastal sea level. Could this be due to the absence of a second active layer? The available literature suggests that the second baroclinic mode is important in the Indian Ocean, especially in the equatorial waveguide [McCreary et al., 1993; Jensen, 1993]. To examine its effect on coastal sea level, we add an extra active layer to the model, making it a $2\frac{1}{2}$-layer model[3]. The model parameters are listed in Table 4.1. Density is constant in each layer and the model is forced by the wind-stress climatology of Hellerman and Rosenstein [1983]. The model sea level plotted in Figure 4.3 is from the tenth year of the simulation.

Table 4.1 Model parameters for the $2\frac{1}{2}$-layer reduced-gravity model.

Parameter (units)	Symbol	Value
Laplacian mixing coefficient for momentum ($cm^2\ s^{-1}$)	ν	5×10^7
Laplacian mixing coefficient for thickness ($cm^2\ s^{-1}$)	κ	1×10^7
Reduced-gravity parameter for the first layer	$\overline{\Gamma}_1$	0.0035
Reduced-gravity parameter for the second layer	$\overline{\Gamma}_2$	0.0020
Initial thickness of the first layer (m)	$\overline{H}_1$	70
Initial thickness the second layer (m)	$\overline{H}_2$	250
Minimum thickness of the first layer (m)	$H_{1,\min}$	10
Maximum thickness of the first layer (m)	$H_{1,\max}$	140
Minimum thickness of the second layer (m)	$H_{2,\min}$	50
Maximum thickness of the second layer (m)	$H_{2,\max}$	450
Grid size (km)	$\Delta x, \Delta y$	55
Time step (minutes)	Δt	72

The $2\frac{1}{2}$-layer model also fails to capture the observed variability, doing no better than the $1\frac{1}{2}$-layer model in simulating the winter peak along the east coast. This failure of the purely wind-forced reduced-gravity models to simulate the seasonal cycle of corrected sea level, even though they are able to simulate that of the alongshore currents, implies that a critical element is missing in these dynamical models. We explore if thermohaline effects constitute this critical element.

[3]The equations are derived in Appendix A; see Section A.2.

Figure 4.4 Effect of temperature on the seasonal cycle of sea level (cm). Monthly anomalies of corrected sea level are plotted along with that of the sea level from the $2\frac{1}{2}$-layer model of McCreary et al. [1993]. Like the dynamical reduced-gravity models, this too fails to simulate the winter peak along the east coast. Since the model does fairly well in simulating the temperature in the upper ocean, this failure implies that seasonal variations in temperature have a minor effect on sea level along the coast of India.

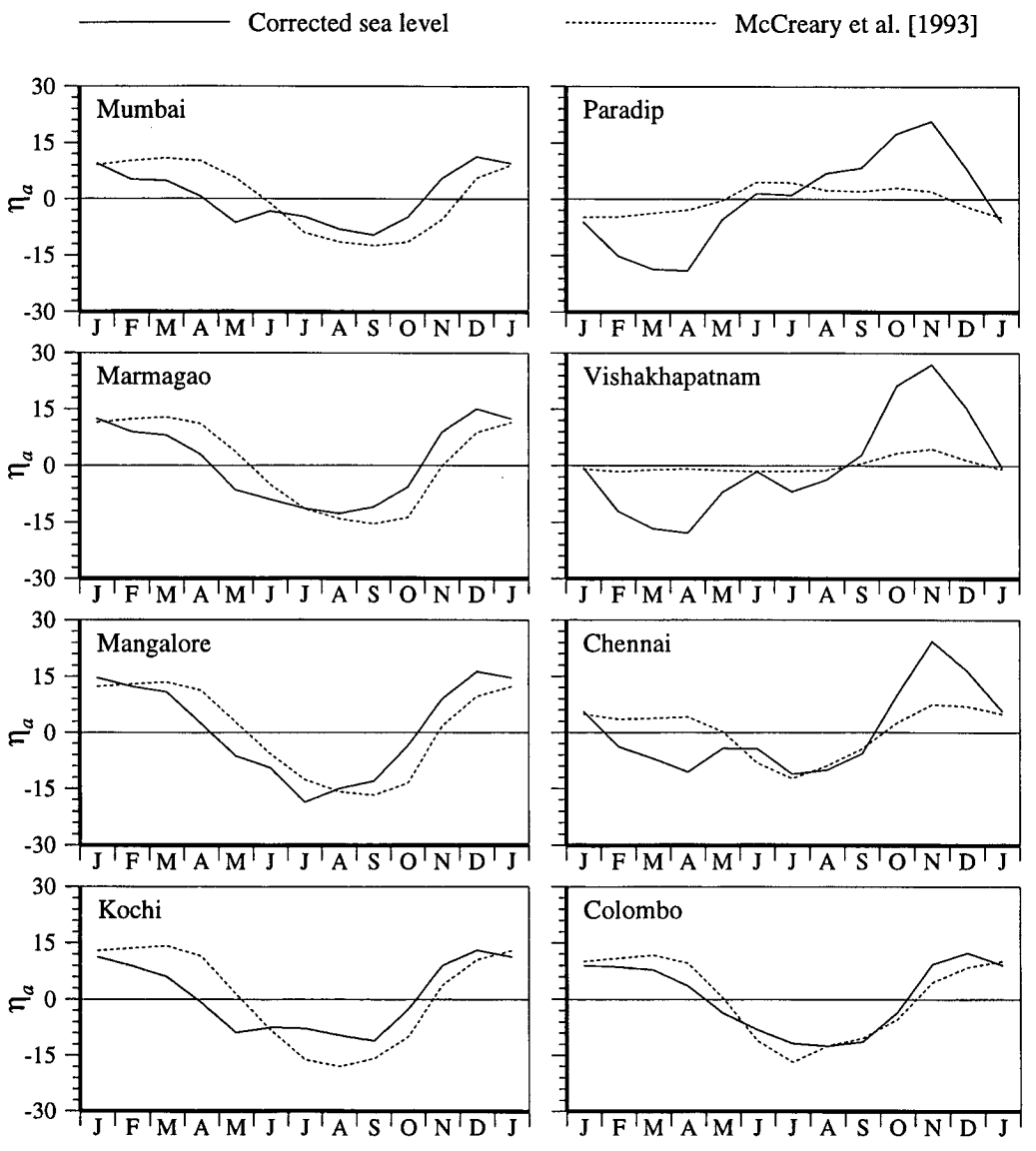

4.2 Effect of Variations in Temperature

In their numerical study of the dynamics and thermodynamics of the Indian Ocean, McCreary et al. [1993] used a $2\frac{1}{2}$-layer reduced-gravity model with a mixed layer embedded in the upper layer. The model, forced by the wind-stress climatology of Hellerman and Rosenstein [1983] and observed surface fluxes of heat, simulates the major features of the observed circulation and sea surface temperature (SST) fairly well. Hence, we expect it to account for the effect of temperature on coastal sea level. It, however, fares no better than the purely wind-forced models (Figure 4.4), implying that temperature changes play but a minor role in forcing seasonal sea-level changes along the Indian coast.

This result, which is not surprising because seasonal variations in temperature are small in the tropics [Clarke and Liu, 1993], leaves us with salinity as the possible cause of the winter peak in sea level along the east coast of India. Since the haline contraction coefficient is roughly five times the thermal expansion coefficient (Table 3.1), a salinity change of 1 PSU is equivalent to a temperature change of 5°C. Though a 5°C change in temperature is not common in the north Indian Ocean, a 1 PSU change in salinity is. The annual mean temperature and salinity, averaged over the top 100 m of the water column, and $\overline{\Gamma}$, are plotted in Figures 4.5, 4.6, and 4.7. The alongshore changes in temperature are small, but there is a large alongshore salinity gradient. Hence, salinity may be a significant cause of the seasonal cycle of sea level along the coast of India.

Figure 4.5 Annual mean temperature (°C), averaged over the top 100 m of the water column, in the north Indian Ocean. The temperature field is from the annual climatology of Levitus and Boyer [1994] and has been interpolated to the model grid.

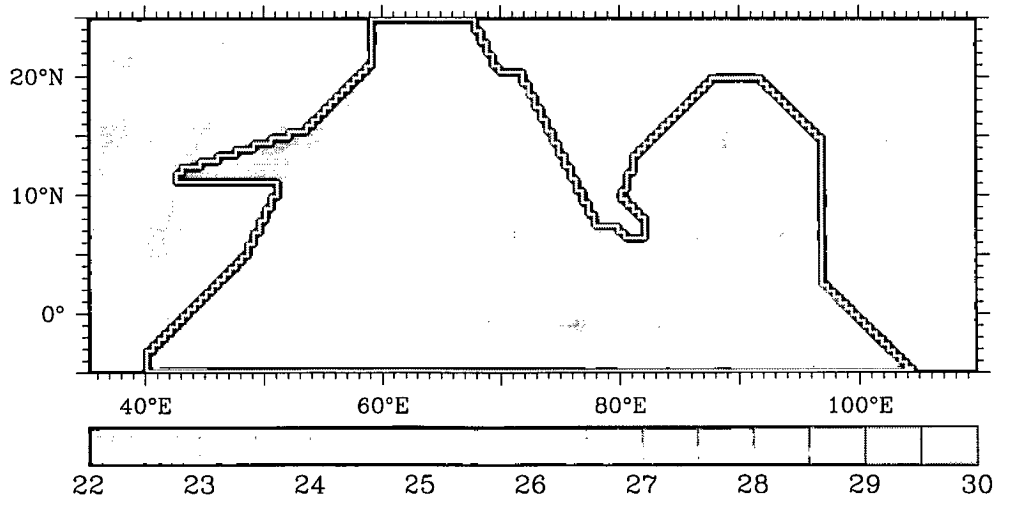

Figure 4.6 Annual mean salinity (PSU), averaged over the top 100 m of the water column, in the north Indian Ocean. The salinity field is from the annual climatology of Levitus et al. [1994] and has been interpolated to the model grid.

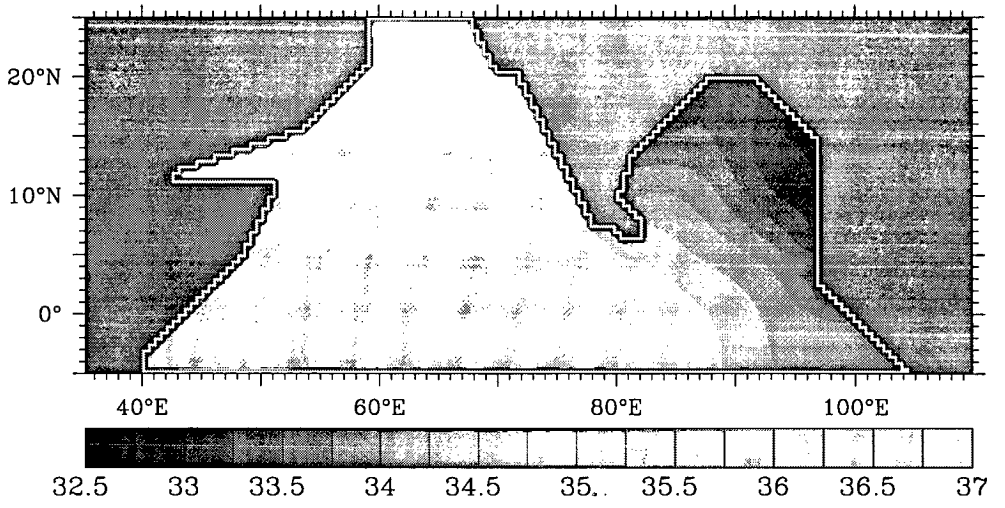

Figure 4.7 Annual mean reduced-gravity parameter $\Gamma = \frac{\rho_2 - \rho_1}{\overline{\rho}}$ in the north Indian Ocean. $\overline{\rho}$ is an average density representative of the ocean (see Appendix A). The temperature field is from the annual climatology of Levitus and Boyer [1994], the salinity field from that of Levitus et al. [1994].

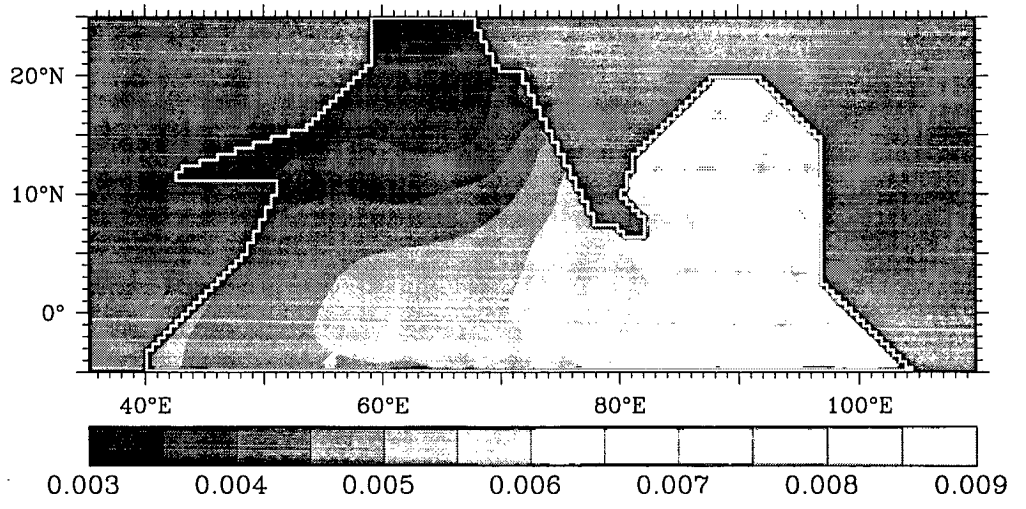

4.3 Effect of Variations in Salinity

The heavy rainfall over the Indian subcontinent leads to a large runoff from rivers into the seas around India, particularly the Bay of Bengal. Together with the rainfall over the ocean, the freshwater inflow from rivers lowers salinity in the bay, especially along the coast of India. The low salinity is bound to raise the steric sea level along the coast.

4.3.1 Simulations With the Salinity Climatology of Levitus et al. [1994]

To examine the impact of salinity on the seasonal cycle of sea level along the Indian coast, we have to permit temperature and salinity to vary in the active upper layer of the $1\frac{1}{2}$-layer model. We do not solve the conservation equations for heat and salt[4]; instead, temperature and salinity are prescribed from the monthly climatologies of Levitus and Boyer [1994] and Levitus et al. [1994]. These monthly fields are averaged over the top 100 m and then interpolated linearly to the model grid at each time-step. The density in the upper layer is still less than that of the constant-density lower layer, but it is now a function of space and time. The resulting seasonal cycle of the reduced-gravity parameter, Γ, is plotted in Figures 4.8 and 4.9. The seasonal cycle of Γ is determined primarily by the changes in salinity in the Bay of Bengal; variations in temperature are important only in the northern Arabian Sea, where cooling by the cold continental winds blowing from the northeast in winter forces a drop in temperature in the upper ocean [Banse, 1984, 1994; Madhupratap et al., 1996], and along the west coast of India during the southwest monsoon, when Γ decreases owing to a decrease in the average temperature of the upper layer due to upwelling associated with the Lakshadweep low.

The model is forced by the wind-stress climatology of Hellerman and Rosenstein [1983] and the resulting sea-level deviation, η, and velocity, $\mathbf{v}$, are shown in Figure 4.10. The variations in density do not perturb the basin-scale circulation much. The alongshore currents also do not change much (Figure 4.11). The range of the seasonal cycle of sea level increases at Paradip (Figure 4.12), but the maximum occurs in June; at Vishakhapatnam and Chennai, there is little change in sea level. This is due to the seasonal cycle of Γ (Figure 4.9), which has a trough in November along the east coast because the coastal salinity in the climatology of Levitus et al. is minimum in September and increases thereafter. This drop in Γ lowers sea level at the coast in November even though the EICC favours downwelling, the effect of the wind-forced rise in sea level being nullified by the rise in salinity.

The monthly climatologies of Levitus and Boyer and Levitus et al. are derived from their seasonal climatologies by interpolation. The sparse distribution of the data in the north Indian Ocean makes it difficult to prepare a monthly climatology. Another problem is the absence of

[4]The equations for this variable-density reduced-gravity model are derived in Appendix A.

Figure 4.8 The seasonal cycle of the reduced-gravity parameter Γ in the north Indian Ocean. Γ is computed from the monthly climatologies of Levitus and Boyer [1994] and Levitus et al. [1994]. There is a large difference in density between the northern Bay of Bengal and the northern Arabian Sea. This difference is determined mainly by the difference in salinity [Shetye, 1984], there being a continuous increase (decrease) in salinity (Γ) from the bay to the Arabian Sea.

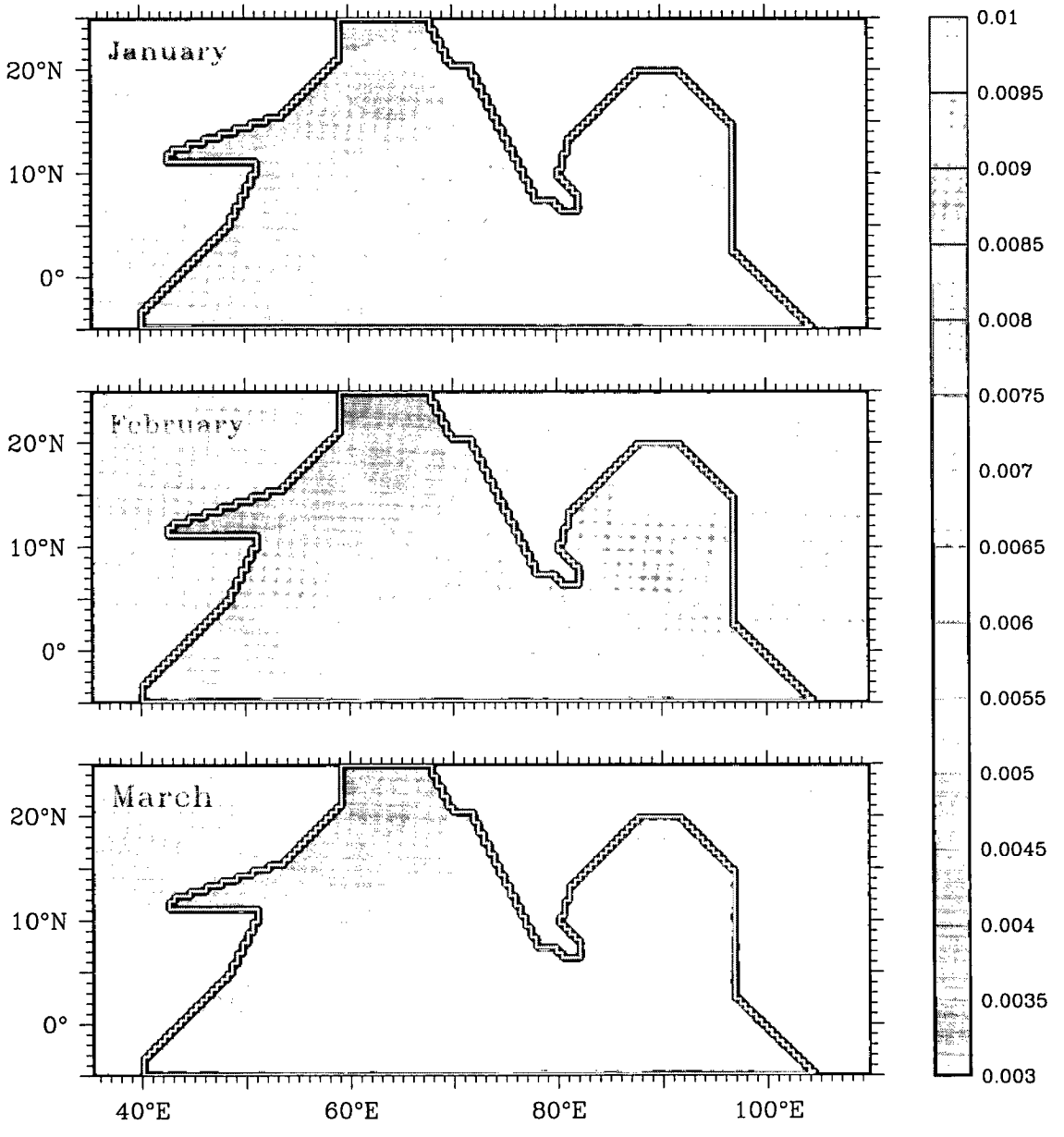

Figure 4.8 (continued) The seasonal cycle of the reduced-gravity parameter Γ in the north Indian Ocean. Γ is computed from the monthly climatologies of Levitus and Boyer [1994] and Levitus et al. [1994]. Γ does not change much during January–May. It drops during the southwest monsoon along the west coast of India because of a decrease in temperature due to upwelling associated with the Lakshadweep low. In June, it starts increasing in the northern Bay of Bengal because of a decrease in salinity.

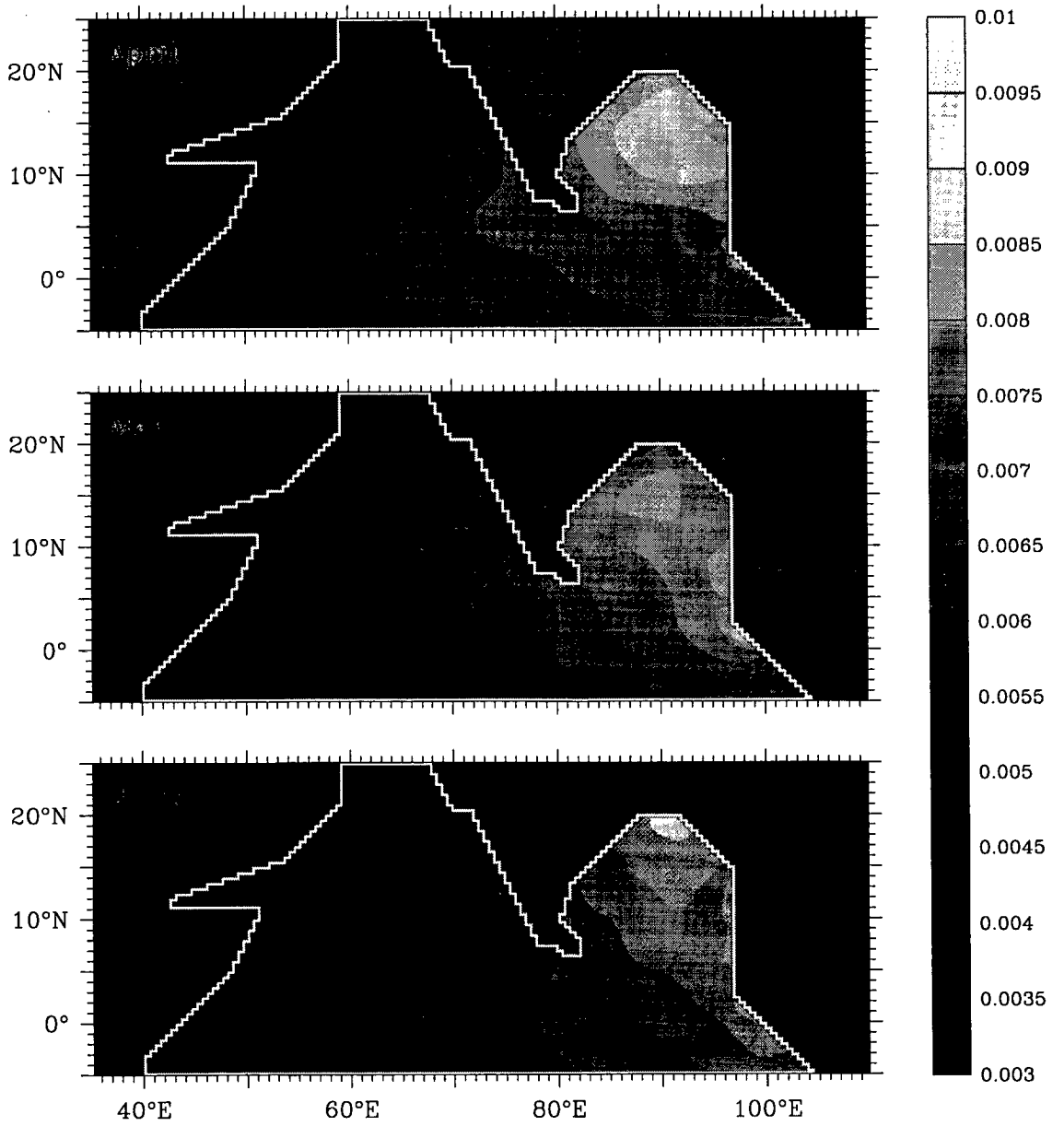

Figure 4.8 (continued) The seasonal cycle of the reduced-gravity parameter Γ in the north Indian Ocean. Γ is computed from the monthly climatologies of Levitus and Boyer [1994] and Levitus et al. [1994]. The southwest monsoon brings about a large change in Γ, especially in the Bay of Bengal. The largest increase (decrease) in Γ (density) is along the east coast of India, and along the west coast of Myanmar (Burma), which forms the eastern boundary of the northern bay. The tongue of low-salinity water (high Γ) in the equatorial Indian Ocean also stretches westward.

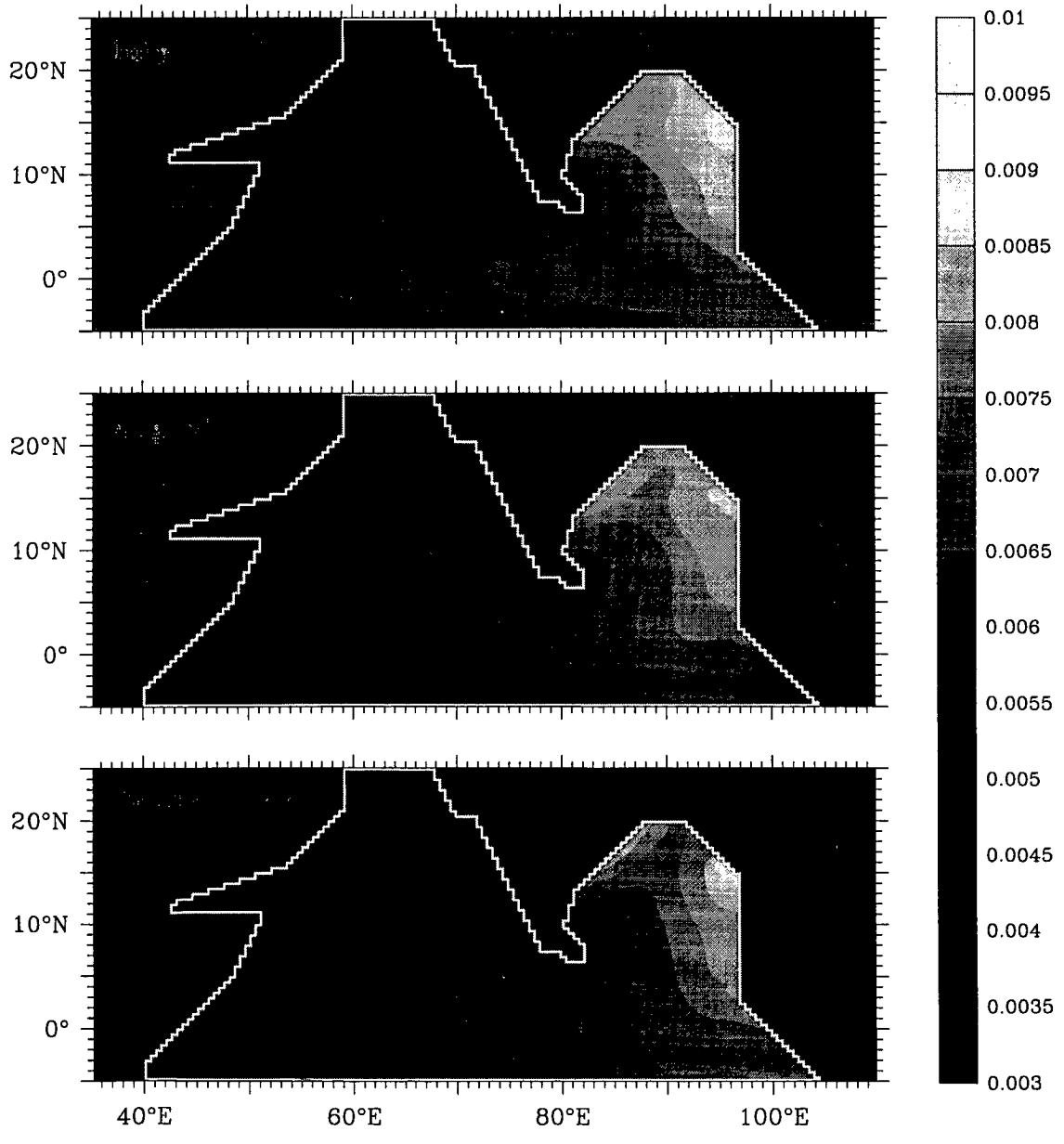

Figure 4.8 (continued) The seasonal cycle of the reduced-gravity parameter Γ in the north Indian Ocean. Γ is computed from the monthly climatologies of Levitus and Boyer [1994] and Levitus et al. [1994]. With the collapse of the southwest monsoon, salinity increases along the east coast of India and Sri Lanka in the monthly climatology of Levitus et al., leading to an increase in Γ. Γ, however, increases along the west coast of India, especially in the south, owing to an inflow of low-salinity water from the bay and the decrease in temperature due to the cessation of upwelling.

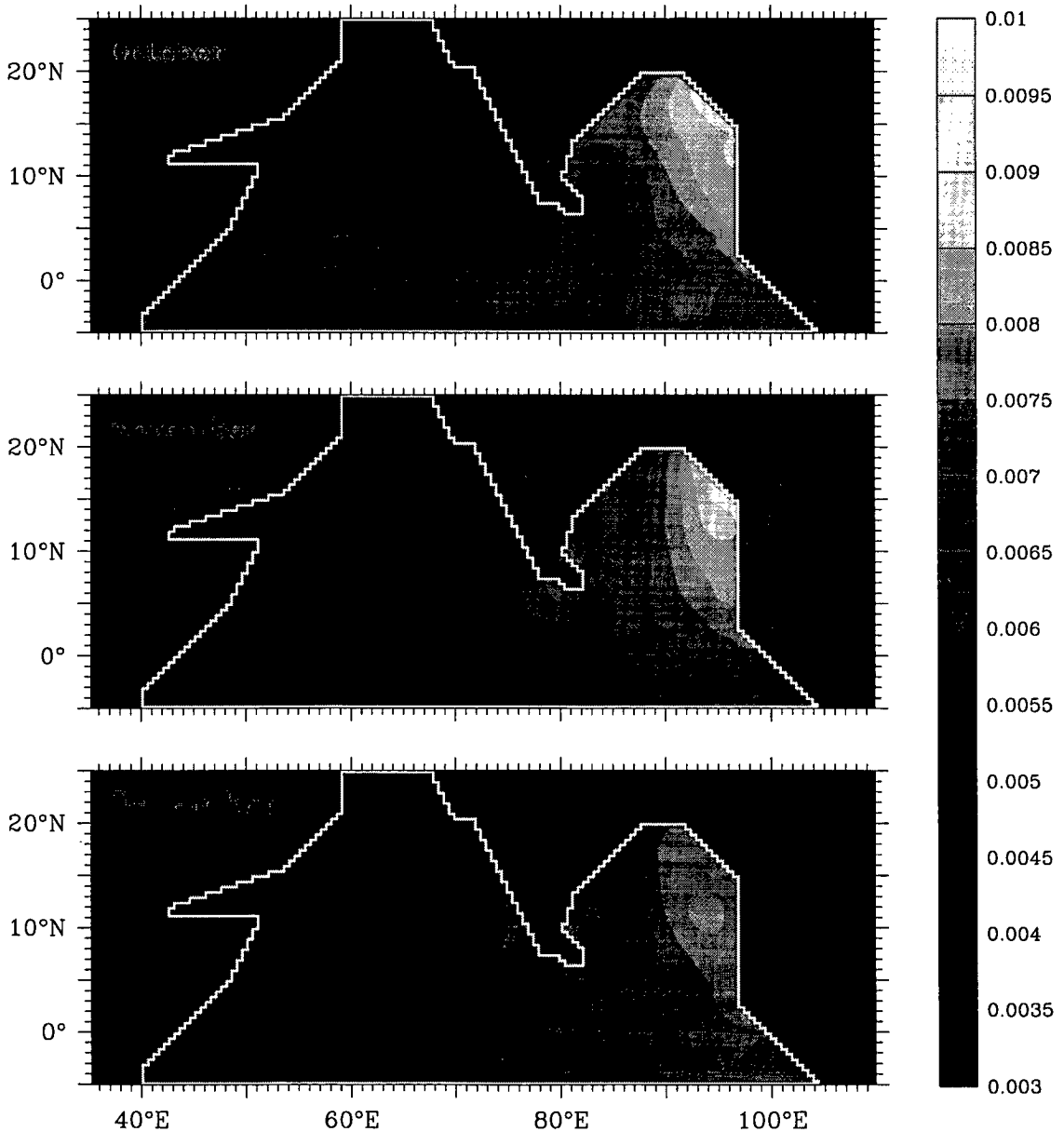

Figure 4.9 The seasonal cycle of Γ along the coast of India. The density of the upper layer is computed from the monthly climatologies of Levitus and Boyer [1994] and Levitus et al. [1994]. The figure shows Γ, Γ_T, and Γ_S; Γ_T and Γ_S are the contributions of temperature and salinity to Γ. Along the west coast, both temperature and salinity are important, the decrease in temperature because of upwelling associated with the Lakshadweep low causing a drop in Γ during the southwest monsoon. After the southwest monsoon, Γ increases because of the cessation of upwelling and an inflow of low-salinity water from the Bay of Bengal. Along the east coast, temperature is unimportant; it is salinity that controls the density in the upper layer. In the monthly climatology of Levitus et al., salinity is minimum, and hence, Γ is maximum, in September. Γ is minimum during November and December.

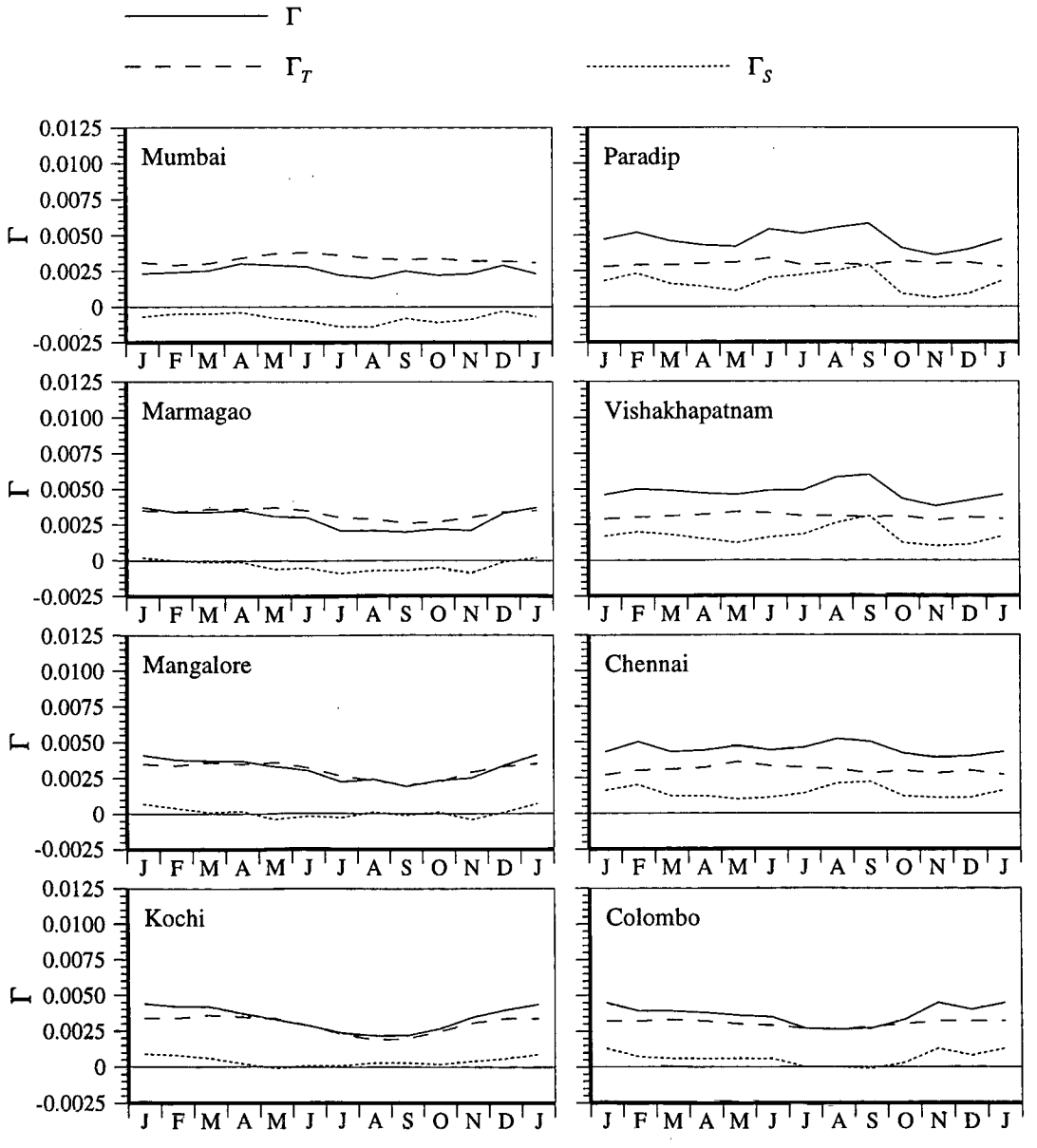

Figure 4.10 Effect of variable density on the seasonal cycle of surface circulation in the north Indian Ocean; apart from the density variation in the upper layer, the simulation is identical to the nonlinear simulation in Section 3.3.2 (Figure 3.5). Sea-level deviation η (cm) and velocity $\mathbf{v}$ (cm s^{-1}) are shown. The variations in density barely perturb the circulation, but there is a change in sea level; for example, sea level is higher in the anticyclonic high in the bay during February–May.

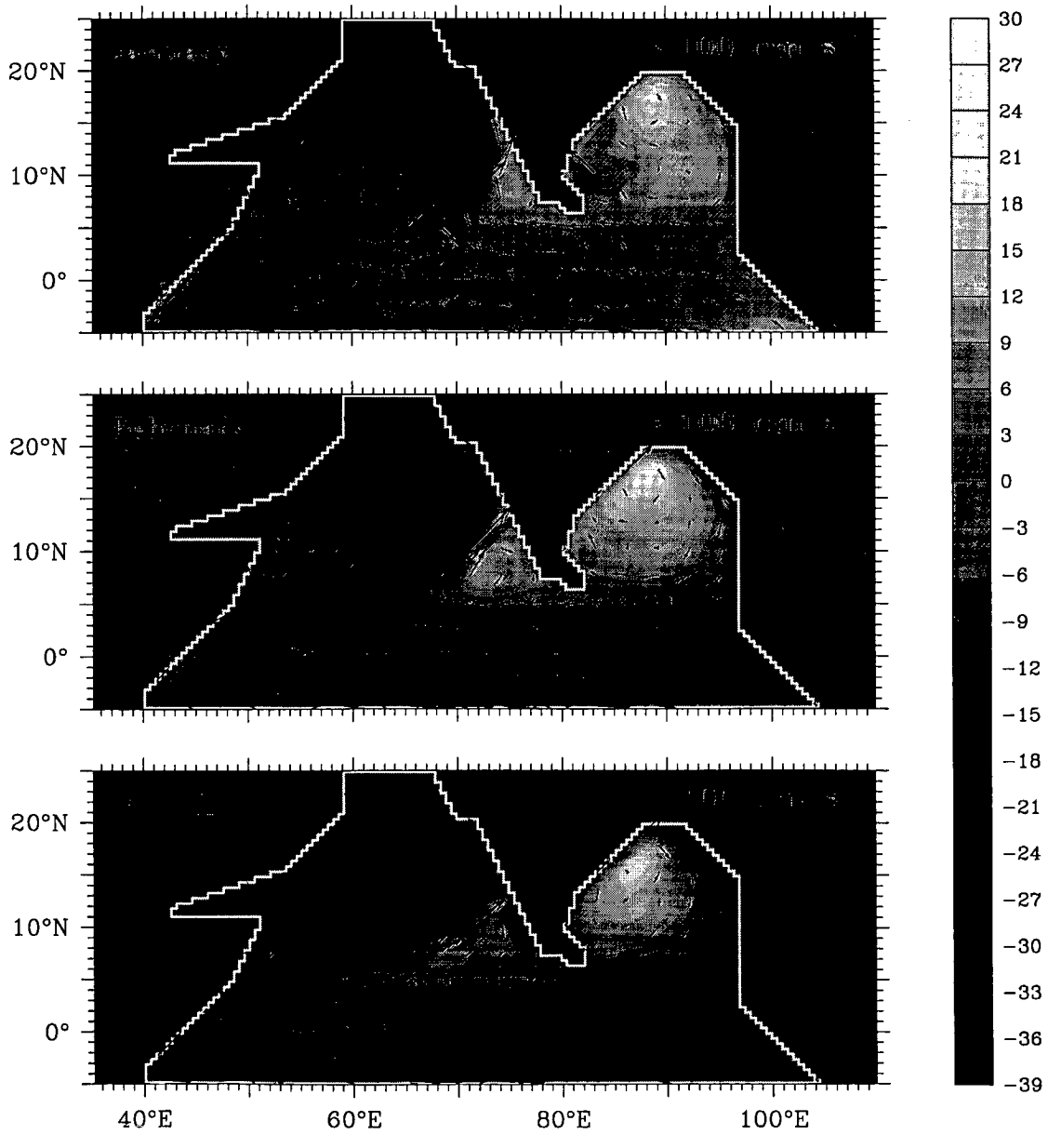

Figure 4.10 (continued) Effect of variable density on the seasonal cycle of surface circulation in the north Indian Ocean; apart from the density variation in the upper layer, the simulation is identical to the nonlinear simulation in Section 3.3.2 (Figure 3.5). Sea-level deviation η (cm) and velocity $\mathbf{v}$ (cm s^{-1}) are shown. Sea level rises in the northern bay and the eastern equatorial Indian Ocean, and it decreases in the northern and western Arabian Sea, the four regions most affected by the variations in density.

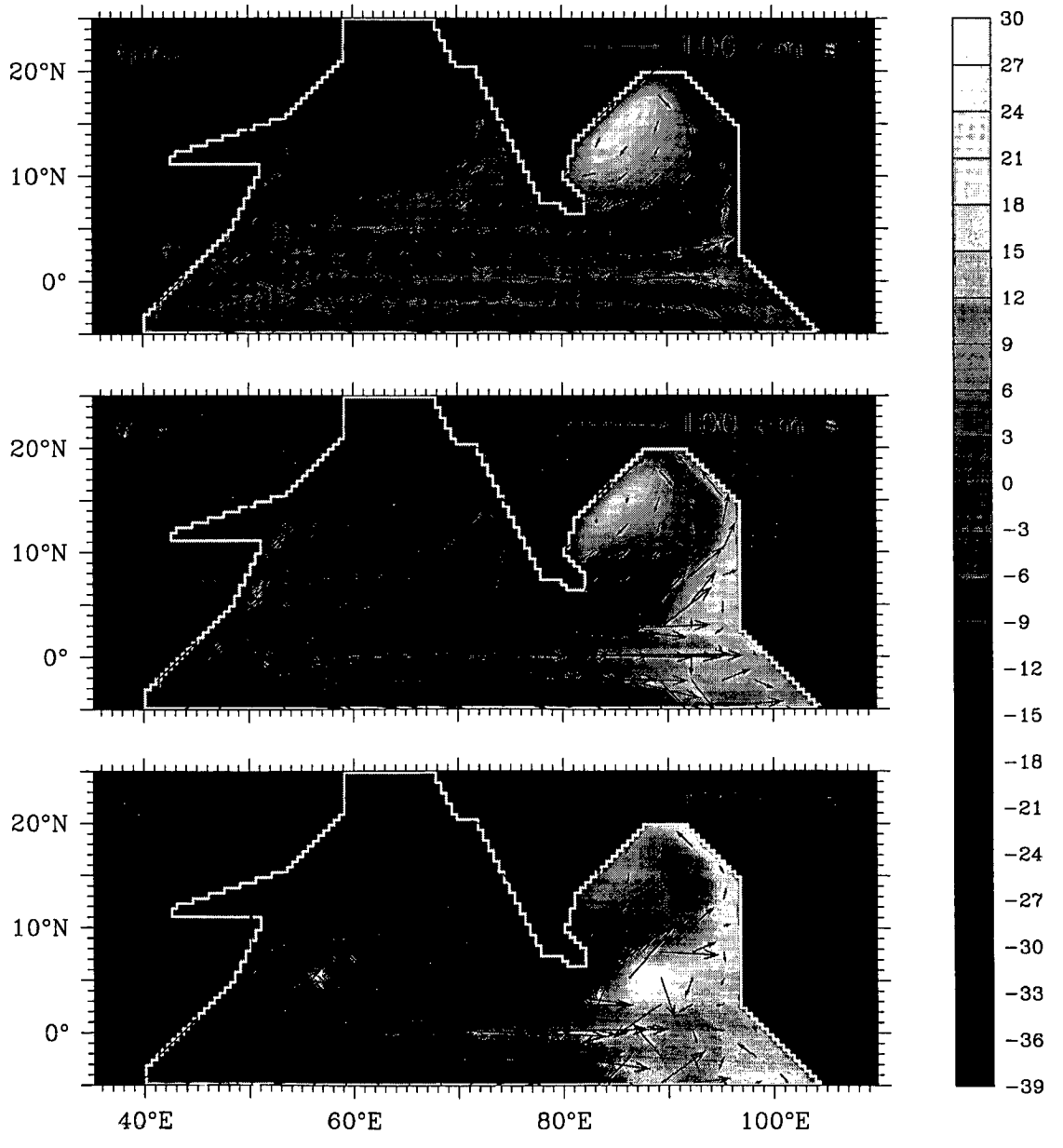

Figure 4.10 (continued) Effect of variable density on the seasonal cycle of surface circulation in the north Indian Ocean; apart from the density variation in the upper layer, the simulation is identical to the nonlinear simulation in Section 3.3.2 (Figure 3.5). Sea-level deviation η (cm) and velocity $\mathbf{v}$ (cm s^{-1}) are shown. The increase in density in the western Arabian Sea has an effect on the sea level and the circulation off the Somali coast; the Great Whirl is weaker than in the constant-density simulation. This is the only occasion when the variations in density have an impact on the circulation.

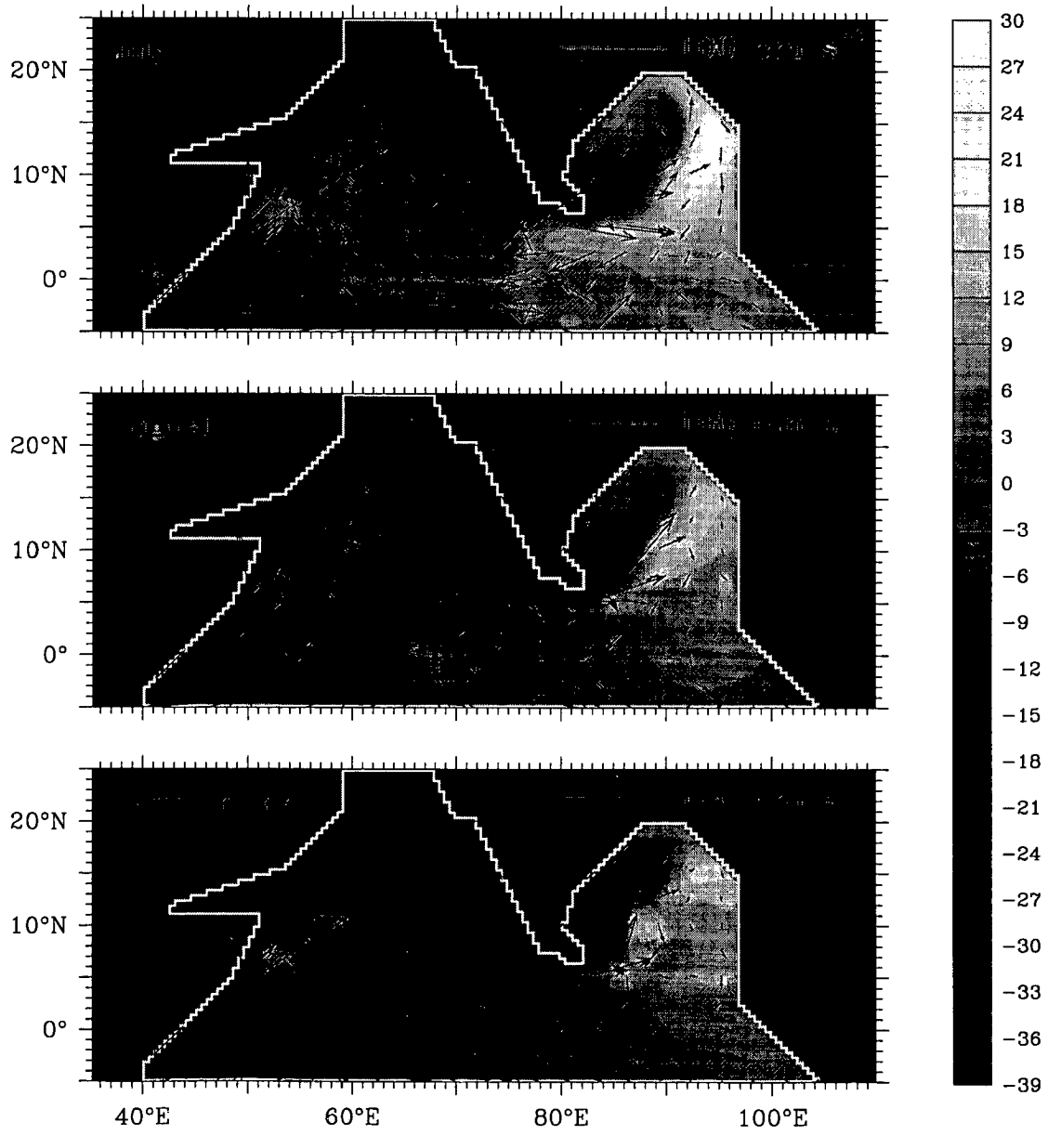

Figure 4.10 (continued) Effect of variable density on the seasonal cycle of surface circulation in the north Indian Ocean; apart from the density variation in the upper layer, the simulation is identical to the nonlinear simulation in Section 3.3.2 (Figure 3.5). Sea-level deviation η (cm) and velocity $\mathbf{v}$ (cm s^{-1}) are shown. The after-effects of the southwest monsoon persist in the western Arabian Sea till December; the sea level there is lower than in the constant-density simulation and the currents are a little weaker.

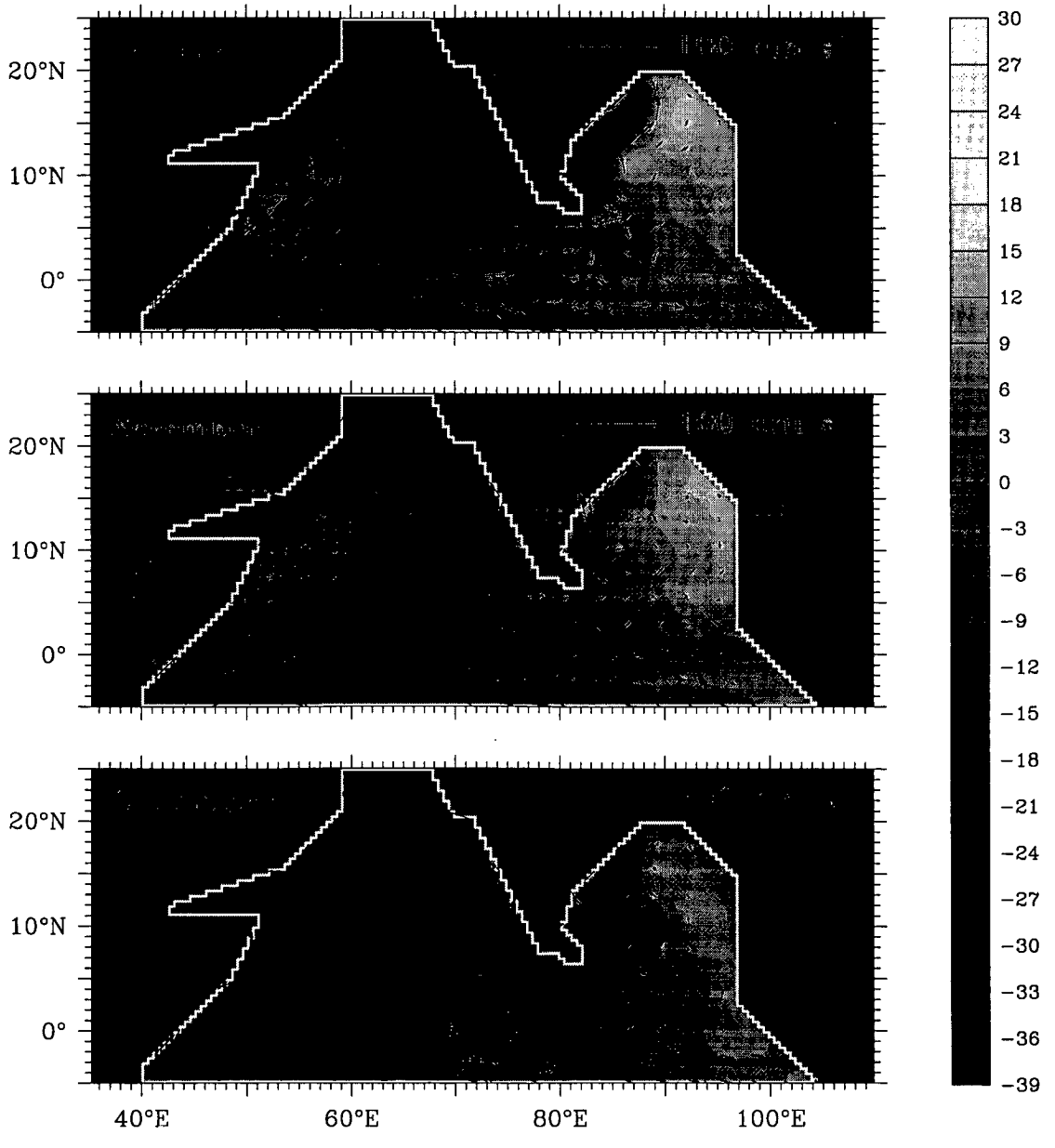

Figure 4.11 Effect of salinity on the seasonal cycle of model alongshore currents. Alongshore ship drifts (cm s^{-1}), from the climatology of Rao et al. [1989], are plotted along with the alongshore currents (cm s^{-1}) from the simulations with constant upper layer density and with variable upper layer density in a $1\frac{1}{2}$-layer reduced-gravity model. The density of the upper layer in the variable-density model is computed from the monthly climatologies of Levitus and Boyer [1994] and Levitus et al. [1994]. All variables plotted are anomalies; the annual mean has been removed. The variations in density force minor changes in the current along the coast of India; the increase in velocity, however, necessitates a change in the scale of the ordinate (see Figure 4.2).

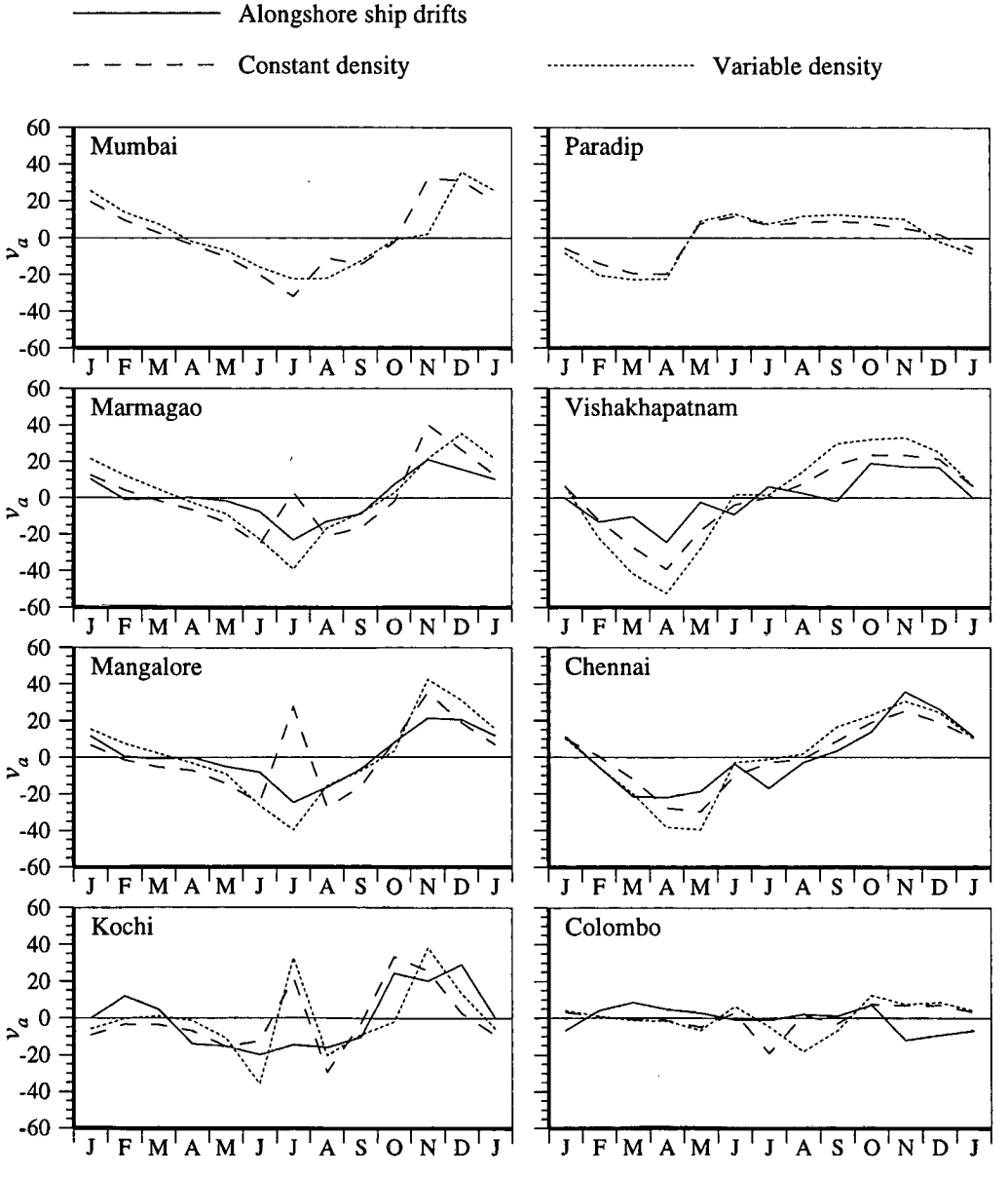

Figure 4.12 Effect of salinity on the seasonal cycle of sea level. Monthly anomalies of corrected sea level (cm) are plotted along with those from the simulations with constant and variable upper layer density in a $1\frac{1}{2}$-layer reduced-gravity model. The increase in Γ along the east coast has an effect on sea level only at Paradip in the northern bay, where the density changes are significant, but this increase is restricted to the southwest monsoon. The effect of a decrease in salinity during September is offset by upwelling forced by the EICC. During November, when the EICC favours downwelling, salinity increases in the monthly climatology of Levitus et al.. Therefore, the model still fails to simulate the maximum along the east coast.

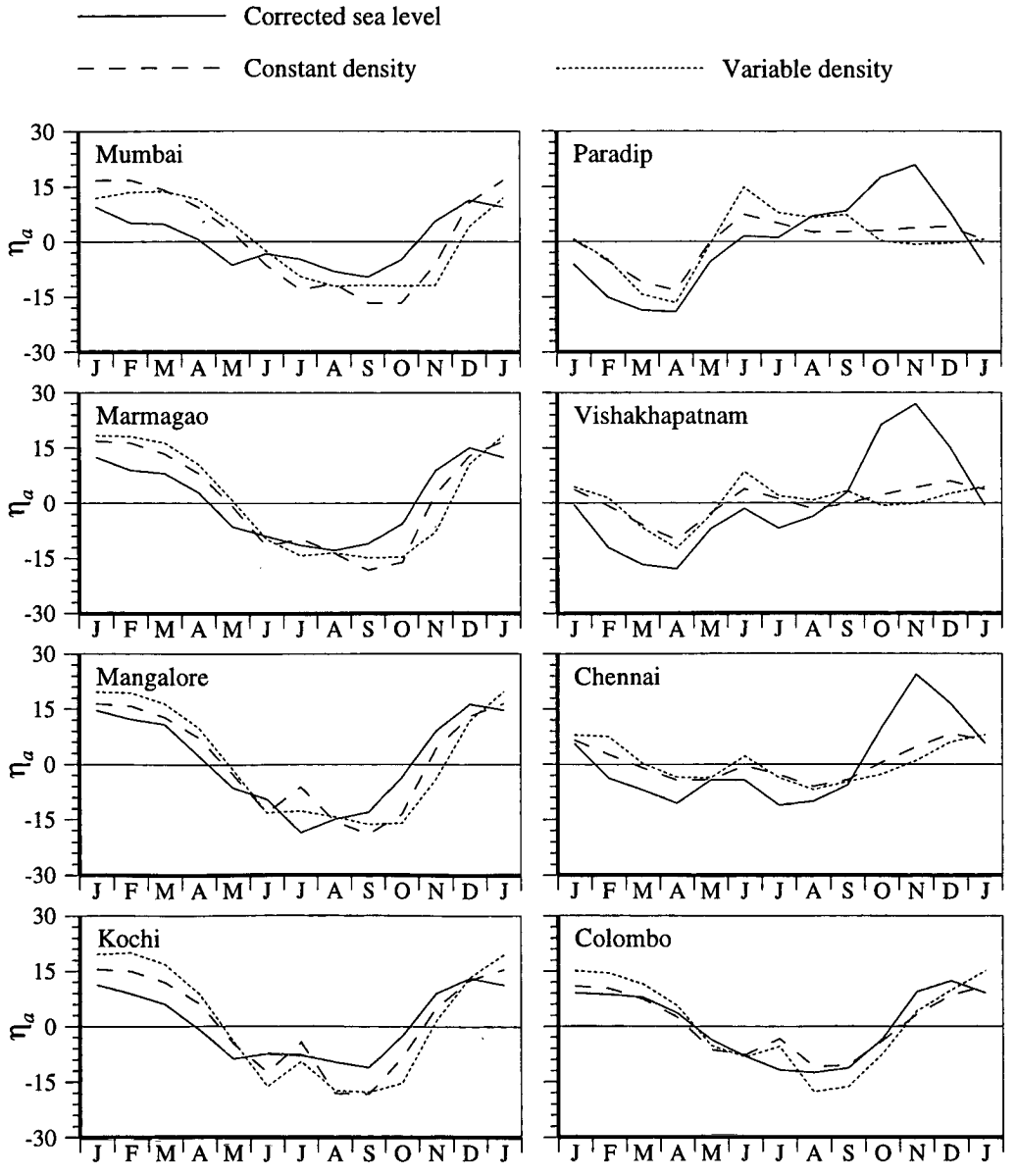

data in the coastal waters of India[5] [Rao, 1998]; this is especially true of salinity. The absence of data in the coastal waters of India makes it necessary to extrapolate from the data in the open bay, which too are sparse. Hence, the monthly climatologies of Levitus and Boyer and Levitus et al. are not reliable in the vicinity of the coast; a comparison with the hydrographic data collected during the six EEZ cruises (Section 2.4) [Shetye et al., 1990, 1991a,b, 1993, 1996] shows that the climatology of Levitus et al. does not capture the seasonal cycle of salinity correctly.

4.3.2 Monsoon Rainfall and the Seasonal Cycle of Salinity

There is considerable spatial and temporal variation in rainfall over the Indian subcontinent and the surrounding ocean, and this leads to the large differences in salinity along the coast. The Indian west coast receives very high rainfall, about 200 cm year^{-1}, almost 90% of which is during the southwest monsoon (June–September). The high rainfall is because of the Sahyadri range (or Western Ghats) running parallel to the coast about 100 km inland (Figure 4.13); this range blocks the moisture-rich monsoon winds. The resulting runoff is carried to the Arabian Sea by numerous swift, seasonal streams. Over the rest of the subcontinent, there is considerable spatial variability in the amount of rainfall, but about 80% is received during the southwest monsoon. Most of this rain falls in the catchment areas of eastward-flowing rivers (Figure 4.13), whose inflow into the Bay of Bengal peaks in August, a month after the peak in rainfall. About 70% of this inflow comes from the Ganga and the Brahmaputra, which discharge about 7.2×10^{11} m^3, the fourth largest discharge in the world, into the northern bay during June–October [Martin et al., 1981; Shetye, 1993]. Therefore, the quantum of freshwater inflow from the rivers into the seas around India is highly seasonal.

Equally seasonal are the coastal currents around India[6]. The weakening of the southwest monsoon winds after July, coupled with remote forcing from the eastern Bay of Bengal and the equatorial Indian ocean, forces an equatorward EICC in the northern bay; the EICC is poleward along the rest of the Indian east coast. Together, these currents trap the runoff in the northern bay. As the southwest monsoon withdraws and the northeast monsoon sets in, the equatorward EICC expands southward, forcing coastal downwelling and advecting the riverine inflow as a coastally-trapped low-salinity plume that is nearly 60 m deep [Shetye et al., 1996]. By November, the EICC is equatorward all along the east coast and there is a sharp drop in the salinity along the coast. The EICC flows into the westward NMC, which bends around Sri Lanka and flows along the western flank of the Lakshadweep high into the poleward WICC; the riverine inflow into the Bay of Bengal is thus transported into the Arabian Sea. This inflow is spread along the west coast

[5]This is due to the restrictions put by India on the use of data, hydrographic or otherwise, collected in the Indian Exclusive Economic Zone (EEZ).

[6]See Chapters 2 and 3.

Figure 4.13 The major rivers of India; the dashed line shows the 200 m isobath. Most of the big rivers flow eastward into the Bay of Bengal. The highest runoff is that of the Ganga and Brahmaputra, which together empty about 7.2×10^{11} m^3 into the northern bay during June–October. Most of these rivers originate either in the Himalayas or in the Sahyadri range (Western Ghats), which is about 1 km high and runs parallel to the west coast of India. Smaller, swift streams flow westward from the Sahyadris into the Arabian Sea, and their combined runoff is about 30% that of the Ganga and the Brahmaputra. This runoff is assumed to be 80% of the total rainfall in the coastal belt that stretches from the southern tip of India to just north of Mumbai and is bounded in the east by the Sahyadri range. The abbreviations used in the figure are as follows: EICC, East India Coastal Current; WICC, West India Coastal Current; NMC, Northeast Monsoon Current; LH, Lakshadweep high; R.G., River Ganga; R.B., River Brahmaputra. The currents are plotted for December, when the EICC flows equatorward and the WICC flows poleward. Together, they transport low-salinity water from the northern bay to the west coast of India.

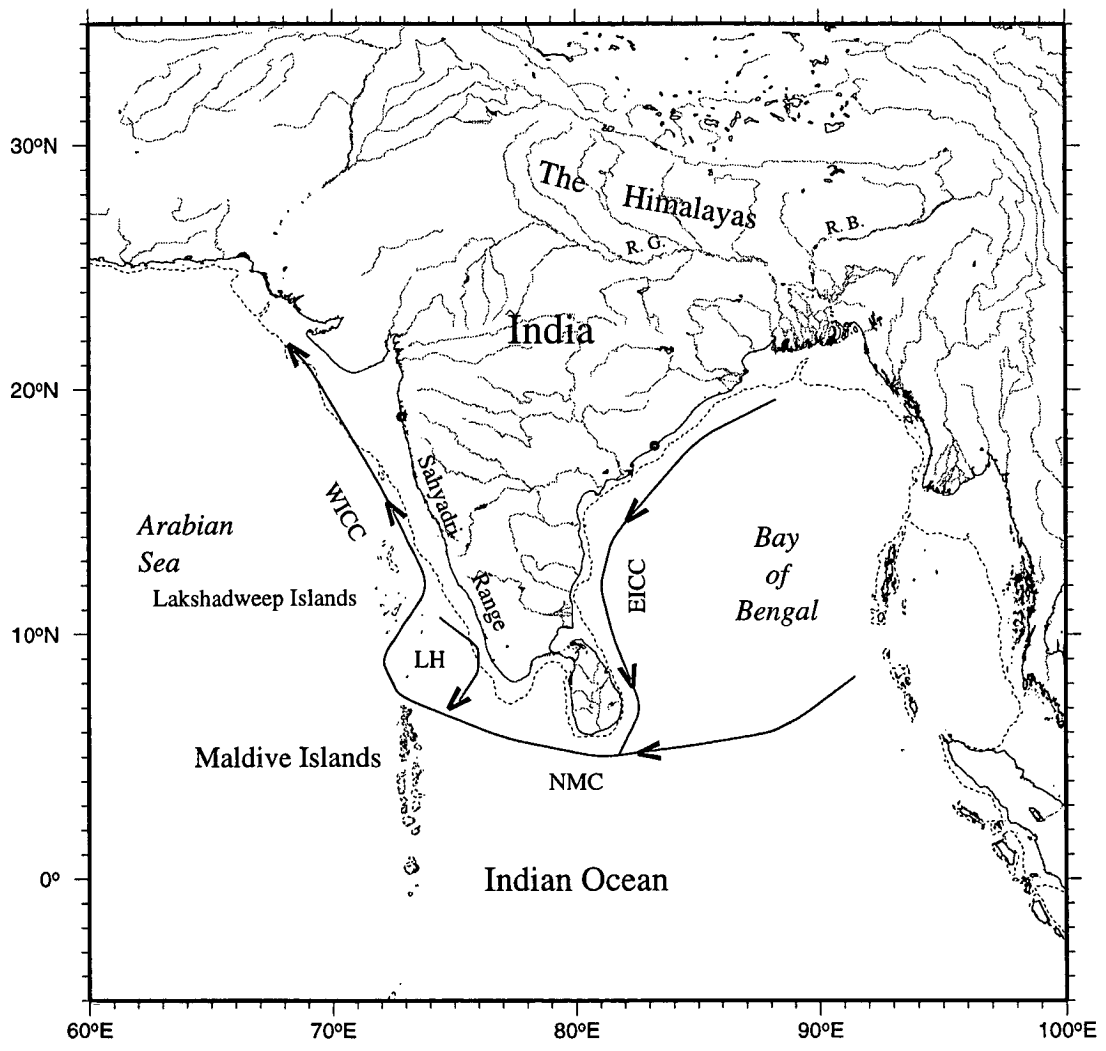

of India by the WICC and is spread offshore in the southern part of the coast by the westward propagating Rossby waves that constitute the Lakshadweep high. By February, the EICC reverses to flow poleward, forcing coastal upwelling and raising salinity along the east coast [Shetye et al., 1993]. The WICC along the northern part of the west coast, however, continues to flow poleward till March, spreading the low-salinity water from the bay, as well as the inflow from local rivers during the southwest monsoon, along the west coast.

During the southwest monsoon, when the freshwater actually enters the Indian coastal regime, the EICC and WICC favour upwelling, and hence, the low-salinity water is trapped at the surface and pushed offshore by the Ekman flow, except in the northern bay, where the remotely-forced equatorward EICC traps the river runoff. It is only after the southwest monsoon, when these currents reverse, that the low-salinity water is pushed towards, and advected along, the coast. Even along the west coast, the lowest salinities at the surface are during the southwest monsoon, but the drop in salinity is restricted to a shallow surface layer. As along the east coast, it is during the northeast monsoon, when the WICC favours downwelling and there is inflow of freshwater from the Bay of Bengal, that the low-salinity layer deepens, this being more pronounced off southwest India where the low-salinity water spreads offshore because of the Lakshadweep high.

The seasonal cycle of salinity along the coast of India is shown in Figures 4.14 and 4.15, which are based on the six EEZ cruises. These data represent but a snapshot and were collected over a few years. Interannual variability is expected to cause changes in these fields, but they nevertheless provide a rough picture of the seasonal cycle of salinity in the coastal waters of India. Unlike in the data of Levitus et al. [1994], salinity, averaged over the top 100 m, is lowest along the east coast *after* the southwest monsoon. The error in the monthly climatology of Levitus et al. is owing to the linear interpolation from their seasonal climatology and the lack of data in the coastal waters of India. Therefore, to examine the effect of salinity on the seasonal cycle of sea level along the east coast of India, we synthesize a seasonal cycle of the coastal salinity field from the available data. We cannot, however, use the data from these six cruises and interpolate to synthesize the seasonal cycle because of the rapid changes in the coastal currents off India and the associated rapid changes in the coastal salinity and temperature fields due to upwelling and downwelling. A better approach is to use all the available salinity data in the vicinity of the coast to construct a climatology of coastal salinity, which can be used in conjunction with the salinity climatology of Levitus et al. [1994] in the simulations.

4.3.3 Synthesis of a Climatology of Temperature and Salinity Along the Coast

To construct the "coastal climatology", we use hydrographic data available at the Indian National Oceanographic Data Centre (INODC). These data were collected over several cruises, the earlier

Figure 4.14 Seasonal cycle of surface salinity (PSU) in the coastal waters of India, based on the six EEZ cruises. The "+" indicate the locations at which the hydrographic profiles were obtained. The time of the cruises are mentioned in addition to the months they are considered representative of. The minimum and maximum salinity and the contour interval (CI) are listed for each cruise.

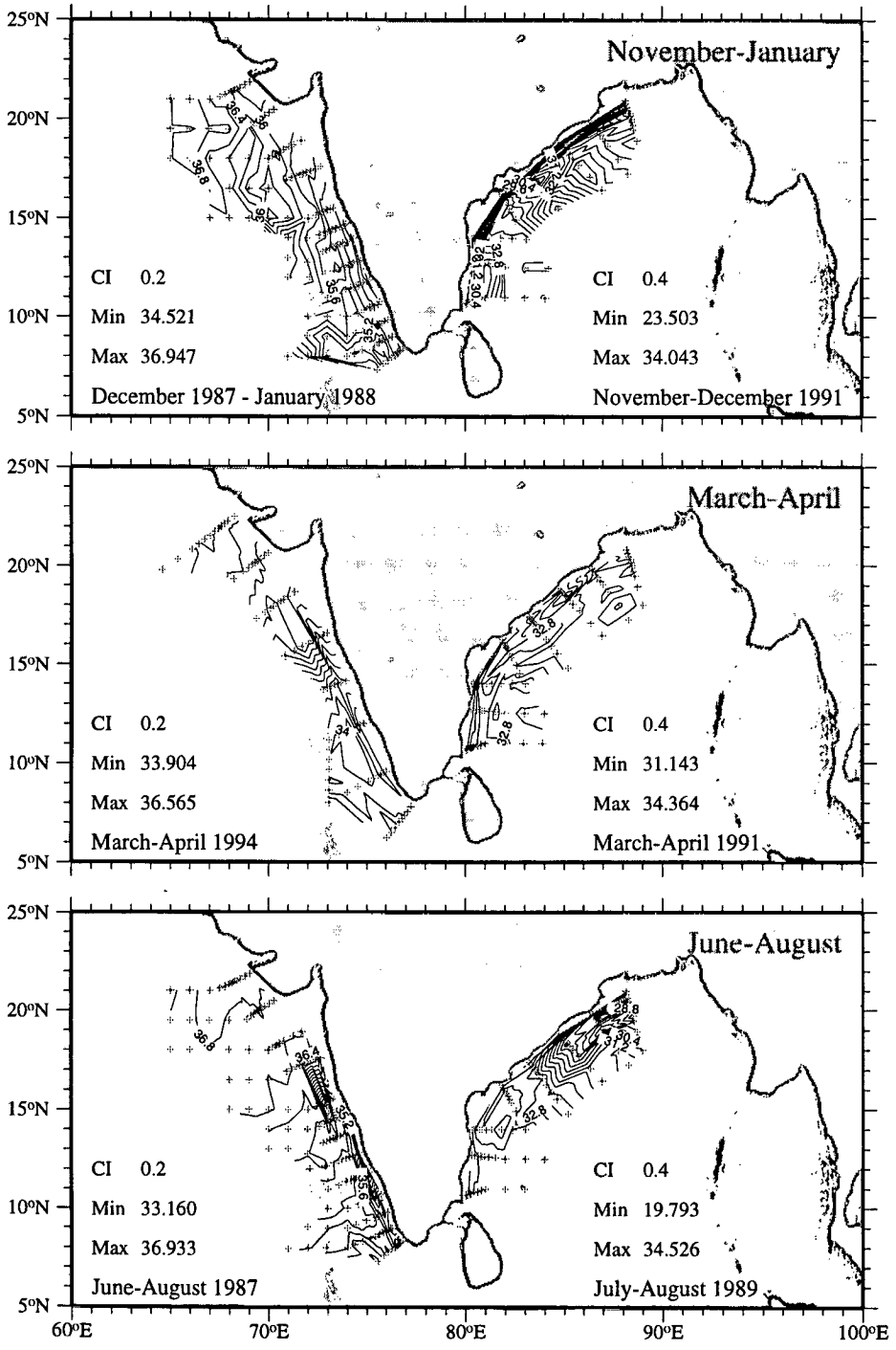

Figure 4.15 Vertical cross-sections of salinity (PSU) off Vishakhapatnam (right) and Marmagao (left). The distance from the coast (km) is plotted on the abscissa and depth (m) on the ordinate. The cross-sections are based on the six EEZ cruises.

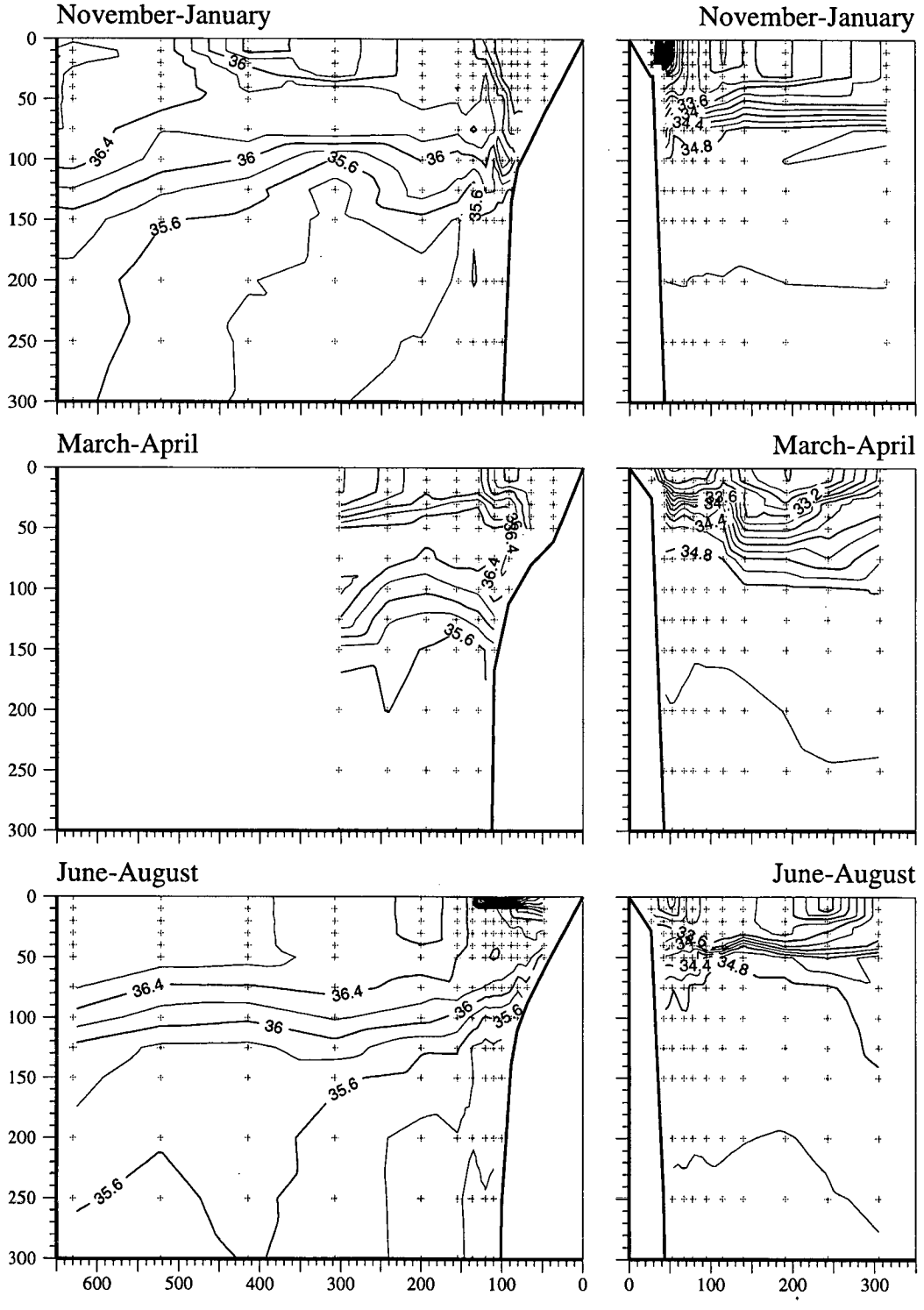

cruises using Nansen bottles and the later cruises using CTDs[7] to obtain a vertical profile of temperature and salinity. The data are available at the standard depths[8]. We bin the data in a $1° \times 1°$ box around Paradip, Vishakhapatnam, Chennai, Kochi, Mangalore, Marmagao, and Mumbai to construct a climatology for these boxes, and then use linear interpolation to obtain a continuous distribution of temperature and salinity along the coast, this process being being repeated for each month[9]. This method works well and yields a better synthesis than is possible using just the six EEZ cruises. The only caveat is that data are not available for some months at some of these seven stations, the data at Paradip having the maximum number of gaps. Given the description of the seasonal cycle of the currents and the available data, it is possible to interpolate to fill these gaps. The difficult month, however, is November, for which no salinity data are available along the east coast! The deep low-salinity plume along the east coast was surveyed in December by Shetye et al. [1996]; hence, the lowest salinity reported along the east coast is for that month. Linear interpolation is ruled out, given the rapid changes in salinity that take place after the collapse of the southwest monsoon. To get over this problem, we use the values for December as a guide, and assume that the salinity in November is *lower* than in December. There are two reasons for making this assumption. First, the equatorward EICC manifests along the coast after the collapse of the southwest monsoon, appearing first in the northern bay. The Kelvin wave that forces it propagates equatorward along the coast and the EICC reverses all along the east coast in October. Since the current speed is of the order of 25 km day^{-1} [Shetye et al., 1996], it would take about a month to transport the low-salinity water down the coast to Chennai; hence, we expect the salinity to be lowest in late October or in early November. Second, the equatorward EICC is strongest in November; it weakens in December and begins reversing in January, forcing coastal upwelling and raising salinity all along the east coast; hence, we expect the salinity to be lower in November than in December.

We choose salinities sufficiently low to produce the sharp peak in sea level observed in November. Then, if these values are not unreasonable, we would have a hypothesis to explain the seasonal cycle of sea level along the coast of India. The synthesized seasonal cycles of temperature and salinity, averaged over the top 100 m of the water column, are shown in Figures 4.16 and 4.17 for the stations along the coast; the seasonal cycle of the resulting reduced-gravity parameter Γ is shown in Figure 4.18.

[7]Conductivity-Temperature-Depth.

[8]The standard depths (m) are 0, 10, 20, 30, 50, 75, 100, 125, 150, 200, 250, 300, 400, 500, 600, 700, 800, 900, 1000, 1100, 1200, 1300, 1400, 1500, 1750, 2000, 2500, 3000, 3500, 4000, 4500, 5000, and 5500.

[9]We interpolate linearly between the climatologies of Levitus and Boyer [1994] and Levitus et al. [1994] at the northeastern corner of the Bay of Bengal and the "new" climatology at Paradip, and between the "new" climatology at Mumbai and the climatologies of Levitus and Boyer and Levitus et al. at Veraval (see Figure 2.1) to obtain a smooth transition along the coast. There still remains a sharp density jump offshore, but this is not of major consequence for our problem.

Figure 4.16 The seasonal cycle of temperature (°C), averaged over the top 100 m of the water column, along the coast. The synthesized seasonal cycle is plotted along with that from the climatology of Levitus and Boyer [1994]. The method used to synthesize the climatological seasonal cycle is described in Section 4.3.3. The synthesized climatology of temperature is similar to that of Levitus and Boyer; the maximum difference in temperature is less than 2°C.

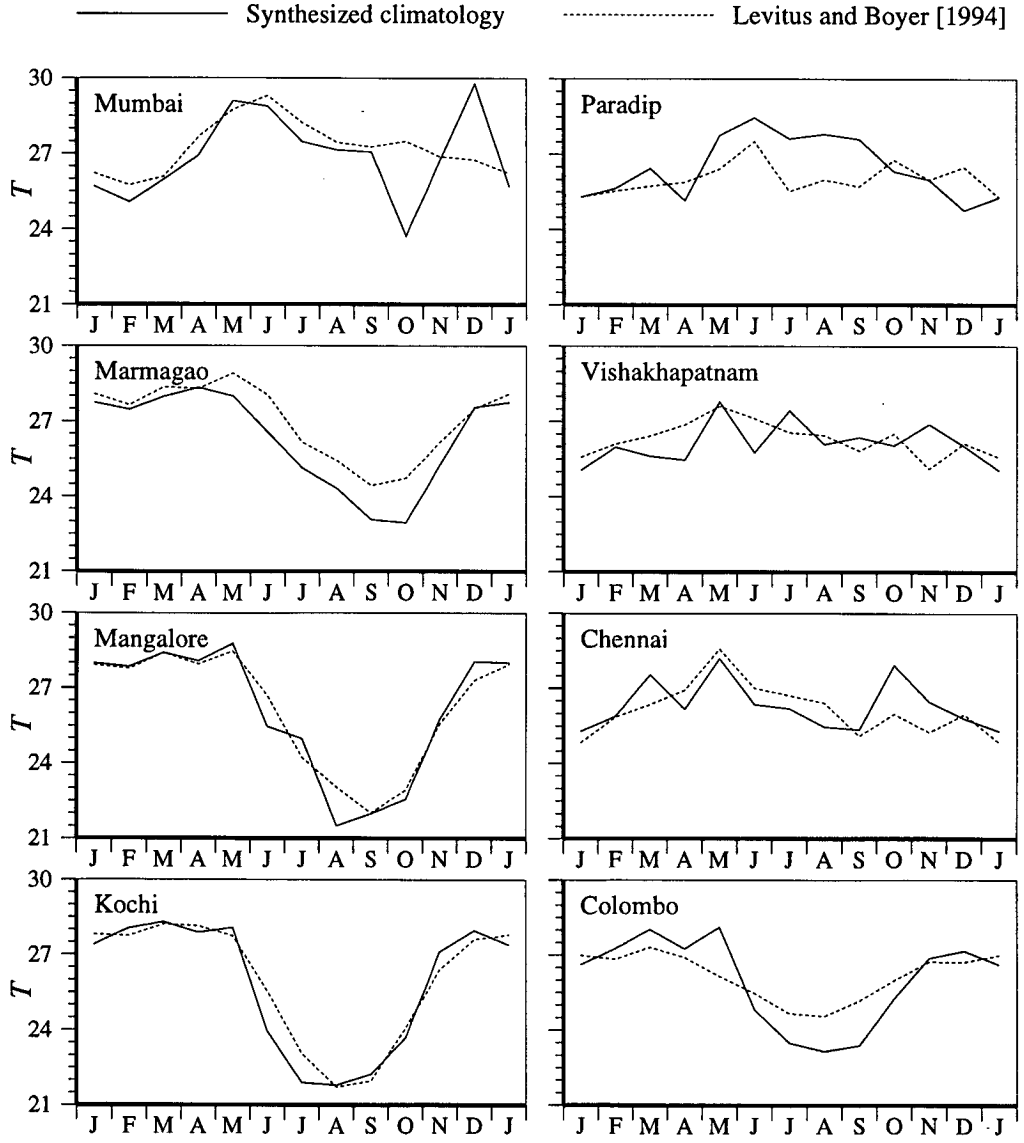

Figure 4.17 The seasonal cycle of salinity (PSU), averaged over the top 100 m, along the coast. The synthesized seasonal cycle is plotted along with that from the climatology of Levitus et al. [1994]. The method used to synthesize the climatological seasonal cycle is described in Section 4.3.3. The synthesized salinity matches that of Levitus et al., except along the east coast after the southwest monsoon. The inflow of freshwater during the southwest monsoon and its advection along the coast by the equatorward EICC after September result in a sharp drop in salinity along the coast.

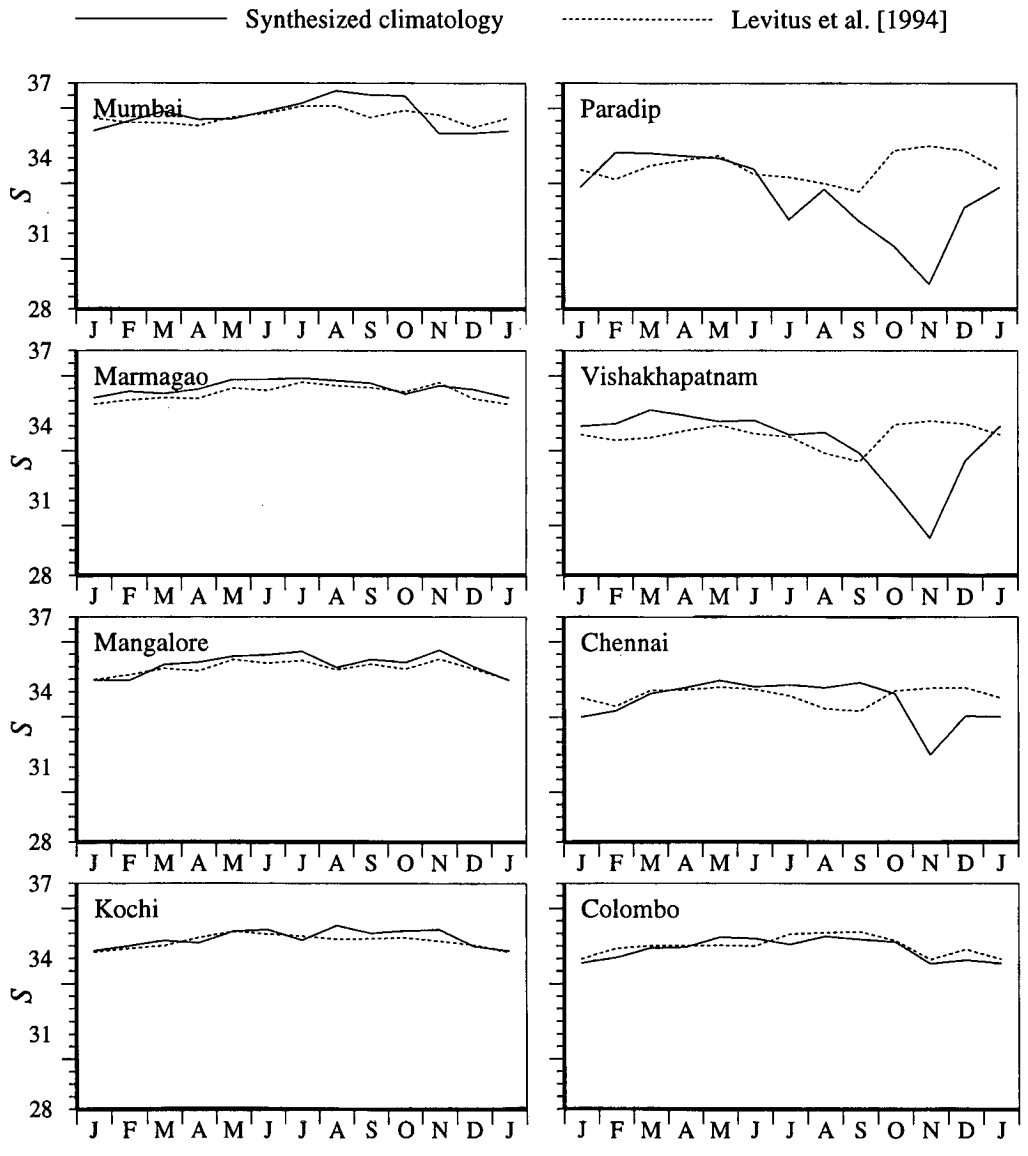

Figure 4.18 The seasonal cycle of Γ along the coast of India. The density of the upper layer is computed from the synthesized monthly climatology of temperature and salinity; the method of synthesis is described in Section 4.3.3. The figure shows Γ, Γ_T, and Γ_S; Γ_T and Γ_S are the contributions of temperature and salinity to Γ. Γ increases rapidly along the east coast after the southwest monsoon as the salinity and density decrease. The major contribution to Γ is from variations in salinity.

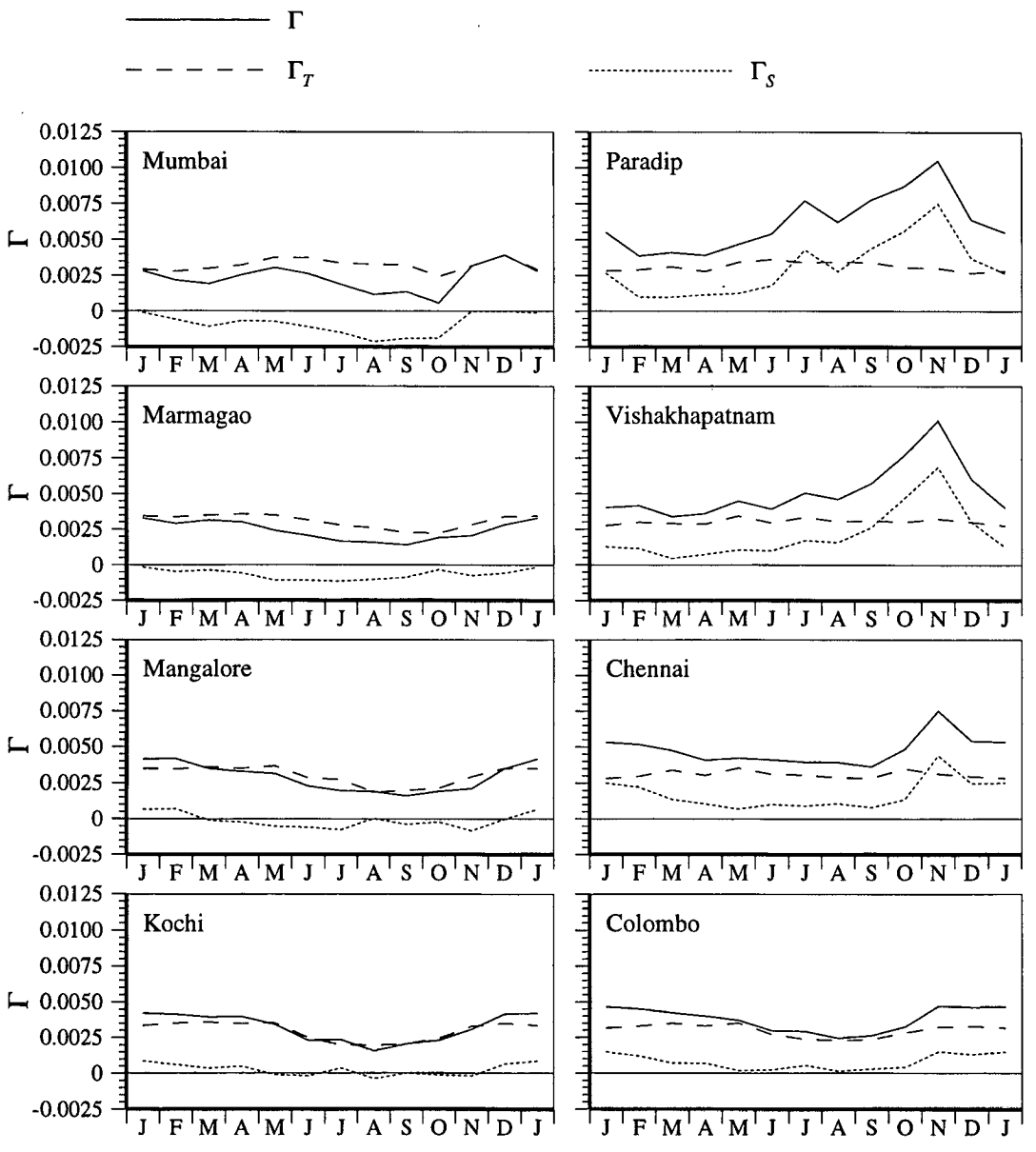

Figure 4.19 Effect of the synthesized salinity on the seasonal cycle of sea level. Monthly anomalies of corrected sea level (cm) are plotted along with those of sea level (cm) from the simulations with constant and variable upper layer density in a $1\frac{1}{2}$-layer reduced-gravity model. The density of the upper layer is computed from the monthly climatologies of Levitus and Boyer [1994] and Levitus et al. [1994], except along the coast of India, where the modified climatology is used. The lower salinity along the east coast in the synthesized climatology enables the model to simulate the sea level maximum in November; the seasonal cycle of model sea level now resembles that of corrected sea level.

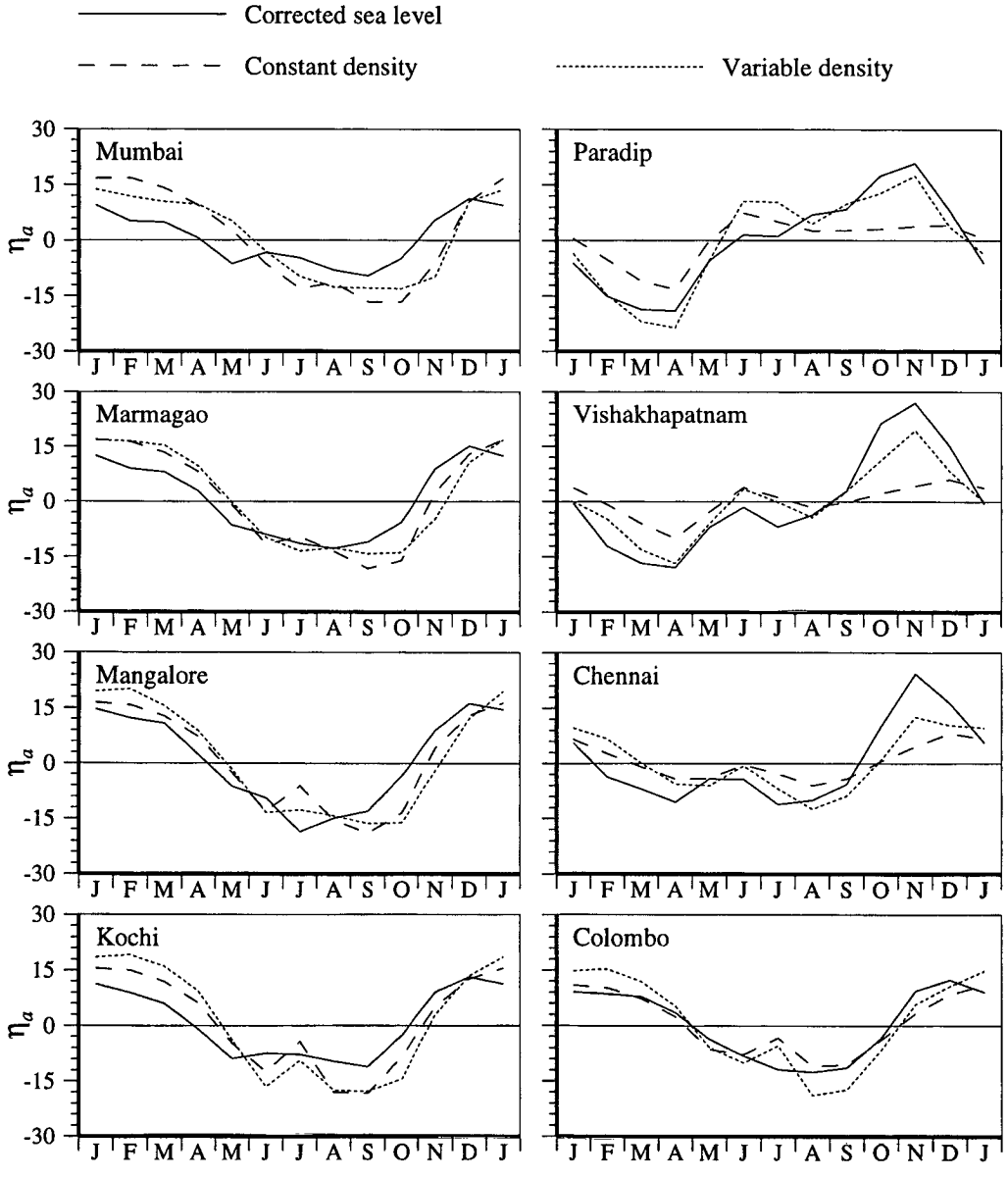

4.3.4 Simulations With the Synthesized Climatology

The synthesized climatology yields alongshore temperature and salinity fields from the northeastern corner of the Bay of Bengal to Veraval on the west coast of India. These are used to replace the coastal temperature and salinity data in the climatologies of Levitus and Boyer [1994] and Levitus et al. [1994], and this new climatology is used to determine Γ for the $1\frac{1}{2}$-layer model. The resulting sea level is shown in Figure 4.19. The synthesized coastal salinity improves the model's ability to simulate the seasonal cycle of sea level along the east coast. The changes made to the coastal salinity field have almost no impact on the west coast, but they raise sea level in November along the east coast, the seasonal cycle of model sea level now being similar to that of corrected sea level. The model sea level is still somewhat lower, implying that the salinity, averaged over 100 m, may be even lower than that assumed. We do not, however, have any data to support or deny this possibility.

In the absence of salinity data along the coast, it is difficult to go farther than this. Our aim has been to diagnose the causes of the seasonal cycle of corrected sea level along the Indian coast, and the somewhat *ad hoc* modifications made to the coastal salinity are justified in this context. A more acceptable approach would be to try to model the salinity, given the rainfall and the river runoff. This, however, is a much more complex task, one that we leave to the future. The simulations, however, are sufficient to warrant the inference that both wind-forced coastal currents and variations in coastal salinity are significant causes of the seasonal cycle of corrected sea level along the coast of India, the decrease in salinity along the east coast in November being responsible for the peak in sea level there. This decrease in salinity is due to the advection of the river runoff along the coast by the EICC. Advection is a nonlinear process; linearization of advection demands the existence of a well-defined mean. Since the variability of the currents and salinity along the coast of India is at least as large as the mean, this process cannot be linearized, unlike the wind-forced model of Chapter 3. The variations in salinity and density, however, have a comparatively minor impact on the alongshore currents; this implies that linear models are sufficient to describe the seasonal cycle of large-scale coastal currents, but not that of sea level, especially along the east coast of India.

4.4 Effect of Bathymetry: The Continental Shelf

One aspect of the reduced-gravity model that needs some discussion is the neglect of the continental shelf. The model assumes that the ocean has a flat bottom and that the continental boundaries are vertical walls. This simplification filters out those continental shelf waves and coastally-trapped waves that depend on shelf-bathymetry for their existence, with coastal Kelvin waves replacing them. In the ocean, the coastal Kelvin waves forced by the large-scale wind field are

modified in the vicinity of a coast, taking the form of continental shelf waves on the shelf in the absence of stratification, and that of coastally-trapped waves in the presence of stratification [Gill and Clarke, 1974; Mysak, 1980]. The Kelvin wave propagates with the shelf-break as the boundary, the continental slope acting as the vertical wall for the Kelvin wave, which therefore has its maximum amplitude at the shelf-break, the amplitude decaying exponentially offshore. Gill and Clarke [1974] showed that the movement of the thermocline due to the large-scale circulation was correlated with the changes in sea level at the coast. Therefore, a simple, heuristic idea of the effect of the shelf is the following. If the upper layer thickness is less than the depth of the continental shelf at the shelf-break, which usually is assumed to coincide with the 200 m isobath, the amplitude of the wave decays inshore too with an e-folding length scale given by the internal Rossby radius of deformation, R_i. If, on the other hand, the upper layer thickness is greater than the depth of the continental shelf at the shelf-break, the amplitude of the wave decays inshore with an e-folding length scale given by the external Rossby radius of deformation, R_e. Since R_i is proportional to the speed of the first baroclinic mode and R_e to the speed of the barotropic mode, $R_i \ll R_e$, and the amplitude decays faster inshore when the depth of the upper layer is less than 200 m. This description may not be valid at higher frequencies, but is reasonable at the seasonal and lower frequencies of interest to us.

The above effect of the continental shelf may be modified under certain circumstances, two of which are of interest to us. First, the strength of the coupling between the Kelvin wave and the shelf wave is of $O(\lambda)$, where $\lambda = \frac{R_i}{L}$, L being the shelf width [Allen, 1975; Mysak, 1980]. Off Mumbai, where the shelf is wide, this implies that the coupling is weak, and therefore the circulation on the shelf may be independent of that offshore. This, however, is unlikely because the seasonal cycle of sea level at Mumbai is similar to that at other stations along the Indian west coast, implying a link between coastal sea level and the large-scale circulation. The increased friction on the wide shelf, however, will alter the momentum balance and a likely consequence is a drop in the sea level at the coast. This would account for the model sea level being higher than the corrected sea level at Mumbai. Second, if there is a strong cross-shore salinity (or temperature) gradient on the shelf, as along the coast of India after the southwest monsoon, the decay in the amplitude inshore will be arrested by the low salinities, and the amplitude may even increase towards the coast. At the low frequencies of interest, this modification will be geostrophic, forcing a coastal current in the same direction as the large-scale coastal current. This would account for the model sea level being lower than the corrected sea level along the east coast. This discussion on the possible effect of the continental shelf on coastal sea level, however, is heuristic, and needs to be confirmed by observations and detailed model studies.

In conclusion, the presence of the continental shelf is not of major consequence for the seasonal cycle of sea level along the coast of India. The causes of this cycle are atmospheric pressure,

the wind-forced coastal currents, and the large changes in salinity, especially along the east coast. The difference in salinity between the east and west coasts of India results in a larger range of the seasonal cycle along the east coast. This alongshore gradient in salinity also has implications for the alongshore gradient in annual sea level, which forms the subject of the following chapter.

Chapter 5

Annual Mean Sea Level

5.1 Observational Background

While concluding the Great Trigonometrical Survey of India, Colonel S. G. Burrard made the following observation [quoted after Ghildyal and Kumar, 1984].

> Whilst therefore the levelling operations 1858–1909 have proved that the mean surface of the Arabian Sea and the Bay of Bengal are very nearly at the same elevation, they have also given rise to a suspicion, that the Bay of Bengal may be perhaps slightly higher of the two. It is but a suspicion, the accuracy of the levelling does not warrant us in pronouncing the divergence to be proved. It will be for our successors to show by means of future lines, whether the suspicion is well-founded, or whether the divergence is a result of levelling errors.

The Great Trigonometrical Survey of India was carried out during 1858–1909 to map the surface topography of the Indian subcontinent, and was, in its time, the most detailed and accurate survey of its kind ever undertaken. It is in the course of this survey that a difference of about 30 cm was noticed between the mean sea level[1] in the Bay of Bengal and the Arabian Sea, an observation that was confirmed during the Adjustment of the First Level Net of India [Ghildyal and Kumar, 1984]. The observations show that the mean sea level at Vishakhapatnam is 32 cm higher than that at Mumbai and that the mean sea level at Chennai is 17 cm higher than that at Mangalore. The permitted error in levelling over 1080 km, the distance along the levelling lines between Chennai and Mangalore, is 9.8 cm; thus, even after accounting for possible errors in levelling, the mean sea level along the east coast of India is higher than that along the west coast [Ghildyal and Kumar, 1984].

[1] By mean sea level, Ghildyal and Kumar mean annual sea level, which is the same as annual mean sea level.

5.2 Theoretical Background

The only study of this difference in mean sea level that we are acquainted with is the one by Ghildyal and Kumar [1984]. They state that "enough levelling data have accumulated to carry forward the investigation from the stage where Colonel Burrard left it for us to complete. The divergence in mean sea level is apparent and this is not due to errors of levelling alone but other factors also." They compute the difference in sea level for several choices of levelling lines before reaching this conclusion. The difference in mean sea level between Chennai and Mangalore is attributed to the lower surface salinity at Chennai (6.7 cm) and higher sea surface temperature (SST) at Chennai (8 cm), with the lower atmospheric pressure at Mangalore reducing the difference by 5 cm. These three factors together account for a difference of about 7 cm between Chennai and Mangalore, less than the permissible error due to levelling. Ghildyal and Kumar state that the apparent difference in mean sea level between the two coasts can be accounted for by these corrections and levelling errors, and that this implies that the mean sea level is not different along these two coasts! The authors are surveyors, and their discomfort at the possibility of a variation in mean sea level along the boundary of the open sea is evident. Hence, though Ghildyal and Kumar on the right track as far as discerning the causes of the observed difference are concerned, their aim is to explain away the difference.

There is no reason for assuming that such a difference in mean sea level cannot exist between the east and west coasts of India. The observations suggest that there is a mean alongshore gradient of sea level along the coast of India. Hence, we accept the observation of Colonel Burrard, confirmed by Ghildyal and Kumar, and see we can discern the causes. As we saw earlier, both wind-forced coastal currents and salinity make a significant contribution to the seasonal cycle of sea level along the coast of India. Of these, salinity is invoked by Ghildyal and Kumar too, except that they use only the surface salinity (and temperature). This is not correct because dynamic heights are determined with respect to a level of no motion, and hence depend on the vertical profile of temperature and salinity between this level and the sea surface, as in the reduced-gravity model.

5.3 Effect of Wind-Forced Coastal Currents

The effect of wind-forced coastal currents on the seasonal cycle of coastal sea level was examined in Section 4.1 using a dynamical $1\frac{1}{2}$-layer reduced-gravity model. The annual sea level[2] from this simulation is plotted for the coastal stations in Figure 5.1. There is an alongshore gradient in sea level, the annual sea level at Vishakhapatnam being higher than that at Mumbai by about 15 cm

[2]Having described the background for this chapter, we return to our preferred terminology.

Figure 5.1 Effect of wind-forced coastal currents on annual sea level η along the coast. The figure shows annual sea level (cm) for two simulations with the $1\frac{1}{2}$-layer model. The first simulation is with the wind-stress climatology of Hellerman and Rosenstein [1983], as in the earlier chapters. The second simulation is for a "more vigorous monsoon circulation", the wind stress of Hellerman and Rosenstein having been multiplied by 1.2. A stronger wind forcing amplifies the alongshore sea-level gradient; the annual sea level behaves like a see-saw along the coast, with its pivot at the southern tip of Sri Lanka.

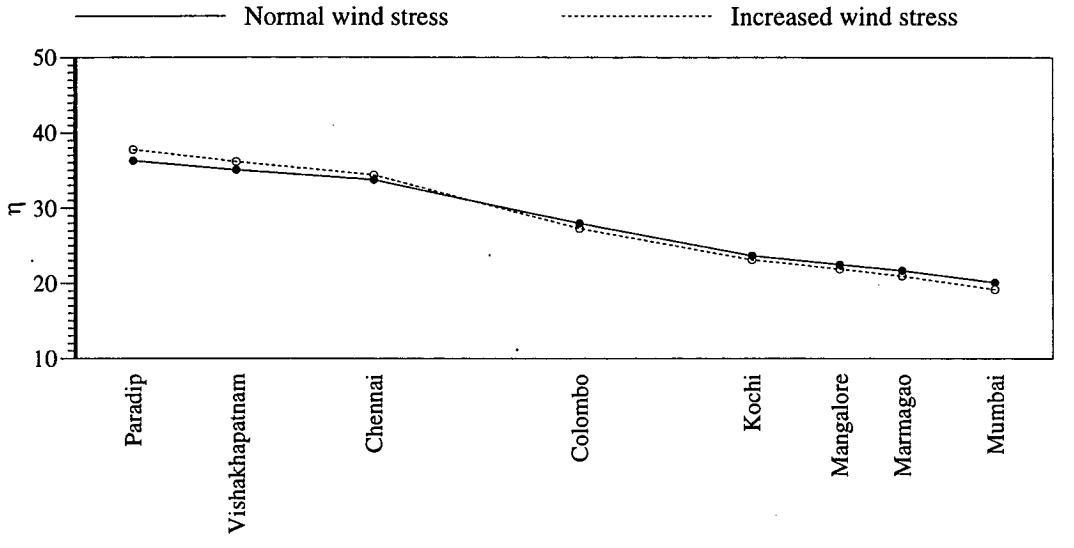

and the annual sea level at Chennai being higher than that at Mangalore by about 11 cm. These values, though lower than the observations, are of the same order. The sea level slopes down continuously along the coast, with highest sea level at Paradip, in the northwestern corner of the Bay of Bengal, and lowest sea level at Mumbai, the northernmost station along the west coast.

In the above simulation, the model was forced by the wind-stress climatology of Hellerman and Rosenstein [1983]. The climatology is an average of data collected over several years, and hence, represents an average, or "normal", monsoon. To see what a more vigorous monsoon would do to the alongshore gradient in sea level, we run a test case with the wind stress of Hellerman and Rosenstein multiplied by 1.2, implying a 10% increase in the strength of the wind all over the basin. The resulting annual sea level is also plotted in Figure 5.1. The sea level is now higher on the east coast, but lower on the west coast, the increase in the difference between Vishakhapatnam and Mumbai being about 13%, and that in the difference between Chennai and Mangalore being about 11%. The annual sea level see-saws along the coast, with its pivot at the southern tip of Sri Lanka. The see-saw goes up in the east if the winds are *uniformly* stronger over the basin throughout the year; it goes down in the east if the winds are weaker.

The observations of Colonel Burrard and Ghildyal and Kumar do not represent a climatology,

unlike our simulation. The observed difference in annual sea level between the two coasts is for a particular year, but it still gives an idea of the alongshore variability. The above simulations show that purely wind-forced circulation accounts for about half the observed difference.

5.4 Effect of the Alongshore Gradient in Salinity

Variations in temperature, as we saw earlier, have only a minor impact on the sea level along the Indian coast; hence, we ignore their effect on annual sea level and examine the contribution of salinity to the alongshore gradient in annual sea level. The effect of salinity is shown in Figure 5.2, which shows the annual sea level along the coast based on the simulation with the climatologies of Levitus and Boyer [1994] and Levitus et al. [1994] (Section 4.3.1) and the simulation with the synthesized climatology (Section 4.3.4). The difference in annual sea level between the two coasts

Figure 5.2 Effect of salinity on the annual sea level η along the coast. The figure shows annual sea level (cm) for three simulations with the $1\frac{1}{2}$-layer model, all forced by the wind-stress climatology of Hellerman and Rosenstein [1983]. In the first simulation, density is constant in the active upper layer. In the second, temperature and salinity are prescribed from the climatologies of Levitus and Boyer [1994] and Levitus et al. [1994]. The third simulation is identical to the second, but the salinity field is modified along the coast from the northeastern corner of the Bay of Bengal to Veraval on the west coast of India, as described in Section 4.3.3. The alongshore gradient in salinity forces an alongshore gradient in annual sea level. The alongshore variations in salinity account for about half the difference in annual sea level between the east and west coasts of India.

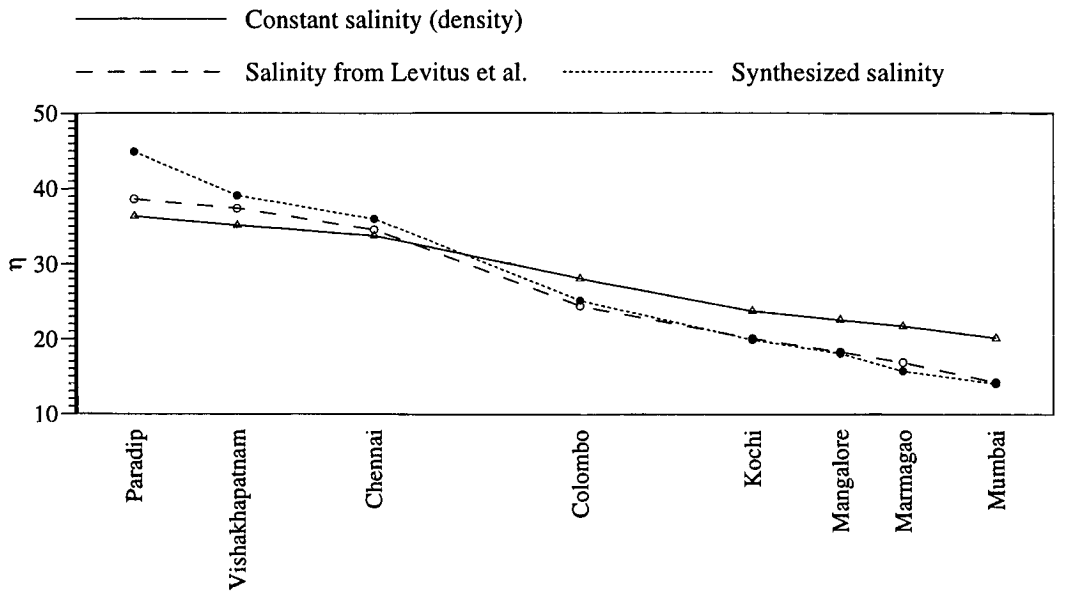

increases because of salinity; there is a marginal decrease in sea level along the west coast because

of a decrease in the annual mean Γ, but there is a large increase along the east coast because of a large increase in the annual mean Γ. The difference in sea level between Vishakhapatnam and Mumbai is now 25 cm and that between Chennai and Mangalore is 18 cm, closer to the observations. There is not much difference between the simulations with and without the modifications in salinity along the coast. This is because the annual mean coastal salinity in the climatology of Levitus et al. [1994] is not very different from that in the synthesized climatology; it is only the seasonal cycle of monthly climatology that departs considerably from observations.

In the presence of horizontal variations in salinity, there is a baroclinic contribution to the average pressure gradient in the upper layer[3] from the horizontal density gradient in the layer. Since the pressure gradient has to vanish in the deeper layer, the presence of the low-salinity plume along the east coast also reduces the upper layer thickness (Figure 5.3). The decrease in layer

Figure 5.3 Effect of salinity on the annual upper layer thickness H along the coast. The figure shows annual upper layer thickness (m) for two simulations with the $1\frac{1}{2}$-layer model, both forced by the wind-stress climatology of Hellerman and Rosenstein [1983]. In the first simulation, density is constant in the active upper layer. In the second, temperature and salinity are prescribed from the climatologies of Levitus and Boyer [1994] and Levitus et al. [1994], except along the coast of the Indian subcontinent from the northeastern corner of the Bay of Bengal to Veraval on the west coast of India, where it is modified as described in Section 4.3.3. The alongshore variation in salinity changes not only the alongshore gradient of annual sea level, but also that of upper layer thickness.

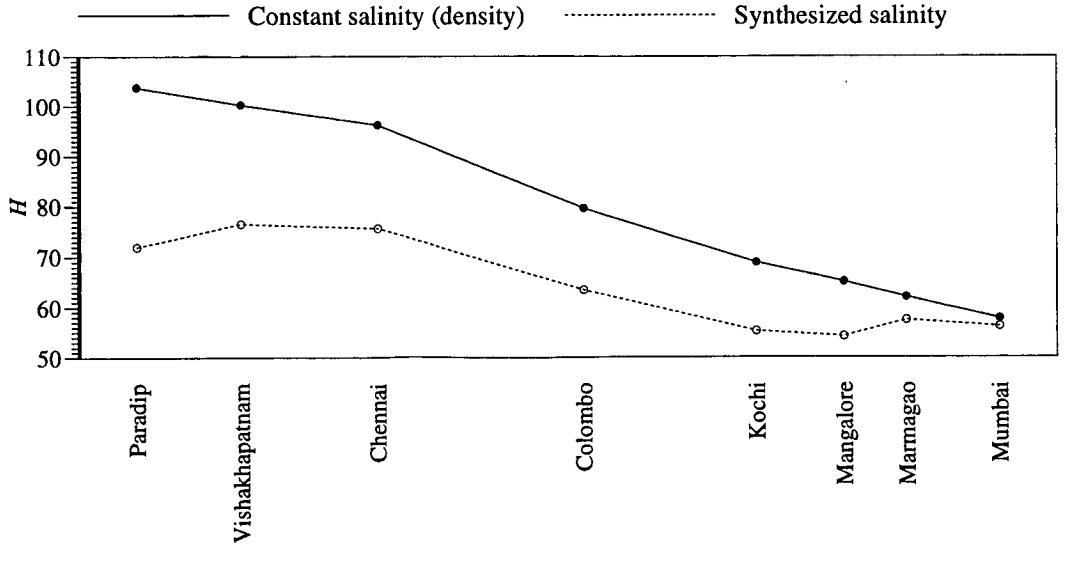

thickness along the east coast reduces the difference in layer thickness between the east and west coasts of India. In the purely wind-forced model, the upper layer is much thicker along the east

[3] See Appendix A.

coast. The presence of the low-salinity plume decreases it, but the layer thickness is still greater in the bay than in the Arabian Sea. Since the thickness of the upper layer is a measure of the thickness of the mixed layer, the higher thickness in the bay contradicts observations. This points to one of the limitations of the reduced-gravity model. It is a discrete model of a continuously stratified system. The large horizontal gradient in salinity, and hence in density, in the north Indian Ocean implies that the vertical structure is coupled to the horizontal structure; a simple decomposition into discrete vertical modes, as in the $1\frac{1}{2}$-layer reduced-gravity model, is not possible, and if attempted, leads to the errors described above. The model is incapable of simulating the higher sea level in the Bay of Bengal without simulating a thicker upper layer also. These simulations show that the lower salinity in the Bay of Bengal, especially in the coastal waters of India, is the likely cause of the thinner mixed layers observed in the bay.

In conclusion, the simulations support the observation of Colonel Burrard, subsequently verified by Ghildyal and Kumar, that the annual sea level is higher on the east coast of India than on the west coast. Both wind-forced coastal currents and salinity contribute to this alongshore gradient in sea level. The impact of winds and salinity on annual sea level and the coupling between that exists between the ocean, the atmosphere, and land imply that variability associated with the monsoon must lead to sea-level variability at lower frequencies; these lower frequencies form the subject of the following chapter.

Chapter 6

Interannual and Interdecadal Variability

The striking aspect of the climate of the Indian subcontinent is the monsoon. The word *monsoon* is derived from the Arabic word *mausam*, which means "season"; it is used to describe the regular reversal of winds with season that determines the climate of the subcontinent. There are two facets of the monsoon. First, the change in weather with season is regular. For example, 1 June is the normal date of onset of the monsoon over southwest India. The seasonal cycle associated with the monsoon is so regular that a departure of more than a few days from this mean date of onset is sufficient cause for concern in the country. It is no different with the progress of the monsoon across the subcontinent; this too follows a definite pattern and is tracked in India by the official herald, the India Meteorological Department. This regular, rhythmic change in winds is responsible for the significant climatological seasonal cycle of sea level along the coast of India (Chapter 4). Thus, regularity, bordering on predictability, is one facet of the monsoon. Second, the monsoon is fickle: it varies a lot from one year to another. Associated with the seasonal changes in winds, which define the monsoonal climate, are changes in atmospheric pressure and, most important, rainfall. Since agriculture is the lifeblood of the subcontinent, it is the variability of rainfall that has the maximum impact and it has aroused interest for a long time, leading to rainfall becoming the best documented climatic variable in the subcontinent. There is considerable interannual and interdecadal variability in the rainfall records; since rainfall directly affects salinity in the ocean, it is inevitable that the interannual variability of the monsoon should lead to interannual variability in sea level along the coast of India. There is evidence for such variability in the tide-gauge record at Mumbai (Figure 1.3). In this chapter, we describe the interannual and interdecadal variations in the sea level along the coast of India and determine their possible causes.

6.1 Interannual Variability of Sea Level Along the Coast

6.1.1 Variability of the Seasonal Cycle

The regularity of the monsoon makes the seasonal cycle a major signal in the sea-level records along the coast of India. We begin our description of interannual variability by examining how the seasonal cycle varies from one year to another. One difficulty in studying sea-level variability at periods greater than an year is the short length of several records. Of the eight tide-gauge records used earlier, only those at Vishakhapatnam (52 years), Chennai (43 years), Kochi (50 years), and Mumbai (111 years) are longer than 40 years. Therefore, we restrict our attention just to these four stations[1]. The anomalies of monthly sea level, computed by subtracting the mean of the time series from the sea level for each month, are plotted in Figure 6.1, which also shows the climatological seasonal cycle. There is considerable scatter about the climatology, the anomalies

Figure 6.1 Anomalies of uncorrected monthly sea level, η_a (cm). The continuous line is the climatological seasonal cycle. The dots represent the anomalies of monthly sea level, computed by subtracting the mean of the time series from the monthly sea level. There is considerable scatter about the climatology, indicating significant interannual variability of sea level along the coast of India.

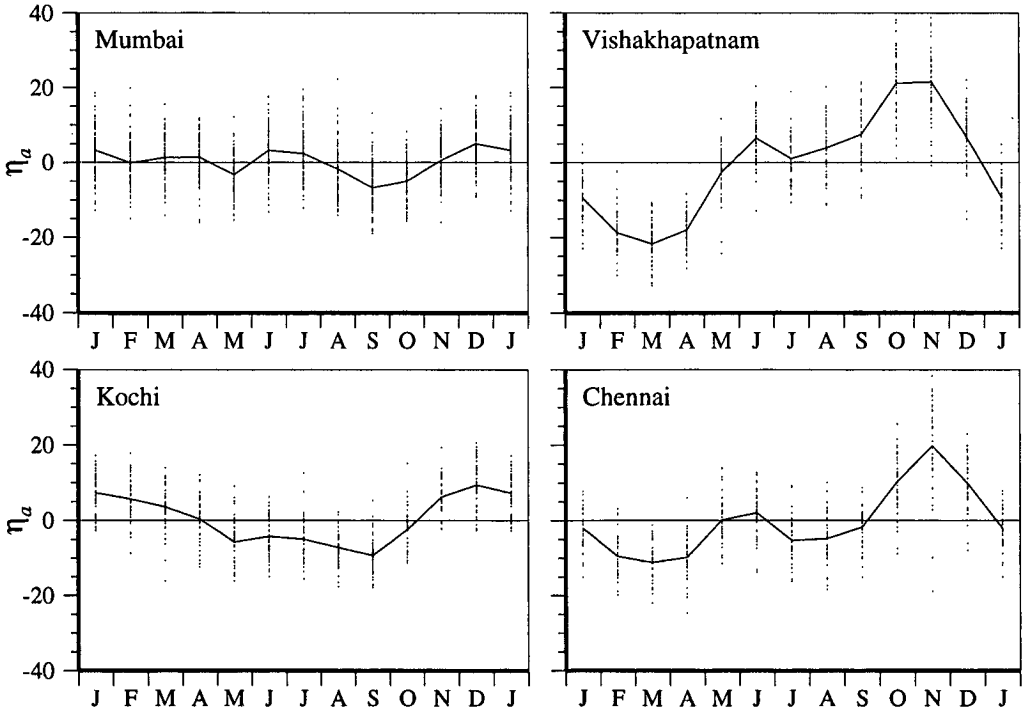

[1]The 40-year cutoff is arbitrary, but, as we shall see, even 40 years is not enough.

of monthly sea level being comparable to the range of the seasonal cycle. Therefore, there is considerable interannual variability in the sea level along the coast of India. The sea-level data used in Figure 6.1 include the effect of atmospheric pressure, which has a strong effect on the seasonal cycle; for example, it changes the sea level by about 10 cm in June at Mumbai. We apply the Inverse-Barometer (IB) approximation (Section 2.2.1) to correct for this effect, using monthly atmospheric-pressure data from the Global Historical Climate Network (GHCN); unfortunately, the GHCN data also have gaps and are not available for the entire span of the sea-level records (Table 6.1), thereby truncating them. In applying the IB approximation, we assume that the average monthly sea-level pressure over the world oceans does not change from year to year, this assumption being necessary since we have only climatological data (from COADS) for the average pressure. The resulting anomalies are plotted in Figure 6.2; there still is considerable scatter about the climatology.

Table 6.1 Sea-level pressure data from the Global Historical Climate Network (GHCN). N_{yr} is the number of years of data available.

Station	Longitude (°E)	Latitude (°N)	Time span	N_{yr}
Vishakhapatnam	83.23	17.72	1941–1988	48
Chennai (Minambakkam)	80.18	13.00	1941–1988	48
Kochi (Fort Cochin)	76.20	10.00	1941–1973	33
Mumbai (Colaba)	72.82	18.90	1921–1988	68

Given that there are large changes in monthly sea level from year to year, how robust is the seasonal cycle? In other words, is the interannual variability such that it warps the seasonal cycle, or does the seasonal cycle repeat almost every year[2], with interannual changes merely perturbing it? One way to determine this is to check the timing of the extrema of the seasonal cycle. Histograms of the month of occurrence of the extrema of the seasonal cycle of sea level, not corrected for the effect of atmospheric pressure, are shown in Figure 6.3. The histograms show that the seasonal cycle is extremely robust on the east coast, there not being much variation in the timing of the maximum; the maximum occurs mostly in October or November at Vishakhapatnam and in November at Chennai. The scatter is more for the minimum, but it occurs mostly during February–April, when the anticyclonic gyre, with a poleward, upwelling-favourable western

[2]For computations related to sea level, the year is defined from July of a given year to June of the following year in the rest of this chapter, unless otherwise stated. This is done because of the effect that salinity has on sea level along the coast of India. Since the changes in salinity are linked to monsoon rainfall, it seems more reasonable to define the year such that the monsoon rains occur "early in the year", rather than in the middle; with this definition, rainfall for a given calendar year has an effect on sea level throughout the "year". Another possible definition would start the year after the monsoon rains, say in October. Note that the calendar year is still used for computations involving rainfall.

Figure 6.2 Anomalies of corrected monthly sea level, η_a (cm). The continuous line is the climatological seasonal cycle. The dots represent the anomalies of monthly sea level, computed by subtracting the mean of the time series from the monthly sea level. There is considerable scatter about the climatology, indicating significant interannual variability of sea level along the coast of India.

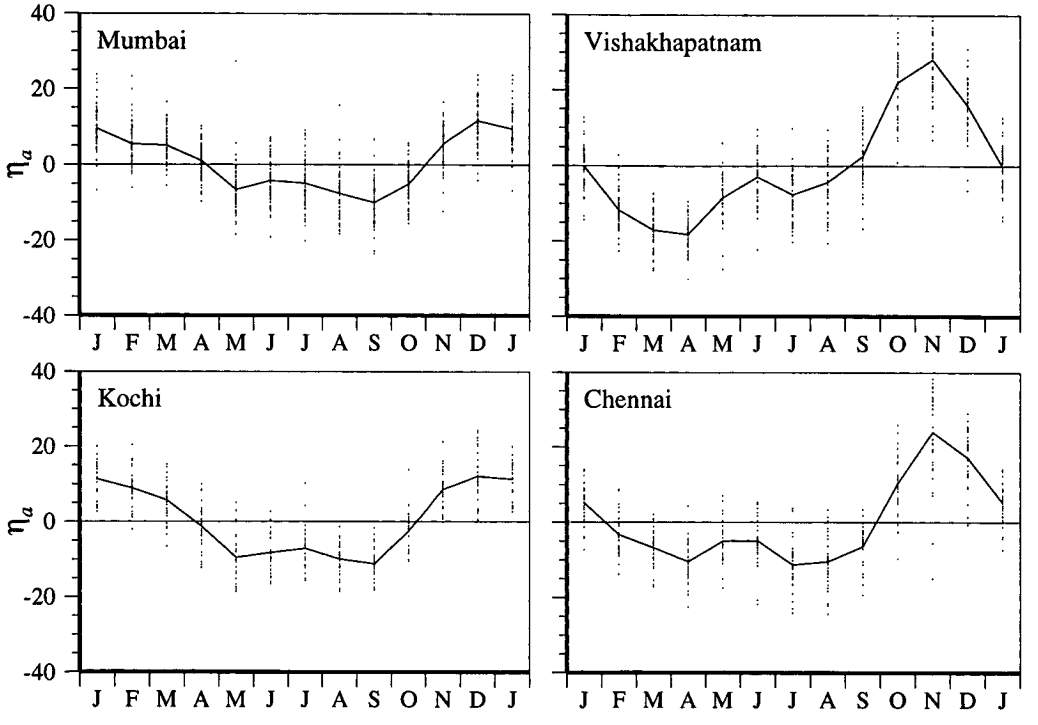

boundary current, forms in the Bay of Bengal. Since Chennai lies close to the southern limit of the gyre and the size of the gyre depends on the wind field over the bay, the greater scatter there is not surprising. Along the west coast, however, there is considerable variation in the timing of the extrema, the scatter increasing poleward along the coast to Mumbai. At Kochi, the maximum occurs mostly during November–January, when the climatological seasonal cycle peaks there. The minimum occurs mostly in May, before the southwest monsoon, or in September, towards the end of the southwest monsoon; this reflects the existence of a minor secondary maximum during the southwest monsoon. At Mumbai, the extrema of the seasonal cycle can occur in almost any month of the year. The maximum occurs during winter, or during the southwest monsoon, or in March, reflecting the multiple peaks of the seasonal cycle before it is corrected for the effect of atmospheric pressure (Figure 4.1). The prominence of the semiannual signal is also reflected in the timing of the minimum, which usually occurs either towards the end of the southwest monsoon, or in May.

Figure 6.3 Histograms of the time of occurrence of the extrema of the seasonal cycle of uncorrected sea level. The number of occurrences of the extremum in a given month is plotted on the ordinate and the month during which the extremum occurs is plotted on the abscissa. The scatter in the timing of the extrema is more on the west coast, implying that the seasonal cycle is more robust along the east coast of India.

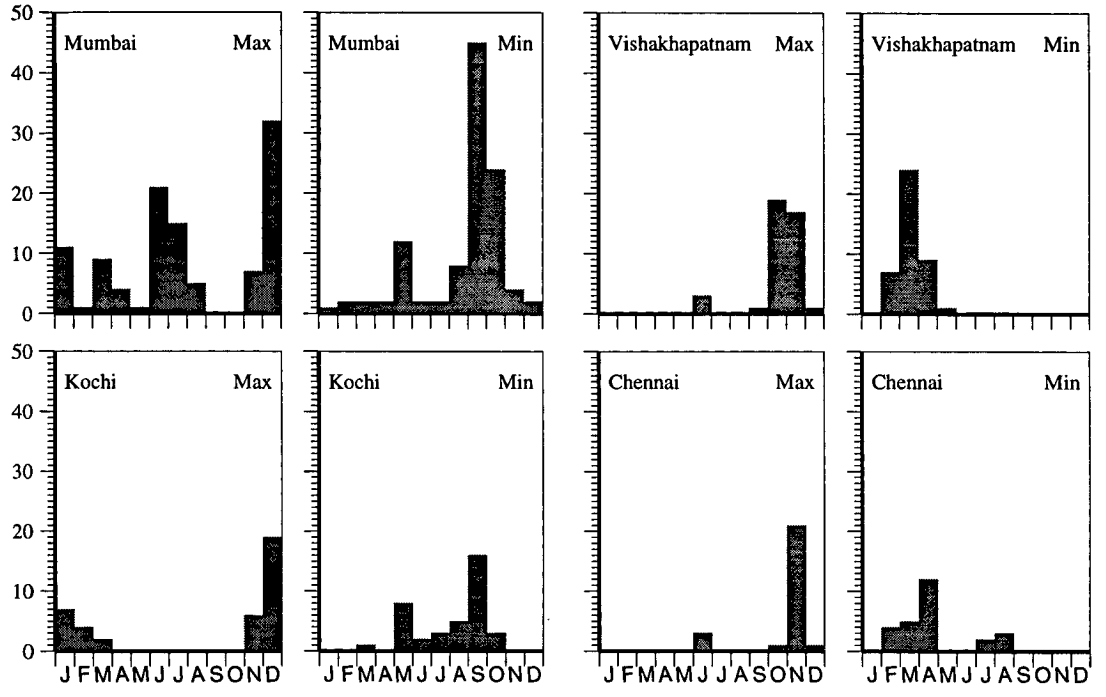

Since the effect of atmospheric pressure on the seasonal cycle is not small, it is necessary to determine how robust the corrected seasonal cycle is. The resulting histograms are shown in Figure 6.4; for comparison, the histograms for the uncorrected sea level are repeated in Figure 6.5, retaining only those years that contribute to Figure 6.4. These figures show that the seasonal cycle is much more robust when corrected for atmospheric pressure. There is a large decrease in the scatter in the timing of the extrema, especially at Mumbai, where the corrected seasonal cycle peaks almost always in winter.

Therefore, the seasonal cycle of sea level, when corrected for the effect of atmospheric pressure, is robust and the basic pattern of the seasonal cycle does not show significant interannual variations, reflecting the regularity with which the monsoon winds and salinity along the coast of India change. Nevertheless, there must be interannual variability in the annual sea level along the coast of India because the anomalies of monthly sea level with respect to the climatological seasonal cycle are not small (Figures 6.1 and 6.2).

Figure 6.4 Histograms of the time of occurrence of the extrema of the seasonal cycle of corrected sea level. The number of occurrences of the extremum in a given month is plotted on the ordinate and the month during which the extremum occurs is plotted on the abscissa. The scatter in the timing of the extrema is much less when the sea level is corrected for the effect of atmospheric pressure. The corrected seasonal cycle is more robust throughout the coast.

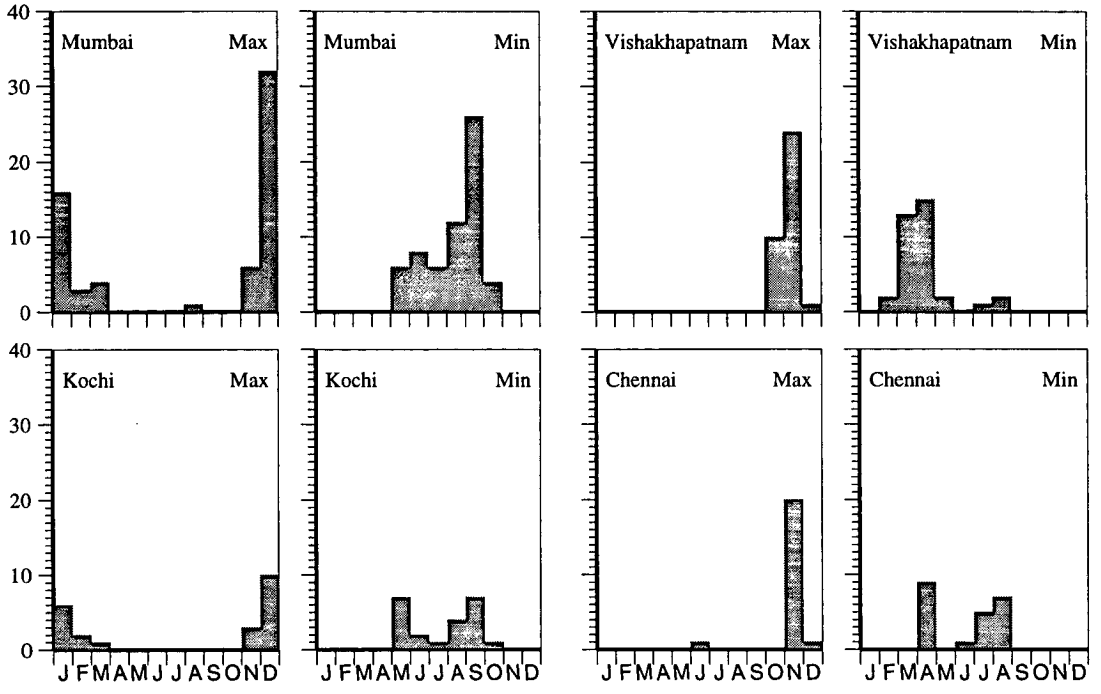

6.1.2 Variability of Annual Sea Level

Annual sea level[3] at a location is computed by averaging monthly sea level over an year. The sea-level records at the four stations are with respect to a given datum, the Revised Local Reference (RLR); hence, it is possible to average the annual sea level over the length of the record and compute anomalies of annual sea level. These anomalies, like the monthly anomalies, can be compared along the coast[4], but, since the reference datum at each station is local to that station and is not linked to that at the others, it is not possible to compute absolute sea level at a station.

The anomalies of annual sea level are plotted in Figure 6.6; the monthly sea level used to compute the annual sea level for this figure are not corrected for the effect of atmospheric pressure. The annual sea level along the coast exhibits significant interannual variability, the range of

[3] Annual sea level is also called "annual mean", or just "mean", sea level in this chapter; the qualification is necessary at times because the annual extrema are also considered along with the annual mean. Nevertheless, "annual sea level", when used as such, still refers to the annual mean.

[4] The difference in the length of the sea-level records, however, introduces some errors.

Figure 6.5 Histograms of the time of occurrence of the extrema of the seasonal cycle of uncorrected sea level, but for the same period as in Figure 6.4. The number of occurrences of the extremum is plotted on the ordinate and the month during which the extremum occurs is plotted on the abscissa. This figure is similar to Figure 6.3, except that the data cover only those years that contribute to Figure 6.4. The scatter in the timing of the extrema is more than for the corrected seasonal cycle, especially at Mumbai, reflecting the significant contribution made by atmospheric pressure to the seasonal cycle there.

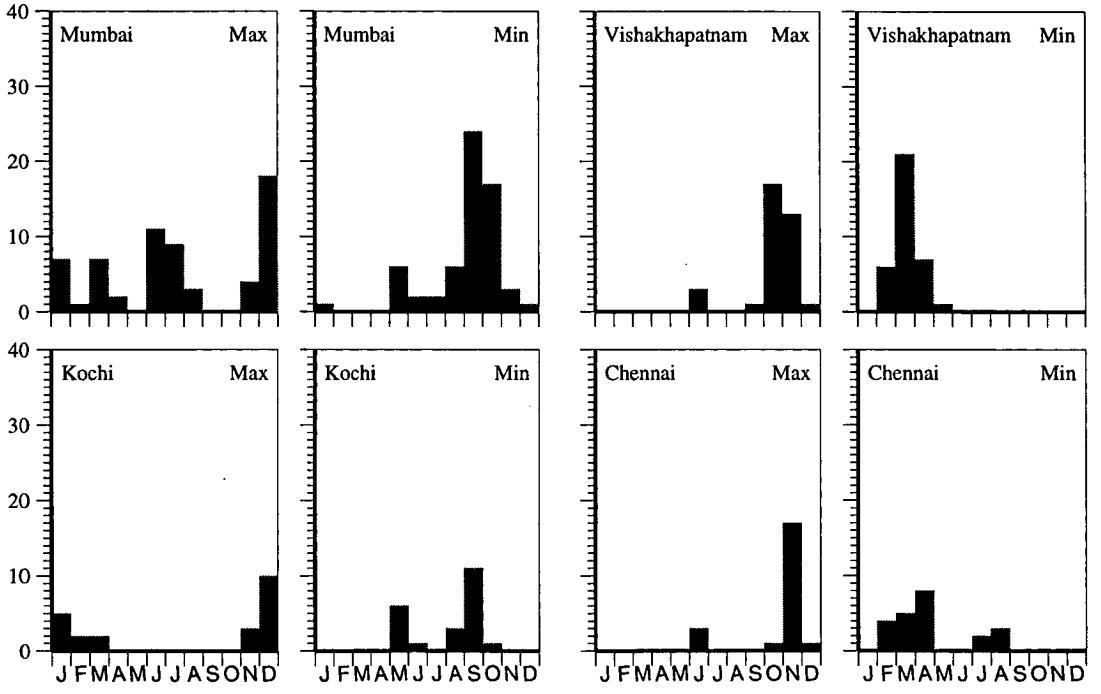

the variation being comparable to that of the climatological seasonal cycle at each station. The anomalies of annual sea level are also coherent along the coast, and this coherence remains when the monthly sea level is corrected for atmospheric pressure before computing the annual sea level (Figure 6.7). This coherence is not just visual; the anomalies are also statistically well correlated[5] along the coast (Table 6.2). The only exception seems to be the tide gauge at Kochi, where sea level rises sharply from the 1940s to 1960; the variation at the other stations is not similar, and this reduces the correlations for Kochi. Annual sea level at Kochi is best correlated with that at Chennai, but this is owing to the absence of data at Chennai during the 1940s.

This coherence along the coast is also seen in the variation of the annual extrema (Figures 6.8, 6.9). The maximum and minimum sea level during an year are in phase with the annual mean; they increase (decrease) when the mean increases (decreases). The correlation between the

[5]See Appendix C for the method used to compute the significance levels.

Table 6.2 Linear correlation statistics for annual sea level. η_V, η_C, η_K, and η_M denote the sea level anomalies at Vishakhapatnam, Chennai, Kochi, and Mumbai; the subscript "m" implies annual mean sea level. r is the linear correlation coefficient between the variables in the first two columns (at zero lag). r_s is the linear correlation at the P% significance level for the required number of degrees of freedom; if the column for P is blank, then r_s is the correlation at the 90% significance level, but the two variables are not correlated even at this level. A "C" in the last column implies that the sea-level data are corrected for the effect of atmospheric pressure (default is no correction). The correlation between Chennai and Kochi for corrected sea level is not computed because only seven degrees of freedom are available.

		r	r_s	P	
$\eta_{V,m}$	$\eta_{C,m}$	0.779	0.561	99.0	
$\eta_{V,m}$	$\eta_{C,m}$	0.772	0.575	99.0	C
$\eta_{V,m}$	$\eta_{K,m}$	0.572	0.449	99.0	
$\eta_{V,m}$	$\eta_{K,m}$	0.482	0.444	95.0	C
$\eta_{V,m}$	$\eta_{M,m}$	0.401	0.316	95.0	
$\eta_{V,m}$	$\eta_{M,m}$	0.474	0.436	99.0	C
$\eta_{C,m}$	$\eta_{K,m}$	0.687	0.590	99.0	
$\eta_{C,m}$	$\eta_{M,m}$	0.593	0.505	99.0	
$\eta_{C,m}$	$\eta_{M,m}$	0.548	0.433	95.0	C
$\eta_{K,m}$	$\eta_{M,m}$	0.216	0.292		
$\eta_{K,m}$	$\eta_{M,m}$	0.398	0.390	90.0	C

annual mean and the annual extrema is excellent (Table 6.3). It is not just the annual extrema that are in phase with the annual mean sea level; even the seasonal averages (for February–April, March–May, and July–September along both coasts, for October–December along the east coast, and for November–January along the west coast) are significantly correlated with the annual mean (Table 6.3). This implies that the major change from year to year is in the mean sea level, superimposed on which is the seasonal cycle. The interannual variations in this superimposed seasonal cycle lead to differential variations in the extrema and the seasonal averages of sea level.

6.2 Interdecadal Variability of Sea Level Along the Coast

An implication of the above statistics is that it is not necessary to correct for atmospheric pressure when determining the annual extrema. This is important because applying the correction using the GHCN pressure data truncates the length of the sea-level record. Not applying the correction implies that the sea-level record at Mumbai extends over 111 years (1878–1988), permitting us to use low-pass filters to examine the variability at even lower frequencies. The next longest record, at Vishakhapatnam, is only 52 years long; hence, only the tide gauge at Mumbai is useful for

Figure 6.6 Anomalies of uncorrected annual sea level (cm). The annual sea level was computed by averaging monthly sea level, not corrected for atmospheric pressure, over an year (July–June), and the mean of the time series was removed to obtain the anomalies. The curve for Mumbai is superimposed on those for the other three stations. The anomalies of annual sea level are coherent along the coast, Kochi being the only exception. The sharp rise in annual sea level at Kochi during 1940–1960 is not seen at the other stations.

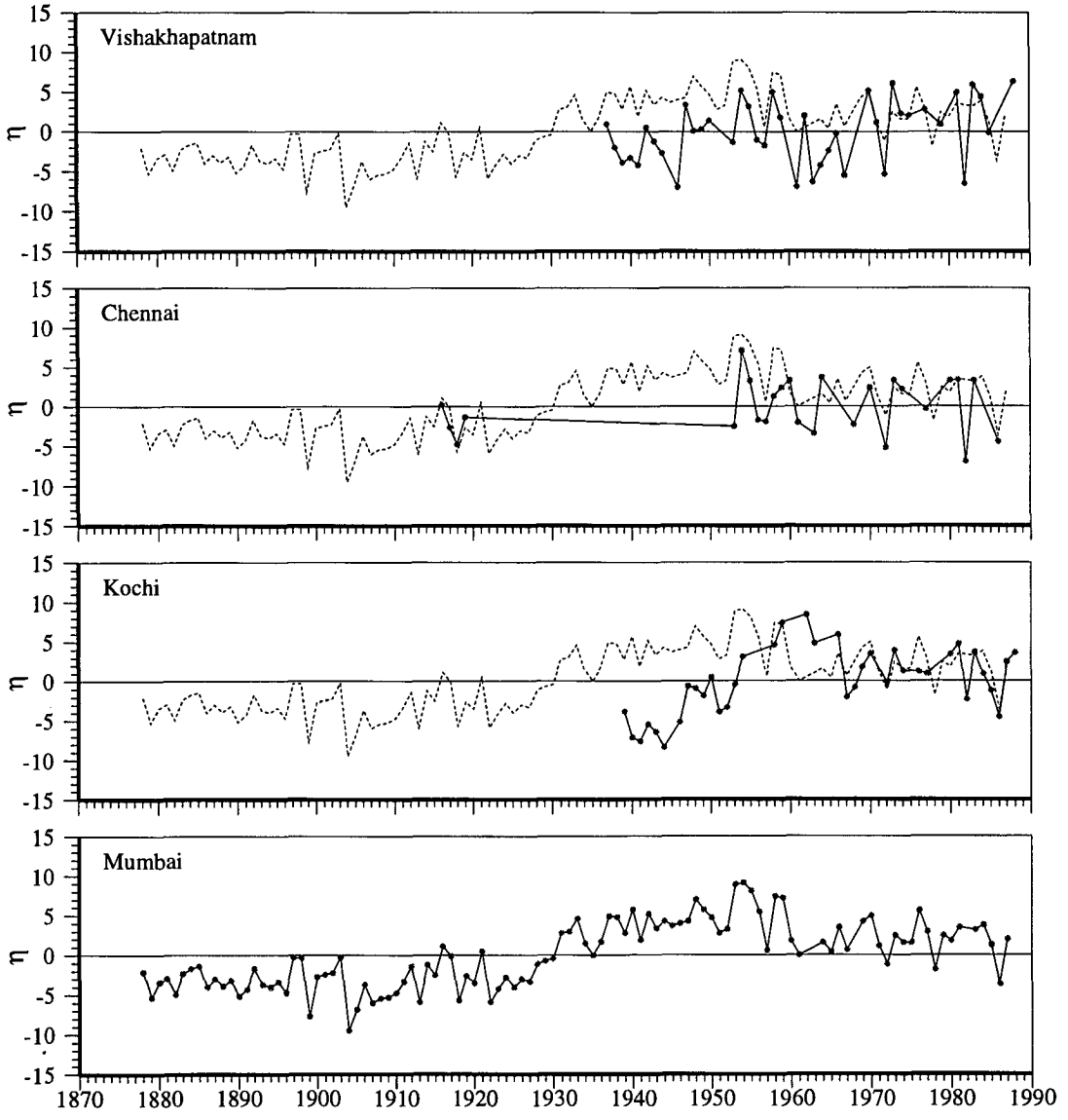

Figure 6.7 Anomalies of corrected annual sea level (cm). The annual sea level was computed by averaging monthly sea level, corrected for the effect of atmospheric pressure, over an year (July–June), and the mean of the time series was removed to obtain the anomalies. The curve for Mumbai is superimposed on those for the other three stations. The corrected annual sea level is also coherent along the coast, Kochi again being the only exception.

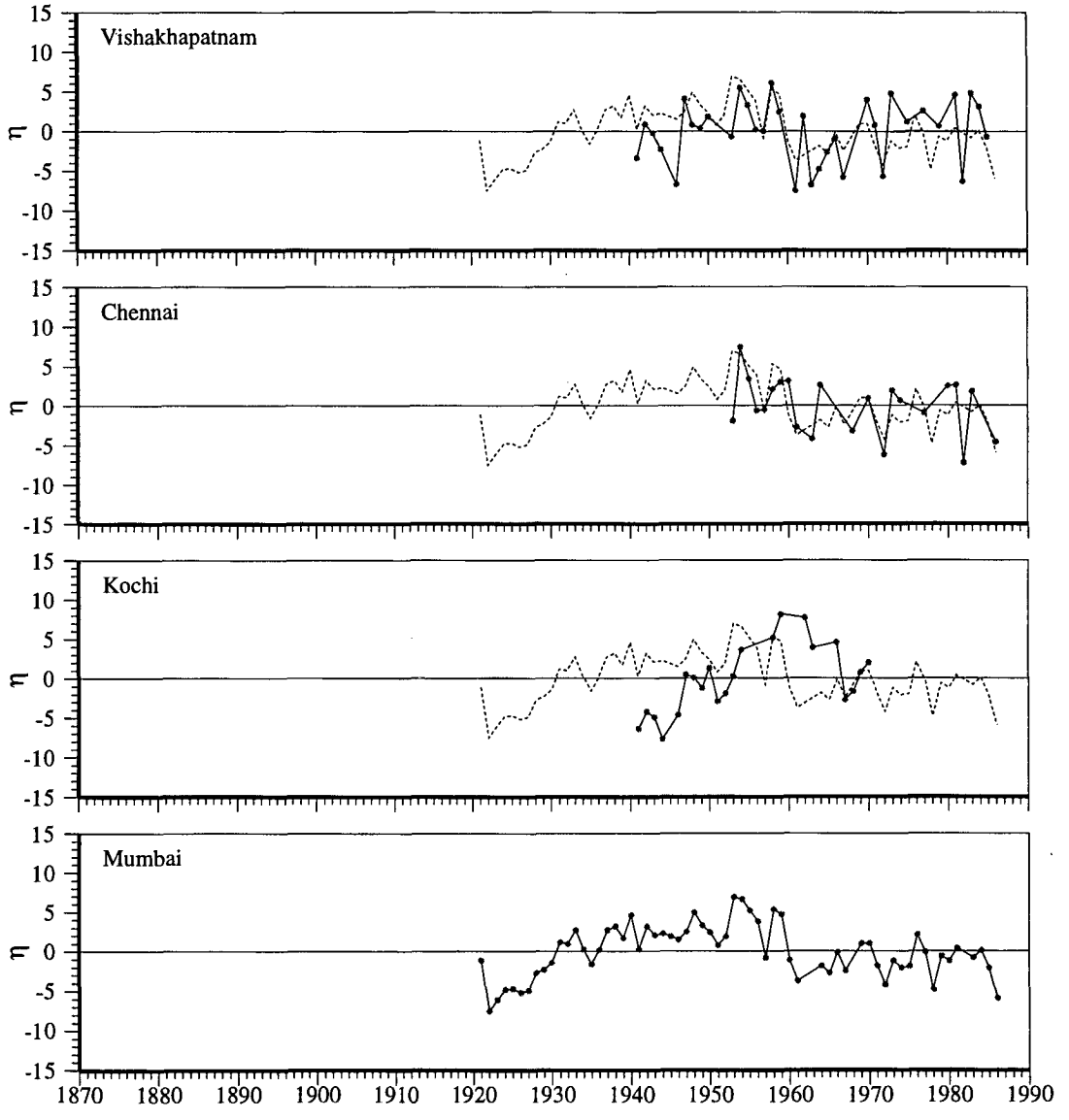

Figure 6.8 Anomalies of the uncorrected annual mean (middle curve), maximum (upper curve), and minimum (lower curve) sea level (cm). The annual mean sea level was computed by averaging monthly sea level, not corrected for atmospheric pressure, over an year (July–June); the annual maximum (minimum) is the maximum (minimum) sea level during July–June. The mean of the time series was removed to obtain the anomalies. The annual extrema are in phase with the annual mean; in general, when the mean sea level increases, so do the maximum and the minimum.

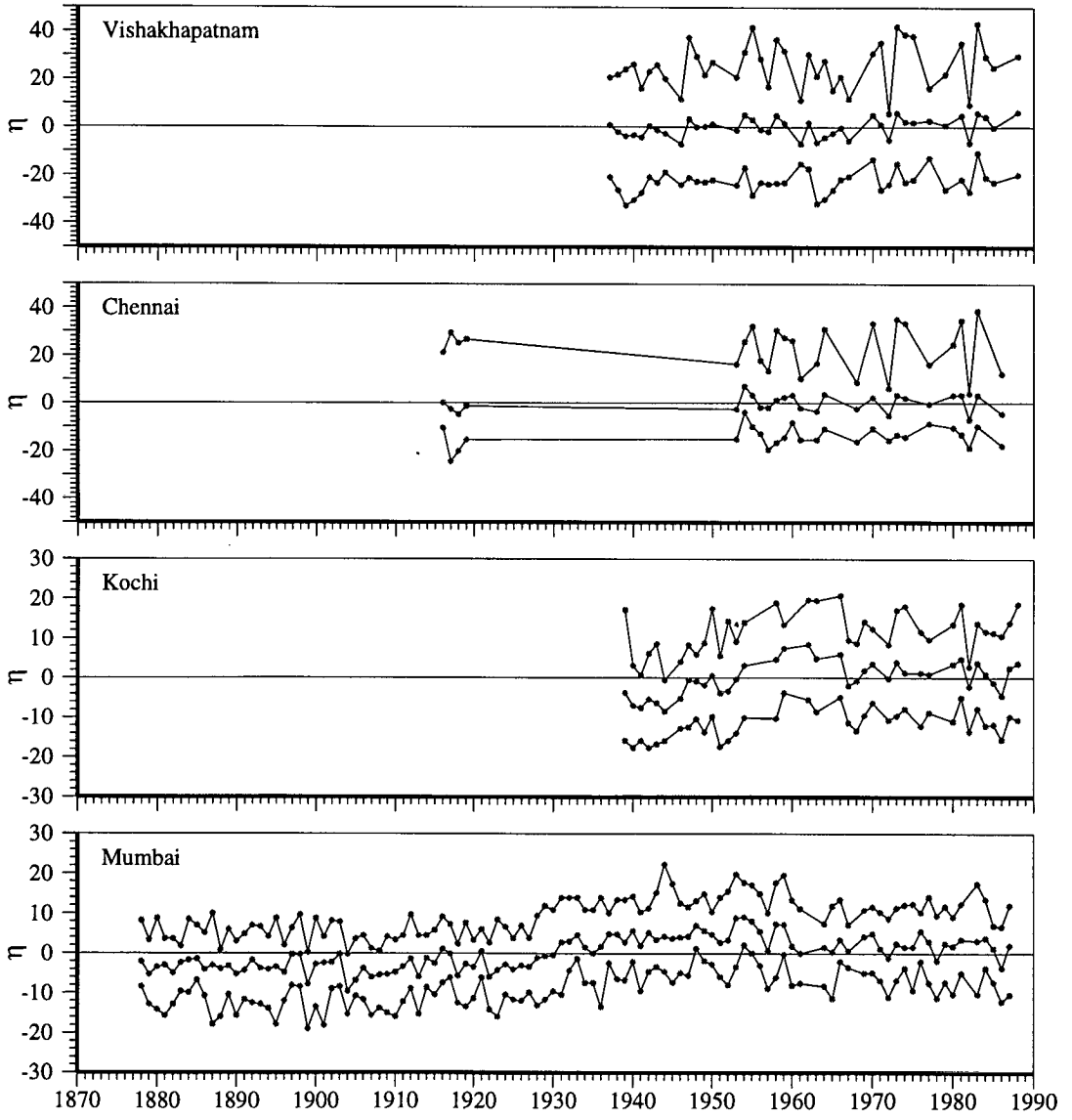

Figure 6.9 Anomalies of the corrected annual mean (middle curve), maximum (upper curve), and minimum (lower curve) sea level (cm). The annual mean sea level was computed by averaging monthly sea level, corrected for atmospheric pressure, over an year (July-June); the annual maximum (minimum) is the maximum (minimum) sea level during July-June. The mean of the time series was removed to obtain the anomalies. The annual extrema of corrected sea level are in phase with the annual mean; in general, when the mean sea level increases, so do the maximum and the minimum.

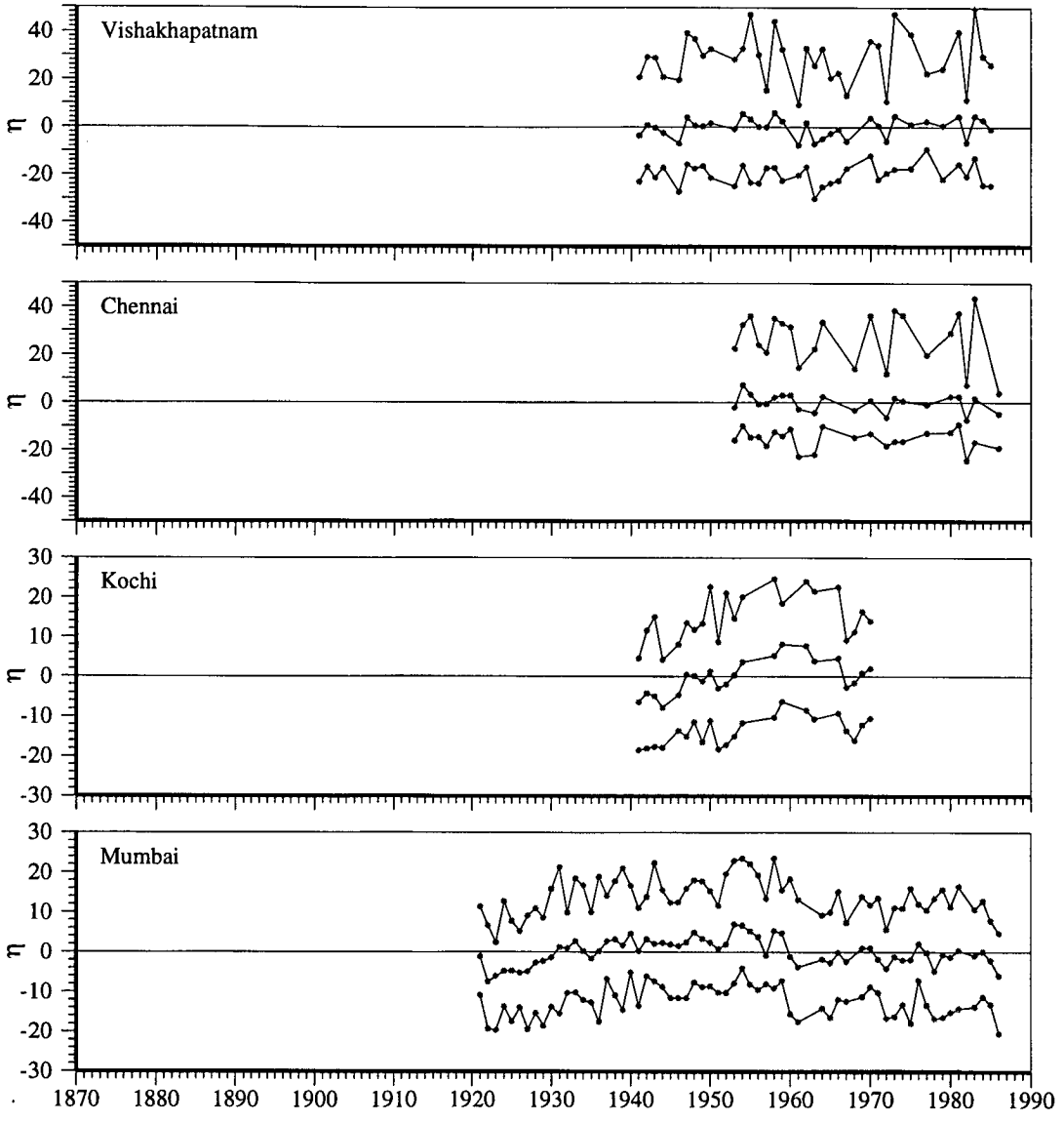

Table 6.3 Linear correlation statistics for annual mean, extrema, and seasonal averages of sea level. η_V, η_C, η_K, and η_M denote the sea level anomalies at Vishakhapatnam, Chennai, Kochi, and Mumbai; the subscripts "m", "max", and "min" imply annual mean, maximum, and minimum sea level, and the subscripts "FMA", "MAM", "JAS", "OND", and "NDJ" imply average sea level for February–April, March–May, July–September, October–December, and November–January. r is the linear correlation coefficient between the variables in the first two columns (at zero lag). r_s is the linear correlation at the P% significance level for the required number of degrees of freedom; if the column for P is blank, then r_s is the correlation at the 90% significance level, but the two variables are not correlated even at this level. A "C" in the last column implies that the sea-level data are corrected for the effect of atmospheric pressure (default is no correction).

		r	r_s	P	
$\eta_{V,m}$	$\eta_{V,max}$	0.789	0.388	99.0	
$\eta_{V,m}$	$\eta_{V,max}$	0.798	0.418	99.0	C
$\eta_{V,m}$	$\eta_{V,min}$	0.530	0.388	99.0	
$\eta_{V,m}$	$\eta_{V,min}$	0.530	0.418	99.0	C
$\eta_{V,m}$	$\eta_{V,FMA}$	0.556	0.388	99.0	
$\eta_{V,m}$	$\eta_{V,MAM}$	0.586	0.388	99.0	
$\eta_{V,m}$	$\eta_{V,JAS}$	0.746	0.388	99.0	
$\eta_{V,m}$	$\eta_{V,OND}$	0.800	0.388	99.0	
$\eta_{C,m}$	$\eta_{C,max}$	0.759	0.478	99.0	
$\eta_{C,m}$	$\eta_{C,max}$	0.831	0.515	99.0	C
$\eta_{C,m}$	$\eta_{C,min}$	0.752	0.478	99.0	
$\eta_{C,m}$	$\eta_{C,min}$	0.789	0.515	99.0	C
$\eta_{C,m}$	$\eta_{C,FMA}$	0.606	0.478	99.0	
$\eta_{C,m}$	$\eta_{C,MAM}$	0.505	0.478	99.0	
$\eta_{C,m}$	$\eta_{C,JAS}$	0.523	0.478	99.0	
$\eta_{C,m}$	$\eta_{C,OND}$	0.850	0.478	99.0	
$\eta_{K,m}$	$\eta_{K,max}$	0.796	0.402	99.0	
$\eta_{K,m}$	$\eta_{K,max}$	0.821	0.515	99.0	C
$\eta_{K,m}$	$\eta_{K,min}$	0.895	0.402	99.0	
$\eta_{K,m}$	$\eta_{K,min}$	0.893	0.515	99.0	C
$\eta_{K,m}$	$\eta_{K,FMA}$	0.891	0.402	99.0	
$\eta_{K,m}$	$\eta_{K,MAM}$	0.905	0.402	99.0	
$\eta_{K,m}$	$\eta_{K,JAS}$	0.873	0.402	99.0	
$\eta_{K,m}$	$\eta_{K,NDJ}$	0.875	0.402	99.0	
$\eta_{M,m}$	$\eta_{M,max}$	0.879	0.247	99.0	
$\eta_{M,m}$	$\eta_{M,max}$	0.785	0.320	99.0	C
$\eta_{M,m}$	$\eta_{M,min}$	0.862	0.247	99.0	
$\eta_{M,m}$	$\eta_{M,min}$	0.828	0.320	99.0	C
$\eta_{M,m}$	$\eta_{M,FMA}$	0.887	0.247	99.0	
$\eta_{M,m}$	$\eta_{M,MAM}$	0.907	0.247	99.0	
$\eta_{M,m}$	$\eta_{M,JAS}$	0.845	0.247	99.0	
$\eta_{M,m}$	$\eta_{M,NDJ}$	0.863	0.247	99.0	

studying interdecadal variability in sea level. Since the annual mean and extrema of sea level are coherent along the coast, it is reasonable to assume that the interdecadal variability at Mumbai is representative of that along the coast of India.

6.2.1 Interdecadal Variability of Sea Level at Mumbai

To determine the variability at periods higher than an year, we low-pass-filter the sea-level data at Mumbai (not corrected for atmospheric pressure) with an N-year running mean. The correlations between the filtered annual mean and annual extrema remain statistically significant at the lower frequencies and the coherence between the annual mean and extrema increases as frequency decreases (Table 6.4, Figure 6.10).

Table 6.4 Linear correlation statistics for low-pass-filtered sea level at Mumbai. η_M denotes the anomaly of low-pass-filtered sea level at Mumbai; the subscripts "m", "max", and "min" imply mean, maximum, and minimum sea level, respectively. r is the linear correlation coefficient between the variables in the first two columns. An N-year running mean is used to filter the sea-level data before computing the correlations ($N = 1$ implies no running mean). r_s is the linear correlation at the $P\%$ significance level for the required number of degrees of freedom.

		r	r_s	P	N
$\eta_{M,m}$	$\eta_{M,max}$	0.879	0.247	99.0	1
$\eta_{M,m}$	$\eta_{M,min}$	0.862	0.247	99.0	1
$\eta_{M,m}$	$\eta_{M,max}$	0.927	0.304	99.0	2
$\eta_{M,m}$	$\eta_{M,min}$	0.917	0.304	99.0	2
$\eta_{M,m}$	$\eta_{M,max}$	0.974	0.450	99.0	5
$\eta_{M,m}$	$\eta_{M,min}$	0.968	0.450	99.0	5
$\eta_{M,m}$	$\eta_{M,max}$	0.990	0.609	99.0	10
$\eta_{M,m}$	$\eta_{M,min}$	0.985	0.609	99.0	10

The filtered data show that sea level was generally low during 1870–1920; it peaked in the late 1950s, decreasing thereafter. The rise in the first half of this century was about 11 cm, the fall after that being about 4.5 cm. This decrease after 1960 was also noted by Emery and Aubrey [1989], who computed the linear trends in sea level along the coast of India. They considered five stations in their analysis, of which four — Vishakhapatnam, Chennai, Kochi, and Mumbai — showed a rise in sea level relative to land over the duration of the tide-gauge record. At Mangalore, however, they noted a decrease in sea level relative to land. The tide-gauge record at Mangalore spans the period 1952–1976 (Table 2.1), during which sea level at Mumbai also shows a decreasing trend. The coherence in the low-frequency variability of sea level along the coast of India suggests a similar behaviour at Mangalore and also at the other tide-gauge stations.

6.2.2 Significance of the Tide Gauge at Mumbai

This decrease in sea level over a decade or more is puzzling because it does not fit in with the idea of "global sea-level-rise". Sea level has been recognized as an excellent marker of climate change and "global" sea level appears to be rising relative to land at the rate of 1 mm year^{-1}; this is attributed, in part, to the warming of the globe due to the greenhouse effect [Gornitz et al., 1982]. The warming is expected to affect sea level in two ways. First, it is expected to raise the temperature in the upper ocean; second, it is expected to melt polar ice caps, releasing the large quantities of freshwater trapped in them. Both processes would increase the volume of water in the world oceans, thereby raising sea level all over the globe.

The issue, however, is more complicated, and it is difficult to obtain a single global index for long-term sea-level changes [Barnett, 1984]. Though there is an apparent increase in sea level in most of the world oceans, there are regions that show a different trend, southeast Asia for example. Apart from this, there is the problem of separating natural, low-frequency sea-level variability from that caused by anthropogenic effects; this calls for long sea-level time-series, and such records are not many. Moreover, the available records are not distributed uniformly, most being from Scandinavia. Between the tropics of Cancer and Capricorn, only three records, those at Mumbai, Honolulu, and Balboa, go back at least to the beginning of this century. Of these, only Mumbai is in the Indian ocean, and its tide gauge has been considered representative of the low-frequency sea-level variability in the basin [Gornitz et al., 1982; Barnett, 1984]. The coherence in the interannual variability of sea level along the coast of India supports this assumption.

6.3 Monsoon Variability and Sub-Annual Changes of Sea Level

Given that the ocean and the atmosphere form a coupled system, it is unquestionable that the changes in sea level must reflect changes in climate. The major aspect of the climate of the Indian subcontinent in particular, and of Asia in general, is the monsoon, which is linked to global climate by the planetary-scale processes in the atmosphere and the ocean. Therefore, there must be a relation between the variability of the Indian monsoon and the sub-annual changes in sea level at Mumbai and other stations along the Indian coast. The best record of monsoon variability is contained in rainfall measurements at meteorological stations scattered over the Indian subcontinent. Since rainfall directly influences salinity, which, in turn, influences coastal sea level, the sub-annual variability of sea level along the coast of India must be related to the sub-annual variability of rainfall over India. Hence, we look for for a connection between the variability of rainfall and that of sea level.

6.3.1 Correlation Between Local Rainfall and Sea Level

A connection between sea level at a location and the local rainfall was tentatively established by earlier studies [Varadarajulu et al., 1982; Prasad and Reddy, 1985; Shetye and Almeida, 1985]. The seasonal cycle of rainfall over southeast India, including Vishakhapatnam and Chennai, differs from that over the rest of India: southeast India receives more rain during the northeast monsoon. Therefore, the seasonal cycles of both local rainfall and sea level peak in November at Vishakhapatnam and Chennai. This, however, is not true along the west coast of India, or at Paradip in the northern Bay of Bengal. Given that the seasonal cycle of sea level is coherent along the east coast, is there any connection between local rainfall and sea level at sub-annual time scales? We examine the possibility, using annual rainfall[6] as a measure of rainfall variability to avoid using two indices, one for the southwest monsoon and another for the northeast monsoon.

Monthly rainfall data for Vishakhapatnam, Chennai, Kochi, and Mumbai are available from GHCN (Table 6.5). Annual rainfall for these stations is plotted along with the annual mean and extrema of sea level in Figure 6.11; the corresponding correlations are listed in Table 6.6. Local rainfall is significantly correlated with annual sea level only at Mumbai. At Chennai and Kochi, local rainfall appears to be unrelated to annual sea level.

Table 6.5 Monthly local rainfall data from the Global Historical Climate Network (GHCN). N_{yr} is the number of years of data available. The symbol in the last column is used for the local rainfall at these four stations.

Station	Longitude (°E)	Latitude (°N)	Time span	N_{yr}	Symbol
Vishakhapatnam	83.23	17.72	1866–1989	124	R_V
Chennai (Minambakkam)	80.18	13.00	1813–1990	178	R_C
Kochi (Willingdon)	76.27	9.95	1842–1973	132	R_K
Mumbai (Colaba)	72.82	18.90	1817–1989	173	R_M

The local rainfall at these four stations are correlated amongst themselves, but the correlation is high only for Vishakhapatnam and Mumbai, the two stations at which local rainfall and sea level yield a non-negligible correlation. Since the connection between rainfall and sea level is through salinity, this implies that salinity along the coast is not influenced simply by the local rainfall, except, perhaps, in the neighbourhood of Mumbai. The correlation at Mumbai remains significant when the rainfall and sea level are low-pass-filtered (Table 6.6, Figure 6.12). Like annual sea level,

[6]Annual rainfall is defined as the sum of monthly rainfall over a calendar year. As mentioned earlier, we use the calendar year for computing rainfall, but compute the mean and extrema of sea level during July–June; for computing correlations between rainfall and sea level, "zero lag" implies (say) rainfall for 1950 is matched against sea level during July 1950 to June 1951.

Table 6.6 Linear correlation statistics for annual local rainfall and sea level. R_V, R_C, R_K, and R_M denote the anomalies of annual local rainfall at Vishakhapatnam, Chennai, Kochi, and Mumbai, and $\eta_{V,m}$ and $\eta_{M,m}$ the anomalies of annual sea level at Vishakhapatnam and Mumbai. r is the linear correlation coefficient between the variables in the first two columns (at zero lag). r_s is the linear correlation at the P% significance level for the required number of degrees of freedom; if the column for P is blank, then r_s is the correlation at the 90% significance level, but the two variables are not correlated even at this level. An N-year running mean has been used to filter the data before computing the correlations; $N = 1$ implies no running mean. Correlations for sea level at Chennai and Kochi are not shown because they are negligible.

		r	r_s	P	N
R_V	$\eta_{V,m}$	0.183	0.272		1
R_M	$\eta_{M,m}$	0.492	0.247	99.0	1
R_M	$\eta_{M,m}$	0.587	0.304	99.0	2
R_M	$\eta_{M,m}$	0.666	0.450	99.0	5
R_M	$\eta_{M,m}$	0.752	0.609	99.0	10
R_V	R_M	0.307	0.235	99.0	1
R_C	R_M	0.138	0.141		1
R_K	R_M	0.136	0.160		1
R_C	R_K	0.163	0.160	90.0	1

rainfall also increases from a low early this century to a peak in the 1950s and then decreases. This implies that there must be a relation between rainfall and sea level, but this relation may not be local.

6.3.2 All-India Rainfall

The lack of correlation between local rainfall and sea level is not surprising because of the strong influence that runoff from the Ganga and the Brahmaputra has on the salinity along the east coast of India (Section 4.3.2). The decrease in salinity along the east coast is mainly due to the runoff from the Ganga and the Brahmaputra, and that along the west coast is due to the runoff from local rivers during the southwest monsoon and the advection of freshwater from the bay during the northeast monsoon. Therefore, the sub-annual variability of salinity along the east coast must be determined by the variability of rainfall in the catchment areas of the Ganga and the Brahmaputra (Figure 6.13), which must also have an effect on the sub-annual variability of salinity along the west coast; the rainfall along the west coast is an additional factor in the variability of salinity there.

There is considerable variation in the rainfall over the Indian subcontinent in both space and time. Nevertheless, meteorologists use an area-weighted average, called "all-India rainfall", as a popular index of monsoon variability. This is often defined for the southwest monsoon (June–

September), during which a large fraction of the subcontinent receives over 75% of the annual rainfall [Mishra and Gadgil, 1996, and references therein]. The major exception is southeast India, where 70% of the rainfall is during October–December. Since the rainfall during these two seasons is positively correlated [Singh, 1994; Mishra and Gadgil, 1996], annual all-India rainfall is a reasonable measure of the variability of monsoon rainfall over India.

There is a strong biennial component in the variation of all-India rainfall, with a good (poor) monsoon followed by a poor (good) monsoon [Mishra and Gadgil, 1996, and references therein]. This interannual variation is embedded in a decadal-scale variation: there have been distinct epochs in the monsoon rainfall over India and in its variability [Joseph, 1976]. There was a high frequency of droughts and variability was large during the periods 1899–1920 and 1965–1987, whereas very few droughts occurred and the variability was low during 1880–1899 and 1929–1964; since 1988, another epoch with a low frequency of droughts appears to have commenced [Mishra and Gadgil, 1996].

Since all-India rainfall is a derived quantity, estimated as the area-weighted average of annual rainfall at stations covering 29 meteorological subdivisions in India [Parthasarathy et al., 1993, 1995; Mishra and Gadgil, 1996], there exists more than one estimate. We use two time series of annual all-India rainfall, the first spanning 1901–1990 ($R_{I,19}$) and the second spanning 1871–1994 (R_I). The anomalies computed from the two time series agree well with each other (Figure 6.14), but there is a difference of 23 cm in the long-term mean rainfall, and hence, in total annual rainfall; the mean of $R_{I,19}$ is 86.5 cm, and that of R_I is 109.1 cm. In the absence of any reason for preferring one time series to the other, we use both for studying the link between the monsoon and sea level along the coast of India.

We have data from the 1871–1994 time series for 29 meteorological subdivisions in India [Parthasarathy et al., 1995]. Three of these — Konkan and Goa, Coastal Karnataka, and Kerala (Figure 6.15) — lie to the west of the Sahyadri Range in a coastal strip that receives very high rainfall; Mumbai lies in the subdivision Konkan-and-Goa and is close to the northern end of the coastal strip; Kochi lies in Kerala and is close to the southern end of the strip. We combine data from these three subdivisions, using an area-weighted average to estimate "West-Coast rainfall" (R_{WC}), which has a mean of 281 cm. Its anomaly is plotted along with that of R_I in Figure 6.14.

It is more difficult to estimate the rainfall in the catchment areas of the Ganga and the Brahmaputra because the catchment areas of these two rivers and their tributaries covers a vast area of India and spans several meteorological subdivisions; it also includes Bangladesh, for which we have no rainfall data. We pick eight of these subdivisions — North Assam, South Assam, Sub-Himalayan West Bengal, Gangetic West Bengal, Bihar Plateau, Bihar Plains, East Uttar Pradesh, and West Uttar Pradesh Plains (Figure 6.15) — and combine the data from them, using an area-weighted average to estimate "Ganga-Brahmaputra rainfall" (R_{GB}), which has a mean of 147 cm.

This gives an idea of the rainfall and its variability in the catchment areas of the Ganga and the Brahmaputra, but is less accurate than West-Coast rainfall because some of the tributaries of the Ganga, especially those flowing south–north, are not accounted for; also ignored in this estimate are the contributions to runoff from rainfall in the Himalayan foothills and from snow-melt in Tibet and the Himalayas, where the Ganga, the Brahmaputra, and some of their major tributaries originate. The rainfall over hilly regions is also not included in estimates of all-India rainfall because of the difficulty in using station rainfall data to compute area-weighted averages; this is prone to large errors in hilly areas, where the spatial variation is large and rapid, unlike in the plains. The anomaly of R_{GB} is plotted along with that of R_I in Figure 6.14.

Though the variability of all-India rainfall is determined primarily by the variability in north-west India because the coefficient of variation is largest there (> 50%) [Mishra and Gadgil, 1996, and references therein], all-India rainfall is significantly correlated with both West-Coast rainfall and Ganga-Brahmaputra rainfall; so is the local rainfall at Mumbai and Kochi with West-Coast rainfall (Table 6.7). The implication of these correlations is that all-India rainfall, from either time

Table 6.7 Linear correlation statistics for annual rainfall. R_I and $R_{I,19}$ denote the anomalies of all-India rainfall for the 1871–1994 and 1901–1990 time series, R_{WC} and R_{GB} the anomalies of West-Coast and Ganga-Brahmaputra rainfall, and R_V, R_K, and R_M the anomalies of annual local rainfall at Vishakhapatnam, Mumbai, and Kochi. r is the linear correlation coefficient between the variables in the first two columns (at zero lag). r_s is the linear correlation at the P% significance level for the required number of degrees of freedom; if the column for P is blank, then r_s is the correlation at the 90% significance level, but the two variables are not correlated even at this level. Rainfall at Chennai is not correlated with all-India rainfall, and hence, the correlation is not listed.

		r	r_s	P
R_I	$R_{I,19}$	0.941	0.267	99.0
R_I	R_{WC}	0.641	0.229	99.0
R_I	R_{GB}	0.587	0.229	99.0
$R_{I,19}$	R_{WC}	0.670	0.267	99.0
$R_{I,19}$	R_{GB}	0.378	0.267	99.0
R_I	R_V	0.384	0.239	99.0
R_I	R_K	0.199	0.194	95.0
R_I	R_M	0.478	0.235	99.0
$R_{I,19}$	R_V	0.265	0.213	99.0
$R_{I,19}$	R_K	0.195	0.198	
$R_{I,19}$	R_M	0.549	0.272	99.0
R_{WC}	R_{GB}	0.177	0.175	95.0
R_{WC}	R_M	0.557	0.235	99.0
R_{WC}	R_K	0.574	0.253	99.0

series, is a reasonable measure of the rainfall over the west coast of India and in the catchment

areas of the Ganga and the Brahmaputra. Therefore, its variability must influence that of salinity, and hence, of sea level along the coast of India.

6.3.3 Correlation Between All-India Rainfall and Sea Level

The anomalies of the annual mean and extrema of sea level are visually correlated with R_I and $R_{I,19}$ (Figures 6.16, 6.17, 6.18, and 6.19). The corresponding correlations are listed in Table 6.8. Except at Kochi, the annual mean sea level is significantly correlated with R_I and $R_{I,19}$. The correlation is best for Mumbai, which is significantly correlated at the 99% significance level irrespective of the all-India-rainfall time series used. At Vishakhapatnam and Chennai, the correlations are better when $R_{I,19}$ is used, and when the correction is applied for the effect of atmospheric pressure. The correlations at these two stations improve considerably when the sea-level data for 1961 are dropped, this year being an outlier. The annual all-India rainfall during 1961 is the second highest for the series $R_{I,19}$ and the fourth highest for R_I. Despite this, the lowest annual mean sea level was recorded in 1961 at Vishakhapatnam; at Chennai, the annual mean was the sixth lowest in 1961 (sea level corrected for atmospheric pressure). We treat this data point as an outlier for the time being, but return to it in Section 6.4.4.

Table 6.8 also lists the correlations between all-India rainfall and the annual extrema; the annual extrema at Kochi also are not correlated with all-India rainfall. At Mumbai, both the maximum and minimum are significantly correlated with both R_I and $R_{I,19}$. At Vishakhapatnam and Chennai, the maximum is significantly correlated with all-India rainfall, the correlation being significant at the 99% significance level when the sea-level data for 1961 are dropped. The minimum at Vishakhapatnam is better correlated with $R_{I,19}$ than with R_I; at Chennai, in either case, the correlation falls just short of the 90% significance level. Therefore, the annual mean and extrema of sea level along the coast of India, Kochi being an exception, are significantly correlated with all-India rainfall, the correlations being lower for the minimum; the best correlations are obtained for the sea level at Mumbai, which has the longest tide-gauge record.

The correlations at Mumbai retain their significance (Table 6.9) when the data are low-pass-filtered with a running mean (Figures 6.20 and 6.21). Annual sea level at Mumbai is significantly correlated with the all-India rainfall from the 1901–1990 data, $R_{I,19}$. Though the filtered rainfall is noisier than the filtered sea level, both rainfall and sea level were low in the first two decades of this century, rose to a peak in the 1950s, and declined thereafter. Annual sea level at Mumbai, however, is not as well correlated with the 1871–1994 all-India rainfall, R_I. R_I was above normal during 1871–1899 and dropped to a low during 1900–1915, but the annual sea level at Mumbai during 1878–1899 was just 2 cm higher than that during 1900–1920; eliminating the data during 1871–1900 improves the correlation. Annual sea level at Mumbai is also correlated with West-Coast rainfall R_{WC}, but not with Ganga-Brahmaputra rainfall R_{GB}; eliminating the data during

Figure 6.10 Low-pass-filtered variability of sea level (cm) at Mumbai. The annual mean (middle curve), maximum (upper curve), and minimum (lower curve) are plotted after the data are low-pass-filtered with a running mean. Plots are shown for no running mean, 2-year running mean, 5-year running mean, and 10-year running mean. The coherence between the annual mean and annual extrema increases as frequency decreases. The interdecadal changes in sea level are apparent even for a 2-year running mean, but are clearer for 5-year and 10-year running means. Sea level at Mumbai was generally low during 1870–1920; it peaked in the late 1950s, decreasing thereafter.

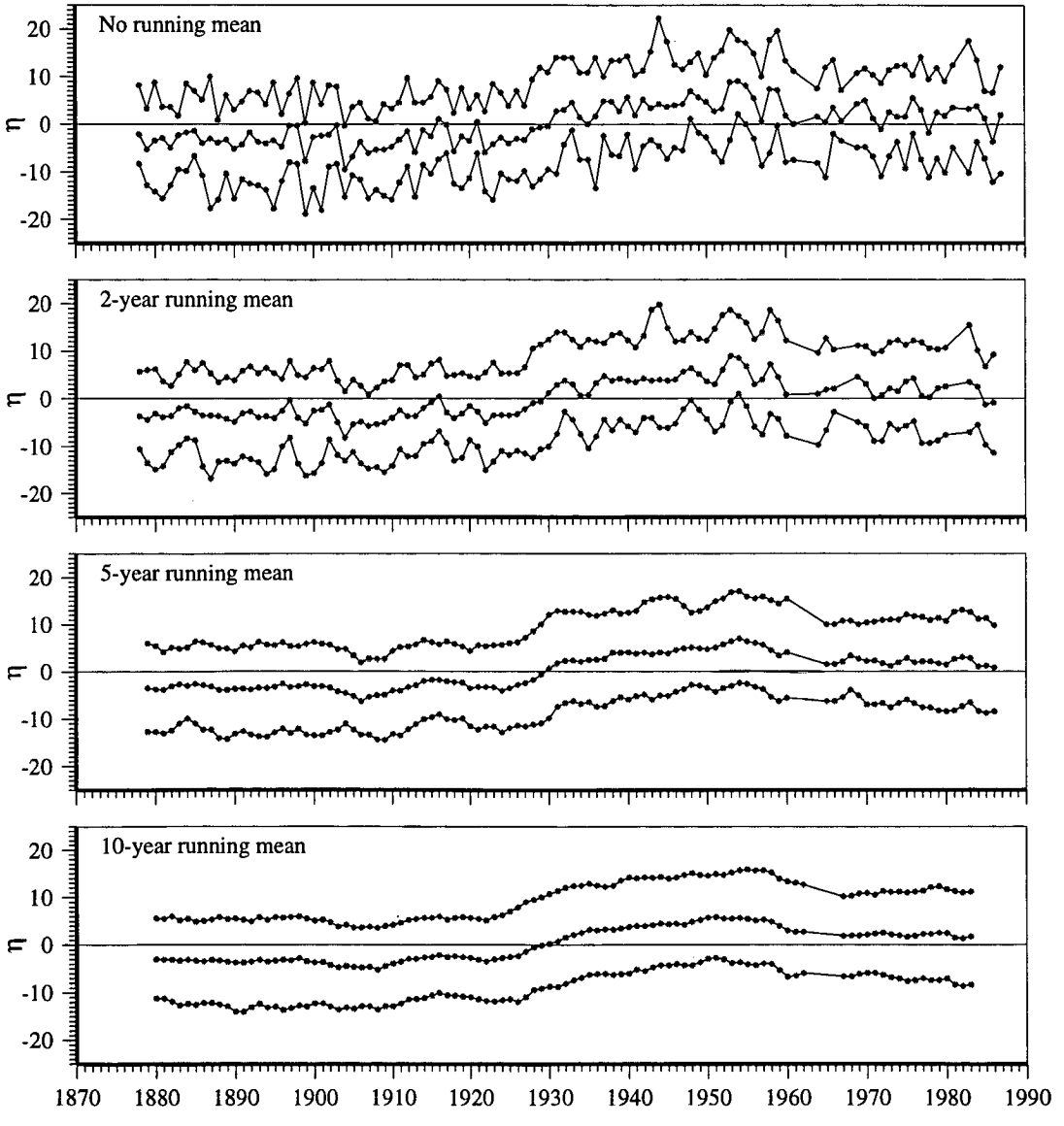

Figure 6.11 Anomalies of local annual rainfall and the annual mean and extrema of sea level at Vishakhapatnam, Chennai, Kochi, and Mumbai. Anomalies of sea level (cm) and rainfall (cm) are plotted on the ordinate and time (year) is on the abscissa. The dashed curve is for rainfall and the solid curves are for the annual mean (middle curve), annual maximum (upper curve) and annual minimum (lower curve) of sea level.

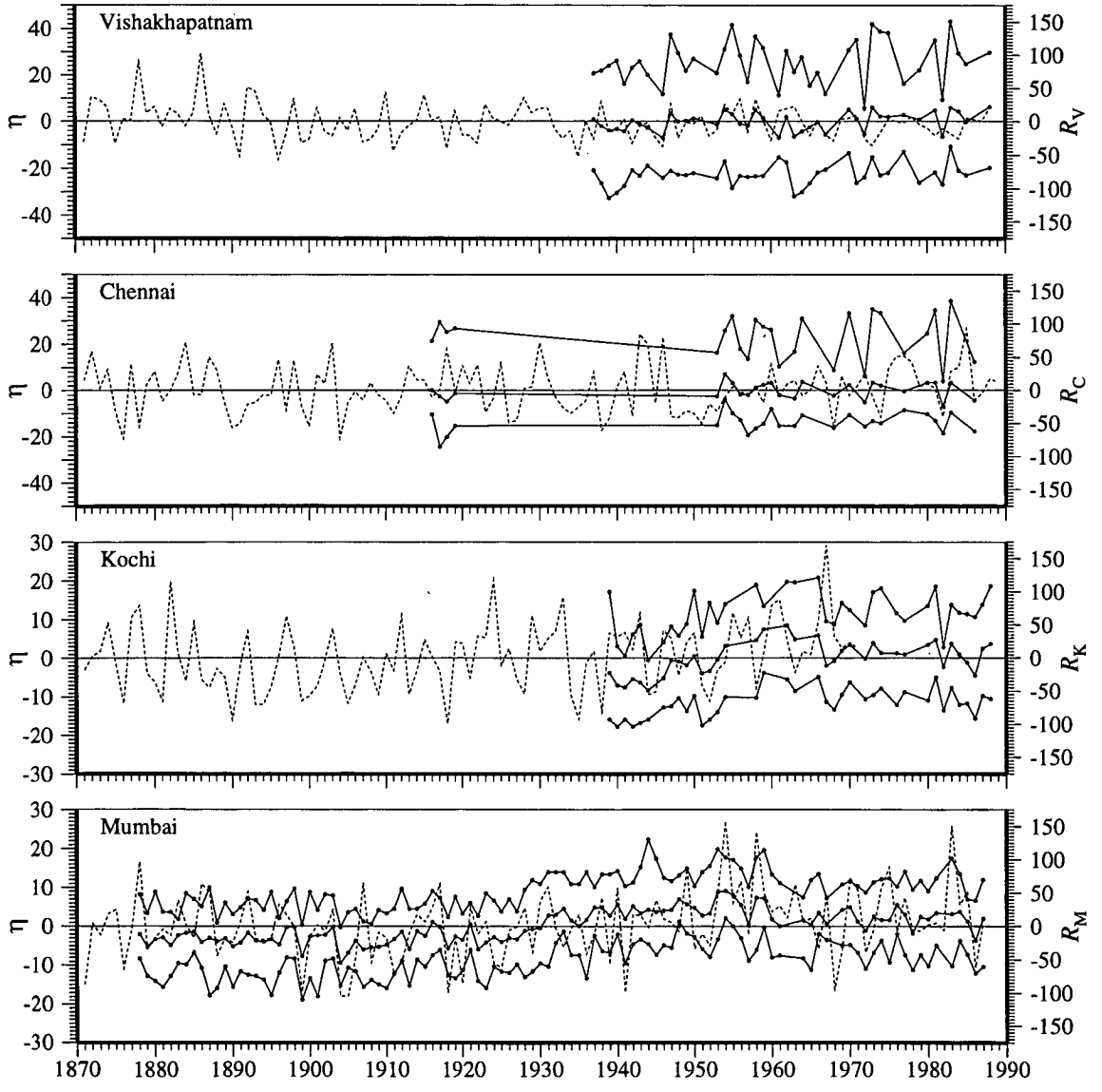

Figure 6.12 Low-pass-filtered variability of local annual rainfall and sea level at Mumbai. Anomalies of sea level (cm) and rainfall (cm) are plotted on the ordinate and time (year) is on the abscissa. The dashed curve is for rainfall and the solid curves are for the annual mean (middle curve), annual maximum (upper curve) and annual minimum (lower curve) of sea level. The data are filtered with a running mean. Plots are shown for no running mean, 2-year running mean, 5-year running mean, and 10-year running mean. Local annual rainfall and the annual mean and extrema of sea level are significantly correlated at Mumbai, the correlation increasing when the data are low-pass-filtered. Like annual sea level, rainfall also increases from a low early this century to a peak in the 1950s and then decreases.

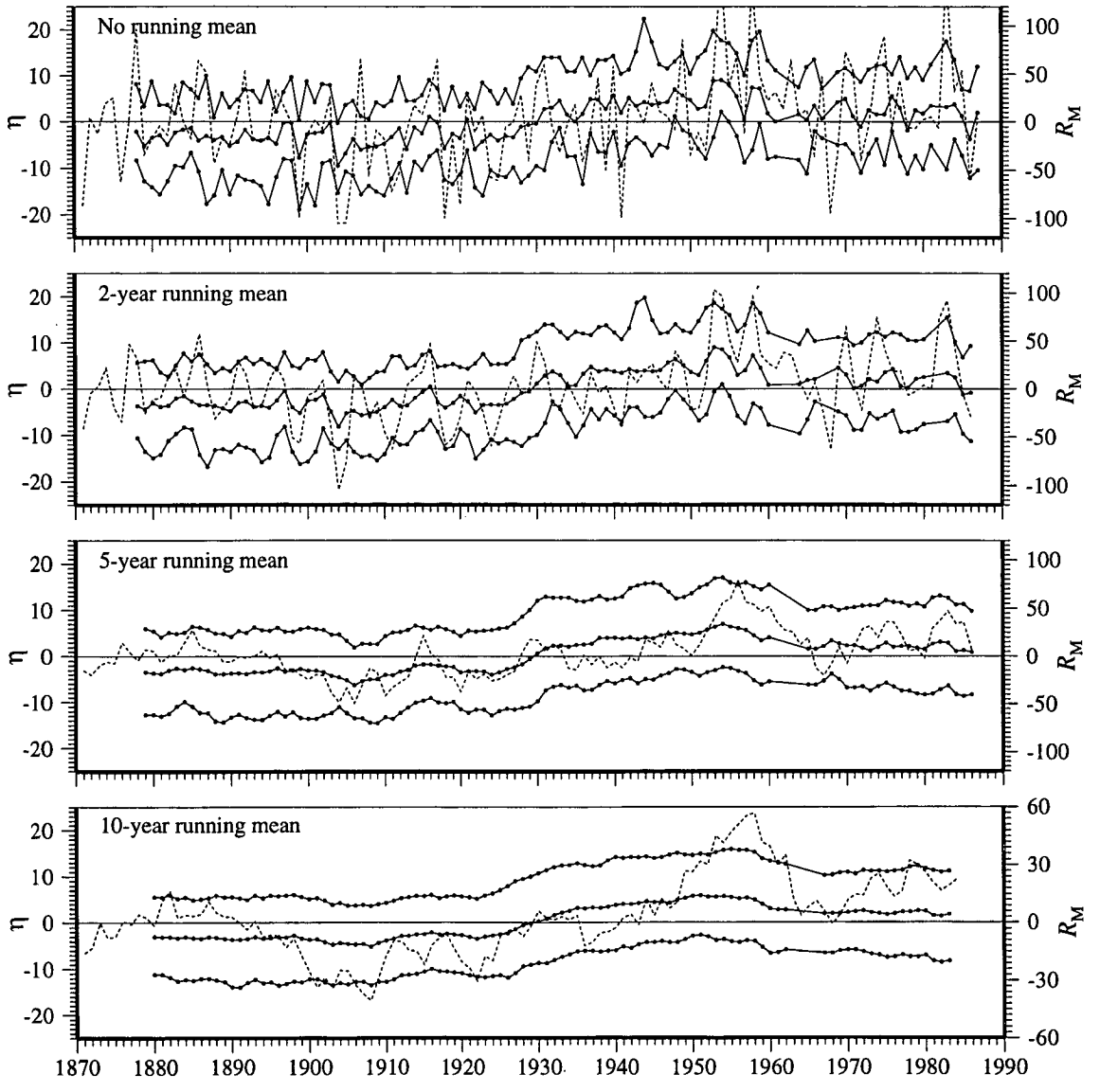

Figure 6.13 The major rivers of India are marked on the map; the dashed line shows the 200 m isobath. Most of the big rivers flow into the Bay of Bengal. The highest runoff is that of the Ganga and Brahmaputra, which together empty about 7.2×10^{11} m^3 into the northern bay during June–October. Most of these rivers originate either in the Himalayas or in the Sahyadri range (Western Ghats), which is about 1 km high and runs parallel to the west coast of India. Smaller, swift streams flow westward from the Sahyadris into the Arabian Sea, and their combined runoff is about 30% that of the Ganga and the Brahmaputra. The runoff into the Arabian Sea is assumed to be 80% of the total rainfall over the three meteorological subdivisions along the west coast of India; this coastal belt stretches from the southern tip of India to just north of Mumbai and is bounded in the east by the Sahyadri range. The abbreviations used in the figure are as follows: EICC, East India Coastal Current; WICC, West India Coastal Current; NMC, Northeast Monsoon Current; LH, Lakshadweep High; R.G., River Ganga; R.B., River Brahmaputra. The currents are plotted for December, when the EICC flows equatorward and the WICC flows poleward. Together, they transport low-salinity water from the northern bay to the west coast of India.

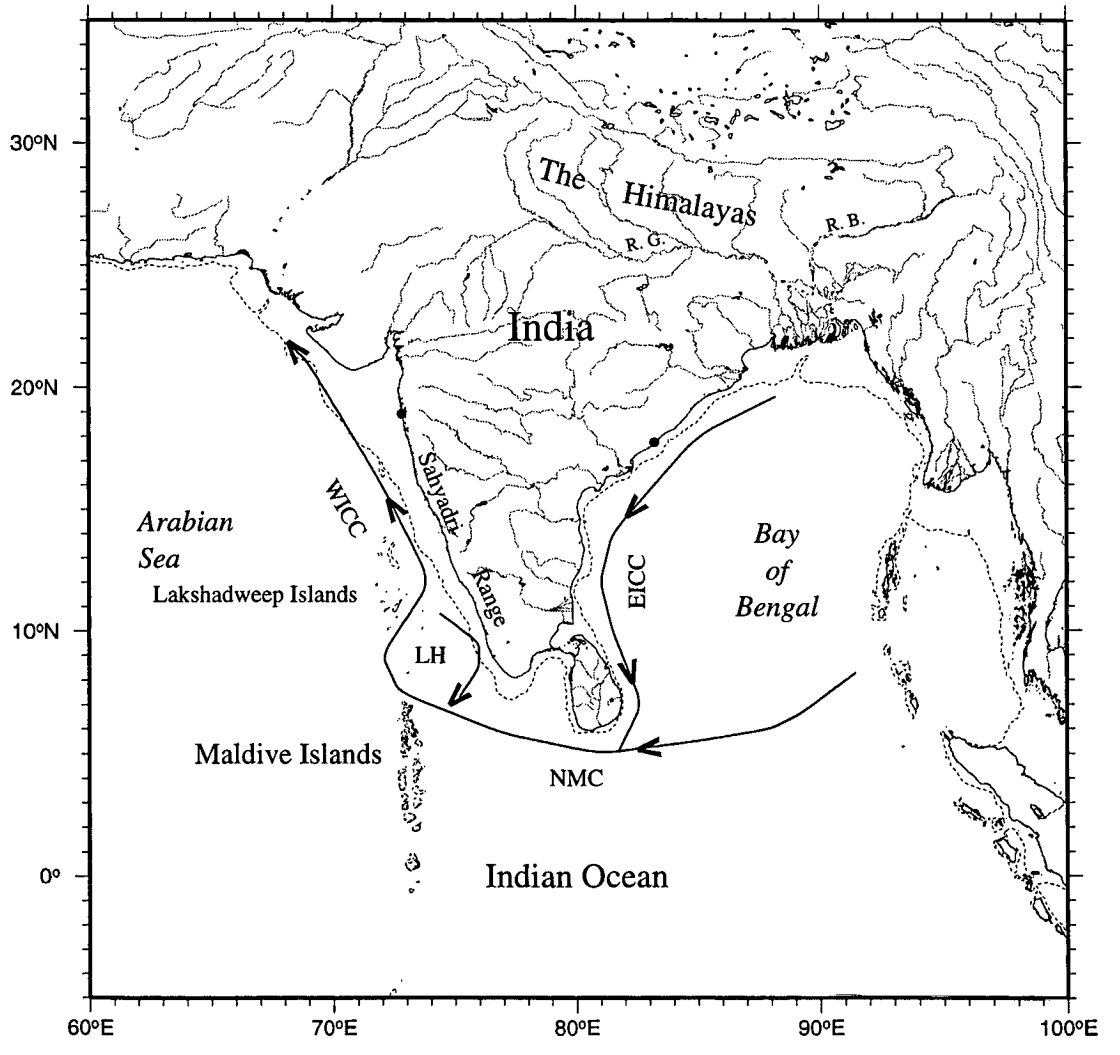

Figure 6.14 Anomalies of annual all-India, West-Coast, and Ganga-Brahmaputra rainfall. The anomalies (cm), are plotted as a function of time (year). The two series of all-India annual rainfall yield different long-term means; the mean of the 1871–1994 (R_I) series is 109.1 cm, and that of the 1901–1990 series ($R_{I,19}$) is 86.5 cm. Though there is a difference in the total rainfall, the anomalies are comparable (top panel). West-Coast rainfall (R_{WC}) is an area-weighted average of annual rainfall over three meteorological subdivisions along the west coast of India — Konkan and Goa, Coastal Karnataka, and Kerala. Anomalies of R_{WC} are correlated with those of R_I (middle panel). Ganga-Brahmaputra rainfall (R_{GB}) is an area-weighted average of annual rainfall over eight meteorological subdivisions in India — North Assam, South Assam, Sub-Himalayan West Bengal, Gangetic West Bengal, Bihar Plateau, Bihar Plains, East Uttar Pradesh, and West Uttar Pradesh Plains. Anomalies of R_{GB} are also correlated with those of R_I (lower panel).

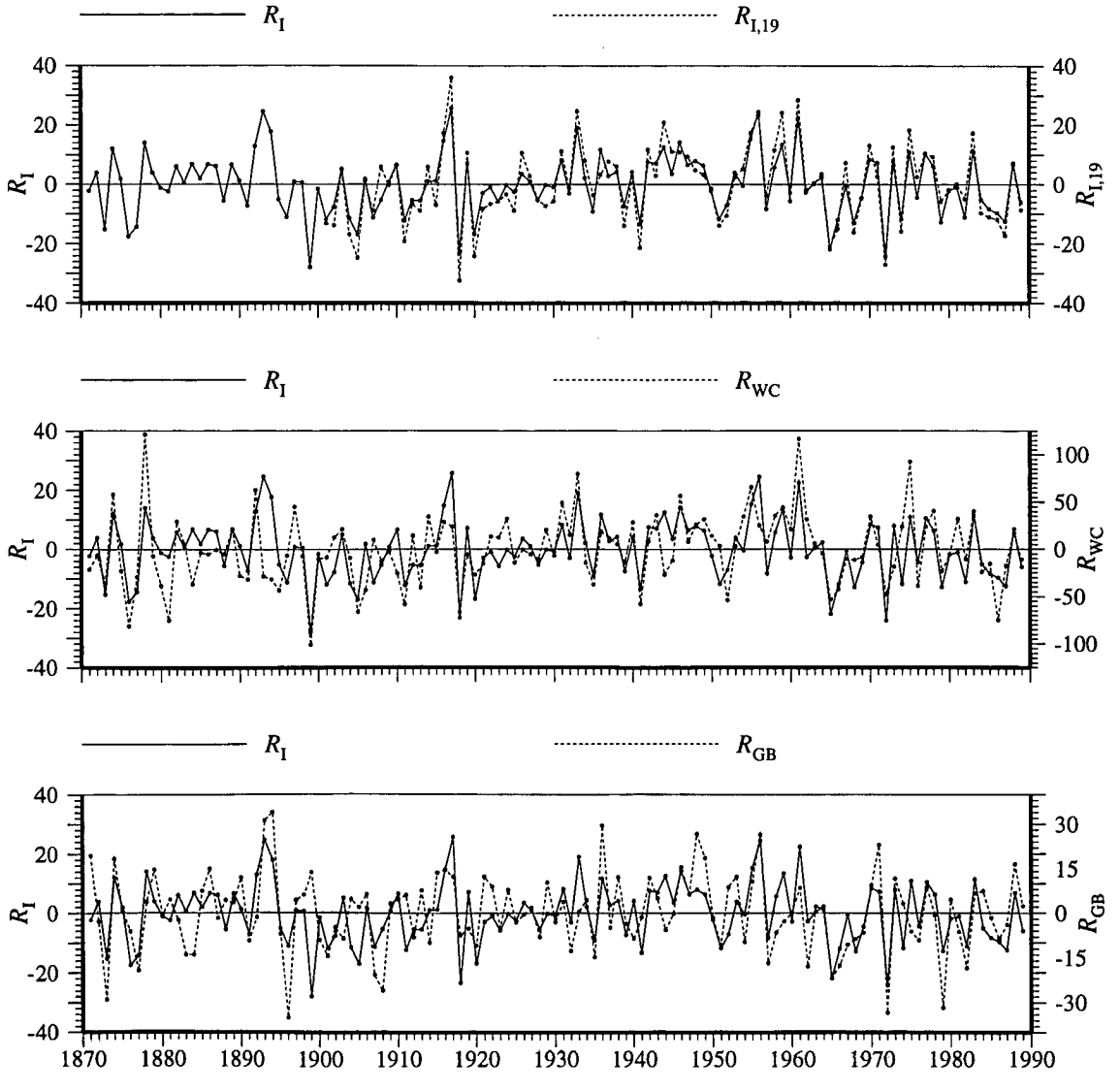

Figure 6.15 The meteorological subdivisions of India referred to in the text. The abbreviations used in the figure are as follows: R.G., River Ganga; R.B., River Brahmaputra; NA, North Assam; SA, South Assam; SHWB, Sub-Himalayan West Bengal; GWB, Gangetic West Bengal; BPn, Bihar Plains; BPu, Bihar Plateau; EUP, East Uttar Pradesh; WUPP, West Uttar Pradesh Plains; KG, Konkan and Goa; CK, Coastal Karnataka; and K, Kerala. The abbreviations, apart from the two for the rivers, refer to meteorological subdivisions of the India Meteorological Department. The first eight of these subdivisions are used to estimate the rainfall in the catchment areas of the Ganga and the Brahmaputra and this estimate is called "Ganga-Brahmaputra rainfall" (R_{GB}). The last three subdivisions are used to estimate the rainfall along the west coast of India till just north of Mumbai and this estimate is called "West-Coast rainfall" (R_{WC}). Both these estimates are significantly correlated with all-India rainfall (R_I and $R_{I,19}$).

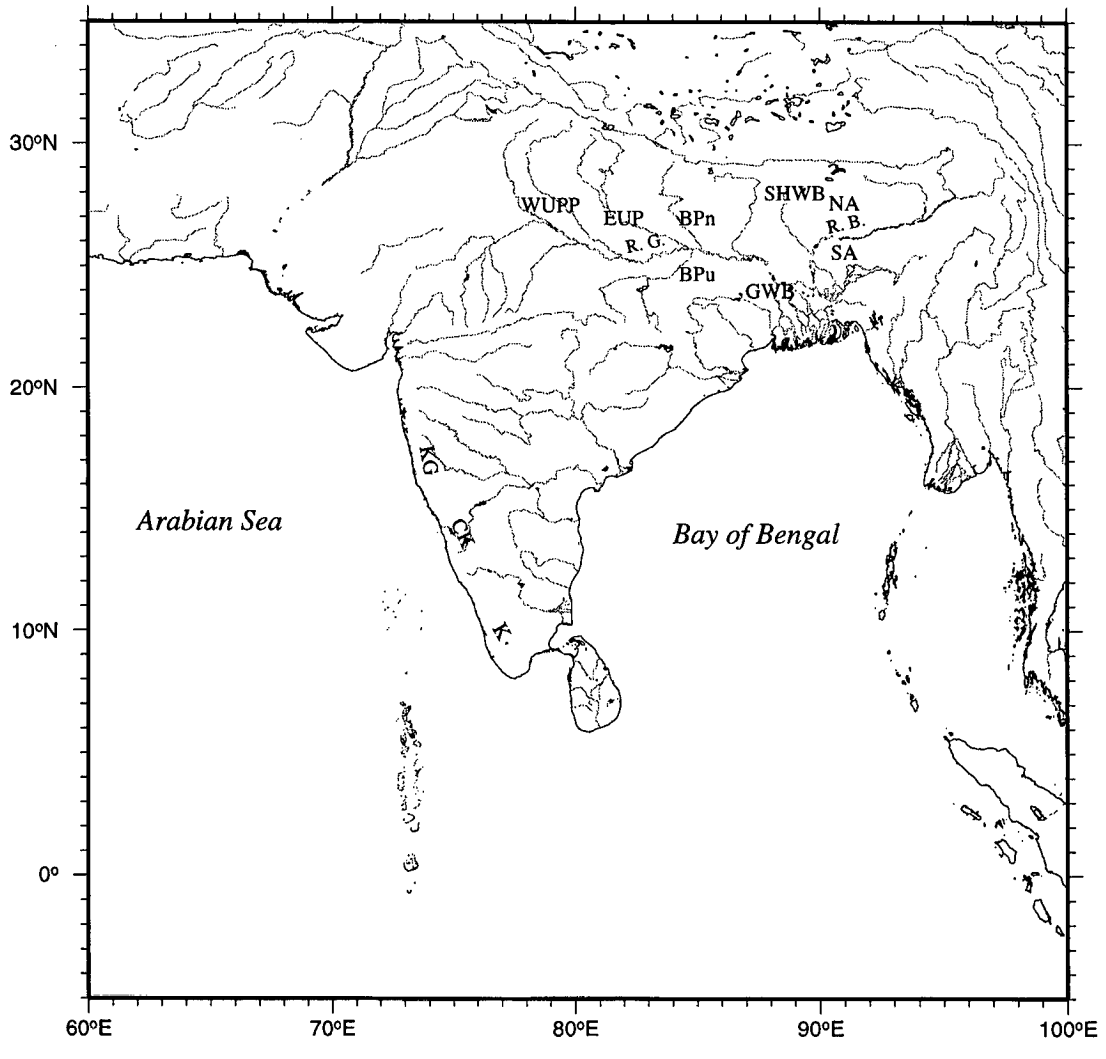

Figure 6.16 Anomalies of annual all-India rainfall (1871–1994) R_I and the annual mean and extrema of uncorrected sea level at Vishakhapatnam, Chennai, Kochi, and Mumbai. The dashed curve is for rainfall and the solid curves are for the annual mean (middle curve), annual maximum (upper curve) and annual minimum (lower curve) of sea level. Anomalies of sea level (cm) and rainfall (cm) are plotted on the ordinate and time (year) is on the abscissa.

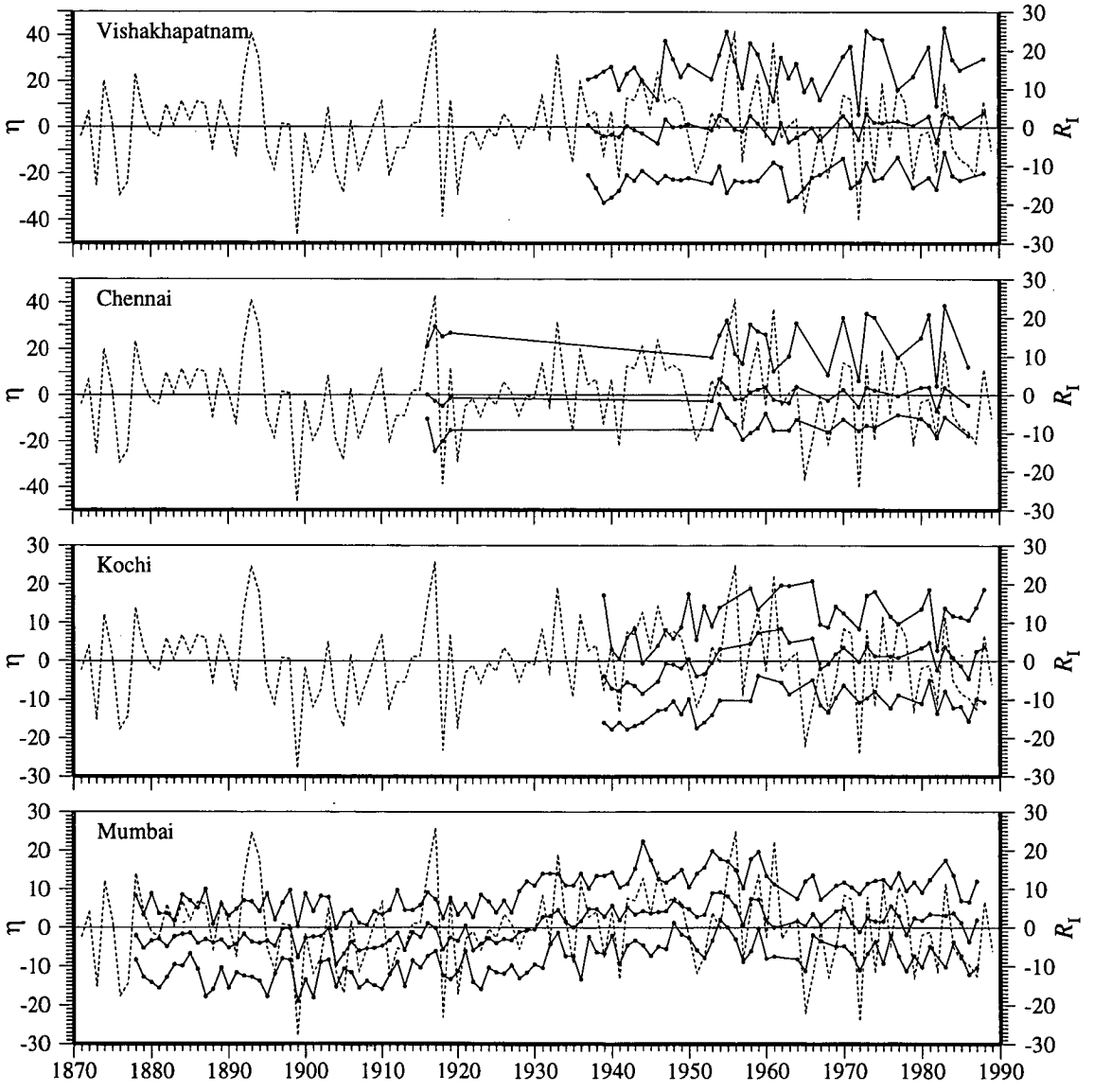

Figure 6.17 Anomalies of annual all-India rainfall (1901–1990) $R_{I,19}$ and the annual mean and extrema of uncorrected sea level at Vishakhapatnam, Chennai, Kochi, and Mumbai. The dashed curve is for rainfall and the solid curves are for the annual mean (middle curve), annual maximum (upper curve) and annual minimum (lower curve) of sea level. Anomalies of sea level (cm) and rainfall (cm) are plotted on the ordinate and time (year) is on the abscissa.

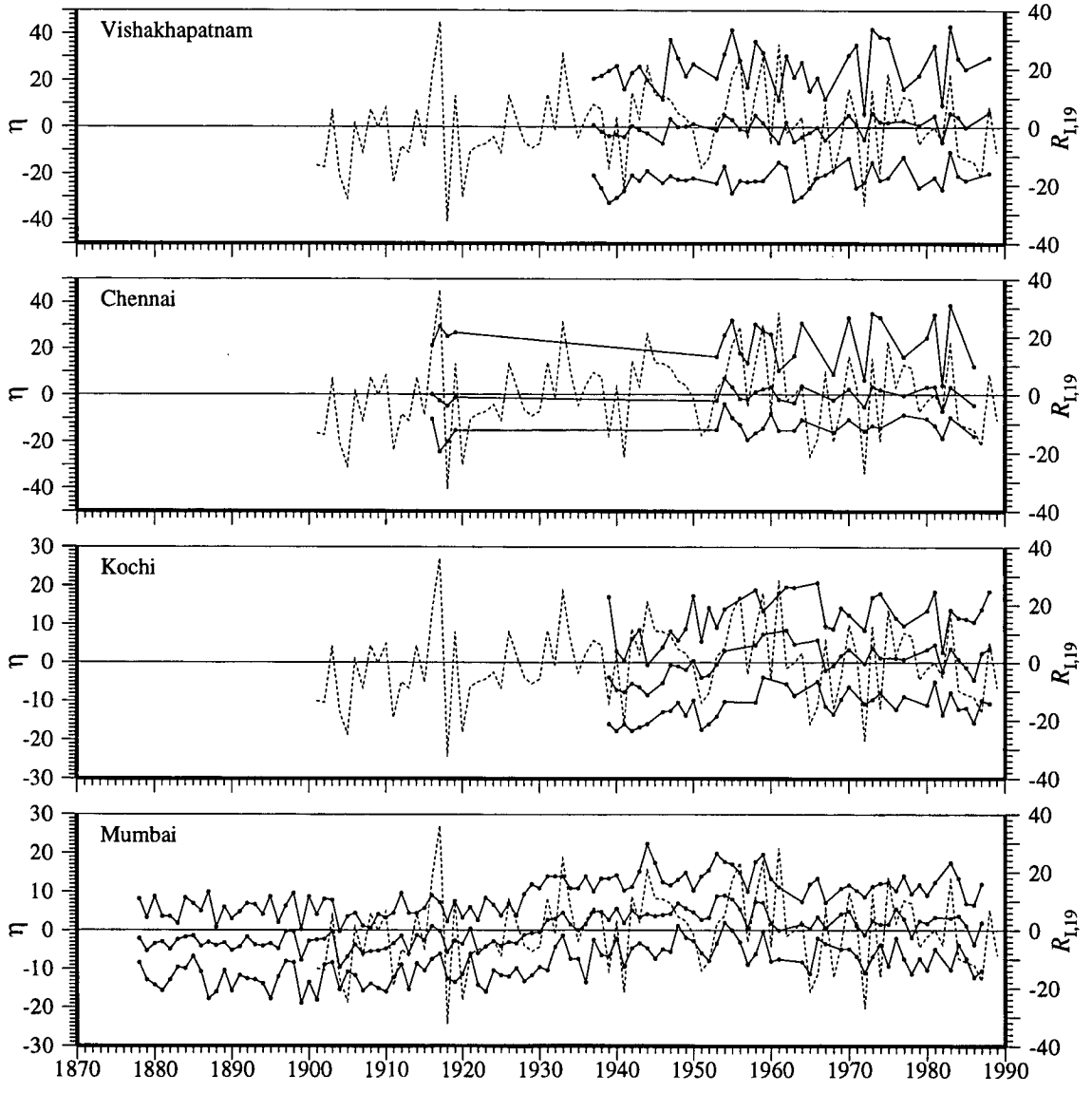

Figure 6.18 Anomalies of annual all-India rainfall (1871–1994) R_I and the corrected annual mean and extrema of sea level, at Vishakhapatnam, Chennai, Kochi, and Mumbai. The dashed curve is for rainfall and the solid curves are for the annual mean (middle curve), annual maximum (upper curve) and annual minimum (lower curve) of sea level. Anomalies of sea level (cm) and rainfall (cm) are plotted on the ordinate and time (year) is on the abscissa.

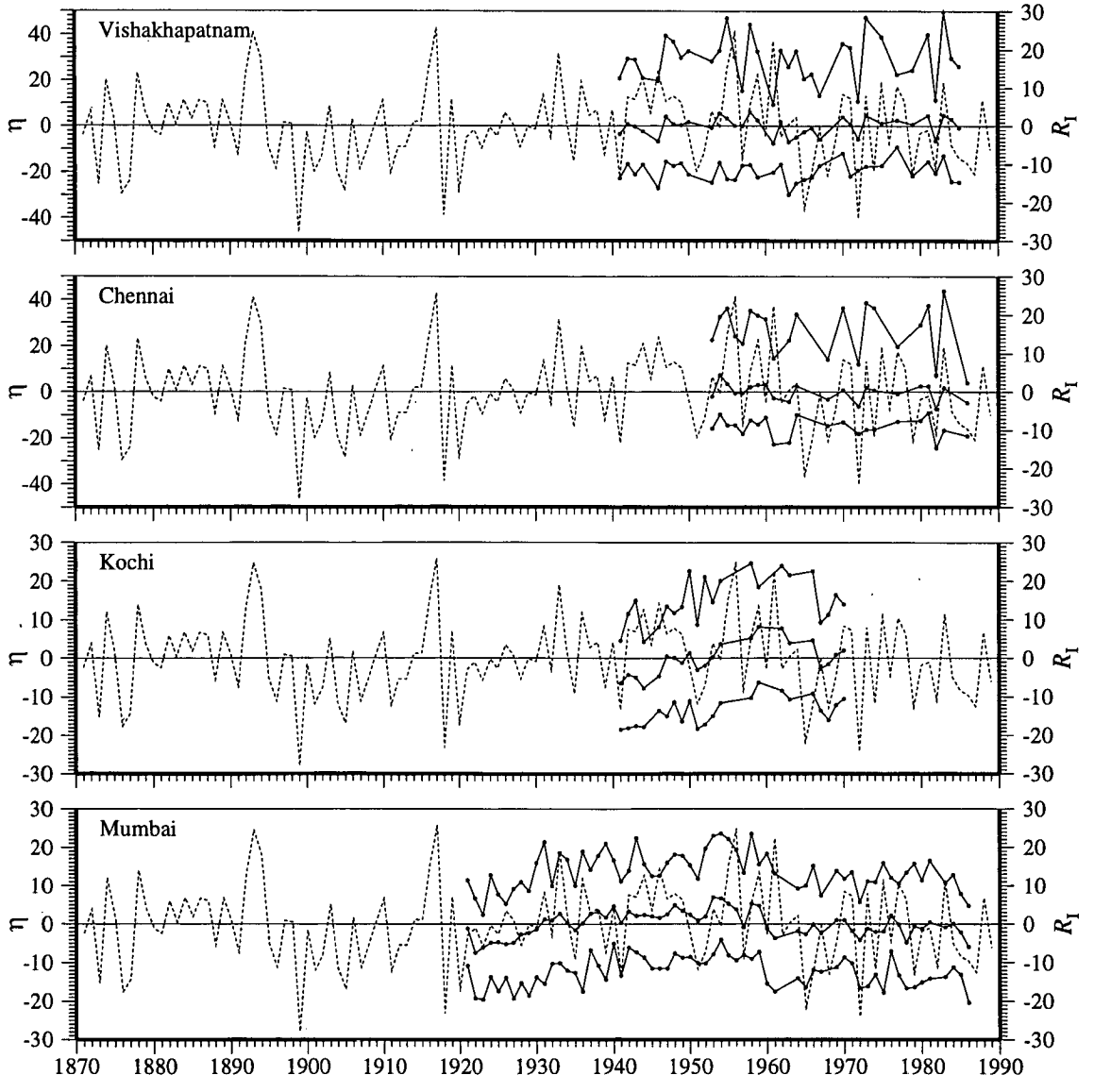

Figure 6.19 Anomalies of annual all-India rainfall (1901–1990) $R_{I,19}$ and the corrected annual mean and extrema of sea level at Vishakhapatnam, Chennai, Kochi, and Mumbai. The dashed curve is for rainfall and the thick solid are for the annual mean (middle curve), annual maximum (upper curve) and annual minimum (lower curve) of sea level. Anomalies of sea level (cm) and rainfall (cm) are plotted on the ordinate and time (year) is on the abscissa.

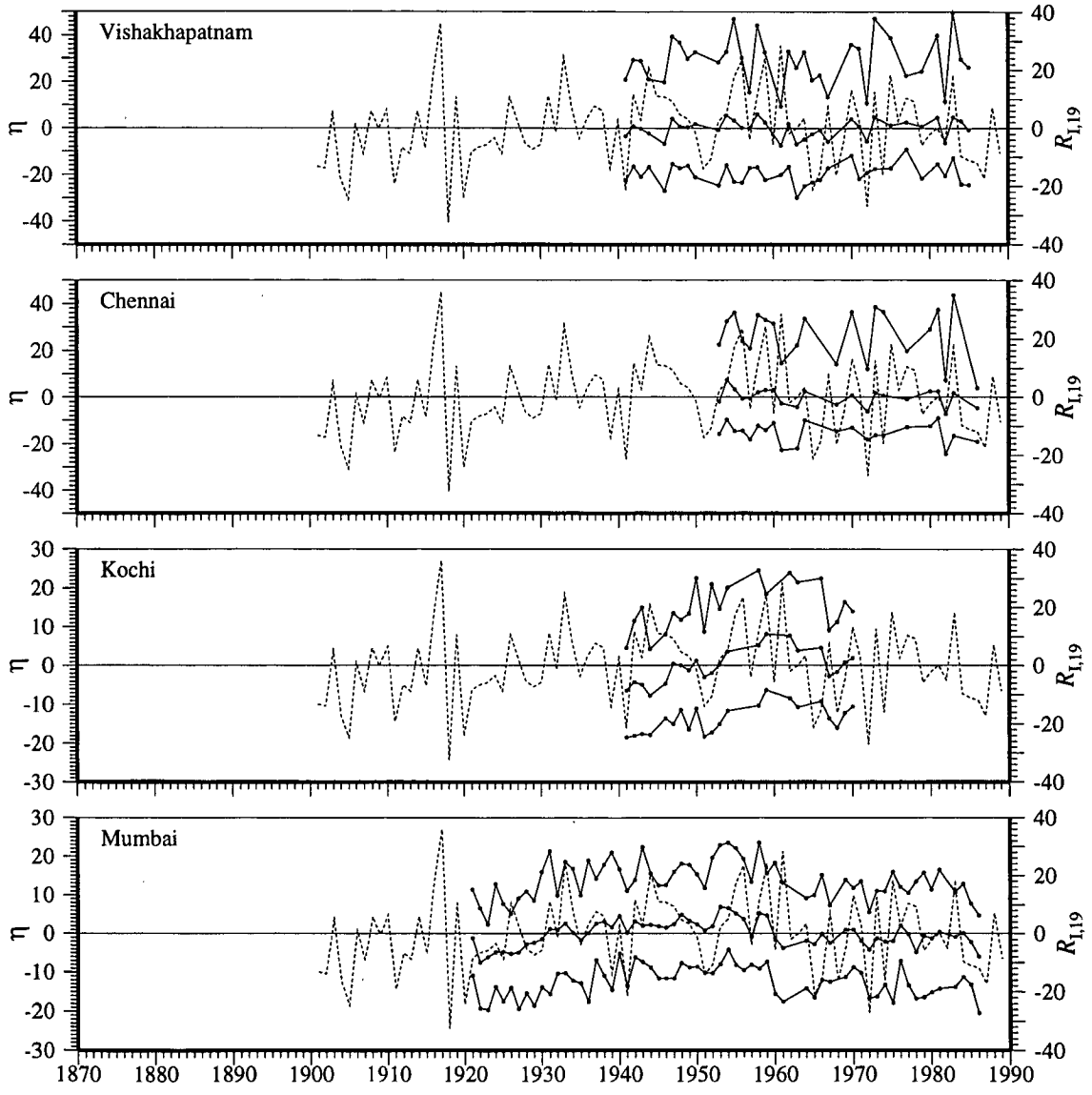

Table 6.8 Linear correlation statistics for annual all-India rainfall and sea level. R_I and $R_{I,19}$ denote the anomalies of annual all-India rainfall (1871–1994 and 1901–1990 time series), and η_V, η_C, η_K, and η_M the anomalies of sea level at Vishakhapatnam, Chennai, Kochi, and Mumbai; the subscripts "m", "max", and "min" imply annual mean, maximum, and minimum. r, r_s, and P are as before. A "C" in the sixth column implies that the sea-level data are corrected for atmospheric pressure (default is no correction); an asterisk (*) in the last (seventh) column implies that sea-level data for 1961 have been dropped while computing the correlations. The annual mean and extrema of sea level at Kochi are not correlated with all-India rainfall, and hence, not shown.

		r	r_s	P		
R_I	$\eta_{V,m}$	0.186	0.260			
R_I	$\eta_{V,m}$	0.211	0.283		C	
R_I	$\eta_{V,m}$	0.297	0.264	90.0		*
R_I	$\eta_{V,m}$	0.352	0.329	95.0	C	*
R_I	$\eta_{V,max}$	0.394	0.325	95.0	C	
R_I	$\eta_{V,max}$	0.550	0.424	99.0	C	*
R_I	$\eta_{V,min}$	0.169	0.283		C	
R_I	$\eta_{V,min}$	0.182	0.287		C	*
$R_{I,19}$	$\eta_{V,m}$	0.241	0.283		C	
$R_{I,19}$	$\eta_{V,m}$	0.393	0.329	95.0	C	*
$R_{I,19}$	$\eta_{V,max}$	0.372	0.325	95.0	C	
$R_{I,19}$	$\eta_{V,max}$	0.534	0.424	99.0	C	*
$R_{I,19}$	$\eta_{V,min}$	0.275	0.283		C	
$R_{I,19}$	$\eta_{V,min}$	0.296	0.287	90.0	C	*
R_I	$\eta_{C,m}$	0.308	0.329			
R_I	$\eta_{C,m}$	0.387	0.361	90.0	C	
R_I	$\eta_{C,m}$	0.384	0.344	90.0		*
R_I	$\eta_{C,m}$	0.520	0.423	95.0	C	*
R_I	$\eta_{C,max}$	0.387	0.361	90.0	C	
R_I	$\eta_{C,max}$	0.545	0.537	99.0	C	*
R_I	$\eta_{C,min}$	0.129	0.361		C	
R_I	$\eta_{C,min}$	0.357	0.379		C	*
$R_{I,19}$	$\eta_{C,m}$	0.410	0.404	95.0	C	
$R_{I,19}$	$\eta_{C,m}$	0.564	0.537	99.0	C	*
$R_{I,19}$	$\eta_{C,max}$	0.405	0.404	95.0	C	
$R_{I,19}$	$\eta_{C,max}$	0.578	0.537	99.0	C	*
$R_{I,19}$	$\eta_{C,min}$	0.086	0.361		C	
$R_{I,19}$	$\eta_{C,min}$	0.325	0.379		C	*
R_I	$\eta_{M,m}$	0.321	0.247	99.0		
R_I	$\eta_{M,m}$	0.356	0.320	99.0	C	
R_I	$\eta_{M,max}$	0.393	0.320	99.0	C	
R_I	$\eta_{M,min}$	0.241	0.211	90.0	C	
$R_{I,19}$	$\eta_{M,m}$	0.362	0.320	99.0	C	
$R_{I,19}$	$\eta_{M,max}$	0.336	0.320	99.0	C	
$R_{I,19}$	$\eta_{M,min}$	0.285	0.246	95.0	C	

Table 6.9 Linear correlation statistics for low-pass-filtered annual rainfall and sea level at Mumbai. R_I and $R_{I,19}$ denote the anomalies of annual all-India rainfall for the 1871–1994 and 1901–1990 time series, R_{WC} and R_{GB} the anomalies of annual West-Coast and Ganga-Brahmaputra rainfall, and $\eta_{M,m}$ the anomalies of low-pass-filtered annual mean sea level at Mumbai. r is the linear correlation coefficient between the variables in the first two columns (at zero lag). r_s is the linear correlation at the P% significance level for the required number of degrees of freedom; if the column for P is blank, then r_s is the correlation at the 90% significance level, but the two variables are not correlated even at this level. A "T" in the sixth column implies that the rainfall and sea-level data have been truncated and only the data from 1901 onwards have been used to compute the correlations. An N-year running mean has been used to filter the data before computing the correlations; $N = 1$ implies no running mean. The long tide-gauge record at Mumbai yields the best correlations between all-India rainfall and sea level. The correlations at Mumbai retain their significance when the data are low-pass-filtered. $\eta_{M,m}$ is significantly correlated with $R_{I,19}$. Though the filtered rainfall is noisier than the filtered sea level, both rainfall and sea level were low in the first two decades of this century, rose to a peak in the 1950s, and declined thereafter (Figure 6.21). $\eta_{M,m}$, however, is not as well correlated with R_I. R_I was above normal during 1871–1899 and dropped to a low during 1900–1915, but the annual sea level at Mumbai during 1878–1899 was just 2 cm higher than that during 1900–1920 (Figure 6.20); eliminating the data during 1871–1900 improves the correlation. $\eta_{M,m}$ is also correlated with R_{WC}, but not with R_{GB}; eliminating the data during 1871–1900 improves this correlation also. Since R_M is significantly correlated with R_{WC}, R_I, and $R_{I,19}$ (Table 6.7), and the annual sea level is well correlated along the coast (Table 6.2), this implies that there exists at least a statistical basis for a relation between the sub-annual variability of rainfall over India and that of sea level along her coast. The physical basis for such a relation is the influence of salinity on the seasonal cycle and alongshore variations of sea level along the coast.

		r	r_s	P		N
R_I	$\eta_{M,m}$	0.321	0.247	99.0		1
R_I	$\eta_{M,m}$	0.334	0.304	99.0		2
R_I	$\eta_{M,m}$	0.328	0.299	90.0		5
R_I	$\eta_{M,m}$	0.464	0.424	90.0		10
$R_{I,19}$	$\eta_{M,m}$	0.437	0.278	99.0		1
$R_{I,19}$	$\eta_{M,m}$	0.501	0.344	99.0		2
$R_{I,19}$	$\eta_{M,m}$	0.556	0.506	99.0		5
$R_{I,19}$	$\eta_{M,m}$	0.752	0.677	99.0		10
R_I	$\eta_{M,m}$	0.416	0.278	99.0	T	1
R_I	$\eta_{M,m}$	0.654	0.557	95.0	T	10
R_{WC}	$\eta_{M,m}$	0.374	0.274	99.0		1
R_{WC}	$\eta_{M,m}$	0.375	0.278	99.0	T	1
R_{GB}	$\eta_{M,m}$	0.091	0.161			1
R_{GB}	$\eta_{M,m}$	0.195	0.182	90.0	T	1

Figure 6.20 Low-pass-filtered variability of all-India annual rainfall (1871–1994) R_I and the annual mean and extrema of sea level at Mumbai. Anomalies of sea level (cm) and rainfall (cm) are plotted on the ordinate and time (year) is on the abscissa. The dashed curve is for rainfall and the solid curves are for the annual mean (middle curve), annual maximum (upper curve) and annual minimum (lower curve) of sea level. The data are filtered with a running mean. Plots are shown for no running mean, 2-year running mean, 5-year running mean, and 10-year running mean.

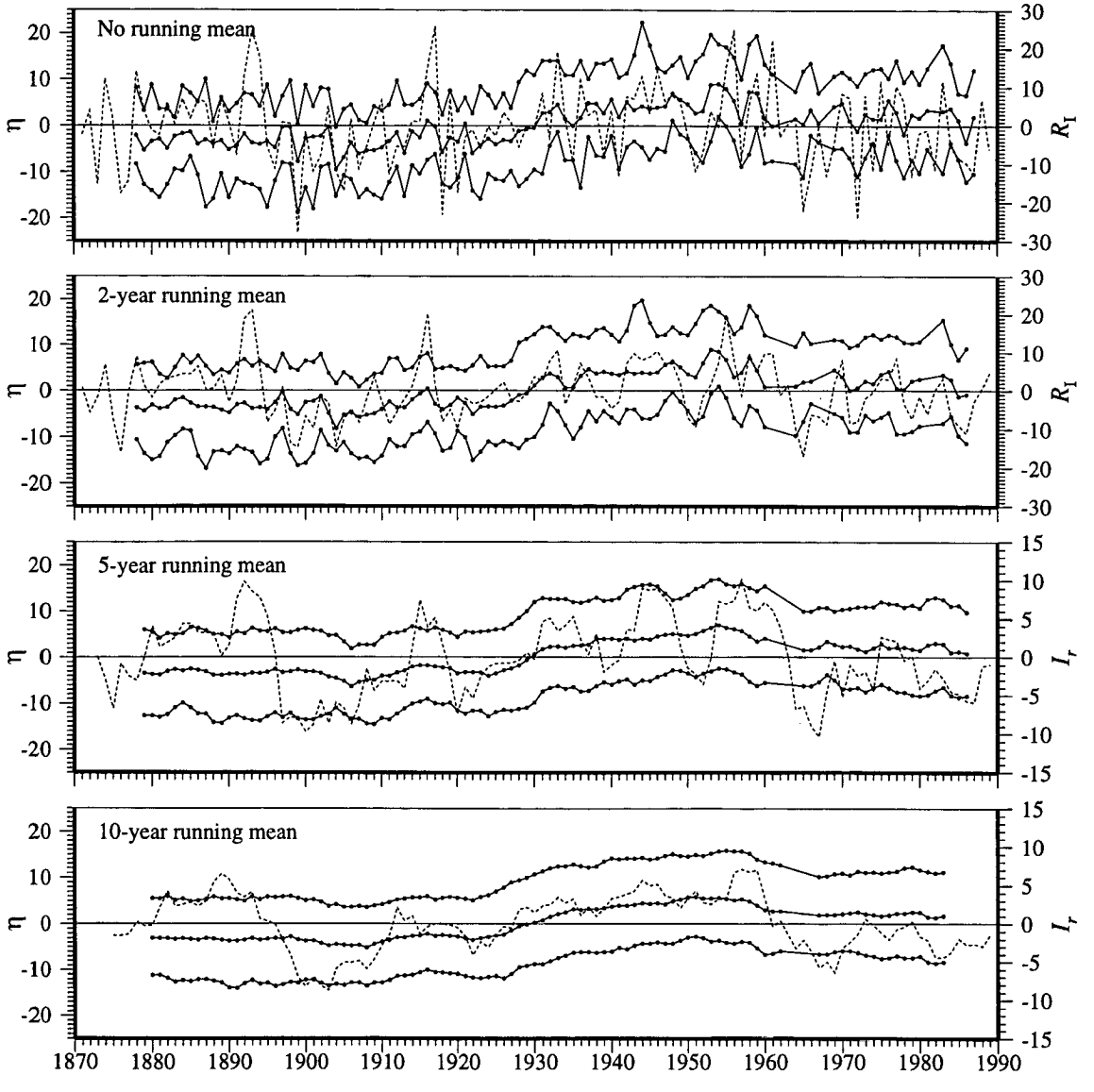

Figure 6.21 Low-pass-filtered variability of all-India annual rainfall (1901–1990) $R_{I,19}$ and the annual mean and extrema of sea level at Mumbai. Anomalies of sea level (cm) and rainfall (cm) are plotted on the ordinate and time (year) is on the abscissa. The dashed curve is for rainfall and the solid curves are for the annual mean (middle curve), annual maximum (upper curve) and annual minimum (lower curve) of sea level. The data are filtered with a running mean. Plots are shown for no running mean, 2-year running mean, 5-year running mean, and 10-year running mean.

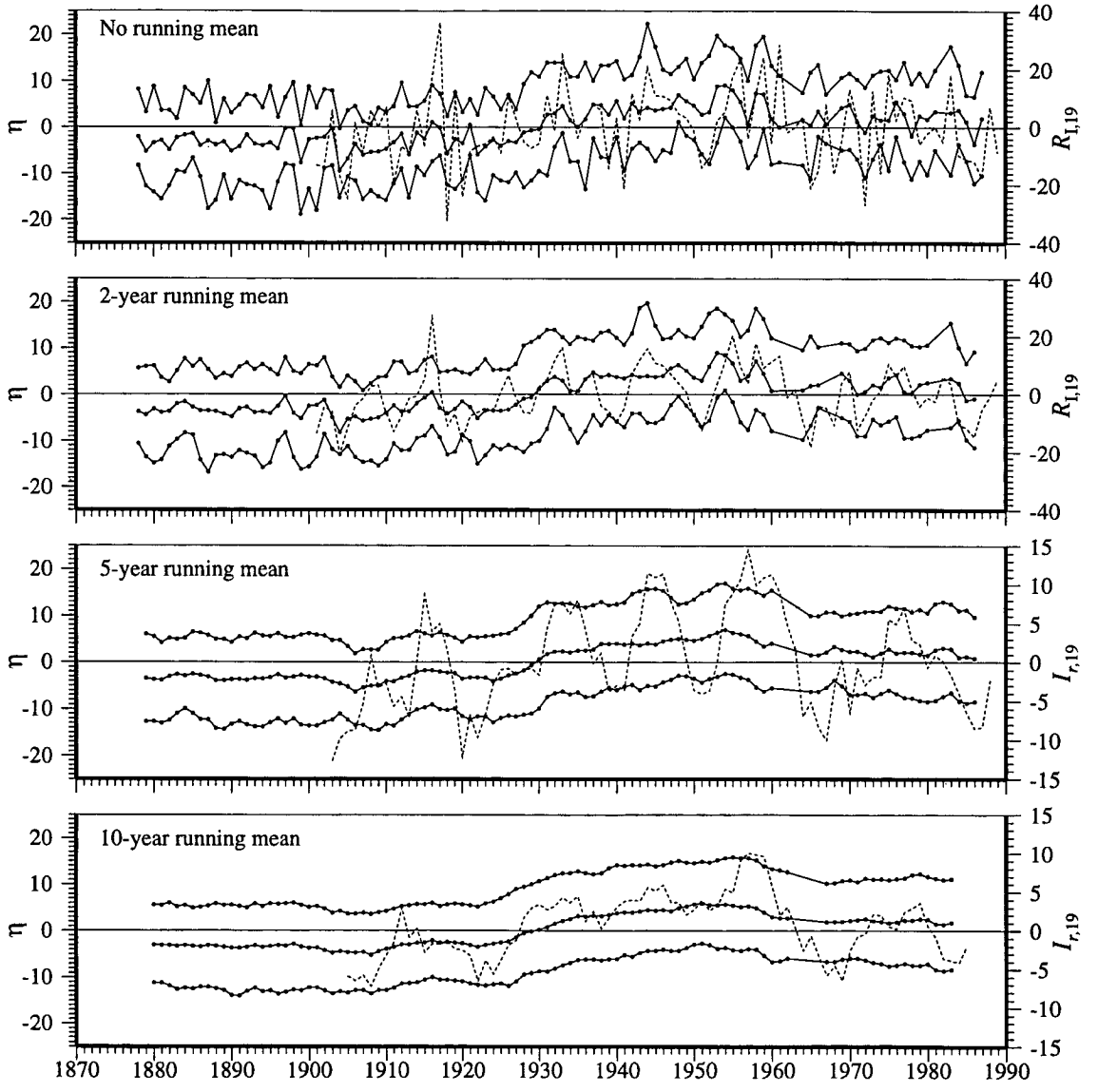

1871–1900 improves this correlation also.

Since R_M is significantly correlated with R_{WC}, R_I, and $R_{I,19}$ (Table 6.7), and the annual sea level is well correlated along the coast (Table 6.2), this implies that there exists at least a statistical basis for a relation between the sub-annual variability of rainfall over India and that of sea level along her coast. The physical basis for such a relation is the influence of salinity on the seasonal cycle and alongshore variations of sea level along the coast.

6.3.4 A Hypothesis Linking Monsoon Rainfall and Sea Level Along the Coast

Our hypothesis is that the seasonal inflow of the monsoon rainfall into the seas around India and the dynamics of currents (EICC and WICC) along her coast provide the link between all-India rainfall and coastal sea level, with the coastal salinity field playing an intermediate role. A simple model for the seasonally reversing EICC and WICC is an annual Kelvin wave, which favours upwelling during the southwest monsoon and downwelling during the northeast monsoon (Section 3.4). Under the influence of such a wave, the currents and sea level at the coast undergo a seasonal cycle; a coastal current favouring downwelling (upwelling) implies an increase (decrease) in coastal sea level (Figure 6.22a). The seasonal cycle of currents alone, however, cannot explain the link between all-India rainfall and the sea level at Mumbai on the interdecadal time scale (Figures 6.12, 6.20 and 6.21), just as it could not explain the seasonal cycle of sea level; the salinity along the coast has a significant effect on sea level (Section 4.3). The changes in coastal salinity are a consequence of the spreading of river runoff along the coast by the seasonal EICC and WICC. The result of the spreading and mixing of this low-salinity water is a gradient of salinity normal to the coast; the time scale associated with the temporal variability of this gradient is much longer than a season or an year because mixing is slow in the ocean. We propose that it is this cross-shore gradient of salinity that drives a weak, quasi-steady circulation (Figure 6.22b), providing the link between the interdecadal variability of all-India rainfall and that of sea level at Mumbai. In the next section, we put together a simple dynamical framework to justify this proposition.

6.4 Mechanics of Interdecadal Sea-Level Change Along the Coast of India

Our primary aim is to examine how the currents and sea level associated with an annual coastal Kelvin wave, which is a good description of the conditions along the coast of India, are modified by a cross-shore variation in density. We begin with the linearized $1\frac{1}{2}$-layer model (Section A.1) that has proven useful in understanding the seasonal cycle of circulation along the coast of India, and then constrain it to reflect the weak, quasi-steady forcing that arises because of the cross-shore

Figure 6.22 **(a)** Schematic of a section normal to the coast, showing the relation between currents and sea level along the coast of India. The current shown by "x" ("·") within a circle is into (out of) the plane of the paper. When there is downwelling (upwelling) at the coast, the current flows with the coast on its right (left), sea level rises (falls) at the coast, and the pycnocline (the top of which is shown by the line marking the bottom of the hatched area) slopes down (up) towards the coast. Along the west coast of India, there is downwelling (upwelling) during the northeast (southwest) monsoon. **(b)** Schematic to show how, according to our hypothesis, the conditions depicted in **(a)** are modified when salinity near the coast is lower than that farther offshore. Wider spacing of the hatched lines indicates lower salinity. The salinity (hence, density) gradient normal to the coast drives a weak, quasi-steady surface current that moves with the coast on its right, introducing a quasi-steady rise in sea level at the coast.

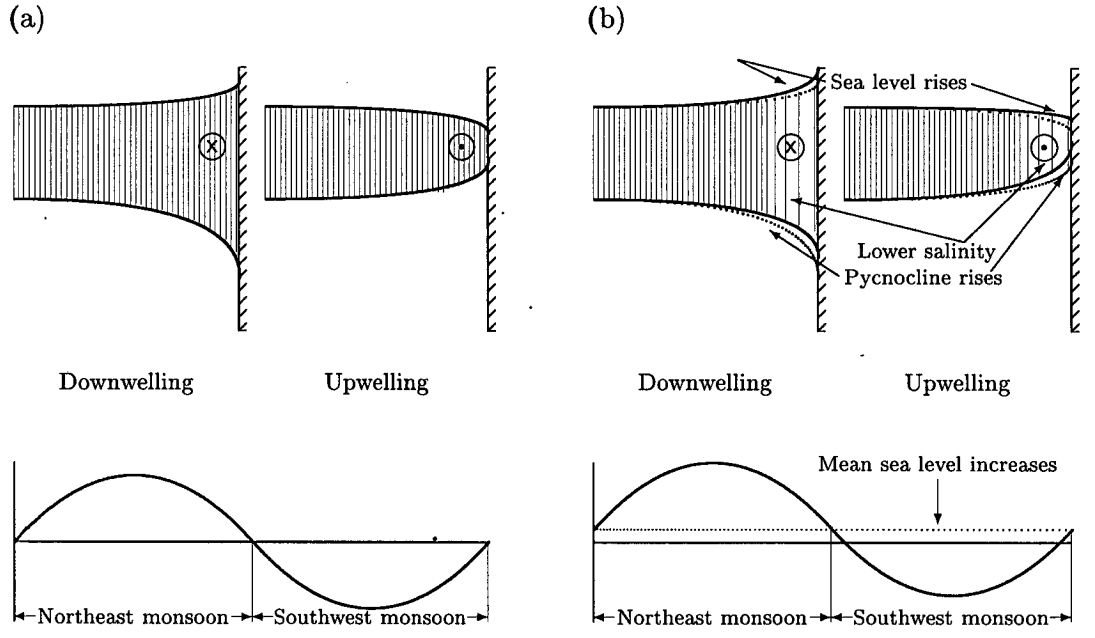

salinity gradient. The density of the active upper layer may vary in space (because of a variation in salinity); it is not allowed to vary in time, implying that the time scale associated with density changes is much longer than the transient motions such as Kelvin waves that are supported by the model. This is because our interest is in the long-term effects of changes in the coastal salinity field: how is the annual Kelvin wave modified by a quasi-steady cross-shore salinity gradient?

6.4.1 The $1\frac{1}{2}$-Layer Model

Consider a coastal Kelvin wave propagating south–north along a meridional eastern boundary. The basic state is one of no motion and constant density in each of the two model layers. This state is perturbed by prescribing a density that is a function of space alone; we solve the equations

for a free Kelvin wave in this perturbed medium. The relevant equations are (A.13), with some constraints. First, since we are considering a coastal Kelvin wave, there is no cross-shore velocity, i.e., $u = 0$. Second, since we are interested only in a Kelvin wave, it is not necessary to solve the equations on a β-plane; hence, the Coriolis parameter f is a constant. Third, since salinity and density vary only in space, $\gamma = \gamma(x,y)$; hence, $q = 0$. Fourth, since we are interested in a free wave, $\tau^x = \tau^y = 0$. Then, dropping the Rayleigh friction coefficient, i.e., setting $r = 0$, and dropping the subscript "0" (which indicates that these are the zeroth-order perturbation equations), we obtain

$$-fv = -g\overline{\Gamma}\frac{\partial h}{\partial x} - \frac{g\overline{H}}{2}\frac{\partial \gamma}{\partial x}, \tag{6.1a}$$

$$\frac{\partial v}{\partial t} = -g\overline{\Gamma}\frac{\partial h}{\partial y} - \frac{g\overline{H}}{2}\frac{\partial \gamma}{\partial y}, \tag{6.1b}$$

$$\frac{\partial h}{\partial t} = -\overline{H}\frac{\partial v}{\partial y}, \tag{6.1c}$$

$$\eta = \overline{\Gamma}h + \overline{H}\gamma. \tag{6.1d}$$

$\overline{H}$ and $\overline{\Gamma}$ are the upper layer thickness and the reduced-gravity parameter in the basic state of no motion, about which the system is perturbed; v, h, η, and γ are the perturbation meridional (alongshore) velocity, upper layer thickness, sea level, and reduced-gravity parameter; the layer thickness and reduced-gravity parameter are $H = \overline{H} + h$ and $\Gamma = \overline{\Gamma} + \gamma$.

We define an "equivalent layer thickness" (ELT)

$$H' = \overline{H} + h', \tag{6.2a}$$

where

$$h' = h + \left(\frac{\gamma}{2\overline{\Gamma}}\right) \tag{6.2b}$$

is the "equivalent perturbation layer thickness" (EPLT). Equations (6.1) and (6.2) yield the free wave equation

$$\frac{\partial h'}{\partial t^2} = c^2\frac{\partial h'}{\partial y^2}, \tag{6.3}$$

where $c = \left(g\overline{\Gamma}\overline{H}\right)^{\frac{1}{2}}$ is the speed of the first-baroclinic-mode Kelvin wave. The solution to (6.3) is

$$h' = \tilde{h}'e^{x/a + \iota(ly - \sigma t)}, \tag{6.4}$$

where $\tilde{h}'$ is the "equivalent" amplitude of the Kelvin wave at the coast and $a = \frac{c}{f}$ is the internal Rossby radius of deformation. Equations (6.1), (6.2), and (6.4) yield the required zeroth-order solution

$$h = \tilde{h}' e^{x/a + \imath(ly - \sigma t)} - \left(\frac{\gamma}{2\overline{\Gamma}}\right), \tag{6.5a}$$

$$v = \left(\frac{g\overline{\Gamma}}{\overline{H}}\right)^{\frac{1}{2}} \tilde{h}' e^{x/a + \imath(ly - \sigma t)}, \tag{6.5b}$$

$$\eta = \overline{\Gamma}\tilde{h}' e^{x/a + \imath(ly - \sigma t)} + \left(\frac{\gamma}{2}\right)\overline{H}. \tag{6.5c}$$

In the absence of spatial variation in density ($\Gamma = \overline{\Gamma}; \gamma = 0$), we obtain the classical Kelvin wave solution. When density varies in space ($\gamma \neq 0$), the Kelvin wave amplitude is modified (it becomes the "equivalent" amplitude), but there is another change that is significant for sea level at the coast. When salinity, and hence density, decreases (increases) from the open sea towards the coast, i.e., when $\frac{\partial \gamma}{\partial x} > 0$ ($\frac{\partial \gamma}{\partial x} < 0$), sea level at the coast increases (decreases). This change in sea level depends only on γ and, hence, is independent of time. Since the low-salinity water is spread along the coast by currents that decay exponentially away from the coast, i.e., they are coastally-trapped, the perturbation in salinity, and hence γ, decays exponentially away from the coast ($\gamma \propto e^{kx}$, $k > 0$). Therefore, the time-independent change in sea level predicted by the model also varies exponentially cross-shore.

The Kelvin wave is superimposed on the time-independent increase in sea level. In the linear system described by equations (6.1), we can ignore the Kelvin wave to look at the quasi-steady state. It consists of an increase in sea level and an upsloping of the pycnocline towards the coast (Figure 6.22b), i.e., when there is no Kelvin wave and density decreases coastward, sea level rises at the coast, the pycnocline upslopes, and there is no current in the layer. This result, which is intriguing because a sloping surface and pycnocline are normally associated with a geostrophic alongshore current, can be understood by extending the model to include another active layer.

6.4.2 The $2\frac{1}{2}$-Layer Model

Consider a $2\frac{1}{2}$-layer reduced-gravity model (Section A.2), but with no difference in density between the two active layers in the basic state, i.e., $\overline{\Gamma}_1 = \overline{\Gamma}_2 = \overline{\Gamma}$; the perturbation density in the two layers, however, is different, i.e., $\Gamma_1 \neq \Gamma_2$. The model now supports velocity shear in the vertical, permitting the existence of a "shear mode". As with the $1\frac{1}{2}$-layer model, the perturbation density varies in the horizontal in the active layers; the interface between the lower active layer and the deep ocean is the model pycnocline. A precise definition of the density field is required because

this model differs from the usual $2\frac{1}{2}$-layer reduced-gravity model, in which $\overline{\Gamma}_1 \neq \overline{\Gamma}_2$, implying the existence of two baroclinic modes. Our interest is restricted to understanding why the $1\frac{1}{2}$-layer model does not yield a quasi-steady velocity along with the quasi-steady rise in sea level, and, for this, the introduction of shear in the vertical is sufficient; the assumption that there is no difference in unperturbed density between the two shear layers ($\overline{\Gamma}_1 = \overline{\Gamma}_2$) simplifies the algebra.

We define the reduced-gravity parameters as follows. Let ρ_1, ρ_2, and ρ_3 be the densities of the three model layers ($\rho_1 < \rho_2 < \rho_3$). Then, by definition,

$$\Gamma_1 = \frac{\rho_3 - \rho_1}{\overline{\rho}} \; ; \; \Gamma_2 = \frac{\rho_3 - \rho_2}{\overline{\rho}},$$

where $\overline{\rho}$ is an average density that is representative of the ocean. In the basic state, $\overline{\Gamma}_1 = \overline{\Gamma}_2 = \overline{\Gamma}$. Hence, we have $\Gamma_1 = \overline{\Gamma} + \gamma_1$; $\Gamma_2 = \overline{\Gamma} + \gamma_2$. Let

$$\overline{\Gamma} = \frac{\rho_3 - \overline{\rho}_{1,2}}{\overline{\rho}}, \tag{6.6a}$$

where

$$\overline{\rho}_{1,2} = \frac{\overline{H}_1 \overline{\rho}_1 + \overline{H}_2 \overline{\rho}_2}{\overline{H}}, \tag{6.6b}$$

and

$$\overline{\rho}_1 = \frac{1}{A} \iint_{\mathbf{A}} \rho_1 dx\, dy, \tag{6.6c}$$

$$\overline{\rho}_2 = \frac{1}{A} \iint_{\mathbf{A}} \rho_2 dx\, dy. \tag{6.6d}$$

$\overline{H}_1$ and $\overline{H}_2$ are the layer thicknesses in the basic state and A is the area of the model domain. $\overline{H}_1$, $\overline{H}_2$, and $\overline{\Gamma}$ define the basic state about which the system is perturbed. Since $\rho_2 > \rho_1$, we have $\overline{\rho}_2 > \overline{\rho}_1$. Then,

$$\gamma_1 = \frac{\overline{\rho}_{1,2} - \rho_1}{\overline{\rho}} = \frac{\overline{\rho}_1 - \rho_1}{\overline{\rho}} + \left(\frac{\overline{H}_2}{\overline{H}}\right)\left(\frac{\overline{\rho}_2 - \overline{\rho}_1}{\overline{\rho}}\right), \tag{6.7a}$$

$$\gamma_2 = \frac{\overline{\rho}_{1,2} - \rho_2}{\overline{\rho}} = \frac{\overline{\rho}_2 - \rho_2}{\overline{\rho}} - \left(\frac{\overline{H}_1}{\overline{H}}\right)\left(\frac{\overline{\rho}_2 - \overline{\rho}_1}{\overline{\rho}}\right). \tag{6.7b}$$

This yields $\gamma_1 - \gamma_2 > 0$, as expected. This definition of the density field and reduced-gravity parameters ensures that $\overline{H}_1$ is a meaningful quantity: it is the depth up to which salinity at the coast

is affected by the runoff from rivers. A consequence of the definition is that $\gamma_2 \neq 0$, but it may be constant.

The zeroth-order, linearized perturbation equations for this $2\frac{1}{2}$-layer model, equivalent to equations (6.1) for the $1\frac{1}{2}$-layer model, follow from equations (A.20) and (A.21) on making the same assumptions as for $1\frac{1}{2}$-layer model.

$$-fv_1 = -g\overline{\Gamma}\frac{\partial}{\partial x}(h_1 + h_2) - \frac{g\overline{H}_1}{2}\frac{\partial \gamma_1}{\partial x} - g\overline{H}_2\frac{\partial \gamma_2}{\partial x}, \tag{6.8a}$$

$$\frac{\partial v_1}{\partial t} = -g\overline{\Gamma}\frac{\partial}{\partial y}(h_1 + h_2) - \frac{g\overline{H}_1}{2}\frac{\partial \gamma_1}{\partial y} - g\overline{H}_2\frac{\partial \gamma_2}{\partial y}, \tag{6.8b}$$

$$\frac{\partial h_1}{\partial t} = -\overline{H}_1\frac{\partial v_1}{\partial y} \tag{6.8c}$$

are the equations for the first layer, and

$$-fv_2 = -g\overline{\Gamma}\frac{\partial}{\partial x}(h_1 + h_2) - \frac{g\overline{H}_2}{2}\frac{\partial \gamma_2}{\partial x}, \tag{6.9a}$$

$$\frac{\partial v_2}{\partial t} = -g\overline{\Gamma}\frac{\partial}{\partial y}(h_1 + h_2) - \frac{g\overline{H}_2}{2}\frac{\partial \gamma_2}{\partial y}, \tag{6.9b}$$

$$\frac{\partial h_2}{\partial t} = -\overline{H}_2\frac{\partial v_2}{\partial y} \tag{6.9c}$$

are the equations for the second layer. The perturbation sea level is given by

$$\eta = \overline{\Gamma}(h_1 + h_2) + \overline{H}_1\gamma_1 + \overline{H}_2\gamma_2. \tag{6.10}$$

Let

$$h = h_1 + h_2, \tag{6.11a}$$

$$\overline{H} = \overline{H}_1 + \overline{H}_2, \tag{6.11b}$$

$$v = \frac{\overline{H}_1 v_1 + \overline{H}_2 v_2}{\overline{H}}, \tag{6.11c}$$

where $\overline{H}$ is the "cumulative layer thickness" in the basic state, h is the "cumulative perturbation layer thickness", and v is the mean velocity. Then, equations (6.8), (6.9), and (6.11) yield the free wave equation

$$\frac{\partial h'}{\partial t^2} = c^2\frac{\partial h'}{\partial y^2}, \tag{6.12}$$

where

$$h' = h + \left(\frac{\overline{H}_1^2 \gamma_1 + 2\overline{H}_1 \overline{H}_2 \gamma_2 + \overline{H}_2^2 \gamma_2}{2\overline{\Gamma} \overline{H}} \right) \tag{6.13}$$

is the "equivalent cumulative perturbation layer thickness" (ECLPT) and $c = \left(g\overline{\Gamma H}\right)^{\frac{1}{2}}$. The solution to (6.12) is

$$h' = \tilde{h}' e^{x/a + \imath(ly - \sigma t)}, \tag{6.14}$$

where $a = \frac{c}{f}$. Then equations (6.13) and (6.14) imply

$$h = \tilde{h}' e^{x/a + \imath(ly - \sigma t)} - \left(\frac{\overline{H}_1^2 \gamma_1 + 2\overline{H}_1 \overline{H}_2 \gamma_2 + \overline{H}_2^2 \gamma_2}{2\overline{\Gamma} \overline{H}} \right). \tag{6.15}$$

The perturbation sea level is

$$\eta = \overline{\Gamma} \tilde{h}' e^{x/a + \imath(ly - \sigma t)} + \left(\frac{\overline{H}_1^2 \gamma_1 + 2\overline{H}_1 \overline{H}_2 \gamma_1 + \overline{H}_2^2 \gamma_2}{2\overline{H}} \right). \tag{6.16}$$

Since we are interested only in the quasi-steady part of the solution, we restrict our attention to it. It is the quasi-steady response that causes the interdecadal changes in sea level, the Kelvin wave being superimposed on it. The quasi-steady component of h is

$$h_s = - \left(\frac{\overline{H}_1^2 \gamma_1 + 2\overline{H}_1 \overline{H}_2 \gamma_2 + \overline{H}_2^2 \gamma_2}{2\overline{\Gamma} \overline{H}} \right), \tag{6.17a}$$

and the quasi-steady sea level is

$$\eta_s = \frac{\overline{H}_1^2 \gamma_1 + 2\overline{H}_1 \overline{H}_2 \gamma_1 + \overline{H}_2^2 \gamma_2}{2\overline{H}}. \tag{6.17b}$$

Substituting (6.17a) in (6.8a) and (6.9a), we obtain the quasi-steady solutions for the alongshore velocity in the two layers. These are

$$v_{1,s} = \left(\frac{g\overline{H}_2}{2f\overline{H}} \right) \frac{\partial}{\partial x} \left(\overline{H}_1 \gamma_1 + \overline{H}_2 \gamma_2 \right), \tag{6.17c}$$

$$v_{2,s} = - \left(\frac{g\overline{H}_1}{2f\overline{H}} \right) \frac{\partial}{\partial x} \left(\overline{H}_1 \gamma_1 + \overline{H}_2 \gamma_2 \right). \tag{6.17d}$$

The introduction of the "shear mode" permits the existence of an undercurrent, but there is no mean velocity, i.e., $v_s = 0$, as in the $1\frac{1}{2}$-layer model, and

$$\frac{v_{1,s}}{v_{2,s}} = - \frac{\overline{H}_2}{\overline{H}_1}.$$

From equations (6.17), we obtain

$$\frac{\partial \eta_s}{\partial x} \gtreqless 0 \quad \forall \quad \frac{\partial \gamma_1}{\partial x} \gtreqless -\tan\theta_\eta \frac{\partial \gamma_2}{\partial x}, \tag{6.18a}$$

$$\frac{\partial h_s}{\partial x} \lesseqgtr 0 \quad \forall \quad \frac{\partial \gamma_1}{\partial x} \gtreqless -\tan\theta_h \frac{\partial \gamma_2}{\partial x}, \tag{6.18b}$$

$$v_{1,s} \gtreqless 0 \quad \forall \quad \frac{\partial \gamma_1}{\partial x} \gtreqless -\tan\theta_v \frac{\partial \gamma_2}{\partial x}, \tag{6.18c}$$

$$v_{2,s} \lesseqgtr 0 \quad \forall \quad v_{1,s} \gtreqless 0, \tag{6.18d}$$

where

$$\tan\theta_\eta = \left(\frac{\overline{H}_2}{\overline{H}_1}\right)^2 \left(1 + \frac{2\overline{H}_2}{\overline{H}_1}\right)^{-1}, \tag{6.19a}$$

$$\tan\theta_h = \left(\frac{\overline{H}_2}{\overline{H}_1}\right)^2 \left(1 + \frac{2\overline{H}_2}{\overline{H}_1}\right), \tag{6.19b}$$

$$\tan\theta_v = \frac{\overline{H}_2}{\overline{H}_1}, \tag{6.19c}$$

with

$$\theta_\eta < \theta_v < \theta_h. \tag{6.19d}$$

Equations (6.18) and (6.19) imply that the velocities in the two active layers, $v_{1,s}$ and $v_{2,s}$, and the cross-shore gradients of η_s and h_s depend on the layer thicknesses in the basic state, $\overline{H}_1$ and $\overline{H}_2$, and on the cross-shore gradients of both γ_1 and γ_2. This is shown graphically in Figure 6.23. The solution shows that there exist conditions under which sea level may rise at the coast; this need not, however, be accompanied by a rise of the pycnocline, or by a surface current that flows with the higher sea level on its right, unlike in the simpler solution obtained for the $1\frac{1}{2}$-layer model. For example, between the solid and dashed lines in the second quadrant in Figure 6.23, sea level falls coastward, but the surface current is still poleward (for an eastern boundary like the Indian west coast); between the solid and dotted lines in the fourth quadrant, sea level rises towards the coast, but so does the pycnocline. An extreme case is that of sea level falling at the coast despite salinity decreasing coastward; this can happen if the density of the lower layer increases coastward at a sufficiently rapid rate (the region to the left of the solid line in Figure 6.23). Thus, there exist a number of possible solutions and it is the prevailing conditions, i.e., the thickness of the layer influenced by runoff ($\overline{H}_1$), the thickness of the layer below ($\overline{H}_2$), and the cross-shore gradients of the reduced-gravity parameters in the two layers (γ_1 and γ_2), that determine whether sea level rises at the coast or not.

Figure 6.23 A graphical representation of the quasi-steady solution to the $2\frac{1}{2}$-layer model equations. The possible quasi-steady solutions (the subscript "s" is dropped in this figure for convenience) are shown as a function of γ_{1x} (abscissa) and γ_{2x} (ordinate); the subscript x denotes a partial derivative w.r.t x, the cross-shore co-ordinate. The lines $h_x = 0$ (dotted), $\eta_x = 0$ (solid), and $v_1 = v_2 = 0$ (dashed) mark the boundaries across which the cross-shore gradients of h and η, and the velocities v_1 and v_2 change sign. To the right (left) of the respective lines, η_x and v_1 are positive (negative), and h_x and v_2 are negative (positive). Unless there is a sufficiently large negative gradient of γ_2, a coastward decrease in the salinity of the upper active layer at an eastern boundary ($\gamma_{1x} > 0$) implies a rise in coastal sea level, a rise of the pycnocline towards the coast, and a surface current (undercurrent) that flows with the coast on its right (left).

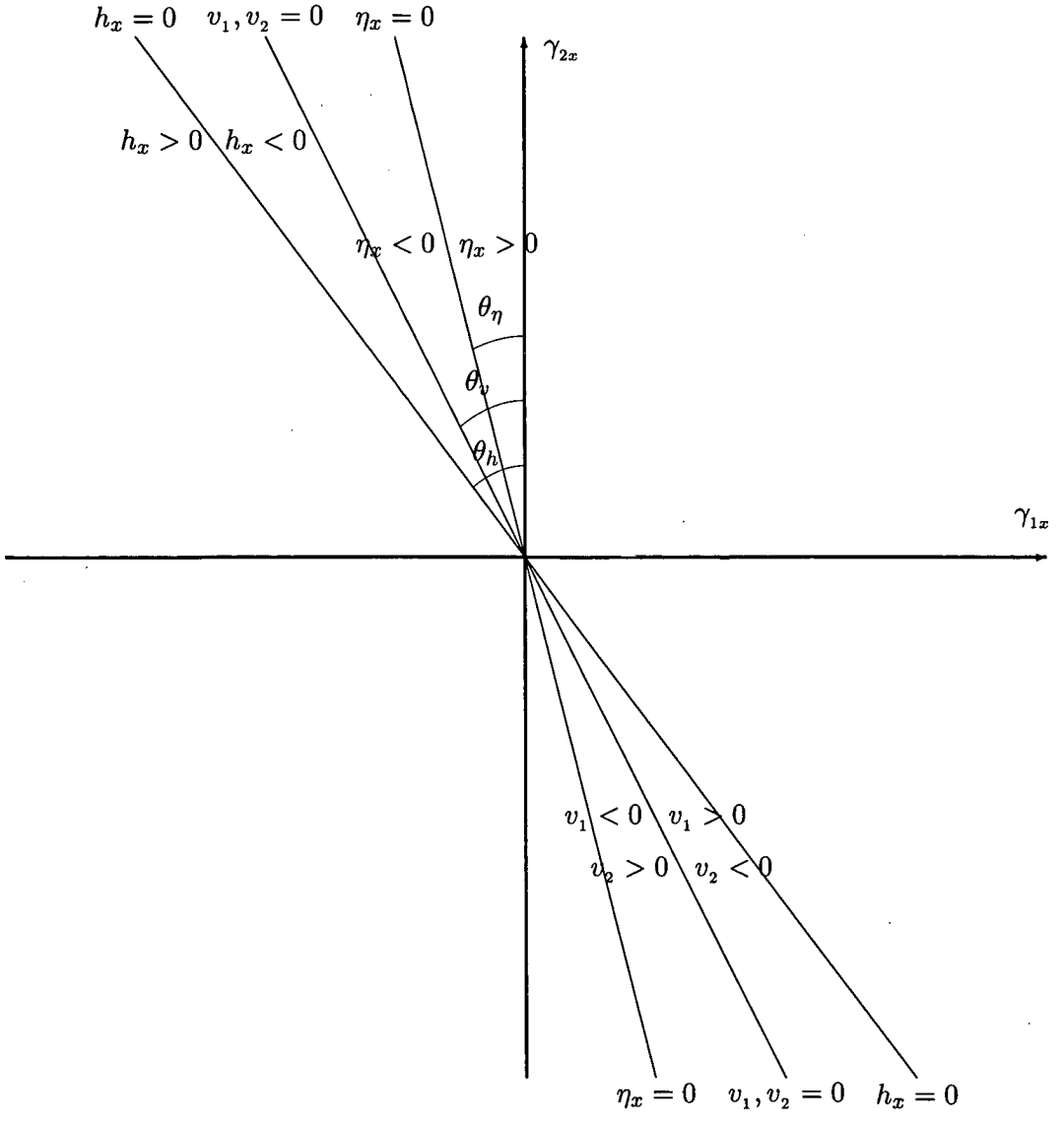

6.4.3 Application to the West Coast of India

Despite the relative complexity of the $2\frac{1}{2}$-layer solution, it is similar to that for the $1\frac{1}{2}$-layer model when there is a coastward decrease of salinity in both layers (but with $\gamma_1 > \gamma_2$). The two solutions are shown in Figure 6.24.

Figure 6.24 Schematic of a section normal to the coast, showing the effect of a decrease in the salinity of coastal waters on sea level at an eastern ocean boundary in the northern hemisphere. The panel on the left shows the response in a $1\frac{1}{2}$-layer model, and that on the right the response in a $2\frac{1}{2}$-layer model. The cross-shore, time-independent variation in salinity forces a rise in coastal sea level and a time-independent geostrophic circulation with a surface current and an undercurrent. The surface current flows with the lighter water on its right and the undercurrent in the opposite direction. The pycnocline (the interface between the undercurrent and the motionless deeper ocean) slopes up towards the coast. The transports of the two currents cancel to yield a zero net transport. The $1\frac{1}{2}$-layer model yields only the mean of the surface current and the undercurrent, and hence predicts a zero current associated with the rise in sea level and the pycnocline at the coast. In the figure, the current shown by "x" ("·") within a circle is into (out of) the plane of the paper, and wider spacing of the hatched lines indicates lower salinity.

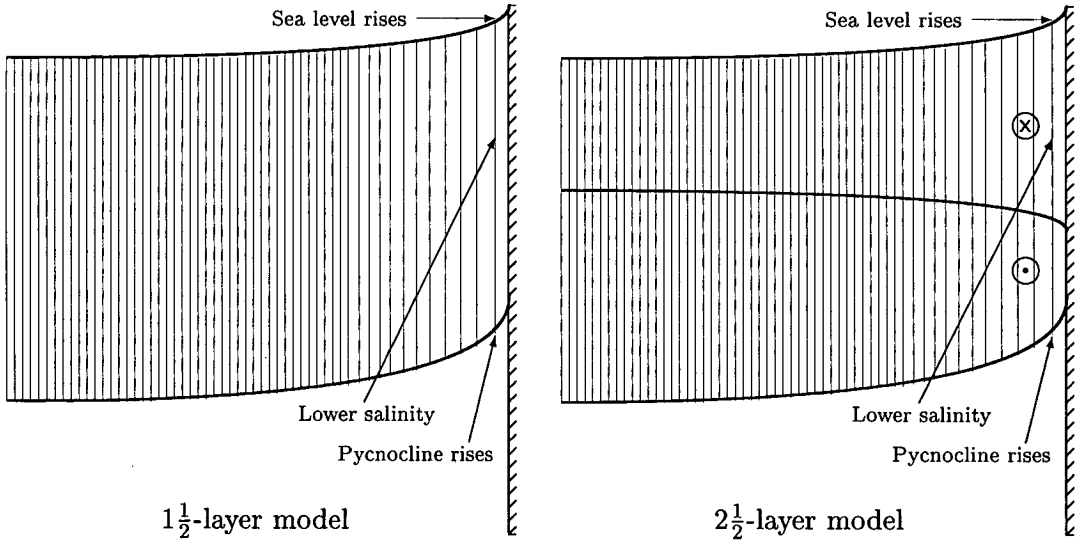

At Mumbai, sea level rose by about 11 cm during 1900–1950 and fell by about 4.5 cm during 1950–1980. By how much does the salinity at the coast have to change to force these interdecadal changes in sea level? Our model domain has an eastern boundary and extends to infinity towards west. The changes in salinity due to runoff from rivers affects only a layer of thickness $\overline{H}_1$ and is restricted to the vicinity of the coast, the slow mixing in the ocean acting over time to reduce the cross-shore density gradient. This cross-shore gradient is quasi-steady because mixing in the ocean is slow; the more rapid changes forced by seasonal Kelvin waves are superimposed on

it. In the lower active layer of thickness $\overline{H}_2$, density, and hence γ_2, is assumed to be constant. Differentiating η_s in (6.17b) then eliminates the contribution from density variations in this layer. Integrating $\frac{\partial \eta_s}{\partial x}$ over $(-\infty, 0]$ for an exponential variation of density in x ($\gamma_1 \propto e^{kx}$, where k^{-1} is a length scale), we obtain

$$\eta_s|_{x=0} = \left(\frac{\overline{H}_1^2 + 2\overline{H}_1\overline{H}_2}{2\overline{H}} \right) \gamma_1|_{x=0}. \tag{6.20}$$

For $\eta_s = 5$ cm and $\overline{H}_1 = \overline{H}_2 = 50$ m, we obtain $\gamma_1 = 0.0013$. If we assume that the change in density is entirely due to a change in salinity, ignoring other processes (for example, temperature changes due to "global warming", melting of ice caps, etc.), this translates to a decrease of 1.07 PSU in the salinity averaged over the top 50 m. A similar approach, using (6.17a) instead of (6.17b), gives the displacement of the pycnocline at the coast.

$$h_s|_{x=0} = -\left(\frac{\overline{H}_1^2}{2\overline{\Gamma}\overline{H}} \right) \gamma_1|_{x=0}. \tag{6.21}$$

For $\overline{\Gamma} = 0.0035$, the value used in the constant-density reduced-gravity model in Chapter 3, we obtain $h_s = -4.8$ m at the coast. To compute the currents associated with the cross-shore density gradient, we need a measure of the length scale k^{-1} associated with the mixing of salt in the Arabian Sea. Horizontal eddy diffusivities in the Arabian Sea range from 1.3×10^6 (zonal) to 3.1×10^6 cm^2 s^{-1} (meridional) [Somayajulu et al., 1996]. Assuming an average value of 2×10^6 cm^2 s^{-1}, we obtain a length scale of 400 km for a time scale of 25 years, the period over which sea level at Mumbai drops by 4.5 cm. Then (6.17c) implies $v_{1,s} = -v_{2,s} = 0.8$ cm s^{-1}; thus, the background thermohaline circulation forced by the cross-shore density gradient is much weaker than the seasonal WICC superimposed on it.

To summarize, a suitable model to explain the link between sea level and all-India rainfall is the following. The ocean responds as a two-layer system to a cross-shore variation in density. When density decreases coastward in a surface layer, sea level rises at the coast, and this is accompanied by a geostrophic surface current that flows with the lighter water on its right; below the surface current is an undercurrent. The sum of the transport of the surface current and the undercurrent vanishes. Geostrophy requires that the interface between the undercurrent and the motionless deeper ocean (the model pycnocline) slope up towards the coast (Figure 6.24). The slow mixing in the ocean makes this response quasi-steady.

Thus, a coastward decrease (increase) in salinity implies an increase (decrease) in both the annual maximum and the annual minimum of sea level, and hence, an increase (decrease) in sea level throughout the year, as seen at Mumbai. This change in sea level occurs on interannual and interdecadal time scales, much slower than the changes associated with the annual and other

Kelvin waves that are superimposed on it. Though it is the currents associated with these waves that spread the low-salinity water along the Indian coast, the long-term effect of spreading this water is to set up a weak, quasi-steady circulation.

6.4.4 Effect of Interannual Variability of Winds

The above hypothesis links the sub-annual changes in sea level along the coast of India to the variability of the monsoon, with the coastal salinity field playing an intermediate role. In building this hypothesis, we have ignored the large-scale winds over the basin, except for the redistribution of salt due to the currents forced by them. This needs some justification because an increase in the intensity of the monsoon is accompanied by an increase in the strength of the winds; rainfall is not the only measure of monsoon intensity.

An increase in the strength of the winds will force stronger upwelling and stronger downwelling, implying an increase in the maximum and a decrease in the minimum, the range of the seasonal cycle increasing as a consequence. Along the coast of India, the annual mean sea level is significantly correlated with the annual extrema and with the seasonal averages of sea level, and the hypothesis links these to changes in the salinity of coastal waters (Figure 6.22). The increase in the maximum usually is higher than that in the minimum, but a decrease in the maximum is not (Figures 6.8 and 6.9); a decrease in the maximum is, at times, accompanied by an increase in the minimum. This may be because of winds. Also, as shown in Chapter 5, a uniform increase in winds over the basin raises annual mean sea level along the east coast, but lowers it along the west coast. Since an increase in the intensity of the monsoon is accompanied by an increase in the strength of the winds, these two causes, rainfall and winds, force similar changes in sea level along the east coast, but opposing changes along the west coast. Thus, the interannual variability of the large-scale winds associated with the monsoon is bound to affect the correlation between all-India rainfall and sea level.

Interannual changes in the large-scale winds directly affect coastal sea level by forcing interannual Kelvin and Rossby waves. Clarke and Liu [1994] showed that friction due to the presence of the continental shelf [Clarke and van Gorder, 1994] allows Kelvin waves at these periods also to propagate along the coast; not all their energy is lost to westward propagating Rossby waves. Such interannual changes in the winds are bound to influence sea level, especially along the east coast of India, which is affected by Rossby waves forced by Ekman pumping in the open bay and by radiation from Kelvin waves forced by winds in the equatorial Indian Ocean. Since Chennai is to the south of Vishakhapatnam, sea level there will be affected more by these Rossby waves.

That the large-scale winds do have an effect on the sub-annual variability of sea level is apparent from the low correlation between all-India rainfall and sea level at Vishakhapatnam and Chennai; the correlation improves when the data for 1961 is dropped (Table 6.8). The annual sea

level for 1961 is an outlier and distorts the correlations. In 1961, rainfall was among the highest, but sea level at Vishakhapatnam and Chennai were among the lowest observed (Section 6.3.3). The deviation of monthly sea level from the long-term mean is plotted for 1956–1965 in Figure 6.25. The monthly sea levels follow the usual seasonal cycle during the decade, but there is a striking anomaly in 1961. The range of the seasonal cycle is anomalously low along the east coast; at Kochi, data for some months are missing during 1961, and at Mumbai, the effect is not so striking. Despite the high rainfall, the annual maximum decreased at Vishakhapatnam, Chennai, and Mumbai, as did the annual mean; the annual minimum also decreased at Chennai and Mumbai, but hardly changed at Vishakhapatnam (Figures 6.8 and 6.9). This implies that the high rainfall over India did not lower the salinity along the coast. This decrease in annual sea level during 1961–1962 is seen better in Figure 6.26, which shows the deviation of the monthly sea level from the climatology.

One cause is the relatively low rainfall in the catchment areas of the Ganga and the Brahmaputra during 1961 (Figure 6.14); the rainfall on the west coast, however, was in phase with all-India rainfall. Another important difference in 1961 was the anomaly in winds over the equatorial Indian Ocean [Reverdin et al., 1986]. These anomalous winds were driven by a reversal in the gradient of sea surface temperature (SST) along the equator. The SST normally is higher in the east and cooler in the west, where the Somali Current forces strong upwelling. In 1961, however, SST in the eastern equatorial Indian Ocean dropped below that in the west, forcing easterly anomalies in the winds. Such wind anomalies often occur during an El Niño [Reverdin et al., 1986], which also has an impact on monsoon rainfall [Mishra and Gadgil, 1996, and references therein], but 1961 was not an El-Niño year.

An anomaly in the winds over the equatorial Indian Ocean, which are an important forcing mechanism for the EICC [Shankar et al., 1996; McCreary et al., 1996], is likely to force anomalies in the seasonal cycle of the coastal currents off India. Anomalous easterlies would weaken the eastward equatorial jets in May and November [Wyrtki, 1973; O'Brien and Hurlburt, 1974; Jensen, 1993]. The weakening of the May jet would weaken the equatorward EICC that forms in the northern bay during the southwest monsoon, enabling the local Ekman flow to push the runoff offshore into the open bay. The weakening of the November jet would weaken the equatorward EICC during October–January, implying weaker downwelling along the coast. This, coupled with the lower runoff due to the decrease in rainfall in the catchment areas of the Ganga and the Brahmaputra (Figure 6.14) and the offshore movement of the runoff, implies a decrease in the annual mean and extrema according to the hypothesis. More of the runoff is likely to reach Vishakhapatnam because it lies north of Chennai; this is a possible reason for the lack of a decrease in the annual minimum there.

On interdecadal time scales, however, the effect of winds is negligible in comparison with that

Figure 6.25 Deviation of corrected monthly sea level (cm) during 1956–1965 from the long-term mean sea level. On the abscissa, the long and small ticks mark the beginning and end of the years and months, respectively. The monthly sea levels during July 1961 to June 1962 show a different behaviour in comparison to the sea level during the rest of the decade; the anomalous behaviour is maximum along the east coast, but is also seen at Kochi. At Mumbai, however, the anomalies are not striking. 1961 was an year of anomalous easterly winds over the equatorial Indian Ocean. The wind anomalies were similar to those seen during an El Niño, but 1961 was not an El-Niño year. Another possible cause of the anomalies is the lower rainfall in 1961 in the catchment areas of the Ganga and the Brahmaputra; though all-India and West-Coast rainfall were higher than normal, Ganga-Brahmaputra rainfall was lower than normal.

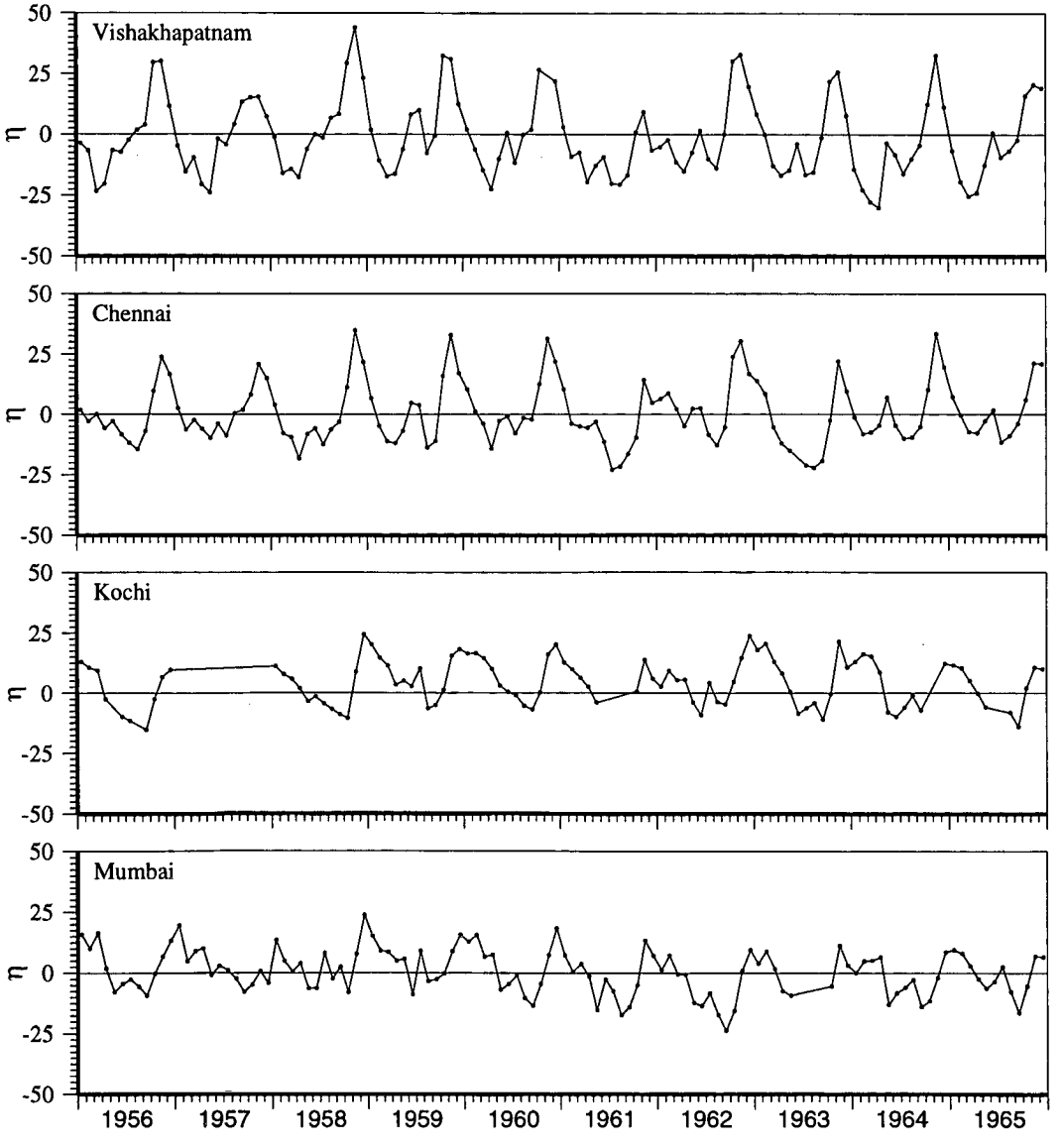

Figure 6.26 Deviation of corrected monthly sea level (cm) during 1956–1965 from the climatology of corrected monthly sea level. On the abscissa, the long and small ticks mark the beginning and end of the years and months, respectively. The monthly sea levels during July 1961 to June 1962 show a different behaviour in comparison to the sea level during the rest of the decade; the anomalous behaviour is maximum along the east coast, but is also seen at Kochi. At Mumbai, however, the anomalies are not striking. 1961 was an year of anomalous easterly winds over the equatorial Indian Ocean. The wind anomalies were similar to those seen during an El Niño, but 1961 was not an El-Niño year. Another possible cause of the anomalies is the lower rainfall in 1961 in the catchment areas of the Ganga and the Brahmaputra; though all-India and West-Coast rainfall were higher than normal, Ganga-Brahmaputra rainfall was lower than normal.

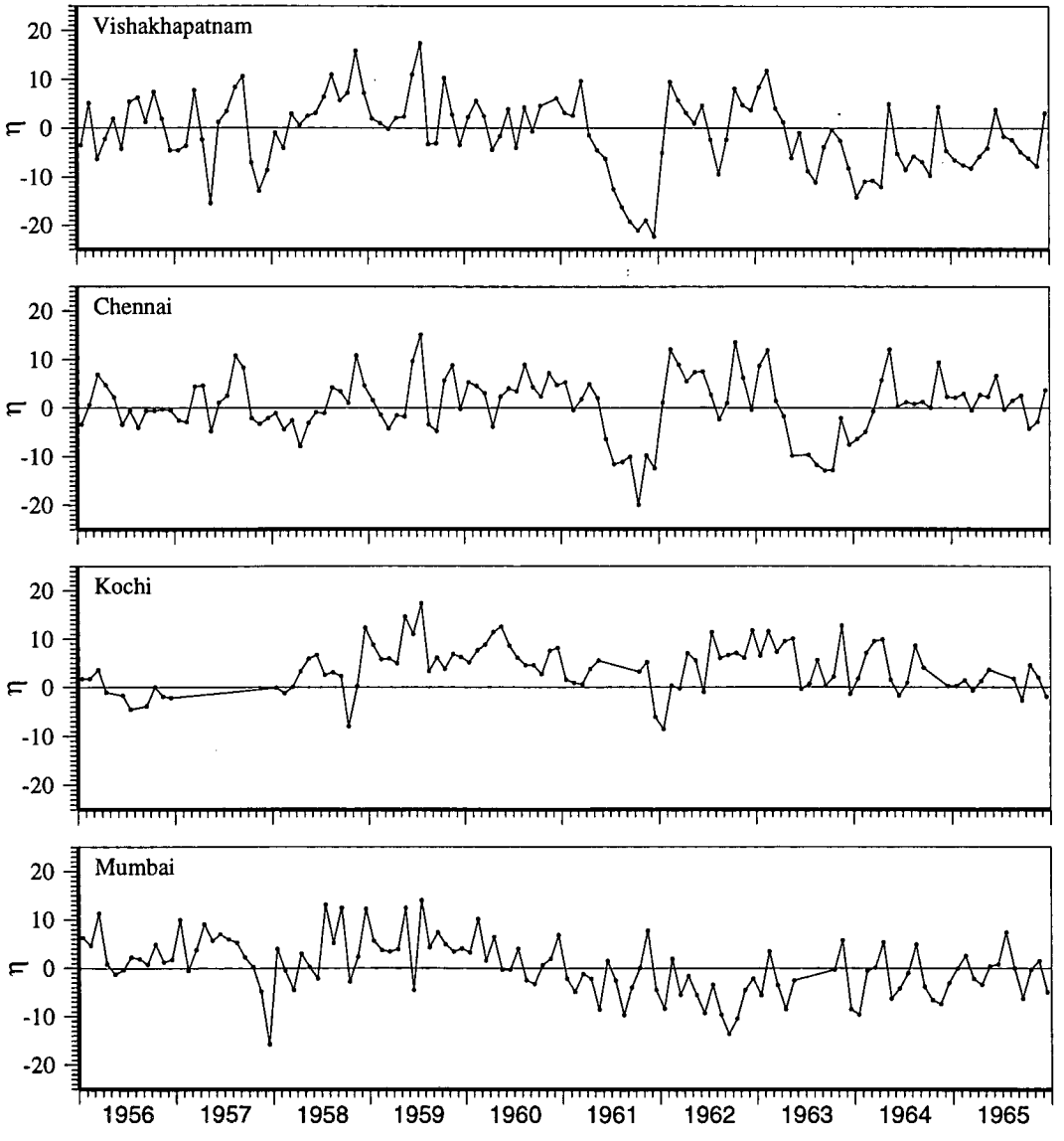

of salinity. The time scale associated with wind-forced changes, determined by the travel time of long baroclinic Kelvin and Rossby waves, is of the order of a few months for the Arabian Sea and the Bay of Bengal [McCreary et al., 1993; Clarke and Liu, 1994]. The effect of a change in salinity survives longer because of the longer time scale associated with the mixing of salt in the ocean; measured values of horizontal eddy diffusivities [Somayajulu et al., 1996] indicate a mixing time of about two years for a length scale of 100 km. Therefore, though monsoon rainfall itself is affected by the monsoon winds, the very low-frequency changes in sea level at Mumbai and elsewhere along the coast of India are mostly because of changes in the salinity of coastal waters caused by variability in monsoon rainfall. Apart from salinity and winds, sea level is affected by ocean temperature and atmospheric pressure; these, however, vary too little in the tropics on these time scales to cause changes of the observed magnitude.

6.5 Implications of the Hypothesis

We have shown that the interdecadal variability of sea level along the coast of the Indian subcontinent is linked to the monsoon rainfall over the subcontinent, the coastal salinity field playing an intermediate role. The most striking feature of this mechanism is the connection between two vastly different time scales, the seasonal and the interdecadal. The bulk of the rainfall over the Indian subcontinent occurs during June–September, and the runoff is carried to the seas around India within a season. The equatorward EICC and the poleward WICC, which transport this low-salinity water along the Indian coast, are also seasonally varying currents. These seasonal phenomena act in concert with the low-frequency variability of monsoon rainfall and the slow mixing of salt in the oceans to force sea-level changes on interdecadal time scales.

A change in the salinity of coastal waters caused by variations in monsoon rainfall, and hence in river runoff, creates a cross-shore density gradient, to which the response is a two-layer, geostrophic circulation with a surface current and an undercurrent. Though this background circulation, on which the seasonal circulation is superimposed, is weak, the associated movements of the sea surface and the isopycnals are observable. When salinity decreases (increases) at an eastern ocean boundary like the Indian west coast, the current at the surface flows poleward (equatorward), there is an opposing undercurrent, sea level rises (falls) at the coast, and the pycnocline, or the interface between the undercurrent and the deeper ocean, slopes up (down) towards the coast. The interdecadal changes in sea level off the Indian coast are thus linked to the dynamics of local coastal currents and to the variability in the rainfall over the Indian subcontinent.

In developing this hypothesis, we were forced to correlate monsoon rainfall directly with sea level, bypassing salinity. This was unavoidable because there is a dearth of data on salinity in the north Indian Ocean. Moreover, the available data are sufficiently scattered in space to preclude

Figure 6.27 Surface salinity along a section normal to the west coast of India. Salinity S (PSU) is plotted as a function of distance D (km) from the coast. The section is off Marmagao, Goa (vertical cross-sections for three cruises along this section are presented in Figure 4.15).

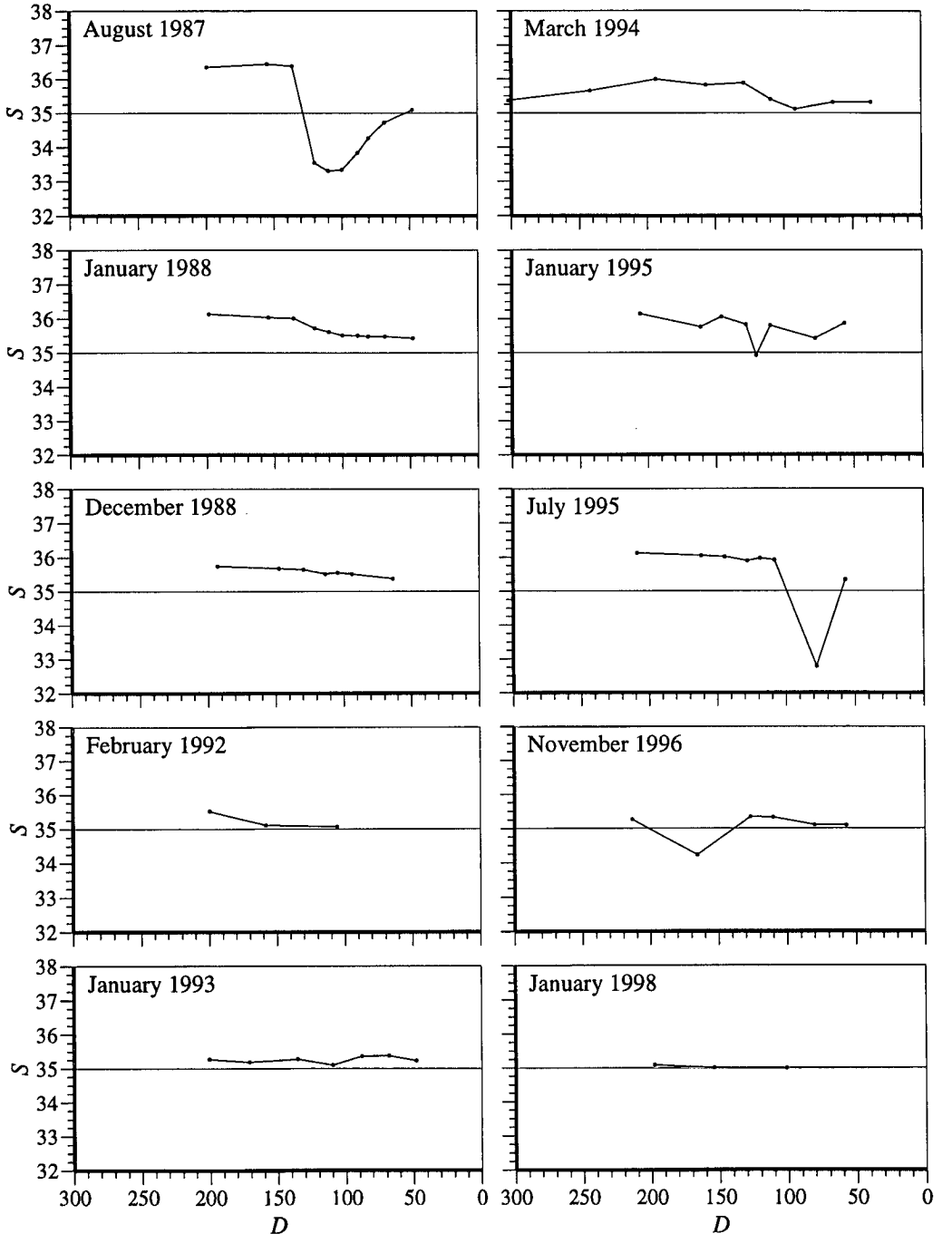

the generation of a time series of salinity along the coast of India. Since the model requires that salinity along the west coast of India change by 1 PSU over a decade, and this is not a small change, a natural question is whether such changes in salinity occur along the coast of India. The only empirical evidence we have is from a hydrographic section normal to the coast off Marmagao in Goa. Hydrographic data for this section based on three cruises were presented in Figure 4.15; these data are for different seasons and two are from the late 1980s, which mark the end of an epoch of low rainfall and high frequency of droughts [Mishra and Gadgil, 1996]. Some cruises since then have added data, and surface salinity from 10 cruises along this section is plotted in Figure 6.27. Four of these sections are during January. There is a difference of about 1 PSU in the salinity, with a high in 1988 and 1995, and a low in 1993 and 1998. This lends credibility to the hypothesis.

This hypothesis, while linking interdecadal changes in sea level to those in the climate of the region, differs from those usually invoked in constructing scenarios of long-term changes in sea level. These hypotheses also link interdecadal sea-level variability to climate change [Gornitz et al., 1982; Wyrtki, 1990], but invoke the rise in temperature in the upper ocean and the melting of polar ice caps. It has been speculated, however, that global climate change is a complex process and will manifest differently in different regions; in the tropics, since ocean temperature is already high, it is expected to change evaporation, and hence, change atmospheric moisture, cloud cover, and rainfall [Wyrtki, 1990]. The rainfall and sea-level observations presented above highlight the complex relationship among the variables that define climate change. They do not, however, allow separation of natural, very low-frequency variability of monsoon rainfall and sea level from that caused by global warming due to anthropogenic effects.

Chapter 7

Summary and Discussion

We have described the variability of sea level along the coast of India on seasonal through inter-decadal time scales, mapping one end of the spectrum of sea-level variability, and have proposed hypotheses to explain the observations. There is significant variability at all these frequencies and the variability is coherent along the coast, which implies that its causes are not purely local; the low-frequency variability of sea level along the coast of India is linked to the large-scale processes in the north Indian Ocean.

In Chapter 3, we presented a theoretical framework for describing this large-scale circulation. Developed over the last decade, the framework invokes equatorial Kelvin and Rossby waves and coastal Kelvin waves, which merge the Bay of Bengal, the Arabian Sea, and the equatorial Indian Ocean into a single dynamical entity, the north Indian Ocean, whose dynamics must be modelled as a whole even to simulate the circulation in its parts. The framework was applied to the dynamics of the Lakshadweep high and low, a high and low in sea level that form off southwest India during the northeast and southwest monsoons, respectively, and propagate westward. Numerical and analytic experiments with a dynamical $1\frac{1}{2}$-layer reduced-gravity model showed that the high and low are explicable by linear dynamics on an equatorial β-plane and do not owe their existence to nonlinearity: the high and low are the result of the radiation of westward propagating Rossby waves from Kelvin waves propagating poleward along the west coast of India. The Kelvin waves must have a period greater than about 50 days to radiate Rossby waves and force the high and low; at lower periods, they are trapped at the coast. The principal forcing mechanism of the high and low are the winds along the east coast of India and Sri Lanka. The winds along the west coast amplify the low, but not the high; other processes, including equatorial Rossby and Kelvin waves, amplify the high, but not the low. The winds along the coasts of India determine the circulation in the eastern and northern Arabian Sea, including the meandering structure of the Southwest Monsoon Current (SMC) in the Arabian Sea; elsewhere in the basin, other processes dominate.

Though the dynamical reduced-gravity model is successful in simulating the essential features

of the circulation in the north Indian Ocean, including the currents along the coast of India, it fails to simulate the seasonal cycle of coastal sea level, which was dealt with in Chapter 4. The seasonal cycle, corrected for the effect of atmospheric pressure using the Inverse-Barometer approximation, is coherent along the coast, with a range of 45 cm along the east coast and 30 cm along the west coast. Along the east coast, the maximum sea level occurs in November and the minimum during March–April; along the west coast, the maximum occurs in December and the minimum during the southwest monsoon. The wind-forced model fails to simulate the winter peak along the east coast, and as a result, forces a higher range of the seasonal cycle along the west coast than along the east coast. Simulations in which temperature and salinity vary in the active model layer, these fields being prescribed from a climatology, show that the drop in salinity along the east coast after the southwest monsoon raises steric sea level and is the cause of the maximum in November. This low salinity is the result of runoff from the Ganga and the Brahmaputra into the northern Bay of Bengal during the southwest monsoon. Thus, three mechanisms — atmospheric pressure, winds on the scale of the basin, and salinity — contribute to the seasonal cycle of sea level along the coast of India.

A lower frequency, the annual mean sea level, was the subject of Chapter 5. Levelling observations conducted during the Great Trigonometrical Survey of India (1858–1909) showed that the annual mean sea level is higher along the east coast of India than along the west, the difference between Vishakhapatnam and Mumbai being about 30 cm. Simulations with the $1\frac{1}{2}$-layer reduced-gravity model show that purely wind-forced circulation accounts for half this difference, the other half being due to the gradient in salinity along the coast.

The variability of annual sea level on interannual and interdecadal time scales was dealt with in Chapter 6. Annual mean sea level along the coast is significantly correlated with the annual extrema and seasonal averages. Cross-correlations of annual mean sea level at the stations along the coast are statistically significant, showing that these changes are coherent and are part of a basin-scale response. The annual mean and extrema of sea level are also correlated with annual all-India rainfall, as is the local rainfall at Mumbai with the annual sea level there. These correlations retain their significance when the rainfall and sea-level data are decimated with a 10-year running mean. The interdecadal changes in monsoon rainfall are reflected in sea-level changes at Mumbai, which has the only century-long tide-gauge record in the Indian Ocean; both increase from a low in the first quarter of this century to a high in the 1950s and decrease thereafter.

Our hypothesis is that the seasonal inflow of the monsoon rainfall into the seas around India and the dynamics of the East and West India Coastal Currents (EICC and WICC) provide the link between monsoon rainfall and coastal sea level, the coastal salinity field playing an intermediate role. The seasonal EICC and WICC spread the runoff along the coast, creating a cross-shore gradient in salinity; the time scale associated with this gradient is much longer than an year because

mixing is slow in the ocean, which responds as a two-layer system to this quasi-steady cross-shore gradient in salinity. When salinity, and hence, density, decreases coastward in the upper layer, sea level rises at the coast, and this is accompanied by a weak, geostrophic, surface current that flows with the lighter water on its right; below it is an undercurrent. Geostrophy also requires that the pycnocline slope up towards the coast.

Thus, there are two main conclusions of this thesis.

1. There are three causes of the low-frequency variability of sea level along the coast of India.

   (a) The large-scale wind-forced circulation of the upper ocean.

   (b) The large changes in salinity that are a result of the high rainfall over the Indian subcontinent and the surrounding seas.

   (c) Atmospheric pressure.

   The first two causes are important at periods ranging from a season to decades; atmospheric pressure contributes significantly only to the seasonal cycle.

2. We propose a hypothesis connecting the interdecadal changes in sea level along the coast of India to the variability of the monsoon, the major aspect of the climate of the region. This hypothesis is different from those generally proposed to link sea level to climate change; these hypotheses invoke the increase in volume due to the change in temperature of the upper ocean and the addition of freshwater because of the melting of polar ice caps.

The hypothesis predicts that sea level rises (falls) along the coast of India when rainfall over India increases (decreases), changes in the ocean thereby reflecting those in the atmosphere. A corollary is that an increase (decrease) in rainfall leads to a rise (fall) of the pycnocline and thermocline, implying a decrease (increase) in the thickness of the surface mixed layer. One implication of this corollary is that coastal sea level is not a good proxy for the movement of the thermocline. The second implication is for ocean-atmosphere coupling. A solution similar to that obtained for the quasi-steady rise in sea level at a coast can be obtained for the interior ocean away from coastal boundaries, a westward propagating Rossby wave replacing the coastal Kelvin wave that is superimposed on the quasi-steady response. This implies that a similar decrease in the thickness of the mixed layer will occur even away from the coast if salinity changes there. This mechanism operates on long time scales and diffusion acts incessantly to increase the area of the region affected by the change in salinity. It is inevitable that the resulting low-frequency variability in the thickness of the mixed layer should have an effect on atmospheric processes.

This is especially true in the Bay of Bengal, where the changes in salinity are much larger than they are in the Arabian Sea. Changes in salinity in the interior of the bay need not be caused by diffusion alone; the Northeast Monsoon Current (NMC), which marks the dynamical boundary

between the equatorial Indian Ocean and the bay during the northeast monsoon, transports low-salinity water from the Andaman Sea, forcing changes in salinity in the middle of the basin. Since this process acts on advective time scales, like the seasonal redistribution of salt along the coast of India by the EICC and the WICC, an implication is that the effect of monsoon rainfall over India and Myanmar (Burma) will be felt within a season in the mixed layer over a large part of the bay.

The Bay of Bengal is believed to play a major role in the dynamics of the monsoon. The Tropical Convergence Zone (TCZ), which determines the large-scale monsoon rainfall, is maintained by the genesis of disturbances over the warm waters of the bay [Mishra and Gadgil, 1996]. Hence, any change in the structure of the mixed layer in the bay is likely to be fed back to the atmosphere. The details of this coupling between the ocean and the atmosphere are not clear, but it must be similar to the "barrier layer" in the western Pacific Ocean [Sprintall and Tomczak, 1992; Vialard and Delecluse, 1998a,b]. The major difference between the western Pacific and the Bay of Bengal is in the magnitude of changes in salinity; the changes in the bay are much larger. In the western Pacific, salinity modifies the thermodynamics of the mixed layer; in the bay, it probably controls the process.

The importance of salinity in the north Indian Ocean points to the need for more measurements, without which further theoretical studies will be difficult. The hypothesis linking monsoon rainfall and sea level along the coast of India relies on statistical and mechanistic models. We have assumed that the changes in monsoon rainfall lead to changes in salinity, producing the cross-shore salinity gradient that forces changes in sea level. How is this cross-shore salinity gradient set up? What is the source of the low-salinity water along the west coast of India? How important is the local rainfall over the west coast in relation to the inflow of freshwater from the bay? To answer these questions, we have to go beyond mechanistic models and try to model the salt balance, given the fluxes and the river runoff; this in turn, calls for better data on runoff and salinity in the north Indian Ocean in general, and along the coast of India in particular.

Appendix A

The Reduced-Gravity Model

Since our aim in this thesis is to formulate a hypothesis to explain the observed low-frequency variability of sea level along the Indian coast, we simplify the problem to the extent possible, making use of models that are malleable enough to permit simple numerical experiments and, at times, yield analytic solutions. The simplest realistic model of the low-frequency surface circulation of the ocean is the $1\frac{1}{2}$-layer reduced-gravity model, in which the ocean is a two-layer system, the denser lower layer being much deeper than the relatively shallow upper layer. The assumption that the pressure gradient in the lower layer is vanishingly small makes it motionless (isostatic) and eliminates the fast-moving barotropic mode; only the first baroclinic mode is retained in this model. This is akin to the assumption of a "level of no motion" in computing dynamic heights from hydrographic data. Therefore, the height of the model surface, computed with reference to the motionless layer, is equivalent to the dynamic height, and is the model equivalent of sea level.

Extension of the model to include higher baroclinic modes is simple; an additional active layer results in a $2\frac{1}{2}$-layer model, and so on. The $\frac{1}{2}$ represents the lowest, motionless model layer. The simplicity and ruggedness of these models makes them malleable; as a result, they are among the most used tools in oceanography. Reduced-gravity models have enjoyed tremendous success in oceanography and have played a major role in the study of El Niño. In the rest of this chapter, we derive the equations for the $1\frac{1}{2}$ and $2\frac{1}{2}$-layer models and manipulate them to obtain the simpler equations solved in this thesis.

A.1 The $1\frac{1}{2}$-Layer Model

A schematic vertical cross-section of the $1\frac{1}{2}$-layer model is shown in Figure A.1. The model ocean has a flat bottom and consists of two incompressible layers, the lower layer being denser

Figure A.1 A schematic vertical cross-section of the $1\frac{1}{2}$-layer reduced-gravity model. The model ocean has a flat bottom and consists of two incompressible layers, the denser lower layer being much deeper than the relatively shallow upper layer. In the reduced-gravity models used in this thesis, there is no mixing between the layers. In the figure, the subscripts 1 and 2 refer to the two layers. $\overline{H}_1$ is the mean, or initial thickness of the upper layer, H_i and ρ_i are the instantaneous thickness and density of layer i, and η is the displacement of the surface from the initial, or undisturbed, state. η, the model sea level, is equivalent to the dynamic height computed from hydrographic data. The interface between the layers is the model pycnocline. H_1, ρ_1, and η are functions of space and time; ρ_2 is constant.

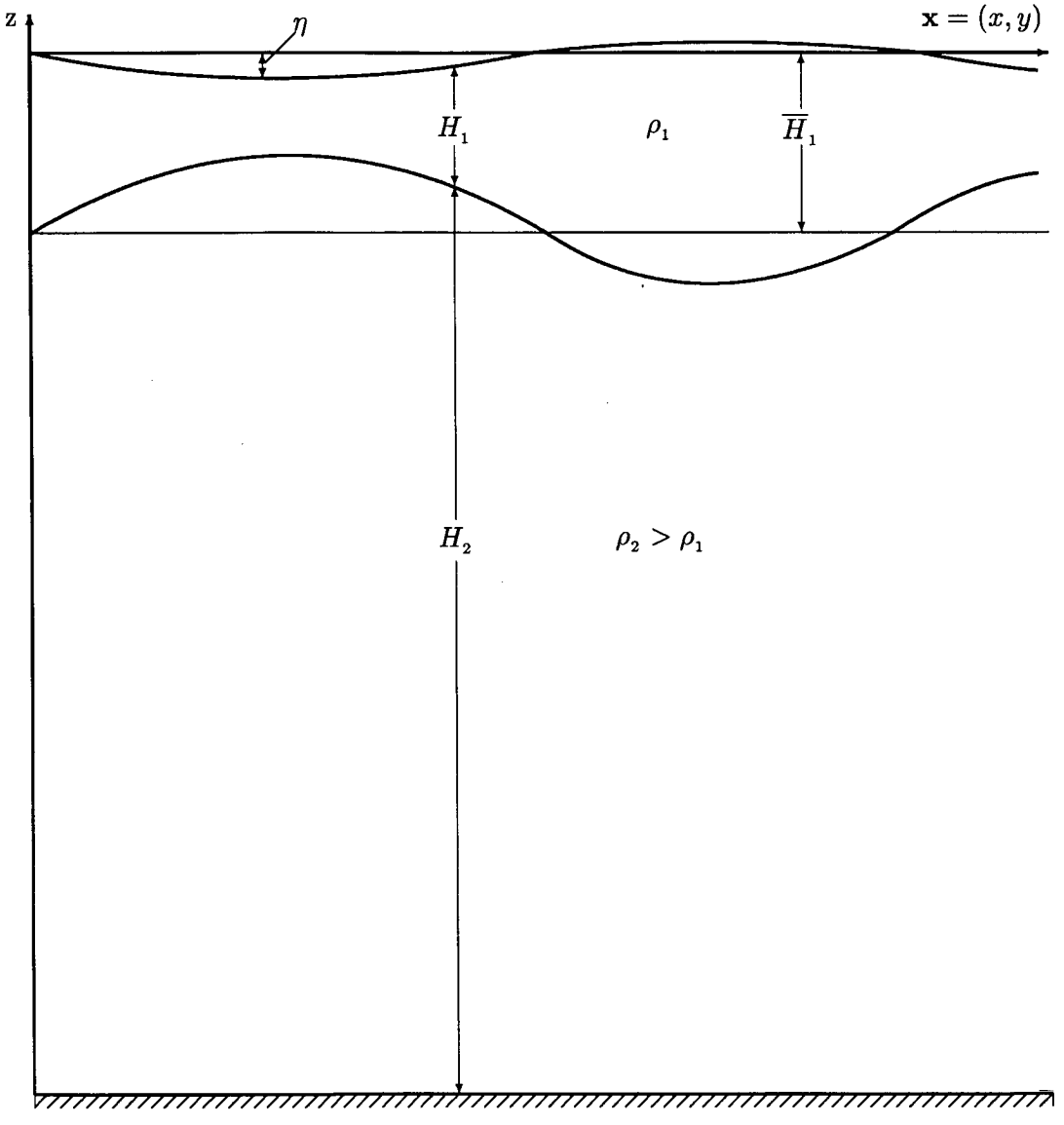

than the upper layer. Each layer is a material layer, i.e., there is no mixing between the layers[1], and is homogeneous in the vertical (in velocity, temperature, and salinity). The interface between the layers represents the model pycnocline, which, in this model, coincides with the thermocline and the halocline. Thermohaline effects are included by permitting horizontal gradients in temperature and salinity in the active layer, but vertical fluxes of heat and salt across the surface, the interface, and the bottom are neglected.

A.1.1 The Nonlinear Model

We begin with the basic conservation equations for zonal, meridional, and vertical momentum, mass, heat, and salt on an equatorial β-plane; for an incompressible fluid, these are given by [Pedlosky, 1979; Gill, 1982]

$$\frac{du}{dt} - fv = -\frac{1}{\rho}\frac{\partial p}{\partial x} + \frac{1}{\rho}\frac{\partial \tau^x}{\partial z} + A'\nabla^2 u, \tag{A.1a}$$

$$\frac{dv}{dt} + fu = -\frac{1}{\rho}\frac{\partial p}{\partial y} + \frac{1}{\rho}\frac{\partial \tau^y}{\partial z} + A'\nabla^2 v, \tag{A.1b}$$

$$\frac{\partial p}{\partial z} = -\rho g, \tag{A.1c}$$

$$\frac{\partial u}{\partial x} + \frac{\partial v}{\partial y} + \frac{\partial w}{\partial z} = 0, \tag{A.1d}$$

$$\frac{dT}{dt} = A'_T \nabla^2 T + Q_T, \tag{A.1e}$$

$$\frac{dS}{dt} = A'_S \nabla^2 S + Q_S, \tag{A.1f}$$

$$\rho = \rho_0 [1 + \alpha_T (T - T_0) + \alpha_s (S - S_0)]. \tag{A.1g}$$

In (A.1), $\mathbf{v} = (u, v)$ is the horizontal velocity, w the vertical velocity, p the pressure, T the temperature, S the salinity, ρ the density, $\tau = (\tau^x, \tau^y)$ the horizontal shear stress, Q_T and Q_S the sources and sinks of heat and salt, $f = \beta y$ the Coriolis parameter, A' the horizontal eddy viscosity coefficient,

[1]This assumption is not necessary. There are many reduced-gravity models that incorporate entrainment and detrainment, mixed-layer physics, surface fluxes, etc.; among them is the model of McCreary et al. [1993].

A_T' and A_S' the horizontal eddy diffusivity coefficients for heat and salt, α_T and α_S the expansion coefficients, ρ_0, T_0, and S_0 determine a reference state about which the system is perturbed, and

$$\frac{d}{dt} = \frac{\partial}{\partial t} + u\frac{\partial}{\partial x}\mathbf{i} + v\frac{\partial}{\partial y}\mathbf{j},$$

where **i** and **j** are the unit vectors in the zonal and meridional directions. The vertical momentum equation (A.1c) reduces to the hydrostatic equation because we are interested in large-scale flows. Equations (A.1) are integrated in the vertical over the depth of the layer, from $-(H_1 - \eta)$ to η, to obtain the required depth-averaged equations for the active layer.

The pressure at a depth z in the two layers is given by

$$p_1 = p_{\text{atm}} + \rho_1 g(-z+\eta), \tag{A.2a}$$

$$p_2 = p_{\text{atm}} + \rho_1 g H_1 + \rho_2 g[-z-(H_1-\eta)], \tag{A.2b}$$

where p_{atm} is the atmospheric pressure, whose horizontal variations are ignored. The assumption that the pressure gradient vanishes in the lower layer, i.e., $\nabla p_2 = 0$, then implies that

$$\nabla\eta = \nabla(\Gamma H_1). \tag{A.3}$$

$$\Gamma = \frac{\rho_2 - \rho_1}{\overline{\rho}} \tag{A.4}$$

is the reduced-gravity parameter, $g\Gamma$ is the "reduced gravity", and $\overline{\rho}$ is an average density that is representative of the ocean (this is equivalent to the Boussinesq approximation). This factor Γ reduces the speed of the internal, or interfacial, wave in the model because it multiplies g. Averaging the pressure gradient term over the layer gives

$$\begin{aligned} H_1\overline{\frac{1}{\rho_1}\nabla p_1} &= gH_1\nabla(\Gamma H_1) + \frac{gH_1^2}{2\overline{\rho}}\nabla\rho_1 \\ &= gH_1\nabla(\Gamma H_1) - \frac{gH_1^2}{2}\nabla\Gamma \\ &= g\Gamma H_1\nabla H_1 + \frac{gH_1^2}{2}\nabla\Gamma. \end{aligned} \tag{A.5}$$

$\overline{\frac{1}{\rho_1}\nabla p_1}$ represents a vertical average of the horizontal pressure gradient over the layer.

Using

$$w|_\eta = \frac{d\eta}{dt}; \quad w|_{-(H_1-\eta)} = \frac{d\eta}{dt} - \frac{dH_1}{dt}$$

and assuming that Laplacian friction acts on a column of fluid the way it does on a fluid parcel, we obtain the required governing equations. In vector form, they are

$$\frac{(\partial H_1 \mathbf{v})}{\partial t} + \nabla \cdot (\mathbf{v} H_1 \mathbf{v}) + f\mathbf{k} \times (H_1 \mathbf{v}) = -H_1 \overline{\frac{1}{\rho_1} \nabla p_1} + \frac{\tau}{\bar{\rho}} + A\nabla^2 (H_1 \mathbf{v}) - r(H_1 \mathbf{v}), \tag{A.6a}$$

$$\frac{\partial H_1}{\partial t} = -\nabla \cdot (H_1 \mathbf{v}), \tag{A.6b}$$

$$\frac{\partial \Gamma}{\partial t} = \mathbf{v} \cdot \nabla \Gamma + A_\gamma \nabla^2 \Gamma + Q, \tag{A.6c}$$

where $\mathbf{k}$ is the unit vector in the vertical and $\overline{\frac{1}{\rho_1} \nabla p_1}$ is given by (A.5). Q combines the sources and sinks of heat and salt into a source-cum-sink term for Γ, and $\tau = (\tau^x, \tau^y)$ now represents the wind stress acting at the surface. The bottom friction, or the friction between the two layers, is set to zero. Instead, a friction term, $r(H_1 \mathbf{v})$, is introduced; it is used to define dampers near open boundaries in numerical simulations. Often called Rayleigh friction when linearized, it is also used to add friction to analytic models. It may be thought of as "bottom friction", but is not necessarily that. (A.6c) combines the equations for conservation of heat and salt. This is done because we do not solve the equations for temperature and salinity in this thesis; we do, however, need this equation because temperature and salinity can vary in the horizontal within the active layer.

From (A.3), the surface dynamic height, or model sea level, is

$$\eta = \overline{\Gamma} h + \overline{H} \gamma, \tag{A.7}$$

the constant of integration being set to zero.

The pressure gradient, given by (A.5), has one depth-dependent term. $g\nabla(\Gamma H_1) = g\nabla\eta$ is the barotropic component and $\frac{gH_1}{2\rho}\nabla\rho_1$ is the baroclinic component. Despite this, the velocity field is independent of depth and the wind stress projects as a body force on the upper layer; this is based on the assumption that the Reynolds stresses $\overline{u'w'}$ and $\overline{v'w'}$ have a vertical structure such that their depth-dependent part cancels that of the pressure gradient. A necessary condition for this cancellation is that the depth-dependent part of the pressure gradient is its average value in the layer, evaluated by substituting $z = \frac{H_1}{2}$ in the baroclinic term[2] [McCreary and Kundu, 1988].

Equations (A.6), with $\Gamma = \overline{\Gamma}$, a constant, and $r = \chi_s$, are solved in Section 3.3; this is a dynamical $1\frac{1}{2}$-layer reduced-gravity model, the only dependent variables being u, v, and H_1.

[2]For a detailed discussion on the consequences of this assumption, see Ripa [1992, 1995].

A.1.2 The Linearized Model

Equations (A.6) are linearized by perturbing the system about a basic state of no motion with thickness $\overline{H}$ and "density" $\overline{\Gamma}$ in the upper layer. Let the perturbations in H and Γ be h and γ, respectively, i.e.,

$$H = \overline{H} + h, \tag{A.8a}$$

$$\Gamma = \overline{\Gamma} + \gamma. \tag{A.8b}$$

To linearize, we scale the variables, expand them in powers of an infinitesimal, ε, and collect terms of the same order in ε; this yields the required linearized, perturbation equations. We first rewrite the momentum equation for transport, (A.6a), in terms of velocity, i.e., we use (A.6b) to eliminate the factor H_1. (The only term that does not yield directly to this simplification is the Laplacian friction because it was an *ad hoc* change that allowed us to write the friction term for the transport.) The equation becomes

$$\frac{\partial \mathbf{v}}{\partial t} + \mathbf{v}\cdot\nabla\mathbf{v} + f\mathbf{k}\times\mathbf{v} = -\overline{\frac{1}{\rho_1}}\nabla p_1 + \frac{\tau}{\overline{\rho} H_1} + A\nabla^2\mathbf{v} - r\mathbf{v}. \tag{A.9}$$

The variables are scaled as follows.

$$(t,x,y,u,v,Q,\tau,\eta) = \left(\mathcal{T}t', \mathcal{L}x', \mathcal{L}y', \mathcal{U}u', \mathcal{U}v', Qq', \mathcal{F}\tau', \mathcal{H}\eta'\right), \tag{A.10a}$$

$$H = \overline{H}\left(1 + \delta^h h'\right); \quad \Gamma = \overline{\Gamma}\left(1 + \delta^\gamma \gamma'\right). \tag{A.10b}$$

Then, with the scalings

$$\frac{1}{\beta\mathcal{L}\mathcal{T}} = \frac{r}{\beta\mathcal{L}} = \frac{A_\gamma}{A} = \frac{\mathcal{F}}{\beta\mathcal{L}\mathcal{U}} = 1, \tag{A.11a}$$

$$\frac{U}{\beta\mathcal{L}^2} = \left(\frac{U}{g\overline{\Gamma}\overline{H}}\right)^{\frac{1}{2}} = \frac{Q}{\beta\mathcal{L}\overline{\Gamma}} = \frac{\mathcal{H}}{\overline{H}} = \delta^h = \delta^\gamma = \varepsilon, \tag{A.11b}$$

$$\frac{A}{\beta\mathcal{L}^3} = \varepsilon^2, \tag{A.11c}$$

where $\varepsilon \ll 1$ and $f = \beta y$, and with the expansion

$$\theta = \theta_0 + \varepsilon\theta_1 + \varepsilon^2\theta_2^2 + \cdots, \tag{A.12}$$

where θ is any of the variables u, v, h, γ, τ, η, or q, we obtain the following zeroth-order perturbation equations.

$$\frac{\partial u_0}{\partial t} - \beta y v_0 = -g\overline{\Gamma}\frac{\partial h_0}{\partial x} - \frac{g\overline{H}}{2}\frac{\partial \gamma_0}{\partial x} + \frac{\tau_0^x}{\overline{\rho H}} - r u_0; \tag{A.13a}$$

$$\frac{\partial v_0}{\partial t} + \beta y u_0 = -g\overline{\Gamma}\frac{\partial h_0}{\partial y} - \frac{g\overline{H}}{2}\frac{\partial \gamma_0}{\partial y} + \frac{\tau_0^y}{\overline{\rho H}} - r v_0; \tag{A.13b}$$

$$\frac{\partial h_0}{\partial t} = -\overline{H}\left(\frac{\partial u_0}{\partial x} + \frac{\partial v_0}{\partial y}\right); \tag{A.13c}$$

$$\frac{\partial \gamma_0}{\partial t} = Q_0, \tag{A.13d}$$

$$\eta_0 = \overline{\Gamma} h_0 + \overline{H}\gamma_0. \tag{A.13e}$$

In (A.13d), $Q_0 = Q q_0$. The subscript "0" indicates that these are the zeroth-order terms in the expansion (A.12).

Equations (A.13), with $\gamma_0 = 0$, are the linear equations solved in Chapter 3. The Laplacian friction terms, however, are retained in the linear numerical simulations to avoid numerical instabilities.

In the analytic model, we seek wave solutions of the form $\theta_0 \propto e^{\iota\omega t}$; writing

$$\iota\omega = \frac{\partial}{\partial t} + r = \iota\sigma + r \tag{A.14}$$

and dropping the wind stress yields the free wave equations (3.3) for the equatorial β-plane.

For a coastal Kelvin wave propagating along a meridional boundary, $u_0 = 0$. The resulting equations are solved in Section 6.4.1 on an f-plane ($f = f_0$, where f_0 is a constant).

A.2 The $2\frac{1}{2}$-Layer Model

A $2\frac{1}{2}$-layer model has two active layers; the third layer is much deeper than these and is motionless (Figure A.2). The equations are similar to those for the $1\frac{1}{2}$-layer model, except for changes in the pressure gradient terms for the layers. The wind stress projects as a body force on the first layer and the second layer is driven by the resulting changes in the pressure field.

As for the $1\frac{1}{2}$-layer model, the conservation equations are averaged over the depth of each layer; the limits of integration are $-(H_1 - \eta)$ and η for the first layer and $-(H_1 + H_2 - \eta)$ and $-(H_1 - \eta)$ for the second layer. The pressure at a depth z in the three layers is given by

$$p_1 = p_{\text{atm}} + \rho_1 g(-z + \eta), \tag{A.15a}$$

Figure A.2 A schematic vertical cross-section of the $2\frac{1}{2}$-layer reduced-gravity model. The model ocean has a flat bottom and consists of three incompressible layers, the lowest layer being much deeper than the relatively shallow layers above. There is no mixing between the layers. In the figure, the subscripts 1, 2, and 3 refer to the three layers. $\overline{H}_1$ and $\overline{H}_2$ are the mean, or initial thicknesses, of the top two layers, H_i and ρ_i are the instantaneous thickness and density of layer i, and η is the displacement of the surface from the initial, or undisturbed, state. η, the model sea level, is equivalent to the dynamic height computed from hydrographic data. The interface between the second and third layers is the model pycnocline. H_1, H_2, ρ_1, ρ_2, and η are functions of space and time; ρ_3 is constant.

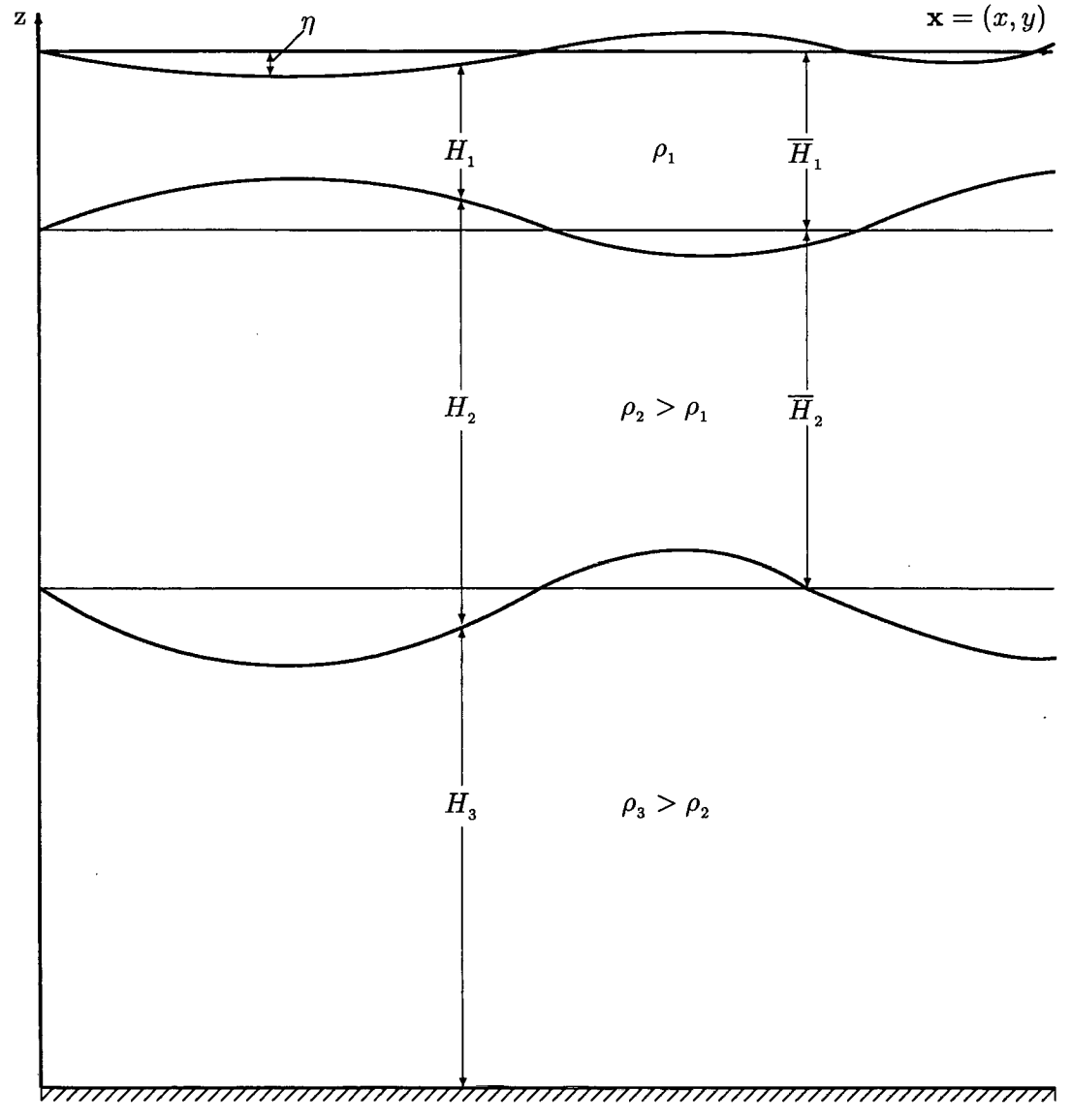

$$p_2 = p_{\text{atm}} + \rho_1 g H_1 + \rho_2 g[-z-(H_1-\eta)], \tag{A.15b}$$

$$p_3 = p_{\text{atm}} + \rho_1 g H_1 + \rho_2 g H_2 + \rho_3 g[-z-(H_1+H_2-\eta)], \tag{A.15c}$$

where p_{atm} is the atmospheric pressure, whose horizontal variations are neglected. The assumption that the pressure gradient vanishes in the lowest layer, i.e., $\nabla p_3 = 0$, then implies that

$$\nabla\eta = \nabla(\Gamma_1 H_1 + \Gamma_2 H_2). \tag{A.16}$$

$$\Gamma_1 = \frac{\rho_3-\rho_1}{\bar{\rho}} \quad \text{and} \quad \Gamma_2 = \frac{\rho_3-\rho_2}{\bar{\rho}} \tag{A.17}$$

are the "reduced-gravity" parameters for the two layers, and $\bar{\rho}$, as before, is an average density that is representative of the ocean. Averaging the pressure gradient term over each layer gives

$$\begin{aligned} H_1\overline{\frac{1}{\rho_1}\nabla p_1} &= gH_1\nabla(\Gamma_1 H_1+\Gamma_2 H_2)+\frac{gH_1^2}{2\bar{\rho}}\nabla\rho_1 \\ &= gH_1\nabla(\Gamma_1 H_1+\Gamma_2 H_2)-\frac{gH_1^2}{2}\nabla\Gamma_1 \\ &= gH_1\left(\Gamma_1\nabla H_1+\Gamma_2\nabla H_2+\frac{H_1}{2}\nabla\Gamma_1+H_2\nabla\Gamma_2\right), \end{aligned} \tag{A.18a}$$

$$\begin{aligned} H_2\overline{\frac{1}{\rho_2}\nabla p_2} &= gH_2\nabla[\Gamma_2(H_1+H_2)]+\frac{gH_2}{\bar{\rho}}\left(H_1+\frac{H_2}{2}\right)\nabla\rho_2 \\ &= gH_2\nabla[\Gamma_2(H_1+H_2)]-gH_2\left(H_1+\frac{H_2}{2}\right)\nabla\Gamma_2 \\ &= gH_2\left(\Gamma_2\nabla H_1+\Gamma_2\nabla H_2+\frac{H_2}{2}\nabla\Gamma_2\right). \end{aligned} \tag{A.18b}$$

$\overline{\frac{1}{\rho_1}\nabla p_1}$ and $\overline{\frac{1}{\rho_2}\nabla p_2}$ represent a vertical average of the horizontal pressure gradient over the layers.

The required governing equations for the $2\frac{1}{2}$-layer model, solved numerically in Chapter 4, are

$$\frac{(\partial H_i\mathbf{v}_i)}{\partial t}+\nabla\cdot(\mathbf{v}_i H_i\mathbf{v}_i)+f\mathbf{k}\times(H_i\mathbf{v}_i) = -H_i\overline{\frac{1}{\rho_i}\nabla p_i}+\delta_i\frac{\tau}{\bar{\rho}}+A\nabla^2(H_i\mathbf{v}_i)-r(H_i\mathbf{v}_i), \tag{A.19a}$$

$$\frac{\partial H_i}{\partial t} = -\nabla\cdot(H_i\mathbf{v}), \tag{A.19b}$$

$$\frac{\partial\Gamma_i}{\partial t} = \mathbf{v}_i\cdot\nabla\Gamma_i + A_\gamma\nabla^2\Gamma_i + Q_i, \tag{A.19c}$$

where the subscript $i = 1,2$ refers to layer i and

$$\delta_i = \begin{cases} 1 & \text{if } i = 1, \\ 0 & \text{if } i = 2. \end{cases}$$

Linearization of (A.19) is done as for the $1\frac{1}{2}$-layer model. The zeroth-order linearized perturbation equations for the $2\frac{1}{2}$-layer model, equivalent to (A.13) for the $1\frac{1}{2}$-layer model, are as follows.

$$\frac{\partial u_1}{\partial t} - \beta y v_1 = -g\overline{\Gamma}_1 \frac{\partial h_1}{\partial x} - g\overline{\Gamma}_2 \frac{\partial h_2}{\partial x} - \frac{g\overline{H}_1}{2} \frac{\partial \gamma_1}{\partial x} - g\overline{H}_2 \frac{\partial \gamma_2}{\partial x} + \frac{\tau^x}{\overline{\rho}\overline{H}_1} - r u_1, \tag{A.20a}$$

$$\frac{\partial v_1}{\partial t} + \beta y u_1 = -g\overline{\Gamma}_1 \frac{\partial h_1}{\partial y} - g\overline{\Gamma}_2 \frac{\partial h_2}{\partial y} - \frac{g\overline{H}_1}{2} \frac{\partial \gamma_1}{\partial y} - g\overline{H}_2 \frac{\partial \gamma_2}{\partial y} + \frac{\tau^y}{\overline{\rho}\overline{H}_1} - r v_1, \tag{A.20b}$$

$$\frac{\partial h_1}{\partial t} = -\overline{H}_1 \left(\frac{\partial u_1}{\partial x} + \frac{\partial v_1}{\partial y} \right), \tag{A.20c}$$

$$\frac{\partial \gamma_1}{\partial t} = Q_1 \tag{A.20d}$$

are the equations for the first layer and

$$\frac{\partial u_2}{\partial t} - \beta y v_2 = -g\overline{\Gamma}_2 \frac{\partial (h_1 + h_2)}{\partial x} - \frac{g\overline{H}_2}{2} \frac{\partial \gamma_2}{\partial x} - r u_2, \tag{A.21a}$$

$$\frac{\partial v_2}{\partial t} + \beta y u_2 = -g\overline{\Gamma}_2 \frac{\partial (h_1 + h_2)}{\partial y} - \frac{g\overline{H}_2}{2} \frac{\partial \gamma_2}{\partial y} - r v_2, \tag{A.21b}$$

$$\frac{\partial h_2}{\partial t} = -\overline{H}_2 \left(\frac{\partial u_2}{\partial x} + \frac{\partial v_2}{\partial y} \right), \tag{A.21c}$$

$$\frac{\partial \gamma_2}{\partial t} = Q_2 \tag{A.21d}$$

are the equations for the second layer. In (A.20) and (A.21), we have dropped the subscript "0" for convenience.

The surface dynamic height, or model sea level, is given by

$$\eta = \overline{\Gamma}_1 h_1 + \overline{\Gamma}_2 h_2 + \overline{H}_1 \gamma_1 + \overline{H}_2 \gamma_2, \tag{A.22}$$

where

$$H_1 = \overline{H}_1 + h_1, \quad H_2 = \overline{H}_2 + h_2, \tag{A.23a}$$

$$\Gamma_1 = \overline{\Gamma}_1 + \gamma_1, \quad \Gamma_2 = \overline{\Gamma}_2 + \gamma_2. \tag{A.23b}$$

$\overline{H}_1$, $\overline{H}_2$, $\overline{\Gamma}_1$, and $\overline{\Gamma}_2$ define the basic state about which the system is perturbed.

Equations (A.20) and (A.21), with the definition (A.14) and $\tau^x = \tau^y = 0$, are solved in Section 6.4.2 for a coastal Kelvin wave on an f-plane.

Appendix B

Linear Waves on an Equatorial β-Plane

Theoretical studies of the dynamics of the north Indian Ocean during the last decade have used free and forced long baroclinic waves to describe the circulation in the basin. For the description of low-frequency dynamics, the most important of these waves are the equatorially-trapped Rossby and Kelvin waves and coastally-trapped Kelvin waves, all of which can exist in a reduced-gravity model at the low frequencies of interest. Here, we discuss the characteristics of these waves in brief; the discussion essentially follows Gill [1982] and Shetye [1998].

B.1 Waves Trapped at the Equator

The properties of the equatorially-trapped waves may be found by looking for solutions proportional to $e^{i(kx-\sigma t)}$. When this expression is used in the linearized equations (3.3), the resulting dispersion relation is [Gill, 1982, p. 438]

$$\left(\frac{\sigma}{c}\right)^2 - k^2 - \frac{\beta k}{\sigma} = (2n+1)\frac{\beta}{c}, \tag{B.1}$$

where c is the baroclinic wave speed, σ the frequency, and k the zonal wavenumber. For $n \geq 1$, the waves subdivide into two classes [Gill, 1982]. For the upper branches, $\frac{\beta k}{\sigma}$ is small, and an approximate dispersion relation is

$$\sigma^2 \approx (2n+1)\beta c + k^2 c^2; \tag{B.2}$$

these are the Poincaré waves. For the lower branches, $\frac{\sigma^2}{c^2}$ is small, and an approximate dispersion relation is

$$\sigma \approx \frac{-\beta k}{k^2 + (2n+1)\frac{\beta}{c}}; \tag{B.3}$$

these are the Rossby waves. $n = -1$ yields the Kelvin wave and $n = 0$ yields the Yanai, or mixed planetary-gravity, wave. All these dispersion curves are shown in Figure B.1. Since there is a large gap between the minimum Poincaré wave frequency and the maximum Rossby wave frequency, it is easy to distinguish between them; only the Kelvin and Yanai waves exist in this frequency gap. All these waves are trapped near the equator, and the trapping scale R_{eq}, called the "equatorial radius of deformation" [Gill and Clarke, 1974; Gill, 1982], is of the same order for them.

$$R_{eq} = \left(\frac{c}{2\beta}\right)^{\frac{1}{2}}. \tag{B.4}$$

For $c = 185$ cm s^{-1}, the speed of the baroclinic wave in the linear models used in this thesis, $R_{eq} \approx 200$ km.

At the low frequencies of interest in this thesis, Poincaré waves do not exist and the only equatorially-trapped waves of consequence are the Kelvin and Rossby waves; at these frequencies, the Yanai waves have very short wavelengths and are quickly dissipated.

B.1.1 Equatorially-Trapped Kelvin Waves

The phase and group velocities (c) of these non-dispersive waves is eastward. The particle velocity associated with the waves is along the equator ($v = 0$) and can be eastward or westward. The equatorial Kelvin waves exist within the equatorial waveguide, which extends about 200 km on either side of the equator.

B.1.2 Equatorially-Trapped Rossby Waves

The equatorially-trapped Rossby waves can have both eastward and westward group velocity, though their phase velocity is always westward. The eastward propagating waves, however, have a short wavelength (Figure B.1) and are dissipated quickly. Therefore, they are not important for large-scale dynamics, except in the neighbourhood of a western ocean boundary. The phase speed of the non-dispersive westward propagating Rossby wave is approximately one-third that of the equatorial Kelvin wave. The particle velocity associated with this wave can have both zonal and meridional components. Away from the equator, a local dispersion relation

$$c_R = \frac{\sigma}{k} = -\frac{c^2}{\beta y^2} \tag{B.5}$$

can be written for these waves; this states that the local phase velocity of the wave decreases with increasing distance from the equator. They are trapped equatorward of a critical latitude given by

$$y_c = \frac{c}{2\sigma}. \tag{B.6}$$

The equatorial Rossby waves cannot exist poleward of this latitude.

Figure B.1 Dispersion curves for linear waves on an equatorial β-plane, obtained by using different values of n in (B.1). On the ordinate is the non-dimensional frequency $\hat{\sigma} = \frac{\sigma}{(2\beta c)^{\frac{1}{2}}}$ and on the abscissa is the non-dimensional zonal wavenumber $\hat{k} = k\left(\frac{c}{2\beta}\right)^{\frac{1}{2}}$. The curves labelled -1 (solid) and 0 (dashed) correspond to the equatorially-trapped Kelvin and Yanai, or mixed planetary-gravity, waves, respectively. The upper curves (dashed) labelled 1 and 2 are the first two Poincaré wave modes and the corresponding lower curves (solid) are the first two Rossby wave modes [the curves for the Poincaré and Rossby waves are based on the approximate relations (B.2) and (B.3)]. The zonal group velocity of these waves is given by $c_g = \frac{d\sigma}{dk}$ and the zonal phase velocity by $c = \frac{\sigma}{k}$. The zonal group and phase velocity of the Kelvin wave is eastward. The zonal group velocity of the Yanai wave is eastward; its zonal phase velocity is eastward (westward) at positive (negative) wavenumbers. A consequence of the approximation (B.2) is that the dispersion curves for Poincaré waves are symmetric w.r.t. $\hat{k}$; hence, the waves with eastward (westward) zonal group velocity also have eastward (westward) zonal phase velocity. At low (high) wavenumbers, i.e., at large (short) wavelengths, the zonal group velocity of the Rossby wave is westward (eastward); its zonal phase velocity, however, is always westward. On the curve for the Rossby wave, the westward (eastward) propagating waves lie to the right (left) of the maximum. Since there is a large gap between the minimum Poincaré wave frequency and the maximum Rossby wave frequency, it is easy to distinguish between them; only the Kelvin and Yanai waves exist in this frequency gap. At positive wavenumbers, the Yanai wave is almost indistinguishable from the Kelvin wave, the only difference being its assymetry about the equator; at high negative wavenumbers, it behaves like the (short) Rossby wave. At the low frequencies of interest, Poincaré waves do not exist. At these frequencies, the eastward propagating Rossby waves and the Yanai wave have short wavelengths and are quickly dissipated; hence, they are not important for the large-scale dynamics in the tropics. Therefore, at the low frequencies of interest in this thesis, the only equatorially-trapped waves of consequence are the westward propagating Rossby waves and the Kelvin wave (solid curves).

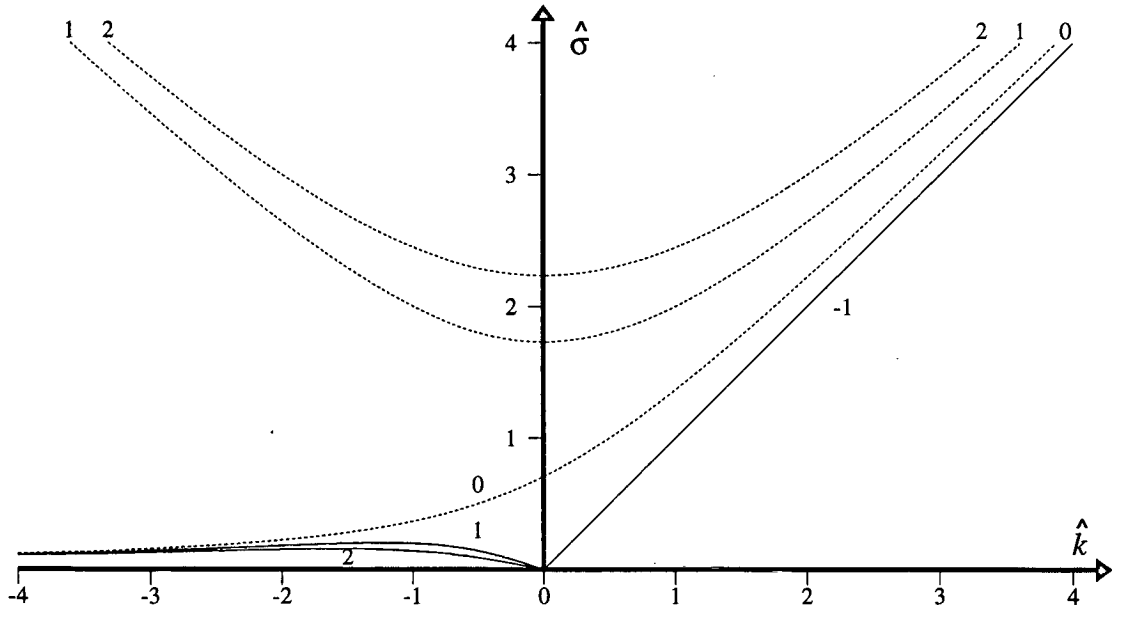

B.2 Waves Trapped at a Coast

Since the models used in this thesis have a flat bottom and ignore the effects of the continental shelf, the only coastally-trapped wave of interest is the Kelvin wave, which propagates along a vertical wall.

B.2.1 Coastally-Trapped Kelvin Waves

These waves propagate with the coast on their right in the northern hemisphere [Gill, 1982]. They are non-dispersive and are trapped at the coast with a trapping scale, or "radius of deformation", given by

$$R_c = \frac{c}{f}, \tag{B.7}$$

where f is the local Coriolis parameter. The coast acts as a waveguide of variable width, R_c decreasing poleward. For $c = 185$ cm s^{-1}, the trapping scale is about 75 km at 10°N and 150 km at 5°N. The particle velocity associated with these waves can be in either direction along the coast.

Equatorward of the critical latitude y_c, given by (B.6), a coastal Kelvin wave is not trapped at the coast; it radiates westward propagating Rossby waves as it propagates meridionally and the coastal waveguide turns "leaky" [Shetye, 1998]. In this case, it is not possible to separate the Kelvin wave from the Rossby wave. Since y_c is 42°and 21°for the annual and semiannual harmonics, the coastal waveguide along the eastern boundary of the Bay of Bengal and along the west coast of India is leaky for these frequencies (Figure B.2).

B.3 Observations of Rossby and Kelvin Waves in the Oceans

Equatorial Rossby and Kelvin waves and coastal Kelvin waves are the three waves invoked when describing the large-scale circulation in the north Indian Ocean. They appear prominently in model simulations, which tend to produce a smoother map of sea level and currents than are actually observed. All these waves, however, have been observed in the oceans, either as oscillations of the sea surface, or as oscillations of the thermocline or pycnocline. In association with these fields, there are changes in the currents. The sea-surface temperature (SST) also shows the influence of these waves, the movement of the model interface (the model thermocline) often having been used as a proxy for SST in model studies of El Niño.

A remarkable manifestation of these waves was reported by Jacobs et al. [1994], who used Geosat altimetry and model simulations to track the positive sea-level anomalies generated in the eastern equatorial Pacific by the 1982–83 El Niño a decade later in the subtropical central Pacific. The sea-level high in the eastern equatorial Pacific was generated by the downwelling equatorial

Figure B.2 A schematic of the "leaky" waveguide in the north Indian Ocean [Shetye, 1998]. The horizontal hatching indicates the equatorial waveguide, which extends about 200 km on either side of the equator; the vertical hatching indicates the coastal waveguide. The equatorial waveguide is connected to the Bay of Bengal at its eastern boundary. This link arises as a consequence of the reflection of the equatorial Kelvin wave at the eastern boundary of the basin; the reflected wave is a summation over several meridional modes of the westward propagating Rossby wave, these being required to satisfy the condition of no normal flow at the boundary [Moore, 1968]. The higher meridional modes are equivalent to a coastal Kelvin wave, which carries a part of the incident energy poleward along the coast in both hemispheres. This Kelvin wave is trapped at the coast poleward of the critical latitude; equatorward of this latitude, westward radiation of energy is possible, and the coastal Kelvin wave is inseparable from the Rossby wave. The same phenomenon is seen off the Indian west coast. For the seasonal cycle, it is the annual and semiannual harmonics that are most important. The critical latitudes for these periods are 42° and 21°, respectively; the former lies poleward of the northern boundary of the basin, and the latter is close to it. Hence, both annual and semiannual Kelvin waves are inseparable from westward propagating Rossby waves in the Bay of Bengal and the Arabian Sea, and energy leaks at these periods from the eastern boundary into the open ocean. The arrows show the direction in which energy leaks out of the coastal waveguide.

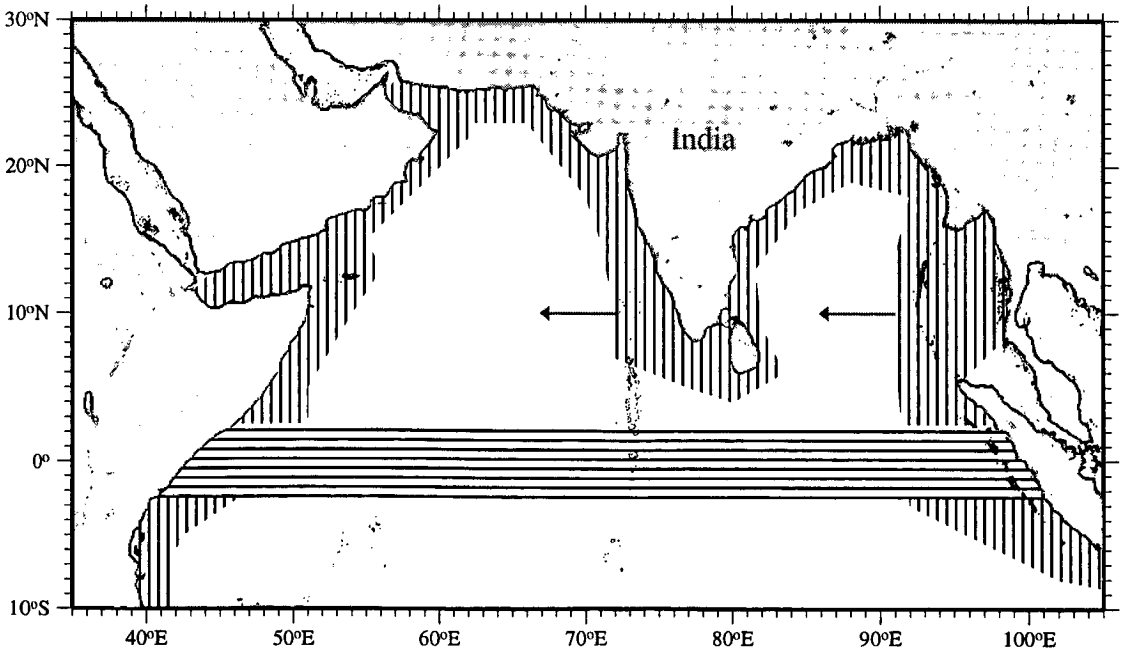

Kelvin waves triggered by a relaxation in the easterly trade winds. The equatorial Kelvin waves generated Rossby waves on reflection at the eastern boundary of the basin. Moore [1968] showed that the zonal velocity of the Kelvin wave cannot be cancelled by a single meridional mode of the westward propagating Rossby wave; an infinity of modes is needed to satisfy the boundary condition. The higher order modes propagate poleward along the coast and Moore showed that this poleward propagation was equivalent to a coastal Kelvin wave. The Kelvin wave at these latitudes cannot be separated from the Rossby wave because it is equatorward of the critical latitude for the sub-annual frequencies that characterise El Niño; hence, a part of the energy "peels" off the coast as a Rossby wave. Jacobs et al. showed that the Rossby wave generated by the strong El Niño of 1982–83 was still propagating across the subtropical Pacific a decade later, forcing changes in the Kuroshio extension. The coastal Kelvin wave generated by the reflection of the equatorial Kelvin wave has been traced as far as the Canadian border and Alaska [Enfield and Allen, 1980; Chelton and Davis, 1982]. The strength of the signal and the improvement in the measuring instruments made it possible to track the effects of the 1982–83 El Niño, but the basic dynamics of this event was no different from that of other manifestations of the phenomenon.

These waves have been detected in the Indian Ocean too. Perigaud and Delecluse [1992, 1993] detected Rossby wave signals in the south Indian Ocean in Geosat data. Kumar and Unnikrishnan [1995], Unnikrishnan et al. [1997], and Rao [1998] used temperature climatologies to show evidence in thermocline oscillation for the existence of Rossby waves in the north Indian Ocean. Equatorial Kelvin waves too are seen in the altimeter data. Coastal Kelvin waves, however, are difficult to detect in the north Indian Ocean because the wind forcing is strong along most of the coast and distorts the phase of the propagating waves; the free and forced waves cannot be separated, making it difficult to track a signal along the coast. The discussion on forcing mechanisms of the Lakshadweep high and low (Section 3.5), however, hints at the possibility of detecting such signals in daily sea-level data along the Indian west coast during the northeast monsoon, when the local winds are relatively weak and the free waves, forced by winds along the Indian east coast, dominate. Unfortunately, there are no tide-gauge data along the eastern boundary of the Bay of Bengal, which appears to be the best place to look for evidence of free coastal Kelvin waves because the local winds blow into the coast, forcing a very weak Kelvin wave (Section 3.5.2). Therefore, the Kelvin wave signal here must consist of free waves forced remotely from the equatorial Indian Ocean.

We close this discussion here, referring the reader to Gill [1982] and Pedlosky [1979] for more details on these waves.

Appendix C

Estimating the Statistical Significance of Correlations

We say that a linear correlation between two variables x and y is statistically significant at a given level, say $P\%$, when the probability of two series of random numbers having the same correlation is less than $(100-P)\%$. For example, the correlation is significant at the 95% significance level if there is but a 5% chance that the correlation between two series of random numbers for the same number of degrees of freedom (the number of valid data points at the given lag) would equal or exceed the correlation between x and y. Therefore, the statistical significance of the linear correlations computed in Chapter 6 is estimated as follows.

Suppose the number of degrees of freedom is M. N_s series of random numbers are constructed using a random-number-generator, each series consisting of M terms. Correlations are computed for each combination of these N_s series, taken two at a time; this yields $N_c = \frac{N_s(N_s-1)}{2}$ correlations. The magnitudes (absolute value) of these correlations are sorted to obtain a monotonic sequence C_n of N_c terms, in which correlations are ordered from the lowest to the highest value. Then, C_p is the required correlation at the $P\%$ significance level, where

$$p = \frac{PN_c}{100} + 1.$$

The correlations computed thus match those in Table 7 in Crow et al. [1960].

The same method is used to estimate the significance levels when x and y are filtered with an N-year running mean. The same filter is applied to the N_s series of random numbers and the correlations are computed for these filtered series. The rest of the procedure is as described above. Application of the filter decreases the randomness of the series; the correlations among the filtered series are higher, and hence, the correlation at given significance level is higher than before.

For the correlations computed in Chapter 6, the random-number series were generated using `function ran2` in Press et al. [1989]; M depends on the variables being correlated because

the tide-gauge sea-level and rainfall records are not of the same length; $N_s = 500$; therefore, $N_c = 124750$. Reducing N_s to 150 decreases N_c to 11175, but there is only a minor change in the correlation at a given significance level. Changing the random number seed `iseed` also does not have an influence on these correlations, implying that the random-number series generated by `function ran2` are sufficiently random for our purpose.

Appendix D

Sources of Data and Software

The observations presented in this thesis were obtained from different sources and processed into graphical form using several software packages. The sources of data and software are listed here.

D.1 Data

- The hourly and daily sea level at Mumbai (Figure 1.3) were obtained from the Survey of India. These data were converted to electronic form by Matthew Dias and processed by D. Sundar.
- Monthly sea level data from tide gauges are the major data used in this thesis. These were obtained from the Permanent Service for Mean Sea Level (PSMSL) at the Bidston Observatory, United Kingdom.
- The Comprehensive Ocean-Atmosphere Data Set (COADS) was the source of the climatology of monthly sea-level atmospheric pressure used to correct the climatology of monthly sea level.
- The monthly sea-level atmospheric-pressure data used to correct the time series of monthly sea level in Chapter 6 were obtained from the Global Historical Climate Network (GHCN); the GHCN was also the source of monthly rainfall data for Mumbai, Kochi, Chennai, and Vishakhapatnam.
- All hydrographic data, except the climatologies of Levitus and Boyer [1994] and Levitus et al. [1994] and the salinity data off Marmagao (Figure 6.27), were obtained from the Indian National Oceanographic Data Centre (INODC) at the National Institute of Oceanography, Goa. A. Suryachandra Rao [Rao, 1998] put these data together and checked their quality, making possible the synthesis of the "coastal climatology" presented in Chapter 4. The

climatologies of Levitus and Boyer [1994] and Levitus et al. [1994] were obtained from the National Oceanic and Atmospheric Administration (NOAA), USA. The salinity data off Marmagao were made available by P. V. Narvekar, National Institute of Oceanography, Goa.

- All-India rainfall data were made available in electronic form by (late) Asha Guruprasad, Sulochana Gadgil, and Sajani Surendran, Indian Institute of Science, Bangalore. The 1871–1994 data were synthesized from the rainfall data for 306 stations in 29 meteorological subdivisions in India by Parthasarathy et al. [1995].

- Julian McCreary, Kevin Kohler, and Weiqing Han (Nova Southeastern University, Florida, USA) made available the results of the numerical simulations of McCreary et al. [1993]; these data were used to compute the sea level plotted in Figure 4.4. The climatology of winds, from Hellerman and Rosenstein [1983], and the climatology of ship drifts, from Rao et al. [1989], were also obtained from them.

D.2 Software

- Most of the figures were made with *GMT* (*Generic Mapping Tools*) and *FERRET*; LaTeX 2ε was used to prepare some of the schematics. *GMT* was written by Paul Wessel and Walter Smith [Wessel and Smith, 1991; Smith and Wessel, 1990]. *FERRET* was developed by the Thermal Modeling and Analysis Project (TMAP) at the Pacific Marine Environmental Laboratory (PMEL) of NOAA, USA; it uses *PlotPlus*, a package developed by Donald Denbo.

- Both *GMT* and *FERRET* use *netCDF*, a data format developed at the University Centre for Atmospheric Research, University of Boulder, Colorado, USA.

- This thesis was typeset using LaTeX 2ε. The manuscript was typed using *GNU Emacs* and *AUCTeX* on a pentium running *Debian GNU/Linux*. *GNU* was also the source of several other packages that were used; notable among these are *ghostscript*, *gv*, and *ghostview*.

Bibliography

J. S. Allen. Coastal trapped waves in a stratified ocean. *Journal of Physical Oceanography*, 5: 300–325, 1975.

D. G. Aubrey and K. O. Emery. Australia — an unstable platform for tide-gauge measurements of changing sea levels. *Journal of Geology*, 94:699–712, 1986.

K. Banse. Hydrography of the Arabian Sea Shelf of India and Pakistan and effects on demersal fishes. *Deep-Sea Research*, 15:45–79, 1968.

K. Banse. Overview of the hydrography and associated biological phenomena in the Arabian Sea. In B. U. Haq and J. D. Milliman, editors, *Marine geology and oceanography of Arabian Sea and coastal Pakistan*, pages 271–303. Van Nostrand Reinhold Co, New York, 1984.

K. Banse. On the coupling of hydrography, phytoplankton, zooplankton, and settling organic particles offshore in the Arabian Sea. *Proceedings of the Indian Academy of Sciences (Earth and Planetary Sciences)*, 103(2):125–161; June 1994. Special issue: Biogeochemistry of the Arabian Sea.

T. P. Barnett. The estimation of "global" sea level change: A problem of uniqueness. *Journal of Geophysical Research*, 89(C5):7980–7988, September 1984.

J. G. Bruce. Comparison of near surface dynamic topography during the two monsoons in the western Indian Ocean. *Deep-Sea Research*, 15:665–667, 1968.

J. G. Bruce, D. R. Johnson, and J. C. Kindle. Evidence for eddy formation in the eastern Arabian Sea during the northeast monsoon. *Journal of Geophysical Research*, 99(C4):7651–7664, April 1994.

J. G. Bruce, J. C. Kindle, L. H. Kantha, J. L. Kerling, and J. F. Bailey. Recent observations and modeling in the Arabian Sea Laccadive high region. *Journal of Geophysical Research*, 103(C4): 7593–7600, April 1998.

D. C. Chapman. Numerical treatment of cross-shelf open boundary conditions in a barotropic coastal ocean model. *Journal of Physical Oceanography*, 15:1060–1075, 1985.

D. B. Chelton and R. E. Davis. Monthly mean sea level variability along the west coast of north America. *Journal of Physical Oceanography*, 12:757–784, 1982.

A. J. Clarke and X. Liu. Observations and dynamics of semiannual and annual sea levels near the eastern equatorial Indian Ocean boundary. *Journal of Physical Oceanography*, 23(2):386–399, February 1993.

A. J. Clarke and X. Liu. Interannual sea level in the northern and eastern Indian Ocean. *Journal of Physical Oceanography*, 24(6):1224–1235, June 1994.

A. J. Clarke and C. Shi. Critical frequencies at ocean boundaries. *Journal of Geophysical Research*, 96(C6):10,731–10,738, June 1991.

A. J. Clarke and S. van Gorder. On ENSO coastal currents and sea levels. *Journal of Physical Oceanography*, 24(3):662–680, March 1994.

E. L. Crow, F. A. Davis, and M. W. Maxfield. *Statistics Manual.* Dover Publications, Inc., New York, 1960. Released within the Department of Defense as NAVORD REPORT 3369-NOTS 948.

A. N. Cutler and J. C. Swallow. Surface currents of the Indian Ocean (to 25°S, 100°E): Compiled from historical data archived by the Meteorological Office, Bracknell, UK. *Report 187*, Institute of Oceanographic Sciences, Wormley, England, 1984. 36 charts, 8pp.

V. K. Das. Seasonal variation in mean-sea level at Mormugao, west coast of India. *Mahasagar*, 12(2):59–67, 1979.

A. T. Doodson. Harmonic development of the tide-generating potential. *Proceedings of the Royal Society of London, Series A*, 100:305–329, 1921.

K. O. Emery and D. G. Aubrey. Tide gauges of India. *Journal of Coastal Research*, 5(3):489–501, Summer 1989.

D. B. Enfield and J. S. Allen. On the structure and dynamics of monthly mean sea level anomalies along the Pacific coast of north and south America. *Journal of Physical Oceanography*, 10(4): 557–578, April 1980.

H. S. Ghildyal and A. Kumar. Global mean sea level investigations: Discrepancy between the local mean sea level of the Bay of Bengal and local mean sea level of the Arabian Sea. Technical Paper, Published by the Surveyor General of India, 1984.

A. E. Gill. *Atmosphere-Ocean Dynamics*, volume 30 of *International Geophysics Series*. Academic Press, Inc., San Diego, CA 92101, USA, 1982.

A. E. Gill and A. J. Clarke. Wind-induced upwelling, coastal currents, and sea-level changes. *Deep-Sea Research*, 21:325–345, 1974.

V. Gornitz, S. Lebedeff, and J. Hansen. Global sea level trend in the past century. *Science*, 215: 1611–1614, 26 mar 1982.

I. S. Gradshteyn and I. M. Ryzhik. *Tables of Integrals, Series, and Products*. Academic Press, fourth edition, 1965. Translated from the Russian by Scripta Technica, Inc. Translation edited by A. Jeffrey.

S. Hellerman and M. Rosenstein. Normal monthly wind stress over the world ocean with error estimates. *Journal of Physical Oceanography*, 13:1093–1104, 1983.

G. A. Jacobs, H. E. Hurlburt, J. C. Kindle, E. J. Metzger, J. L. Mitchell, W. J. Teague, and A. J. Wallcraft. Decade-scale trans-Pacific propagation an warming effects of an El Niño anomaly. *Nature*, 370:360–363, 1994.

T. G. Jensen. Equatorial variability and resonance in a wind-driven Indian Ocean model. *Journal of Geophysical Research*, 98:22,533–22,552, 1993.

P. V. Joseph. Climatic change in monsoon and cyclones 1891–1974. In *Proceedings of the Symposium on Tropical Monsoons*. Indian Institute of Tropical Meteorology, Pune, 1976.

S. P. Kumar and A. S. Unnikrishnan. The seasonal cycle of temperature and associated wave phenomena in the Bay of Bengal. *Journal of Geophysical Research*, 100:13,585–13,593, 1995.

S. Levitus and T. P. Boyer. World Ocean Atlas 1994, Volume 4: Temperature. NOAA Atlas NESDIS 4. 117 pp., 1994.

S. Levitus, R. Burgett, and T. P. Boyer. World Ocean Atlas 1994, Volume 3: Salinity. NOAA Atlas NESDIS 3. 99 pp., 1994.

M. J. Lighthill. Dynamic response of the Indian Ocean to the onset of the southwest monsoon. *Philosophical Transactions of the Royal Society of London, Series A*, 265:45–92, October 1969.

A. R. Longhurst and W. S. Wooster. Abundance of oil sardine (*Sardinella longiceps*) and upwelling on the southwest coast of India. *Canadian Journal of Fisheries and Aquatic Sciences*, 47:2407–2419, 1990.

M. Madhupratap, S. P. Kumar, P. M. A. Bhattathiri, M. D. Kumar, S. Raghukumar, K. K. C. Nair, and N. Ramaiah. Mechanism of the biological response to winter cooling in the northeastern Arabian Sea. *Nature*, 384:549–552, 12 December 1996.

J. M. Martin, J. D. Burton, and D. Eisma. *River inputs to ocean systems.* United Nations Press, 1981.

J. P. McCreary. Modeling wind-driven ocean circulation. Technical Report JIMAR 80-0029, Hawaii Institute of Geophysics, University of Hawaii, Honolulu, Hawaii 96822, December 1980.

J. P. McCreary. A linear stratified ocean model of the equatorial undercurrent. *Philosophical Transactions of the Royal Society of London, Series A*, 298(1444):603–635, January 1981.

J. P. McCreary, W. Han, D. Shankar, and S. R. Shetye. Dynamics of the East India Coastal Current, 2. Numerical solutions. *Journal of Geophysical Research*, 101(C6):13,993–14,010, June 1996.

J. P. McCreary and P. Kundu. A numerical investigation of the Somali current during the south-west monsoon. *Journal of Marine Research*, 46:25–58, 1988.

J. P. McCreary, P. K. Kundu, and R. L. Molinari. A numerical investigation of the dynamics, thermodynamics and mixed-layer processes in the Indian Ocean. *Progress in Oceanography*, 31: 181–244, 1993.

S. K. Mishra and S. Gadgil. *Indian Climate Research Programme. Science Plan.* Department of Science and Technology, Government of India, New Delhi, November 1996.

D. W. Moore. *Planetary-Gravity Waves in an Equatorial Ocean.* PhD thesis, Harvard University, Cambridge, Massachusets, February 1968.

L. A. Mysak. Recent advances in shelf wave dynamics. *Reviews of Geophysics and Space Physics*, 18(1):211–241, February 1980.

S. W. A. Naqvi, M. D. George, P. Narvekar, D. A. Jayakumar, M. S. Shailaja, S. Sardesai, V. V. S. S. Sarma, D. M. Shenoy, H. Naik, P. A. Maheshwaran, K. Krishnakumari, G. Rajesh, A. K. Sudhir, and M. S. Binu. Severe fish mortality associated with 'red tide' observed in the sea off Cochin. *Current Science*, 75(6):543–544, September 1998.

R. S. Nerem, E. J. Schrama, C. J. Koblinsky, and B. D. Beckley. A preliminary evaluation of ocean topography from the TOPEX/POSEIDON mission. *Journal of Geophysical Research*, 99 (12):24,565–24,583, December 1994.

J. J. O'Brien and H. E. Hurlburt. Equatorial jet in the Indian Ocean: Theory. *Science*, 184: 1075–1077, 1974.

B. Parthasarathy, A. A. Munot, and D. R. Kothawale. All-India monthly and seasonal rainfall series; 1871–1993. *Theoretical and Applied Climatology*, 49:217–224, 1993.

B. Parthasarathy, A. A. Munot, and D. R. Kothawale. Monthly and seasonal rainfall series for all-India homogeneous regions and meteorological subdivisions: 1871–1994. IITM Research Report No. RR–065, ISSN 0252-1075, Indian Institute of Tropical Meteorology, Pune, 1995.

J. Patullo, W. Munk, R. Revelle, and E. Strong. The seasonal oscillation in sea level. *Journal of Marine Research*, 14(1):88–113, January 1955.

J. Pedlosky. *Geophysical Fluid Dynamics*. Springer-Verlag, New York, first edition, 1979.

C. Perigaud and P. Delecluse. Annual sea level variations in the southern tropical Indian Ocean from Geosat and shallow-water simulations. *Journal of Geophysical Research*, 97(C12):20,169–20,178, December 1992.

C. Perigaud and P. Delecluse. Interannual sea level variations in the tropical Indian Ocean from Geosat and shallow water simulations. *Journal of Physical Oceanography*, 23(9):1916–1934, September 1993.

G. L. Pickard and W. J. Emery. *Descriptive physical oceanography*. Pergamon Press, fourth edition, 1982.

R. M. Ponte. Variability in a homogeneous global ocean forced by barometric pressure. *Dynamics of Atmospheres and Oceans*, 18:209–234, 1993.

J. T. Potemra, M. E. Luther, and J. J. O'Brien. The seasonal circulation of the upper ocean in the Bay of Bengal. *Journal of Geophysical Research*, 96(C7):12,667–12,683, July 1991.

K. V. S. R. Prasad and B. S. R. Reddy. Sea level variations off Madras, east coast of India. *Indian Journal of Marine Sciences*, 14:206–209, December 1985.

W. H. Press, B. P. Flannery, S. A. Teukolsky, and W. T. Vetterling. *Numerical Recipes. The Art of Scientific Computing (FORTRAN version)*. Cambridge University Press, first edition, 1989.

D. T. Pugh. *Tides, surges, and mean sea level*. John Wiley and Sons Ltd., 1987.

A. S. Rao. *Rossby Waves in the Bay of Bengal: Observations and Simulations*. PhD thesis, Andhra University, Vishakhapatnam, India, March 1998.

R. R. Rao, R. L. Molinari, and J. F. Festa. Evolution of the climatological near-surface thermal structure of the tropical Indian Ocean, 1. Description of mean monthly mixed-layer depth and sea-surface temperature, surface-current, and surface meteorological fields. *Journal of Geophysical Research*, 94:10,801–10,815, 1989.

G. Reverdin, D. L. Cadet, and D. Gutzler. Interannual displacement of convection and surface circulation over the equatorial Indian Ocean. *Quarterly Journal of the Royal Meteorological Society*, 112:43–67, 1986.

P. Ripa. Conservation laws for primitive equations models with inhomogeneous layers. *Geophysical and Astrophysical Fluid Dynamics*, 70:85–111, 1992.

P. Ripa. On improving a one-layer ocean model with thermodynamics. *Journal of Fluid Mechanics*, 303:169–201, 1995.

B. C. Roy. Activities of Indian Cell for Monitoring and Analysis of Sea level (CMAS). In *IOC-UNEP-WMO-SAREC Planning Workshop on an Integrated Approach to Coastal Erosion, Sea Level Changes and their Impacts*, volume 96 of *IOC Workshop Reports*, pages 37–47, Zanzibar, Tanzania, 17–21 January 1994.

F. Schott. Seasonal variation of the cross-equatorial flow in the Somali Current. *Journal of Geophysical Research*, 91:10,581–10,584, 1986.

D. Shankar, J. P. McCreary, W. Han, and S. R. Shetye. Dynamics of the East India Coastal Current, 1. Analytic solutions forced by interior Ekman pumping and local alongshore winds. *Journal of Geophysical Research*, 101(C6):13,975–13,991, June 1996.

D. Shankar and S. R. Shetye. On the dynamics of the Lakshadweep high and low in the southeastern Arabian Sea. *Journal of Geophysical Research*, 102(C6):12,551–12,562, June 1997.

S. S. C. Shenoi, D. Shankar, and S. R. Shetye. On the sea surface temperature high in the Lakshadweep Sea before the onset of the southwest monsoon. *Journal of Geophysical Research*, 104:15,703–15,712, July 1999.

S. R. Shetye. Seasonal variability of the temperature field off the southwest coast of India. *Proceedings of the Indian Academy of Sciences (Earth and Planetary Sciences)*, 93(4):399–411, 1984.

S. R. Shetye. The movement and implications of the Ganges-Brahmaputra runoff on entering the Bay of Bengal. *Current Science*, 64(1):32–38; January 1993.

S. R. Shetye. West India Coastal Current and Lakshadweep high/low. *Sadhana*, 23:637–651, 1998.

S. R. Shetye and A. M. Almeida. An examination of the factors that influence the monthly-mean sea level along the coast of India. In *IOC/Unesco Workshop on Regional Co-operation in Marine Science in the Central Indian Ocean and Adjacent Seas and Gulfs*, volume 37 of *IOC Workshop Reports*, pages 87–104, Colombo, Sri Lanka, 8–13 July 1985.

S. R. Shetye and A. D. Gouveia. *Coastal circulation in the north Indian Ocean. Coastal segment (14,S–W)*, volume 11 of *The Sea*, chapter 18, pages 523–556. John Wiley and Sons, Inc, 1998.

S. R. Shetye, A. D. Gouveia, D. Shankar, S. S. C. Shenoi, P. N. Vinayachandran, D. Sundar, G. S. Michael, and G. Nampoothiri. Hydrography and circulation in the western Bay of Bengal during the northeast monsoon. *Journal of Geophysical Research*, 101(C6):14,011–14,025, June 1996.

S. R. Shetye, A. D. Gouveia, S. S. C. Shenoi, G. S. Michael, D. Sundar, A. M. Almeida, and K. Santanam. The coastal current off western India during the northeast monsoon. *Deep-Sea Research*, 38(12):1517–1529, December 1991a.

S. R. Shetye, A. D. Gouveia, S. S. C. Shenoi, D. Sundar, G. S. Michael, A. M. Almeida, and K. Santanam. Hydrography and circulation off the west coast of India during the southwest monsoon 1987. *Journal of Marine Research*, 48:359–378, 1990.

S. R. Shetye, A. D. Gouveia, S. S. C. Shenoi, D. Sundar, G. S. Michael, and G. Nampoothiri. The western boundary current of the seasonal subtropical gyre in the Bay of Bengal. *Journal of Geophysical Research*, 98(C1):945–954, January 1993.

S. R. Shetye, S. S. C. Shenoi, A. D. Gouveia, G. S. Michael, D. Sundar, and G. Nampoothiri. Wind-driven coastal upwelling along the western boundary of the Bay of Bengal during the southwest monsoon. *Continental Shelf Research*, 11(11):1397–1408, November 1991b.

N. Singh. *Variability of moisture and thermal fields over India.* Ph.D. Dissertation, Department of Geophysics, Banaras Hindu University, Varanasi, India, 1994.

W. H. F. Smith and P. Wessel. Gridding with continuous curvature splines in tension. *Geophysics*, 55:293–305, 1990.

B. L. K. Somayajulu, M. M. Sarin, and R. Ramesh. Denitrification in the eastern Arabian Sea: Evaluation of the role of continental margins using Ra isotopes. *Deep-Sea Research, Part B*, 43: 111–117, 1996.

J. Sprintall and M. Tomczak. Evidence of the barrier layer in the surface layer of the tropics. *Journal of Geophysical Research*, 97:7305–7316, 1992.

B. D. Tapley, D. P. Chambers, C. K. Shum, R. J. Eanes, J. C. Ries, and R. H. Stewart. Accuracy assessment of the large-scale dynamic ocean topography from TOPEX/POSEIDON altimetry. *Journal of Geophysical Research*, 99(C12):24,605–24,617, December 1994.

M. N. Tsimplis and P. L. Woodworth. The global distribution of the seasonal sea level cycle calculated from coastal tide gauge data. *Journal of Geophysical Research*, 99(C8):16,031–16,039, August 1994.

A. S. Unnikrishnan, S. P. Kumar, and G. S. Navelkar. Large-scale processes in the upper layers of the Indian Ocean inferred from temperature climatology. *Journal of Marine Research*, 55: 93–115, 1997.

R. Varadarajulu, M. Harikrishna, and K. H. Rao. Sealevel changes at Paradip, east coast of India. *Indian Journal of Marine Sciences*, 11:32–34, March 1982.

M. J. Varkey, V. S. N. Murty, and A. Suryanarayana. Physical oceanography of the Bay of Bengal and Andaman Sea. *Oceanography and Marine Biology*, 34:1–70, 1996.

J. Vialard and P. Delecluse. An OGCM study for the TOGA decade. Part I: Role of salinity in the physics of the western Pacific fresh pool. *Journal of Physical Oceanography*, 28(6):1071–1088, June 1998a.

J. Vialard and P. Delecluse. An OGCM study for the TOGA decade. Part II: Barrier-layer formation and variability. *Journal of Physical Oceanography*, 28(6):1089–1106, June 1998b.

P. N. Vinayachandran. *The Bay of Bengal Circulation in an OGCM*. PhD thesis, Indian Institute of Science, Bangalore 560012, India, December 1995.

P. N. Vinayachandran, S. R. Shetye, D. Sengupta, and S. Gadgil. Forcing mechanisms of the Bay of Bengal circulation. *Current Science*, 71(10):753–763, November 1996.

P. N. Vinayachandran and T. Yamagata. Monsoon response of the sea around Sri Lanka: Generation of thermal domes and anticyclonic vortices. *Journal of Physical Oceanography*, 28(10): 1946–1960, October 1998.

P. Wessel and W. H. F. Smith. Free software helps map and display data. *EOS Transactions of the American Geophysical Union*, 72:441, 445–446, 1991.

K. Wyrtki. *Oceanographic Atlas of the International Indian Ocean Expedition*. National Science Foundation, Washington, D.C., November 1971. 531 pp.

K. Wyrtki. An equatorial jet in the Indian Ocean. *Science*, 181:262–264, 1973.

K. Wyrtki. Sea level rise: The facts and the future. *Pacific Science*, 44(1):1–16, January 1990.

L. Yu, J. J. O'Brien, and J. Yang. On the remote forcing of the circulation in the Bay of Bengal. *Journal of Geophysical Research*, 96(C11):20,449–20,454, November 1991.